BIOGEOCHEMISTRY OF MARINE DISSOLVED ORGANIC SULFUR: QUANTIFICATION, DISTRIBUTION, MOLECULAR COMPOSITION, AND REACTIVITY

Dissertation zur Erlangung eines
Doktors der Naturwissenschaften
– Dr. rer. nat. –

vorgelegt von

Kerstin B. Ksionzek

Dipl. Chem.

2019

an der Universität Bremen
im Fachbereich Biologie/Chemie

Gutachter:

Prof. Dr. Boris Koch
Prof. Dr. Kai-Uwe Hinrichs

Kolloquium: 15.08.2019
Korrektur: 11.10.2019

AWI Universität Bremen marum Zentrum für Marine Umweltwissenschaften

Gutachter (*Evaluators*):

1. Gutachter (*Evaluator*) **Prof. Dr. Boris Koch**
Universität Bremen, Fachbereich 2
Alfred-Wegener-Institut, Helmholtz-Zentrum für Polar- und Meeresforschung
MARUM – Zentrum für Marine Umweltwissenschaften der Universität Bremen
Hochschule Bremerhaven

2. Gutachter (*Evaluator*) **Prof. Dr. Kai-Uwe Hinrichs**
Universität Bremen, Fachbereich 5
MARUM – Zentrum für Marine Umweltwissenschaften der Universität Bremen

Prüfer (*Examiner*):

1. Vorsitzender (*Chair*) **Prof. Dr. Tilmann Harder**
Universität Bremen, Fachbereich 2
Alfred-Wegener-Institut, Helmholtz-Zentrum für Polar- und Meeresforschung

2. Prüfer (*Examiner*) **Prof. Dr. Boris Koch**
Universität Bremen, Fachbereich 2
Alfred-Wegener-Institut, Helmholtz-Zentrum für Polar- und Meeresforschung
MARUM – Zentrum für Marine Umweltwissenschaften der Universität Bremen
Hochschule Bremerhaven

3. Prüfer (*Examiner*) **Prof. Dr. Christian Wild**
Universität Bremen, Fachbereich 2

4. Prüfer (*Examiner*) **Prof. Dr. Kai-Uwe Hinrichs**
Universität Bremen, Fachbereich 5
MARUM – Zentrum für Marine Umweltwissenschaften der Universität Bremen

Universität Bremen

Ort, Datum: Bremen, 24.06.2019__

Versicherung an Eides Statt

Ich, Kerstin Ksionzek, Busestraße 9, 28213 Bremen, Matr.-Nr. 1956464 (Vorname, Name, Anschrift, Matr.-Nr.)

.

versichere an Eides Statt durch meine Unterschrift, dass ich die vorstehende Arbeit selbständig und ohne fremde Hilfe angefertigt und alle Stellen, die ich wörtlich dem Sinne nach aus Veröffentlichungen entnommen habe, als solche kenntlich gemacht habe, mich auch keiner anderen als der angegebenen Literatur oder sonstiger Hilfsmittel bedient habe.
Ich versichere an Eides Statt, dass ich die vorgenannten Angaben nach bestem Wissen und Gewissen gemacht habe und dass die Angaben der Wahrheit entsprechen und ich nichts verschwiegen habe.
Die Strafbarkeit einer falschen eidesstattlichen Versicherung ist mir bekannt, namentlich die Strafandrohung gemäß § 156 StGB bis zu drei Jahren Freiheitsstrafe oder Geldstrafe bei vorsätzlicher Begehung der Tat bzw. gemäß § 161 Abs. 1 StGB bis zu einem Jahr Freiheitsstrafe oder Geldstrafe bei fahrlässiger Begehung.

_____
Ort, Datum Unterschrift

Acknowledgements

Numerous people - colleges, friends and my family - supported me during the last years in the preparation of my thesis. First of all, my biggest thanks go to my supervisor Prof. Dr. Boris Koch for giving me the opportunity to conduct my thesis and to become part of the working group *Marine Chemistry* at AWI. Boris, you introduced me to this exciting but also demanding topic. I deeply appreciate your continuous support, enthusiasm, expertise and patience during my studies. I also want to thank my other thesis advisory committee members – Prof. Dr. Gerhard Kattner and Dr. Walter Geibert for their support, time and helpful discussions whenever I needed them.

I am thankful to Prof. Dr. Kai-Uwe Hinrichs for his willingness to review my thesis and to Prof. Dr. Tilmann Harder, who agreed to be the chair of my PhD examination committee.

My special thanks go to Doreen Kohlbach for sharing all the ups and downs during the years we spend together at AWI. I really enjoyed sharing office with you. Thank you for your friendship, your support and your always-open-ear.

Furthermore, I also want to thank my other office mates Ivan Dubinenkov, Tim Leefmann, and Kai-Uwe (KUL) Ludwichowski. Thank you for the time we spend together and for the pleasant atmosphere.

Many thanks to all my colleges from the Marine Chemistry group at AWI, namely Boris Koch, Gerhard Kattner, Claudia Burau, KUL, Dieter Janssen, Martin Graeve, Ivan Dubinenkov, Ruth Alheit, Valeria Adrian, Jana Geuer, Heiner Baumgarten, Tim Leefmann, Sinah Müller, Lauris Boissonnont, Mandy Kiel and Steffi Baßler. You all supported me with your helpfulness and expertise in the lab and pleasant scientific and non-scientific discussions during our coffee breaks. I am very pleased for being part of *our* group.

A big "Thank you" to Ingrid Stimac, for introducing me to ICP-MS analysis and for all your help and advice whenever I had trouble with the instrument. I also want to thank you for your support in DOS analysis during my pregnancy.

In particular, I would like to thank from my heard my family, who supported me all the years: My parents - who gave me all the Chemistry sets when I was a child, and my husband – who accompanied me through these years with unlimited support, patience and love. I would not have made it here without your help.

Table of contents

Abstract

Dissolved organic matter (DOM) is ubiquitous in natural waters and plays a central role in the biogeochemistry of riverine, estuarine and marine environments. The heteroatomic fraction of DOM consists mainly of nitrogen, phosphorous, and sulfur. While the biogeochemical cycling of C, N, and P has been intensely studied, dissolved organic sulfur (DOS) has been only marginally addressed. Nevertheless, it is an essential element for marine primary production and organic sulfur compounds play a critical role in biogeochemistry, ecology, and climate processes. The analysis of DOS quantity and distribution in marine environments as well as its chemical characterization is of urgent need to further understand the underlying processes of DOS biogeochemistry.

This study is based on more than 600 samples from different marine environments, from the surface to the deep ocean, and thus, represents the so far most comprehensive dataset of DOS in the ocean. Within this thesis, a basin-scale distribution of extractable DOS in the East Atlantic Ocean, the Atlantic sector of the Southern Ocean, and the Weddell Sea is presented. A first conservative global inventory of the marine non-volatile DOS stock was calculated using a combination of state-of-the-art approaches. The results suggest that the marine DOS inventory is by far the largest oceanic reservoir of organic sulfur (OS), exceeding the atmospheric stock and the volatile marine DOS by several orders of magnitude. Decades of research on the marine DOS cycle have focused on only ~2 % of the total OS inventory (DMSP cycle).

The marine DOS distribution and stoichiometry was compared to radiocarbon age of dissolved organic carbon (DOC), suggesting a primarily autochthonous biogenic origin and an active involvement of this DOS in the microbial loop - similar to organic nitrogen. The contribution of the sulfur-containing amino acid methionine to extractable DOS was found to be only ~2 %. Additionally, ultrahigh-resolution mass spectrometry identified a diverse suite of sulfur containing molecular formulas and their relative contribution suggested shorter residence times relative to DOC supporting the active involvement of DOS in biogeochemical cycles, ecological processes and ecosystem functions.

Rivers are also important sources of (sulfur containing) organic matter to marine environments. Here I quantified DOS and trace metals along a salinity gradient and explored the complexation of trace metals with organic matter, in particular with sulfur-containing compounds. Despite decreasing DOM concentrations along the salinity gradient due to estuarine mixing, we showed that DOS is degrading faster than DOC, underpinning the active involvement of DOS in biogeochemical cycles and ecological processes. We found indication for complexation of trace metals with (sulfur containing) organic ligands and confirmed that the stability of metal-organic complexes followed the Irving-Williams order.

The results of this thesis challenge current views of DOS dynamics and suggest that there remain major gaps in our understanding of the marine sulfur cycle, which will be of interest to ocean (biogeo-) chemists, atmospheric scientists, microbial ecologists, and ocean-/climate modelers.

Zusammenfassung

Gelöstes organisches Material (DOM) ist allgegenwärtig in natürlichen Gewässern und spielt eine zentrale Rolle in der Biogeochemie flussartiger, ästuariner und mariner Umwelten. Die heteroatomare Fraktion des DOM besteht hauptsächlich aus Stickstoff, Phosphor und Schwefel. Während die biogeochemischen Wechselwirkungen von C, N, und P bereits intensiv untersucht wurden, wurde gelöster organischer Schwefel (DOS) bisher nur wenig thematisiert. Gleichwohl ist es ein essentielles Element für die marine Primärproduktion und spielt eine maßgebliche Rolle in der Biogeochemie, Ökologie und klimatischen Prozessen. Die Quantifizierung und Analyse der Verteilung von DOS in marinen Milieus und auch dessen chemische Charakterisierung ist für das weitere Verständnis der zugrunde liegenden Prozesse der Biogeochemie von DOS zwingend notwendig.

Diese Studie basiert auf mehr als 600 Proben aus unterschiedlichen marinen Umgebungen - von der Meeresoberfläche bis zum tiefen Ozean – und repräsentiert somit den bisher umfangreichsten Datensatz über DOS im Ozean. Im Rahmen dieser Arbeit wird die Verteilung von DOS in den Ozeanbecken des Ostatlantiks, des atlantischen Sektors des Südlichen Ozeans und des Weddellmeeres vorgestellt. Eine erste, konservative Berechnung des marinen nicht-volatilen DOS Reservoirs erfolgte mittels modernster Ansätze. Die Ergebnisse legen nahe, dass der Bestand an marinem DOS das bei weitem größte ozeanische Reservoir organischen Schwefels (OS) ist und den atmosphärischen Bestand, sowie den des marinen volatilen OS, um mehrere Größenordnungen übertrifft. Jahrzehnte der Forschungen zu marinem DOS haben sich auf nur ~2 % des gesamten OS Bestandes fokussiert (DMSP Zyklus).

Die Verteilung und Stöchiometrie des marinen DOS wurde mit dem Radiocarbonalter von gelöstem organischem Kohlenstoff (DOC) verglichen. Die Ergebnisse legen einen primären autochthonen biogenen Ursprung und aktive Beteiligung des DOS in der mikrobiellen Schleife nahe – ähnlich wie es bei organischem Stickstoff der Fall ist. Der Anteil der schwefelhaltigen Aminosäure Methionin an extrahierbarem DOS betrug nur ~2 %. Außerdem wurden mit Hilfe ultrahochauflösender Massenspektrometrie diverse schwefelorganische Verbindungen mit verkürzten Residenzzeiten relativ zu gelöstem organischen Kohlenstoff identifiziert, was eine aktive Einbindung von DOS in biogeochemische Kreisläufe, ökologische Prozesse und Funktionen des Ökosystems nahelegt.

Für die marine Umwelt sind Flüsse wichtige Quellen (schwefelhaltigen) organischen Materials. In dieser Studie wurden DOM und Spurenmetalle entlang eines Salzgehaltsgradienten analysiert und die Komplexbildung von Spurenmetallen mit organischem Material, insbesondere mit schwefelhaltigen Verbindungen, untersucht. Trotz abnehmender DOM Konzentrationen entlang des Salzgehaltsgradienten aufgrund ästuariner Mischungsprozesse, haben wir gezeigt, dass DOS schneller

abgereichert wird als DOC. Dies untermauert die aktive Einbindung von DOS in biogeochemischen Kreisläufen und ökologischen Prozessen. Wir fanden Anzeichen für die Komplexbildung von Spurenelementen mit (schwefelhaltigen) organischen Liganden und konnten bestätigen, dass die Stabilität metall-organischer Komplexe der Irving-Williams-Reihe folgt.

Die Ergebnisse dieser Arbeit hinterfragen die aktuelle Auffassung von DOS Dynamiken und zeigen auf, dass noch große Lücken in unserem Verständnis des marinen Schwefelkreislaufs existieren, welche von Interesse für Meeres(biogeo)chemiker, Atmosphärenforscher, mikrobielle Ökologen und Ozean-/ Klimamodellierer sein werden.

Abbreviation list

Chemical components

CDOM	Colored/chromophoric dissolved organic matter
OCS	Carbonyl sulfide
DMS	Dimethyl sulfide
DMSO	Dimethyl sulfoxide
DMSP	Dimethylsulfoniopropionate
DOC/N/P/S	Dissolved organic carbon / -nitrogen / -phosphorus / -sulfur
DOM	Dissolved organic matter
Metal-DOM_{SPE}	Trace metal in solid-phase extracted sample
MSA	Methanesulfonic acid
OPA	Ortho-phthalaldehyde
OS	Organic sulfur
POS	Particulate organic sulfur
TOC/N	Total organic carbon / -nitrogen
VOSCs	Volatile organic sulfur compounds

Methods and methodological terms

AOU	Apparent oxygen utilization
CTD	Conductivity temperature depth
EE	Extraction efficiency
FT-ICR-MS	Fourier transform ion cyclotron resonance mass spectrometry
HPLC	High-performance liquid chromatography
IC	Ion chromatography
ICP-MS	Inductively coupled plasma mass spectrometry
LOD	Limit of detection
MS	Mass spectrometry
MW	Molecular weight
SPE	Solid phase extraction
XANES	X-ray absorption near edge structure

Oceans and Water masses

AASW	Antarctic Surface Water

EA	East Atlantic Ocean
ESW	East Shelf Water
ISW	Ice Shelf Water
MWDW	Modified Warm Deep Water
SO	Southern Ocean
WDW	Warm deep water
WSBW	Weddell Sea Bottom Water
WSDW	Weddell Sea Deep Water
WW	Winter Water

Preface

This project was part of the larger MARUM GB2 initiative „Biogeochemical processes fueling sub-seafloor life: transformations of C, S, and Fe“. The thesis was prepared in the Marine Chemistry group of the Alfred-Wegener Institute in Bremerhaven.

The overall research focus within this thesis was on the quantification of dissolved organic sulfur (DOS) in marine environments and the investigation of its biogeochemical role. The introductory chapter gives a general overview about dissolved organic matter (DOM): its definition, classification, sources, sinks, and biogeochemical role in aquatic systems. The second part of the introduction focusses on DOS: its sources and sinks, biogeochemistry, and interactions with adjoined environments, such as sediment and atmosphere. The second chapter deals with the challenges in the analysis of DOS. The analytical methods applied in this study are presented. An overview about the major research questions is given in Chapter III. Reprints of the cumulative manuscripts are provided in Chapter IV. Chapter V summarizes this study and chapter VI gives an overview about future research perspectives.

I. Introduction

I.1 Definition and classification of DOM

Organic matter in aquatic systems exists in dissolved and suspended/particulate form. The dissolved fraction of organic matter is operationally defined as the fraction of organic matter that passes through a filter, usually with 0.2 - 0.7 μm pore size. However, the size distribution of organic matter is a smooth transition between truly dissolved organic matter (DOM), colloidal (molecular size of 0.001 – 1 μm (Guo and Santschi, 1997)) and particulate organic matter (POM) (Fig. 1).

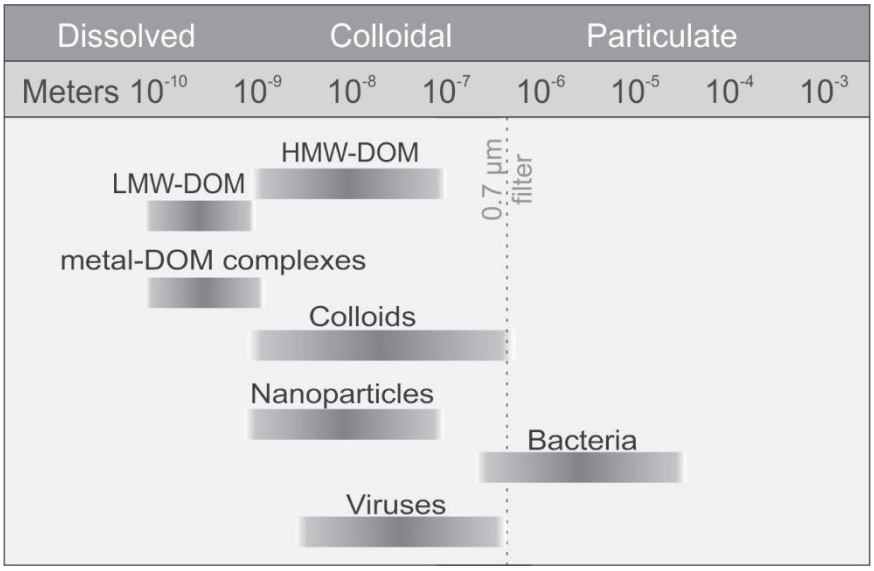

Figure 1. Size ranges of different organic matter classes. The cutoff for the filter pore size used in this study (0.7 μm) is marked. Adapted with permission from (Aiken et al., 2011). Copyright 2011 American Chemical Society.

DOM not only consists of dissolved organic carbon (DOC) but is a complex mixture of organic compounds. It is approximated that DOC contributes about half of the dry weight of DOM (Krogh, 1934). Other major DOM constituents are oxygen, hydrogen, nitrogen (DON), phosphorous (DOP) and sulfur (DOS). The high complexity of DOM makes it difficult to fully characterize its structure and composition. Depending on the source of DOM, a maximum of only ~20 % of DOM can be assigned to specific compound classes, such as carbohydrates (~10 % contribution to the average DOM composition in riverine water), amino acids (~4 %), fulvic acids (~39 %) and others (Hedges et al., 2000; Thurman, 1985). Therefore, a classification of DOM is often based on environmental and/or operational parameters, which will be presented in the following.

Classification of DOM according to the environmental compartment. This classification is either based on the sampling location or – more precise - on the origin of DOM (e.g. terrestrial, marine, atmospheric, or sedimentary DOM). DOM derived from terrestrial sources contains e.g. higher amounts of lignin phenols than DOM from marine or atmospheric sources, turning lignin into an important tracer for terrestrial DOM (Hedges and Mann, 1979). Thus, different pools of the global carbon cycle can be defined.

Classification of DOM according to its source. Allochthonous sources of DOM to the ocean are: input of terrestrial DOM via rivers, precipitation of organic matter from the atmosphere (90 Tg C a^{-1} (Willey et al., 2000)), and input of DOM via seafloor hydrocarbon seeps and submarine groundwater discharge (amount unknown). Allochthonous DOM consists mainly of high molecular weight humic substances, which have a non-labile character (Thurman, 1985; Toming et al., 2013). Autochthonous DOM in contrast, is produced by phytoplankton and other photosynthetic organisms. It consists of more labile compounds (e.g., monomeric sugars, carboxylic acids, and amino acids) and can be easily degraded by microorganisms (Bertilsson and Jones Jr, 2003; Thurman, 1985; Toming et al., 2013).

Classification of DOM according to its molecular weight. High molecular weight (HMW, < 10 kDa and > 3 kDa) and low molecular weight (LMW, < 1 kDa) fractions in DOM samples (Fig. 1) can be separated using ultrafiltration techniques (Benner et al., 1992; Kaiser and Benner, 2009). LMW-DOM accounts for 65 – 80 % of the marine bulk DOC and is thus the major size fraction throughout the water column (Ogawa and Tanoue, 2003). The HMW fraction is relatively reactive and is degraded preferentially by microbial activity. Its proportion decreases with depth, thus the majority of DOM in the deep ocean consists of LMW-DOM (Ogawa and Tanoue, 2003). In rivers in contrast, high molecular weight compounds dominate DOM.

Classification of DOM according to reactivity. This classification is based on DOM turnover rates. Labile DOM is characterized by turnover rates of hours to days. It consists of highly reactive compounds and can be primarily found in surface waters/the eutrophic zone, where it is produced by phytoplankton. Non-labile DOM has very long turnover rates, which is reflected in the high lifetime of the non-labile DOM fraction of ~16000 years (Hansell, 2013). This fraction is almost resistant to microbial degradation and can thus accumulate in the ocean. Usually this non-labile fraction is further separated into semi-labile and semi-refractory DOM (Hansell, 2013). Although it is certainly intuitive and useful to define discrete organic matter fractions such as labile, semi-labile, or refractory organic matter, it is also important to consider that DOM degradation is likely to be determined by a continuum of reactivities of the contributing compounds rather than discrete degradation stages (Flerus et al., 2012). Thus, in this thesis the classification according to DOM reactivity only distinguishes the

truly labile and non-labile fraction. Additionally, lifetimes of DOC and other DOM compounds can be calculated to compare reactivities of different DOM fractions/compound classes.

The analysis of DOM according to bulk elemental ratios/composition can serve as a basis to assess these classification approaches. The elemental ratio, e.g. ratio of DOC and DON (C/N ratio) in a sample varies significantly between different environments and thus allows understanding DOM origin and processing. According to the Redfield ratio of C:N:P = 106:16:1, which reflects the stoichiometry of C, N, and P in phytoplankton, the C/N ratio in marine phytoplankton is ~7 (Redfield et al., 1963). Marine DOM has a C/N ratio of ~10 – 20 and terrestrial DOM is characterized by C/N ratios of ~30 – 60. It was found that HMW-DOM in marine waters consists of mainly carbon-rich compounds, such as carbohydrates, resulting in higher C/N ratios of ~13 – 20 (Aluwihare et al., 1997; Benner et al., 1992; Ogawa and Tanoue, 2003). Nitrogen-rich compounds, such as amino acids and proteins are degraded preferentially. This leads to higher C/N ratios in "older" non-labile marine DOM compared to truly labile DOM.

DOM concentrations in aquatic environments are usually represented as DOC concentrations and are highly variable throughout different aquatic environments. The lowest concentrations of ~50 µmol L^{-1} can be found in marine waters, whereas the highest DOC concentrations can be found in soils and peat water (Fig. 2A). DOC concentrations additionally vary with depth and typical marine depth profiles are characterized by higher concentrations of (more labile) DOC in the surface ocean and decreasing DOC concentrations with depth (Fig. 2B).

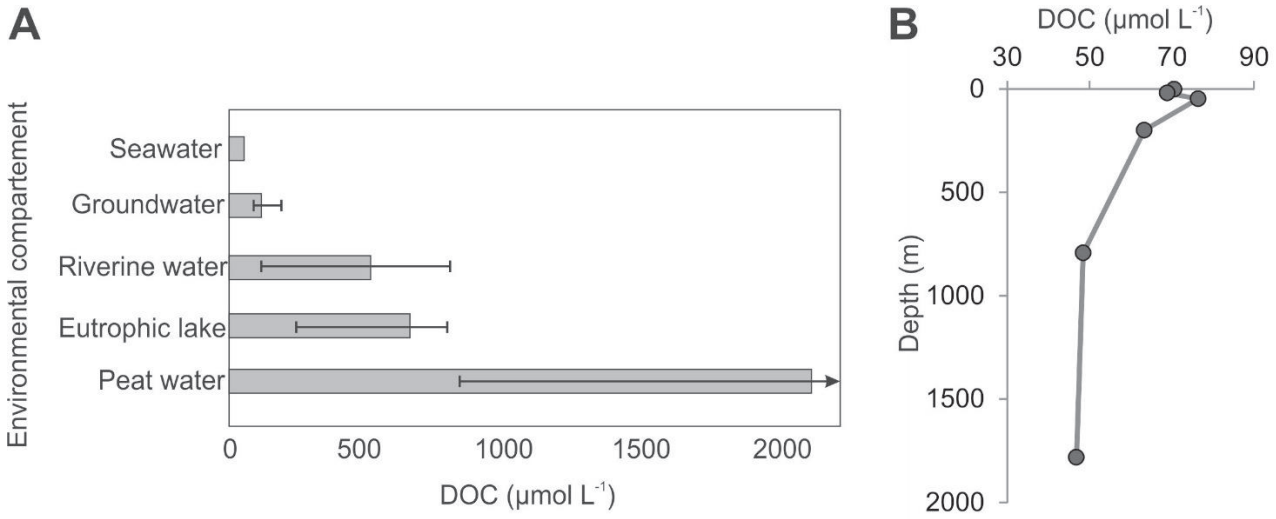

Figure 2. Extend of DOC concentrations. (A) Typical DOC concentrations in different aquatic environments (Modified from (Thurman, 1985)) and (B) typical DOC depth profile from a station in the East Atlantic Ocean (Station 056 of cruise ANT XXV/1: 17° 44.17' S, 23° 07.53'E).

I.2 Sources, sinks and biogeochemical role of marine DOM

As mentioned in Chapter I.1, the sources of DOM in the ocean can be classified into allochthonous and autochthonous sources. Although rivers transport about 0.2 Pg DOC a^{-1} from land to the oceans (Eglinton and Repeta, 2006), terrestrial (allochthonous) DOM contributes to only ~1 – 2 % of the oceanic DOM content (Opsahl and Benner, 1997). Autochthonous primary production plays a minor role in riverine systems. In marine systems in contrast, the major part of DOM is produced via primary production from marine phytoplankton in the surface ocean (euphotic zone). Most of the DOM produced belongs to the labile DOM pool, which is immediately removed via different processes grouped in (i) biotic processes, such as consumption by heterotrophic microbes, or (ii) abiotic processes, such as photochemical processes (Mopper et al., 1991; Moran and Zepp, 1997) or sorption onto sinking particles followed by deposition in sediments (Armstrong et al., 2001). However, there is a significant remaining fraction (>95 %), which is transformed to become refractory and resistant to microbial breakdown. This non-labile DOM pool accumulates, persists in the ocean and interacts with several biogeochemical cycles.

Comparison of different organic matter pools shows that the total amount of ~662 Pg DOC (Hansell et al., 2009) in marine DOM represents one of the largest organic carbon reservoirs on earth (Table 1). The ubiquity of DOM in natural waters and the enormous size of global DOM pools are of great potential to influence biogeochemical cycles. Thus, already small changes can influence the global carbon cycle, CO_2 balance (the annual oceanic net uptake of CO_2 is ~1.9 Pg C^{-1} (Sarmiento and Gruber, 2006)), and its storage in the ocean. Additionally, it can affect other biogeochemical processes, such as trace metal and radionuclide cycling (Santschi et al., 1997), microbial growth (Crump et al., 2003) and the biological carbon pump (Jiao et al., 2010). Thus, the significance of the marine DOM pool is not only caused by its size. It interconnects the atmospheric CO_2 pool with the sedimentary organic matter pool. For instance, it was found that the sequestration of reduced sulfur in sediments affects the carbon and sulfur cycles in a way, that it has also influence on the development of atmospheric CO_2 concentrations over geologic time (Werne et al., 2004).

Table 1. Global inventory of different organic carbon reservoirs on earth

Carbon reservoir	Amount of carbon	Reference
Marine DOC	~662 Pg C	(Hansell et al., 2009)
Atmospheric CO_2	~870 Pg C	National Oceanic and Atmospheric Administration (NOAA) https://www.esrl.noaa.gov/gmd/ccgg/trends/ Status: 11.06.2019
C in living biomass	600 – 1000 Pg C	(Falkowski et al., 2000)
C stored in arctic permafrost	~1600 Pg C	(Tarnocai et al., 2009)
C in marine sediments	$3.7*10^5$ Pg C	(Lipp et al., 2008)

I.3 Heteroatoms in DOM

The determination of the chemical composition of DOM is a prerequisite to further understand its origin and fate and to improve our knowledge on its role in different aquatic environments. DON and DOP are part of several important compound classes for living organisms, such as amino acids, peptides and proteins, vitamins, nucleic acids, phosphonates, and phospholipids. Due to their contribution to numerous biomolecules, N- and P-containing compounds are typically remineralized faster than other organic compounds (Kaiser and Benner, 2009). The Redfield ratio shows that the DON pool is smaller than the DOC pool, whereas the DOP pool is even less abundant (Lechtenfeld, 2012; Redfield et al., 1963). While surface concentrations of marine DOC range between 40 – 80 μmol C L^{-1} (Hansell et al., 2009), concentrations of marine DON and DOP are only 0.3 – 7 μmol N L^{-1} and ~0.1 – 0.3 μmol P L^{-1}, respectively (Sipler and Bronk, 2015).

Sulfur is a reactive element, present in stable valence states from -2 to +6 and can thus participate in various biogeochemical reactions. It is also incorporated in several organic compounds, such as amino acids, proteins, vitamins, sulfolipids, sulfated polysaccharides and coenzymes and is thus essential to living organisms. The high stability of some of these sulfur compounds results from strong covalent disulfur bonds. Examples of important DOS compound classes/functional groups are given in Table 2. Pohlabeln and Dittmar (2015) performed different alteration experiments with model compounds and marine DOM samples to detect specific functional DOS groups. They concluded that only persistent DOS compounds, such as sulfonic acids, thiophenes and sulfones occur in marine DOS. Other compounds, such as thiols, thioesters, sulfonic acid esters and others were not found to be part of marine DOM. Steric hindrance, however, was excluded *a priori* and a discrimination of small polar compounds (such as thiols) by SPE was assumed. Other studies indeed identified thiols and alkylsulfonates in marine DOM (Al-Farawati and Van Den Berg, 2001; Lechtenfeld et al., 2013). As

part of this thesis, also the amino acid methionine (a thioether) was quantified in marine DOS samples (Chapter IV.1).

The contribution of heteroatoms influences the chemical properties of DOM. For instance, heteroatoms are known to play an important role for interactions of DOM with trace metals (Ravichandran, 2004; Smith et al., 2002). However, in contrast to DOC, DON, and DOP, which were intensively studied in the recent past, our knowledge on quantity, distribution and biogeochemical role of DOS is very limited.

Table 2. Chemical sulfur containing compound classes.

Class	Functional group*	Example
Thiol	R-SH (-II)	Cysteine
Sulfide / Disulfide / Polysulfide	R-S-R' (-II) / R-S-S-R' (-I) / R-$(S)_{n<2}$-R' (-I)	Methionine / Diphenyl disulfide / Varacin
Thioester	R-S-C(O)-R' (-II)	Acetyl Coenzyme A
Sulfoxide	R-S(O)-R' (0)	DMSO
Sulfone	R-$S(O)_2$-R' (+II)	Methylsulfonylmethane (MSM)
Sulfonic acid and its derivatives	R-$S(=O)_2$-OH (+IV)	Taurine
Sulfonamide	R-$SO_2NR'_2$ (+IV)	
Thiazol	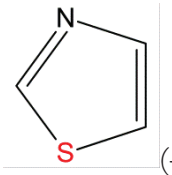 (-II)	Thiamine (Vitamin)

* R and R' are any organic groups. Roman numerals in brackets are referring to the oxidation states of sulfur.

I.4 The marine sulfur cycle and biogeochemical interactions of DOS with adjoining environments

Several organic sulfur (OS) compounds are known to exist in the ocean and other aquatic environments and some of them are known to be actively involved in important climate processes (see "Ocean-atmosphere interactions of volatile DOS") and other biogeochemical processes, such as the complexation of trace metals (e.g. see "DOS as ligand for trace metal complexation"). This chapter aims to provide an overview about the sources, sinks and biogeochemical role of DOS in the ocean and adjoining environments.

The marine sulfur cycle

The marine sulfur cycle is driven by microbial metabolic reactions which reduce sulfate to sulfide (Bentley and Chasteen, 2004). Sulfate is abundant in the marine environment (29 mmol L^{-1} or $38*10^6$ Tmol S total inventory). Organic sulfur containing compounds are produced in ocean surface water by phytoplankton (Yoch, 2002). The assimilation of dissolved sulfate results in an average molar elemental ratio of $C_{124}H_{16}O_1S_{1.3}$ in marine phytoplankton biomass grown under non-limiting conditions (Ho et al., 2003). Based on this C/S ratio of ~95, the global net primary production in the ocean of 48.5 Pg C yr^{-1}

(or 4.2 Pmol C yr^{-1}) (Field et al., 1998) requires an annual net sulfur assimilation of 1.36 Pg S yr^{-1} (or 0.042 Pmol S yr^{-1}). Organic sulfur in phytoplankton biomass (e.g in the green alga *Chlorella*) is primarily bound in two proteinogenic amino acids - methionine (~58 %) and cysteine (~38 %) (Andreae, 1990; Giovanelli et al., 1980), whereas sulfate is only a minor constituent (< 1 % in *Chlorella*) (Giovanelli, 1987). Dissolution of these particulate OS compounds (POS) arises from e.g. grazing, exudation, viral lysis and cell mortality.

Additionally to the biotic DOS production, abiotic transformations to organic sulfur compounds can occur. Such abiotic processes can be (indirect) photochemical transformation (Mopper et al., 2015) or abiotic sulfurization (incorporation of inorganic sulfur compounds to organic matter) (Gomez-Saez et al., 2016). Abiotic processes mostly produce organic sulfur compounds, which are resistant to degradation processes (non-labile) and can accumulate in the ocean.

Labile DOS compounds, such as amino acids and dimethylsulfoniopropionate (DMSP), which represents an important energy source for heterotrophs (Vila-Costa et al., 2006), are rapidly cycled within the ocean. The major sinks for (labile) organic sulfur compounds are remineralization to sulfate, incorporation into microbial biomass, export to the atmosphere, and transformation to the large pool of marine non-labile DOM.

Mixing of water masses with different DOS concentrations is also an important process influencing the distribution of DOS (and DOM in general). Due to the low reactivity (non-lability) of DOC in the deep ocean, DOC is assumed to behave conservative. Thus, changes in the DOC distribution are mainly a result of mixing of different water masses, rather than biogeochemical processes. However, it is unclear, whether DOS behaves in a same way. In this study, DOC and DOS were studied in the East Atlantic Ocean and the Weddell Sea –areas that are characterized by mixing of several different water masses (Chapter IV.1 and IV.4). In another section of this thesis (Chapter IV.3.), the concentration gradients as well as changes in stoichiometry of DOC, DOS and trace metals were studied in the Elbe-Weser estuary, where mixing of riverine freshwater and marine water occurs.

The current state of knowledge on the global sulfur cycle is summarized in the first manuscript (Chapter IV.1, Fig. M1.3). Some DOS compounds, such as the climate relevant volatile DOS compound dimethyl sulfide (DMS), are well studied with regard to their concentration, distribution and flux rate to the atmosphere. However, until now, it is unknown to which extent these compounds contribute to the total DOS pool, respectively, how large the unknown and uncharacterized fraction of DOS is.

DOS as ligand for trace metal complexation

Trace metals are known to have an important biological role, e.g. as structural elements in proteins or as cofactors in enzymes (Morel and Price, 2003) and some trace elements (e.g. Cu and Co) are essential for phytoplankton growth (Sunda, 2012). Thus, depth profiles of trace metals involved in

biological processes show a depletion in pelagic surface waters, similar to nutrient depth profiles (Wu et al., 2001). Although many trace metals are important for biological processes, they can also cause toxic effects if they are present in high concentrations (Paytan et al., 2009). It was found that a considerable fraction of trace metals in the ocean is complexed by organic ligands (Laglera and van den Berg, 2003; Vraspir and Butler, 2009). This complexation increases the retention time of trace metals in seawater. It is indicated, that the uptake of organically bound trace metals requires more energy and thus, free trace metal ions can be acquired faster by organisms (Shaked and Lis, 2012).

DOS and other sulfur-containing compounds, such as phytochelatins, sulfur-rich proteins, and other thiols (-SH) can contribute as organic ligands to form organic metal complexes (Bell and Kramer, 1999; Laglera and van den Berg, 2003; Smith et al., 2002). Microorganisms for instance, can release thiols e.g. in response to oxidative or toxic metal stress (Payne and Price, 1999). Thiols, in turn, can build complexes with toxic metals and can thus reduce their bioavailability and toxicity (De Schamphelaere et al., 2004; Schwartz et al., 2004). Thiols are present at very low concentrations in seawater (< 10 nmol L^{-1}) (Dupont et al., 2006; Tang et al., 2000). Nevertheless, according to the "Hard-Soft-Acids-Bases" (HSAB) theory, soft B-type metals (e.g. Ag, Au, Cd, Cu, Hg, Pb, Pd, and Pt) prefer S and/or N binding sites over O binding sites (Chuang et al., 2015).

The complexation of organic ligands with trace metals can affect, both, the biogeochemistry of DOM and trace metals:

- Metal complexation may provide a protective effect against oxidation of reduced-sulfur groups in DOM (Hsu-Kim, 2007).
- It can influence speciation and mobility (transport and distribution) and thus, bioavailability and toxicity of trace metals in the ocean (Ravichandran, 2004). This indirectly also influences bioproductivity, species composition and – in the long term – food web dynamics.

In surface waters, photochemistry plays an important role effecting DOM and trace metal speciation. Photochemical decomposition can decrease the concentration of organic ligands and thus, the complexation of trace metals (Moffett et al., 1990), resulting in increased bioavailability of free trace metal ions. In reverse, the impact of trace metals on the photochemical reactivity of DOM is widely unknown (Mopper et al., 2015).

It is known, that the binding ability of DOM with Hg(II) is significantly affected by salinity (Wufuer et al., 2014). But the response of other (e.g. sulfur containing) organic metal complexes on salinity remains still unclear. Thus, a better understanding of the environmental factors that control organic metal characteristics is required. This topic is further addressed in Chapter IV.3: "Stoichiometry, polarity, and organometallics in solid-phase extracted dissolved organic matter of the Elbe-Weser estuary".

Ocean-atmosphere interactions of volatile DOS

The knowledge of the contribution of some organic sulfur compounds (but also anthropogenic sulfur gases emitted from fossil fuel burning, e.g. SO_2) to climate processes, such as cloud condensation, global warming, and acid precipitation resulted in numerous studies addressing those volatile organic sulfur compounds (VOSCs) with focus on the DMSP cycle (Andreae, 1990; Charlson et al., 1987; Kiene and Linn, 2000).

DMSP is the precursor of all VOSCs produced in the ocean (Fig. 3). It is an important sulfur-containing compound and is produced in large amounts (~2 Pg a^{-1}) by marine phytoplankton (Moran et al., 2012). DMSP can be degraded enzymatically to DMS (Kiene and Linn, 2000). DMS in turn is the predominant VOSC in ocean waters and can diffuse to the atmosphere. Its concentration is high in the ocean surface and decreases with increasing depth, similar to DMSP and DOC. Although most DMS on earth originates from marine sources (Yoch, 2002), only a small fraction of DMSP in the ocean (1-2 %) is converted into DMS (Bates et al., 1994; Kwint and Kramer, 1996). The major fraction of DMSP is cycled within the ocean (Kiene and Linn, 2000). In a recent study, the DMSP cycle was extended due to the discovery of dimethylsulfoxonium propionate (DMSOP), which is produced from DMSP and metabolized to dimethylsulfoxide (DMSO) (Thume et al., 2018). DMS, which is not emitted to the atmosphere, can also be oxidized to DMSO (Lee et al., 1999). In the atmosphere, DMS is a major precursor of sulfate aerosols, forming cloud condensation nuclei (Vogt and Liss, 2013). It can be oxidized to methanesulfonic acid (MSA), an intermediate product during the photochemical oxidation of DMS to sulfate aerosols (Jasinska et al., 2012; Quinn and Bates, 2011).

Other climate relevant sulfur gases in the atmosphere are carbonyl sulfide (OCS) and carbon disulfide (CS_2). OCS is a volatile component derived from UV-dependent photo–production of DOS (Ferek and Andreae, 1984). It is the most abundant sulfur gas in the atmosphere (Liss et al., 2014) and affects the planetary radiation budget by maintaining the stratospheric sulfate aerosol layer (Cutter et al., 2004). In the ocean, OCS can be hydrolyzed to hydrogen sulfide (Cutter et al., 2004), which is known to be an important metal chelator. CS_2 is the most important precursor for OCS (and SO_2) in the atmosphere. It is produced photochemically from chromophoric DOM (CDOM), like OCS, but is also produced biologically by marine algae (Xie and Moore, 1999). Oceanic emissions are a major source of these gases and account for 20 - 35 % and 40 % of the total atmospheric CS_2 and OCS budgets respectively (Liss et al., 2014). Nevertheless, these estimates are associated with high uncertainties of ~50 % (Kremser et al., 2016; Whelan et al., 2018) and several studies revealed a missing source of atmospheric OCS, which was attributed to the ocean (Berry et al., 2013; Glatthor et al., 2015; Kuai et al., 2015; Launois et al., 2015). A recent study, however, found that oceanic emissions are too low to fully account for the missing source to the atmospheric budget (Lennartz et al., 2017). To reduce the uncertainties in the estimates of oceanic OCS emissions, a better understanding of the underlying processes is needed. In Chapter IV.5 (a study for which I performed DOS_{SPE} analysis), the drivers of

marine OCS and CS_2 production – including the potentially limiting factor of DOS availability - are discussed.

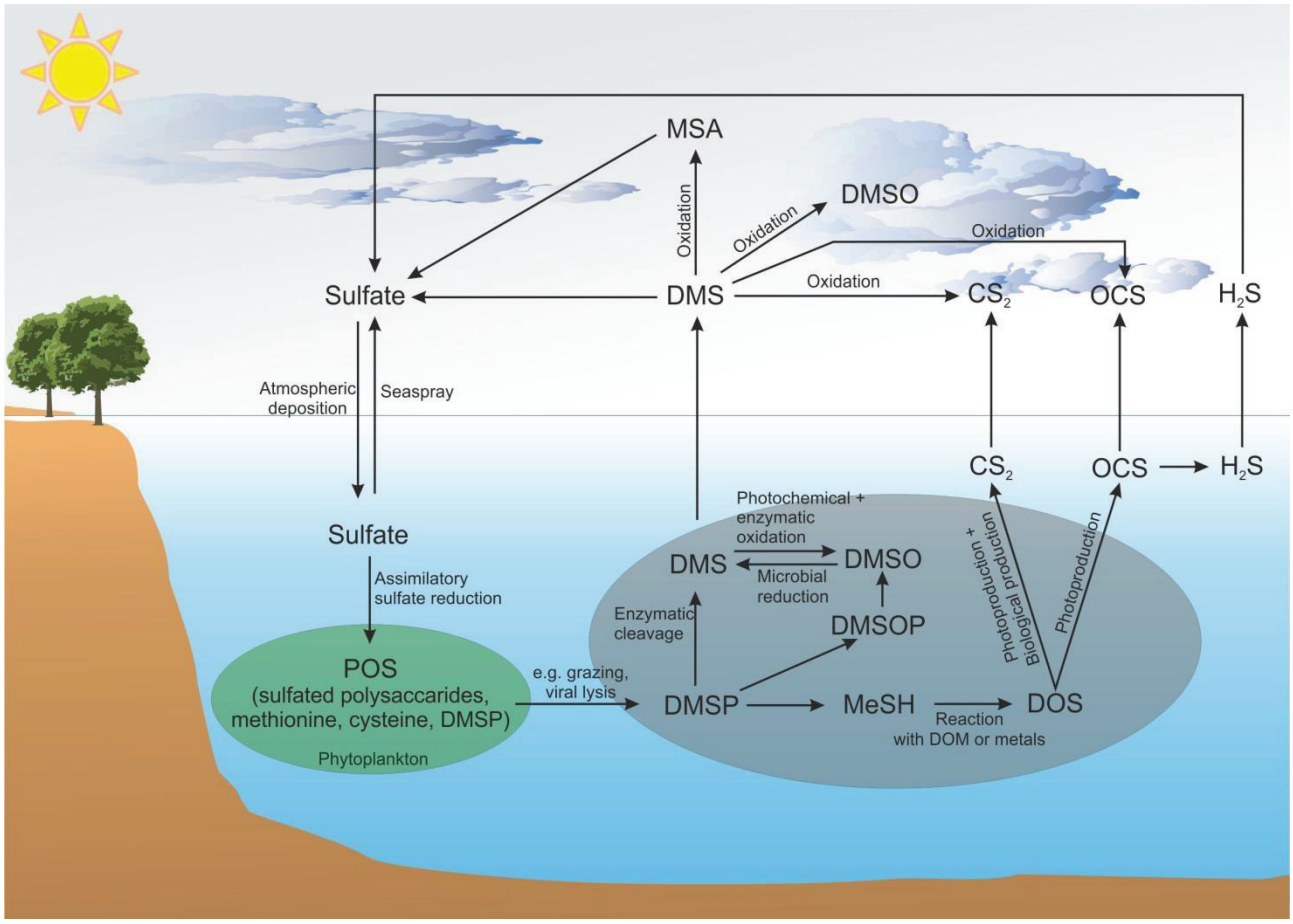

Figure 3. Sulfur cycle at the ocean-atmosphere interface. Schematic overview about the major DOS production and reaction pathways in the ocean and ocean-atmosphere interactions of sulfur compounds. The particulate organic sulfur (POS) pool produced by phytoplankton is indicated by the green ellipse. The pool of DOS compounds is represented by the grey ellipse. See the text of this chapter for corresponding explanations and references.

DOS at the sediment-water interface

Sedimentary processes are the major sinks removing sulfate from the ocean (Fig. 4) (Jørgensen and Kasten, 2006). Globally, ~11 Tmol sulfate are reduced in marine sediments every year (Bowles et al., 2014). One pathway results in the formation of sulfide minerals, particularly pyrite. Another pathway forms organic sulfur, which represents the second largest reduced sulfur pool in sediments besides pyrite, accounting for 35 – 80 % of the reduced sulfur pool (Brüchert and Pratt, 1996; Passier et al., 1999; Wasmund et al., 2017). Reaction pathways are similar for the DOS and particulate organic sulfur (POS) pool (and are therefore described for OS in general). Both pools are closely connected by dynamic processes, such as dissolution of POS to DOS and flocculation of DOS, producing POS. The majority of OS compounds in sediments is formed via abiotic sulfurization. This pathway includes the

dissimilatory reduction of sulfate to H_2S (from which microorganisms converse energy), followed by the reaction with organic molecules forming organically bound sulfur. In competition with the formation of OS is the reaction of H_2S to pyrite: The reaction of reactive iron species with reduced sulfur (e.g. H_2S) to pyrite formation is believed to be faster than the reaction organic matter with reduced sulfur (Vairavamurthy et al., 1995a). Thus, the formation of OS is favored by OM abundance, active microbial sulfate reduction, and limited reactive iron amounts (Vairavamurthy et al., 1995a).

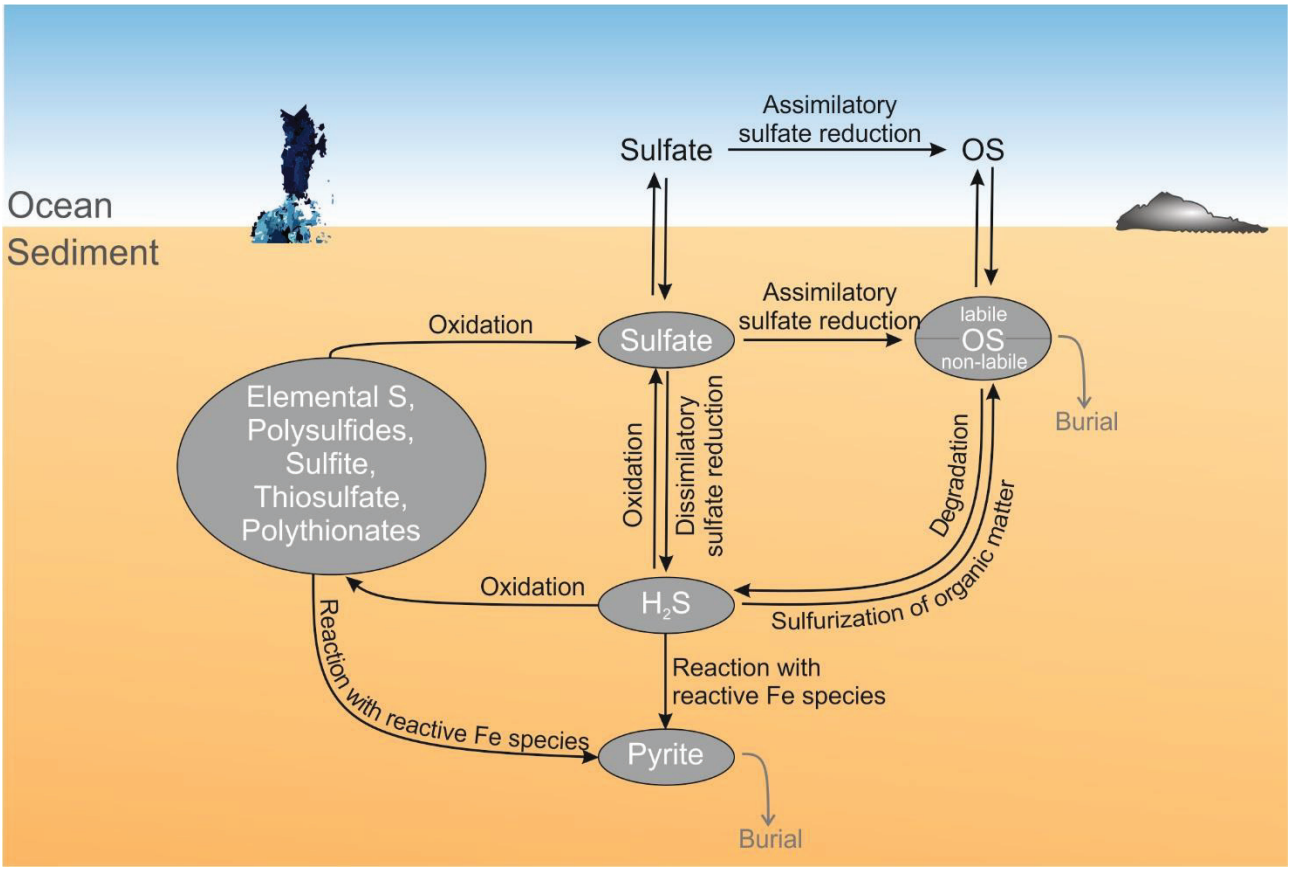

Figure 4. Biogeochemical sedimentary sulfur cycle during diagenesis. The major pathways of sulfate reduction are shown: (i) Dissimilatory sulfate reduction and further reaction of reduced sulfur species (e.g. H_2S) with (a) iron minerals resulting in the formation of pyrite and/or (b) organic matter (OM) leading to formation of organically-bound sulfur in sediments; (ii) assimilatory sulfate reduction resulting in the formation of biogenic organic (labile) sulfur compounds.

The abiotic incorporation of reactive sulfur species into pyrite and OS in near-surface sediments is one of the major geochemical sulfur transformation pathways during early diagenesis (Schmidt et al., 2009; Vairavamurthy et al., 1995a) and leads to the formation of non-labile OS compounds. It affects the preservation of organic matter by protecting it from microbial alteration or remineralization, whereupon the structural information of organic matter (e.g. reactive biomarkers) is preserved (Anderson and Pratt, 1995; Burdige, 2007; Kohnen et al., 1992). Evidence for this OS production was also found in marine hydrothermal systems (Gomez-Saez et al., 2016) and it is speculated, that this process might also contribute to the stabilization of DOM in the ocean water column (Dittmar, 2015).

In contrast, assimilatory sulfate reduction results in biosynthesized organic sulfur. This primarily leads to the formation of labile mainly proteinaceous sulfur compounds, which are most likely respired during diagenesis (Vairavamurthy et al., 1995b). Estimates from sulfur isotope mass balance analysis revealed that this biogenic OS represents ~10 – 25 % of the total sedimentary OS (Anderson and Pratt, 1995; Wakeham et al., 1997; Werne et al., 2003).

The flux of non-labile DOS from abiotic sulfurization processes in sulfidic sediments into the ocean was estimated from sulfurization experiments to be 30 - 200 Tg S a^{-1} (Pohlabeln et al., 2017). Nevertheless, aerobic degradation of labile, biosynthesized DOS (e.g. essential amino acids, proteins) plays an important role for sedimentary communities. Depending on the chemical composition of OM, aerobic degradation can be ~10 times faster than anaerobic degradation (Kristensen et al., 1995).

II. Challenges in the chemical characterization of DOS: Methodological approaches

Very low concentrations of DOM and its high complexity and heterogeneity are the major challenges for the chemical analysis of DOM. Although studies on DOM include thousands of analyses, there is no general analytical procedure which all studies have in common. The choice of pre-treatment conditions, sample preparation and analytical methods strongly depends on the aim and research question of the different studies.

Bulk DOM parameters such as DOC, total dissolved nitrogen (TDN) and dissolved inorganic nitrogen (DIN) concentrations can already be determined from (filtered) original water samples. However, most analytical techniques require desalting and enrichment of DOM samples for further chemical analysis. In the following, an overview about the methods of pre-treatment and the analytical techniques used in this thesis is given (see also Fig. 5).

II.1 Sample preparation

The first step of sample preparation is the filtration of water samples. Fortunately, although filters with different pore sizes are used throughout DOM studies (0.2, 0.45, 0.7 μM), it was found that this does not influence the molecular composition of DOM and that comparability between the studies is given (Denis et al., 2017). In this study (and several others), glass microfiber filters (GF/F) with a pore size of 0.7 μm were used. Those filters can easily be cleaned by pre-combustion and are used for highly sensitive chemical studies. Nevertheless, some bacteria and viruses are smaller than 0.7 μm and might pass the filter and thus contribute to the "DOM".

Sulfate concentrations in marine environments of ~29 mmol S L^{-1} can exceed the concentration of DOS by up to five orders of magnitudes. Thus, the analysis of DOM and especially DOS in marine systems is hampered, due to the high background concentrations of sea salt. Since most analytical techniques require desalting and enrichment of DOM samples, different pre-treatment methods were developed and can be used to remove sulfate/salt from the samples. However, none of them is able to recover 100 % of DOM from the samples.

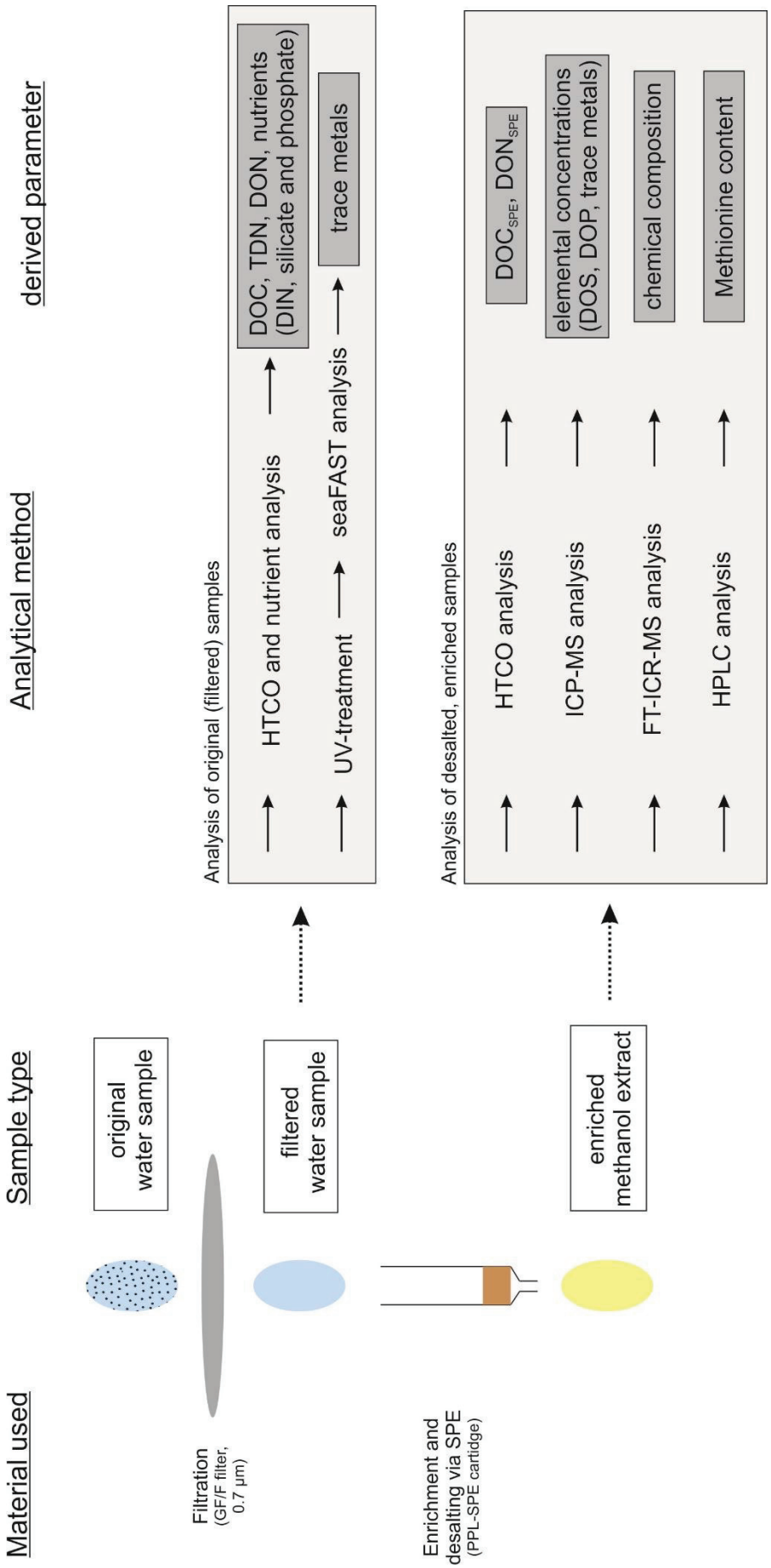

Figure 5. Sample processing scheme.

Solid-phase extraction

Solid-phase extraction (SPE) has been applied for desalting and enrichment of all DOM samples in this study. It is based on retention/sorption of DOM onto a solid sorbent. Due to the lower polarity of DOM relative to sea salt (Repeta, 2015), it is possible to separate DOM from the salt. In this study, the polystyrene based PPL sorbent was used. This sorbent is suitable to extract a broad range of highly polar to non-polar DOM components, whereas e.g. the C18 sorbent used in other studies shows a higher affinity to non-polar/hydrophilic compounds. DOM was extracted according to Dittmar et al. (2008) (Fig. 6): First, the absorber is rinsed with methanol to remove possible contaminations (Step 1 in Fig. 6A). Afterwards, the absorber is rinsed with ultrapure water (acidified to pH 2) to adjust the absorber material to the same milieu/pH as the sample. In the next step, the filtered and acidified water sample (pH 2) is passed through the cartridge. The solid-phase extractable DOM (DOM_{SPE}) interacts with the absorber material and remains on the cartridge, whereas inorganic compounds (such as sea salt) pass the cartridge to be discarded. To entirely remove the salt from the sample, the cartridge is rinsed with ultrapure (pH 2). The sorbent is dried with nitrogen gas (or clean air) to remove any remains of water. In the end, methanol (or another organic solvent) is used to elute DOM_{SPE} from the absorber.

The extraction efficiency (EE) gives the percentage of original DOC that can be extracted using SPE:

$$EE_{DOC} = \frac{[DOC_{SPE}]*100}{[DOC]} \quad (1)$$

where $[DOC_{SPE}]$ is the molar concentration of solid-phase extractable DOC (DOC_{SPE}) in the water and [DOC] the molar DOC concentration in original seawater, respectively. DOC extraction efficiencies are ~65 % for freshwater samples and ~ 45% for marine samples (Dittmar et al., 2008). For DON, the extraction efficiency is less (~15-22 %), due to its high electronegativity and the discrimination of polar compounds by SPE (Lechtenfeld et al., 2011). In contrast, the extraction efficiency of DOS remains unknown, since the DOS concentration in original seawater cannot be analyzed, due to the high sulfate background. However, as long as there is no suitable method to analyze DOS in seawater, knowledge of the DOS extraction efficiency is an urgent need to back-calculate DOS concentrations in original water samples from DOS concentrations in solid-phase extracts (DOS_{SPE}). In preparation to this study, peat water samples with very low sulfate content were extracted and analyzed. To determine the DOS concentration in the original peat water, we analyzed the total sulfur concentration by inductively coupled plasma mass spectrometry (ICP-MS) and subtracted the sulfate concentration analyzed by ion chromatography (IC). DOS_{SPE} extraction efficiency was calculated from the DOS concentration in original and extracted peat water and were 9.35 ± 0.51

% (n = 4, Table 3). The low DOS extraction efficiency reflects the discrimination of polar DOS compounds by PPL-SPE, as previously observed for DON. However, there might be slight differences between the extraction efficiencies of sulfur-containing compounds derived from peat water and seawater samples. Since the electronegativity of nitrogen is higher than for sulfur, the maximum extraction efficiency for DOS should be at least as high as for DON. In another thesis (Pohlabeln, 2017), the extraction efficiencies of some sulfur-containing model compounds (thiols, sulfonic acids, sulfones, thioethers, and thiophenes) were tested. However, there, only EE_{DOC} of these sulfur compounds was determined and found to be similar to other DOC recoveries, suggesting that DOS compounds show similar extraction features as DOC. Nevertheless, an exact evaluation of the EE_{DOS} based on DOS analysis in the stock solution of the model compounds and the extracts is still missing.

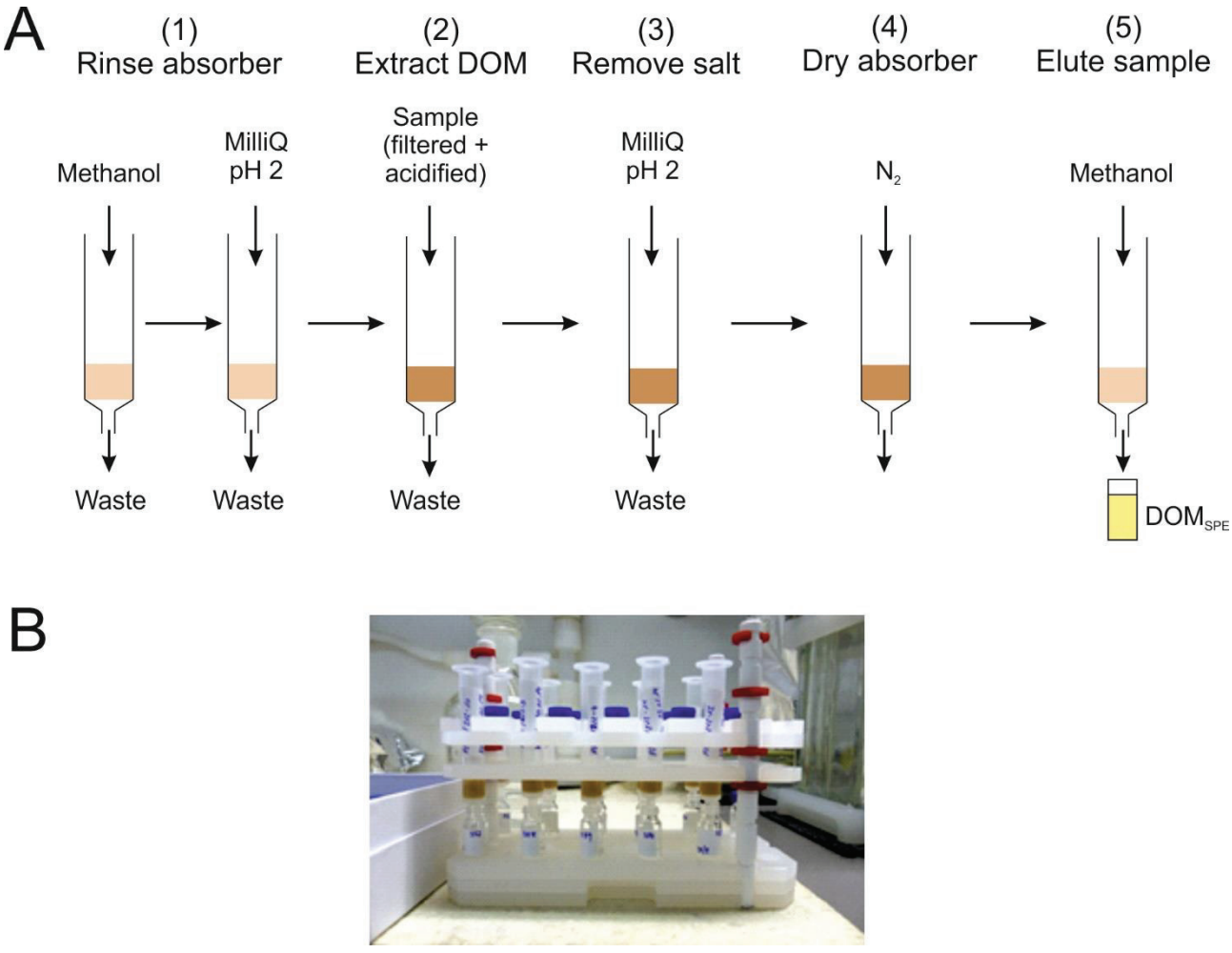

Figure 6. Isolation of the DOM_{SPE} from water samples. (A) Working scheme for the isolation of DOM via SPE adapted from Dittmar et al. (2008). (B) Picture of DOM_{SPE} isolation (Step (5) of Fig. 6A) in the laboratory or on board of a research vessel.

Table 3. Results of the extraction experiment of pea water (PW) samples for the assessment of DOS extraction efficiency.

Sample	Sample volume [mL]	Enrichment factor	DOS in original sample [µmol L^{-1}]	SO_4^{2-} in original sample [µmol L^{-1}]	DOS_{SPE} [µmol L-1]	DOS Extraction efficiency
PW_1	100	38	1155	197	115.65	10.01
PW_2	100	37	1155	197	99.49	8.61
PW_3	100	37	1155	197	106.78	9.25
PW_4	100	37	1155	197	110.08	9.53

Sulfate precipitation

Another experiment performed within the framework of this thesis was the removal of sulfate from water samples, which would allow analyzing DOS in the original water sample. Therefore, two samples from the Southern Ocean/East Atlantic were analyzed. The total sulfur concentration in the samples was determined by ICP-MS. Afterwards, sulfate was precipitated as $BaSO_4$ using $BaCl_2$. The precipitate was removed from the sample via centrifugation. $BaSO_4$ was dried and weighted, to determine the original sulfate concentration. An aliquot of the original sample was extracted and DOS_{SPE} was analyzed. However, the calculated extraction efficiencies were < 1 %, indicating that organic sulfur was co-precipitated.

Cutter et al. selectively removed sulfate from seawater samples followed by the analysis of total DOS concentration (Cutter et al., 2004). The sulfate removal procedure includes (1) the removal of sulfate via $BaSO_4$ precipitation on a cation exchange resin, (2) precipitation of chloride via AgCl precipitation on an Ag/cation exchange resin and (3) removal of the remaining sulfate with an anion exchange resin. Finally, the residual sulfate is analyzed by ion chromatography. Recovery rates of this procedure were tested with some model compounds and found to be >95 %. Nevertheless, several extraction procedures are included in this method and the applicability in the field/onboard of a research vessel should be tested.

II.2 Analytical techniques

In the field of marine DOM research, some of the methods used can be applied directly to the filtered original samples (e.g. DOC, nutrient- and high-performance liquid chromatography (HPLC) analysis) while others are only applicable with desalted and enriched DOM extracts (e.g. inductively coupled plasma mass spectrometry (ICP-MS)/ inductively coupled plasma optical emission spectrometry (ICP-OES) and Fourier transform ion cyclotron resonance mass spectrometry (FT-ICR-MS) analysis). Fundamental DOM analysis comprises the analysis of bulk parameters, e.g. DOC and DOS concentrations or the chemical composition (bulk elemental ratios). Furthermore, the molecular

DOM composition can be analyzed using targeted and non-targeted approaches. Most of the methods used are non-targeted methods, which means, that they are applied to simultaneously analyze a broad range of molecular components. In this study, compositional information was obtained by the application of FT-ICR-MS analysis, resulting in the determination of hundreds of molecular formulas in DOM_{SPE} samples. Targeted methods, in contrast, focus on specific compounds or compound classes. For the first manuscript of this thesis, the sulfur containing amino acid methionine was analyzed. Since ICP-MS analysis represents the key methods used in this thesis, this method will be explained in more detail. Details about specific methodological conditions can be found in the cumulative manuscripts (Chapter IV).

DOC and TDN/DON analysis

DOC can be analyzed in both, the original sample and the solid-phase extracted sample by high temperature catalytic oxidation (HTCO). Analysis of TDN in the original sample and solid-phase extractable DON (DON_{SPE}), respectively, can be performed simultaneously with DOC. First, the sample is acidified to convert all inorganic carbon, such as carbonate and bicarbonate, to CO_2 and purged with O_2 to remove inorganic carbon from the sample. In the next step, the remaining DOC (and DON) is oxidized by HTCO to CO_2 (and NO). During this step, the sample is injected onto a platinum catalyst at 680°C. An oxygen rich atmosphere ensures complete oxidation of carbon and nitrogen. Subsequent nondispersive infrared spectroscopy and chemiluminescence detection allows the analysis of CO_2 and NO, respectively.

The DON concentration in the original sample is determined by subtracting the concentration of dissolved inorganic nitrogen (DIN, determined by nutrient analysis) from the TDN concentration. Dissolved inorganic nutrients (silicate, phosphate and the nitrogen containing nutrients nitrate, nitrite and ammonium) were analyzed according to standard seawater methods (Kattner and Becker, 1991).

Optical methods: UV and fluorescence spectroscopy

These methods can be applied on both, the original and the solid-phase extracted samples. The fraction of DOM which can be analyzed using optical methods is called chromophoric or colored DOM (CDOM). In this study, sample fractions separated based on their polarity by HPLC were detected using UV absorption and fluorescence spectroscopy in order to discuss differences in the polarity of samples from different locations. The strong correlation of UV absorbance peak areas with DOC concentrations allows conclusions on the DOC concentration of the different fractions (Lechtenfeld et al., 2011).

Nevertheless, several more applications were found for UV absorbance and fluorescence spectroscopy. Thus, absorbance ratios at specific wavelengths can be used for the analysis of CDOM quality (e.g. molecular size, aromaticity, carboxyl content, and others) (Chen et al., 1977; Peuravuori and

Pihlaja, 1997; Piccolo et al., 1992; Summers et al., 1987; Weishaar et al., 2003), whereas fluorescent characteristics allow conclusions about sources, quantity and composition of DOM (Chari et al., 2013; Yamashita and Tanoue, 2003).

Analysis of sulfur containing amino acids

The quantification of amino acids (AAs) by HPLC is based on the derivatization of free or hydrolyzed AAs with ortho-phthalaldehyde (OPA) and separation of the derivatization products (Fitznar et al., 1999; Lindroth and Mopper, 1979; Mopper and Lindroth, 1982). The sulfur containing AAs cysteine and methionine represent up to 10 % of total AAs in the surface ocean, with decreasing amounts in deeper regions (Mopper and Lindroth, 1982). Within the framework of a project closely linked to this study, analysis of methionine in DOM_{SPE} samples via HPLC was optimized (Geuer, 2015). The analysis of the thiol cysteine by HPLC was also tested using different methods for derivatization. The presence of thiols could be shown. Their quantity, however, could not be accessed with the methods applied.

ICP-MS/ICP-OES analysis

The ICP-MS method is a highly sensitive technique, which allows for multi-element and even multi-isotope analyses. Thus, the concentrations of almost all elements of the periodic table can be determined in bulk DOM samples. This study focused on the analysis of DOS_{SPE} (Manuscript 1-5) and some trace metals (metal-DOM_{SPE}, Manuscript 3) by ICP-MS or ICP-OES. A schematic representation of the ICP-MS methods is shown in Fig. 7. The basic steps during ICP-MS analysis are:

Sample preparation, uptake, and introduction into the nebulizer. Since methanol affects the plasma stability during analysis, DOM_{SPE} samples were evaporated to dryness and redissolved in double distilled (dd) nitric acid (HNO_3). The samples analyzed in the cumulative manuscripts were calibrated externally. However, also calibration via standard addition is possible and probably even more accurate when analyzing very low concentrated samples. Calibration standards in different concentrations were prepared from a sock solution and diluted with HNO_3 (dd). An internal standard (Rh) was added to each sample and standard solution. Bidestilled HNO_3 was also used for blank analysis. The liquid samples were taken up by an autosampler and introduced into the nebulizer.

Conversion of the liquid samples into aerosol. The nebulizer converts the liquid sample into an aerosol by use of argon gas. For most samples of this study, an Apex desolvation nebulizer was used. This nebulizer unit can be heated to effectively remove/evaporate (organic) solvents from the sample. The received aerosol droplets represent only 1-2 % of the sample (Thomas, 2008). The aerosol is introduced into a spray chamber, where fine aerosol droplets are separated from larger ones, due to inefficient dissociation of large droplet inside the plasma.

Injection of the sample aerosol into the plasma and ionization. The sample aerosol is then transported into the plasma torch. During its flow through the different heating zones of the plasma, the aerosol is dried, vaporized, atomized, and finally ionized to positively charged ions (Thomas, 2008). The plasma itself has a temperature of 6000 - 7000 K. It is ionized by inductively heating Argon gas with a radio-frequency (RF) coil.

Transport of ions through an interface region into the mass separation device. The ions are conducted and extracted from the plasma through an interface region consisting of sampler and skimmer cone into the mass spectrometer. This interface region is operated at a vacuum of 1 - 2 Torr. After passing sampler and skimmer cone, the ions are directed through the ion optics - a series of electrostatic lens maintained at ~10^{-3} Torr – to focus the ion beam toward the mass separation device.

Mass separation and detection of the ions. The focused ion beam then enters the mass separation device, which is operated at ~10^{-6} Torr. The separation of ions is based on their particular mass-to-charge (m/z) ratio. The instrument used in this study is a double focusing sector field mass spectrometer. The ions are directed through a magnetic sector for mass separation and an electrostatic sector for energy separation and focusing. The ions are detected by a secondary electron multiplier (SEM). The signal of the detected ions increases proportionally to their concentration.

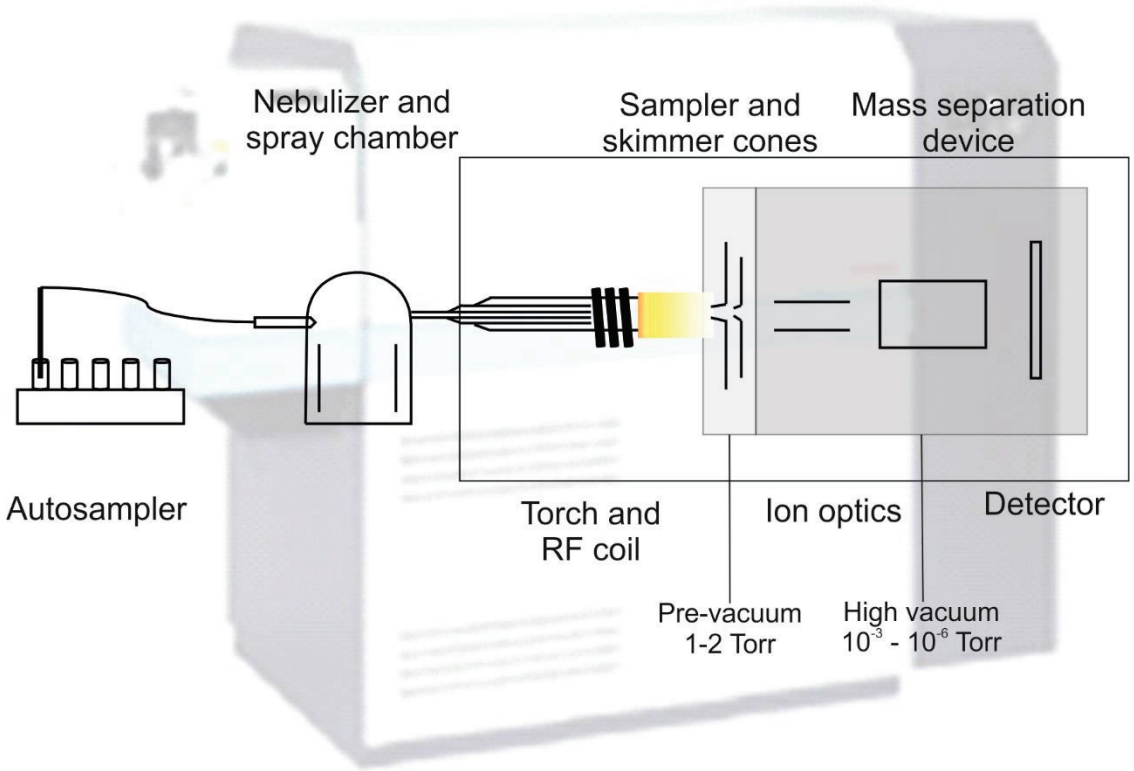

Figure 7. Schematic representation of the ICP-MS instrument.

Although the application of this technique is quite simple for most elements, some challenges occurred:

- Background concentrations of sulfur in the system were higher compared to other elements. Different attempts were carried out to reduce the blank concentration:

  (a) Exchange of all parts of the sample introduction system, such as nebulizer, sampler and skimmer cones, and torch

  (b) Additionally to the bidestilled HNO_3, destilled MilliQ was tested for blank analysis

  (c) To avoid possible sulfur-contamination of the Argon gas used, a filter was installed. However, higher background concentrations of sulfur still caused higher limits of detection (LOD) for sulfur than for all other elements analyzed (see supplementary material to manuscript 3 in addendum). Although LOD was low enough to analyze DOS_{SPE} in our samples, it may still be reduced when reducing background concentration of sulfur.
- Decreasing normalized intensities of S analyzed in the standard solution used for external calibration of S compared to the internal standard (Rh) indicated aging and removal of sulfur from the non-metal standard used. In order to detect such aging of standard solutions in time, a regular comparison of normalized intensities is recommended. Additionally, the frequent analysis of a reference compound with known concentration is useful.

seaFAST analysis

Usually, ICP-MS requires salt-free samples, since salt ions can cause matrix effects and salt buildup on the sampler cone, resulting in a suppression of the signal and partial or total plugging of the sampler cone orifice. Thus, we focused on the analysis of SPE samples. A newly developed method introduced a pre-concentration and matrix elimination process prior to ICP-MS analysis and thus allows direct analysis of trace metals in undiluted seawater samples (Hathorne et al., 2012). Elements such as Co, Cu, Ni, Zn and several others are pre-concentrated on a column, whereas seawater ions (Na, Cl, Mg, and Ca) pass through the column to be discarded. After the separation of elements from the matrix ions, the elements are eluted from the column and analyzed by ICP-MS.

ICP-OES analysis

The ICP-OES method is also used to analyze the concentrations of several elements. Similar to ICP-MS, the sample is introduced into an inductively coupled plasma. Inside the plasma, the sample is ionized. Electrons are emitted from the sample atoms at a specific wavelength characteristic for a particular element. In contrast to the mass spectrometer used for ICP-MS, the detection unit for ICP-OES consists of an optical spectrometer. The emitted light is separated into different wavelengths and the intensities are measured with a photomultimeter. The intensity of the signal increases proportional to the corresponding elemental concentration.

The results from ICP-OES analysis were verified by comparison with results from previous ICP-MS analysis for the measurements of the SLRS-5 reference standard. Although sulfur is not certified for SLRS-5, Yeghicheyan et al. (2013) reported S concentrations of 2347 – 2428 μg S L^{-1} (73.2 – 75.7 μmol L^{-1}). Average values analyzed by ICP-MS and ICP-OES were 2445 ± 32 μg S L^{-1} and 2372 ± 27 μg S L^{-1}, respectively. Thus, a high accuracy is given.

FT-ICR-MS analysis

FT-ICR-MS allows the analysis of complex organic mixtures and provides information on the exact masses of single organic compounds in DOM samples. These masses can be translated into elemental molecular formulae. This method has been applied for characterization of DOM from different origin, e.g. marine water, sediments, and rivers (Hertkorn et al., 2006; Koch et al., 2005; Schmidt et al., 2009). Although this method does not yield the exact chemical structure, some structural information, such as saturation state/aromaticity can be obtained (Koch and Dittmar, 2006).

III. Major research questions and objectives

The aim of this thesis was to elucidate the distribution, composition, sources, and biogeochemistry of DOS in aquatic environments with a focus on the marine system. Fundamental DOS research is based on DOS quantification and chemical characterization, which is crucial to further investigate its biogeochemical cycling. The target was to (1) develop a suitable method for the analysis of DOS_{SPE} by ICP-MS and (2) analyze DOM samples to further investigate DOS_{SPE} characteristics. In this regard, the following research questions/hypotheses were approached in the studies presented in chapter IV:

(i) What is the concentration/distribution of DOS in aquatic environments and how large is the marine DOS reservoir?

Previous studies on organic sulfur compounds mostly focused on VOSCs dissolved in surface waters of the global oceans and their precursor DMSP (see Chapter I.4). The concentration ranges and distribution of those compounds in the oceans are well studied, whereas studies on the non-volatile marine DOS are scarce: DOS in seawater was analyzed locally at one station in the Sargasso Sea and ranged between 0.04 – 0.4 μmol L^{-1} (Cutter et al., 2004). In the area of the Gulf of Bothnia, which is highly influenced by riverine input, DOS concentrations of ~6 - 19 μmmol L^{-1} were found (Alling et al., 2008). Additionally, DOS_{SPE} was analyzed at one station in the North Pacific Ocean and the North Sea, respectively (Pohlabeln and Dittmar, 2015). A DOS depth profile was only analyzed in the study from the Sargasso Sea, where DOS concentrations were found to decrease with depth (Cutter et al., 2004). Due to the limited number of studies, quantification of DOS in a higher spatial resolution and a global assessment of marine DOS relative to DMSP is still pending. Hence, a larger sample set is needed to analyze regional and depth related differences in marine DOS concentrations.

(ii) What is the chemical composition of marine DOS?

In this study, two approaches for the analysis of the chemical composition were applied: The analysis of bulk elemental stoichiometry (e.g. DOC_{SPE}/DOS_{SPE} and DOS_{SPE}/DON_{SPE} ratios) and analysis of the molecular composition (e.g. by FT-ICR-MS and methionine analysis). Using these approaches, the following research questions/hypotheses were studied:

(a) *What are the differences in DOS stoichiometry between samples from different aquatic environments?* I hypothesize that the elemental/molecular composition of DOS changes with the water source and biogeochemical transition processes. For example, terrestrial DOS in riverine systems should have a different stoichiometry than marine DOS. In this study, elemental DOC_{SPE}/DOS_{SPE} ratios were calculated for most samples. Riverine samples were analyzed to gain insights into the stoichiometry of fluvial DOS and differences between riverine and marine

DOS were discussed (Chapter IV.3). Additionally, differences between marine samples from different regions, water masses and depths were analyzed (Chapter IV.1 and IV.4).

(b) *What is the molecular elemental composition of marine DOS?* This question follows up on the previous hypothesis of a variation in the elemental/molecular composition respective to different water sources and biogeochemical transition processes. To answer this question, a sample subset from the East Atlantic Ocean and Southern Ocean was analyzed by FT-ICR-MS. Differences in the diversity and molecular elemental composition of DOS compounds from different depth and locations were discussed (Chapter IV.1).

(c) *What is the contribution of labile DOS to the total DOS pool?* Labile DOS compounds, such as sulfur containing amino acids, are essential for microbial activity. Thus, the majority is turned over rapidly and e.g. transformed to less labile molecules (see Chapter I.4). Consequently, I hypothesize that a major fraction of the total DOS pool consists of non-labile DOS. To test this hypothesis, specific samples were analyzed for their methionine content. The methionine sulfur yield was calculated to discuss differences in the contribution of labile DOS in samples from different depth and ages (Chapter IV.1). Additionally, DOS_{SPE} concentrations were compared with DMS concentrations (analyzed by (Zindler et al., 2014)) to assess the contribution of labile (and volatile) DOS compounds to the total DOS pool.

Based on the knowledge of DOS concentration, stoichiometry, and composition, several biogeochemical questions can be discussed:

(iii) What are the sources of marine DOS?

The major part of marine DOM is produced by phytoplankton in the surface ocean. Thus, DOS stoichiometry was evaluated for indication of biogenic imprint (Chapter IV.1 and IV.4). But also a benthic DOM flux might contribute to the marine DOM pool. For instance, elevated DOC concentrations were found during several expeditions in the bottom water of the Southern Ocean. Within this thesis, numerous DOC and DOS depth profiles were analyzed, some of them with a special focus on the upper- and lowermost water column, to elucidate DOM sources not only to the surface water, but also to bottom water (Chapter IV.1 and IV.4).

(iv) What are the sinks and removal processes of marine DOS? How reactive/bioavailable is marine DOS?

The reactivity of DOS was analyzed and discussed based on relative changes in DOC and DOS concentrations throughout the water column (Chapter IV.1). Additionally, a long-term net removal rate of non-labile DOS was calculated (Chapter IV.1) and DOS removal/transformation was analyzed at different salinities in the Elbe-Weser estuary (Chapter IV.3). As it was suggested, that water mass

mixing alone can be responsible for DOS distribution (Dittmar et al., 2017), the contribution of additional removal processes to changes in DOS concentration, distribution, and composition was discussed (Chapters IV.1 to IV.4).

Biological activity contributes to DOS removal. Apparent oxygen utilization (AOU) is the difference between the measured dissolved oxygen concentration and its equilibrium saturation concentration in water, due to microbial consumption. Thus, AOU might control organic sulfur speciation in the water column. This was tested in chapter IV.4 for samples from the Weddell Sea.

DOS is also suspected as a precursor for some climate relevant volatile sulfur compounds, such as OCS and CS_2. In Chapter IV.5, the potentially limiting factor of DOS availability on marine OCS and CS_2 production is discussed.

(v) How is the relation of DOS to trace element distribution/fluxes?

As introduced in Chapter I.4, sulfur-containing compounds (such as thiols) are known to play a significant role for trace metal-DOM interactions. In this study, we analyzed DOS and trace metal concentrations and the DOS/trace metal stoichiometry in samples along a salinity gradient in the Weser-Elbe estuary. The influence of DOS on trace element complexation is discussed in Chapter IV.3.

IV. Cumulative manuscripts and declaration of author's contributions

This cumulative dissertation is composed of five manuscripts as listed below. Chapters IV.1 to IV.5 are reprints of independent research papers of three published manuscripts (Manuscripts 1 - 3), one submitted manuscript (Manuscript 5, under review) and one manuscript in preparation (Manuscript 4). Manuscripts 1 to 3 were published in international peer-review journals. The content is unchanged and the (reference) style and labeling of figures and tables is adapted to the general format of this thesis. The references are included in the reference chapter at the end of this thesis. Datasets in supplement to Manuscripts 1, 3 and 4 are published (or in preparation for publication) at PANGAEA. Further supplementary information to the manuscripts can be found as an addendum to this thesis.

Chapter IV.1: MANUSCRIPT 1

Dissolved organic sulfur in the ocean: Biogeochemistry of a petagram inventory

Kerstin B. Ksionzek, Oliver J. Lechtenfeld, S. Leigh McCallister, Philippe Schmitt-Kopplin, Jana K. Geuer, Walter Geibert, Boris P. Koch

This manuscript has been published in *Science*, Vol. 354, Issue 6311, pp. 456-459 in October 2016 (doi: 10.1126/science.aaf7796). I performed the DOS analysis and data evaluation and wrote the article with contribution of all coauthors.

In supplement to this manuscript, a dataset was published at PANGAEA: doi 10.1594/PANGAEA.858568.

A comment on the paper "Dissolved organic sulfur in the ocean: Biogeochemistry of a petagram inventory" (Manuscript 1) was published under the doi 10.1126/science.aam6039 (Dittmar et al., 2017).

Chapter IV.2: MANUSCRIPT 2

Response to Comment on "Dissolved organic sulfur in the ocean: Biogeochemistry of a petagram inventory"

Boris P. Koch, Kerstin B. Ksionzek, Oliver J. Lechtenfeld, S. Leigh McCallister, Philippe Schmitt-Kopplin, Jana K. Geuer, Walter Geibert

This manuscript has been published in *Science*, Vol. 356, Issue 6340, pp. 813 in May 2017 (doi: 10.1126/science.aam6328). I conducted parts of the experiments, performed the data evaluation and commented on the manuscript.

Chapter IV.3: MANUSCRIPT 3

Stoichiometry, polarity, and organometallics in solid-phase extracted dissolved organic matter of the Elbe-Weser estuary

Kerstin B. Ksionzek, Jing Zhang, Kai-Uwe Ludwichowski, Dorothee Wilhelms-Dick, Scarlett Trimborn, Thomas Jendrossek, Gerhard Kattner, Boris P. Koch

This manuscript has been published in *PLOSone,* Vol. 13, Issue 9, e0203260 in September 2018 (doi: 10.1371/journal.pone.0203260). I partially performed the analysis of the samples, evaluated the data and wrote the manuscript with contribution of all coauthors.

In supplement to this manuscript, a dataset was published at PANGAEA: doi 10.1594/PANGAEA.895909.

Chapter IV.4: MANUSCRIPT 4

Quantification and biogeochemistry of dissolved organic sulfur in the southeastern Weddell Sea

Kerstin B. Ksionzek, Walter Geibert, Kai-Uwe Ludwichowski, Ingrid Stimac, Svenja Ryan, Boris P. Koch

This manuscript is in preparation for submission. I participated in the design of the research, sampled and processed the samples, performed sample and data analysis, and wrote the manuscript with input from all coauthors.

In supplement to this manuscript, a dataset is in preparation to be published at PANGAEA.

Chapter IV.5: MANUSCRIPT 5

The influence of dissolved organic matter on the marine production of carbonyl sulfide (OCS) and carbon disulfide (CS2) in the Peruvian Upwelling

Sinikka T. Lennartz, Marc von Hobe, Dennis Booge, Henry Bittig, Tim Fischer, Rafael Gonçalves-Araujo, Kerstin B. Ksionzek, Boris P. Koch, Astrid Bracher, Rüdiger Röttgers, Birgit Quack, Christa A. Marandino

This manuscript is under review in Ocean Science Discussion. I explained the SPE method for application onboard to S.T.L., partially performed DOS_{SPE} analysis and data interpretation and commented on the manuscript.

IV.1 Manuscript 1

Dissolved organic sulfur in the ocean: Biogeochemistry of a petagram inventory

Kerstin B. Ksionzek[1,2]*, Oliver J. Lechtenfeld[1,7], S. Leigh McCallister[3], Philippe Schmitt-Kopplin[4,5], Jana K. Geuer[1], Walter Geibert[1], Boris P. Koch[1,2,6]*

1 Alfred Wegener Institute Helmholtz Center for Polar and Marine Research, Am Handelshafen 12, 27570 Bremerhaven, Germany.

2 MARUM – Center for Marine Environmental Sciences, Leobener Straße, D-28359 Bremen, Germany.

3 Virginia Commonwealth University, Department of Biology, Center for Environmental Studies, 1000 West Cary Street, Richmont, VA 23284, USA.

4 Helmholtz Zentrum München (HMGU), German Research Centre for Environmental Health, Institute for Ecological Chemistry, Analytical BioGeoChemistry (BGC), Ingolstädter Landstraße 1, D-85764 Neuherberg, Germany.

5 Technische Universität München, Chair of Analytical Food Chemistry, Alte Akademie 10, 85354 Freising, Germany.

6 University of Applied Sciences, An der Karlstadt 8, 27568 Bremerhaven, Germany.

7 UFZ-Helmholtz Centre for Environmental Research, Department of Analytical Chemistry, Permoserstraße 15, D-04318 Leipzig, Germany.

* Corresponding author. Email: kerstin.ksionzek@awi.de (K.B.K); boris.koch@awi.de (B.P.K.)

Abstract: Although sulfur is an essential element for marine primary production and critical for climate processes, little is known about the oceanic pool of non-volatile dissolved organic sulfur (DOS). We present a basin-scale distribution of solid phase extractable DOS in the East Atlantic Ocean and the Atlantic sector of the Southern Ocean. While molar DOS versus dissolved organic nitrogen (DON) ratios of 0.11 ± 0.024 in Atlantic surface water resembled phytoplankton stoichiometry (S/N ~ 0.08), increasing dissolved organic carbon (DOC) versus DOS ratios and decreasing methionine-S yield demonstrated selective DOS removal and active involvement in marine biogeochemical cycles. Based on stoichiometric estimates, the minimum global inventory of marine DOS is 6.7 Pg S, exceeding all other marine organic sulfur reservoirs by an order of magnitude.

In the early 30s, Alfred Redfield noted that the ratio of carbon, nitrogen and phosphorus in algal phyla remains surprisingly consistent across marine biomes. The canonical 106:16:1 Redfield ratio (Redfield et al., 1963) originated from these observations and has since become a cornerstone of ocean biogeochemistry. Subsequent stoichiometric studies quantified the cellular quota of organic sulfur (OS) and found it to be similar to that of organic phosphorus ($C_{124}N_{16}P_1S_{1.3}$) (Ho et al., 2003). The magnitude of S acquisition, assimilation and metabolism is not trivial given an average molar elemental ratio of $C_{124}N_{16}P_1S_{1.3}$ for marine algae (Ho et al., 2003). Based on this C/S ratio of ~95, the global phytoplankton biomass (~1 Pg C) (Falkowski et al., 1998) contains 0.028 Pg S and the annual net marine primary production (48.5 Pg C a^{-1}) (Field et al., 1998) requires a sulfur assimilation of 1.36 Pg S a^{-1}. Whereas regional marine DOS budgets have been constructed (Cutter et al., 2004), quantification of the global inventory and its ties to other elemental biogeochemical cycles (C, N, P, Fe) has been analytically hampered by the background concentration of sulfate (29 mmol S L^{-1}), which exceeds the concentration of DOS by five orders of magnitude.

The discovery of OS coupling to climate processes (Charlson et al., 1987) generated a surge of interest in the OS cycle and dimethylsulfoniopropionate (DMSP) specifically. DMSP is the precursor of dimethylsulfide (DMS) (Andreae, 1990), a gas, which is assumed to contribute to aerosol formation and climate regulation (Charlson et al., 1987). The estimated annual production of DMSP by phytoplankton of 3.8 Pg C a^{-1} or 2.0 Pg S a^{-1} (Galí et al., 2015) represents an important sulfur assimilation pathway with rapid turnover rates and provides a significant source of reduced carbon and sulfur for heterotrophic bacteria (Kiene et al., 1999; Tripp et al., 2008). At the cellular level, the organic S and N cycles are intimately coupled

through algal biosynthesis of the amino acids methionine and cysteine (Giovanelli et al., 1978). Sulfur-rich peptides can also form metal-organic complexes, and thus influence the speciation and mobility of trace metals in the ocean (Smith et al., 2002) with cascading impacts on phytoplankton production, community composition and carbon storage. Non-volatile DOS is tightly linked to other major mineral assimilation pathways, because it also comprises amino acids, vitamins, osmolytes, and primary metabolites (Durham et al., 2015; Moran et al., 2016). The major sinks for these marine biogenic sulfur compounds are (i) remineralization to sulfate, (ii) incorporation into microbial biomass, (iii) efflux to the atmosphere (Schmitt-Kopplin et al., 2012), and (iv) transformation into the sizeable pool of non-volatile marine dissolved organic matter (DOM; 662 Pg C) (Hansell et al., 2009). Despite the relevance of marine DOS for ocean biogeochemistry, its quantitative depiction and connections and feedbacks to the C and N cycle remain elusive.

This study is based on water samples from the East Atlantic (EA) and the Southern Ocean (SO) collected in November and December 2008 between 50.2° N and 70.5° S (Fig. M1.1A) (Flerus et al., 2012; Lechtenfeld et al., 2014). The concentrations of solid-phase extractable DOS (DOS_{SPE} in μmol L^{-1} seawater) were analyzed by inductively coupled plasma sector field mass spectrometry (ICP-MS). Similar to the ambient DOC concentration (Flerus et al., 2012; Lechtenfeld et al., 2014), DOS_{SPE} in the EA decreased significantly from 0.14 ± 0.02 μmol L^{-1} at surface depths of 0 – 105 m to ≤ 0.08 ± 0.01 μmol L^{-1} in deeper water ≥ 200 m ($p < 0.001$, Fig. M1.1B, Table M1.1). DOS_{SPE} correlated linearly with both, DON_{SPE} and DOC_{SPE} ($p < 0.001$, $R_{DOC} = 0.86$, $R_{DON} = 0.75$; Fig. M1.1C and Fig. M1.S1A), whereas the slopes differed significantly ($p < 0.001$). The molar DOS_{SPE}/DON_{SPE} ratios of 0.11 ± 0.024 were almost constant (slope of 5.3) throughout the water column and comparable to phytoplankton stoichiometry (S/N ~ 0.08, C:N:S = 124:16:1.3) (Ho et al., 2003) suggesting a predominantly biogenic DOS imprint (Gonsior et al., 2011) rather than abiotic incorporation of S into DOM as found in oxygen-limiting conditions (Sleighter et al., 2014). In contrast, molar DOC_{SPE}/DOS_{SPE} ratios in the EA increased with depth from 213 ± 25 in the surface to 268 ± 39 in deeper water (slope of 99.7; $p < 0.001$), suggesting higher biological reactivity of DOS relative to DOC. This is supported by earlier studies showing that microbial growth can be limited by the availability of reduced sulfur sources such as DMSP (Kiene et al., 1999; Tripp et al., 2008).

DOS_{SPE} concentrations in the SO were pervasively low, while primary production was relatively high (see Fig. M1.S2 for chlorophyll concentrations). Depth-related changes in DOS_{SPE} concentrations of 0.08 ± 0.01 μmol L^{-1} in the surface and 0.07 ± 0.01 μmol L^{-1} at ≥ 200 m depth and changes in molar DOC_{SPE}/DOS_{SPE} ratios of 262 ± 28 in the surface and 254 ± 26 at ≥ 200 m were insignificant ($p > 0.05$, Table M1.1). Molar DOS_{SPE}/DON_{SPE} ratios of 0.10 ± 0.027 were similar to those found in the EA. A correlation of chlorophyll *a* with DOC or DOS was not observed. We speculate that the

biogenic signature of DOS production was not detected due to short residence times in the mixed surface water and upwelling of old (5226 ± 64 a), non-labile DOS from the deep SO (Hansell et al., 2009) with low DOS_{SPE} concentrations (0.07 ± 0.001 µmol S L^{-1}, Table M1.1).

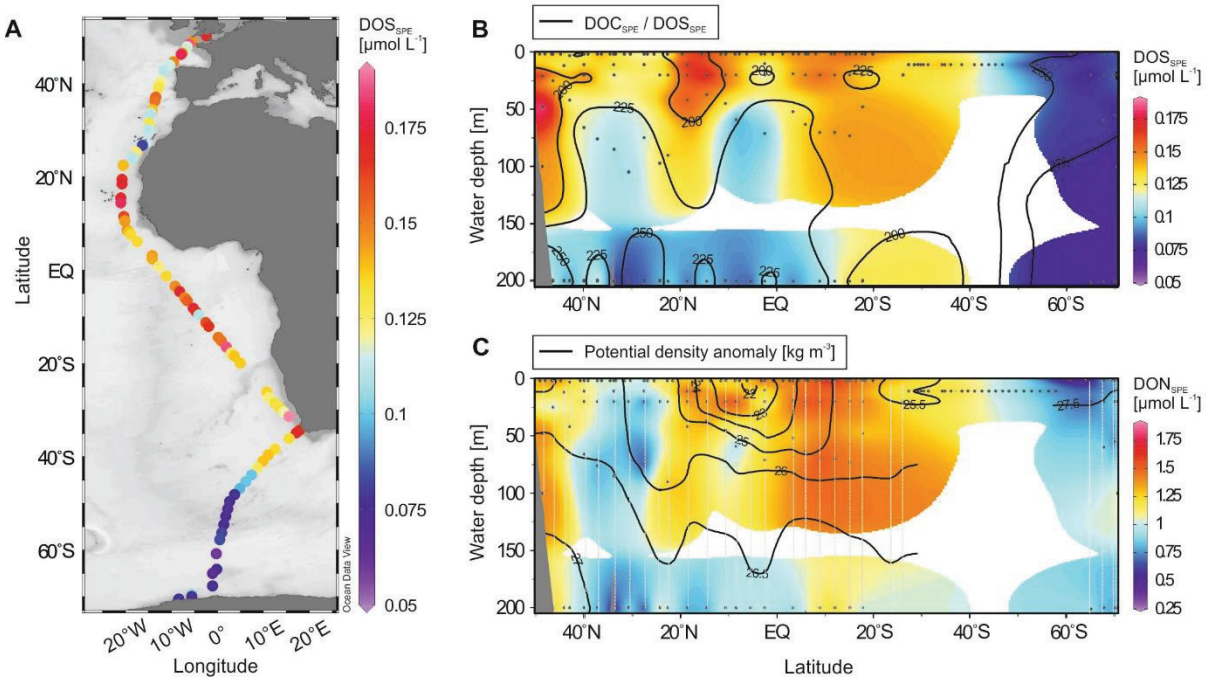

Figure M1.1. Cruise track and distribution of DOS_{SPE} and DON_{SPE} and molar DOC_{SPE}/DOS_{SPE} ratios in the surface ocean. (A) Surface DOS_{SPE} concentrations (µmol L^{-1}, colors) along the cruise track of R/V Polarstern expeditions ANT XXV/1+2. (B) DOC_{SPE}/DOS_{SPE} ratios (contours) and DOS_{SPE} concentrations (µmol L^{-1}, colors). (C) Potential density anomaly σ_0 (kg m^{-3}, contours) and DON_{SPE} concentrations (µmol L^{-1}, colors). For data below 200 m water depth, refer to Table M1.1.

To provide an estimate of non-labile DOS removal, we correlated measured and reconstructed DOC_{SPE} radiocarbon ages (Flerus et al., 2012; Lechtenfeld et al., 2014) with DOS_{SPE} concentrations (Fig. M1.S1B, supplementary material). Based on first order kinetics, we found a strong correlation ($R = 0.75$, $p < 0.01$) of DOS_{SPE} concentration with age, similar to that previously determined for DOC_{SPE} (Flerus et al., 2012; Lechtenfeld et al., 2014) ($R = 0.61$, $p < 0.01$). The long-term degradation rate coefficients for DOS_{SPE} of $k_{DOS} = 2.54*10^{-4}$ a^{-1} and DOC_{SPE} of $k_{DOC} = 1.53*10^{-4}$ a^{-1}differed significantly ($p < 0.001$) and reflected a higher reactivity (lability) of DOS_{SPE} compared to DOC_{SPE}. The long-term net removal rate of $2.7*10^{-5}$ µmol S L^{-1} a^{-1} for this non-labile DOS_{SPE} pool (see supplementary material for definition) results in stoichiometric changes in DOM over time and depth, similar to the preferential remineralization of N (and P) relative to C (Hopkinson et al., 2002). In contrast, degradation rate coefficients for DOS_{SPE} and DON_{SPE} were similar and consequently molar DOS_{SPE}/DON_{SPE} ratios did not change significantly with age. Differences between DOS_{SPE} and DOC_{SPE} degradation kinetics are also reflected in DOS_{SPE} and DOC_{SPE} lifetimes (time at which the DOM concentration decreases to $1/e$ of its initial value): We calculated the average lifetime of DOS_{SPE}

of τ = 3937 a, which is lower than the lifetime for DOC of τ = 4500 a (Lechtenfeld et al., 2014) and DOC_{SPE} of τ = 6536 a (see supplementary material for details). As the molecular composition of the DOC and DOS pools differs, a direct comparison of DOS_{SPE} degradation kinetics with commonly applied DOC fractions (labile, semi-labile, or refractory), which are based on the DOC removal rate and lifetime (Hansell, 2013) cannot be applied. Our results also indicate that DOS degradation kinetics, similar to previous studies on DOC (Flerus et al., 2012), are determined by a continuum of reactivities of the contributing sulfur compounds rather than discrete degradation stages.

Relative changes in the contribution of labile DOS derived from biogenic production to the total DOS pool were assessed from two depth profiles analyzed for total hydrolysable methionine-sulfur yield (i.e. mol% of methionine-S versus total DOS_{SPE}). In the EA, we found a higher molar methionine-sulfur yield of 1.02 ± 0.14 % in the surface water compared to 0.21 ± 0.10 % in deeper water (≥ 200 m). Accordingly, we observed a considerable decrease of the methionine-sulfur yield with age (Fig. M1.S3). In the SO, the methionine-sulfur yield of 0.18 ± 0.04 % was consistently low throughout the water column. Assuming a methionine-S:cysteine-S ratio of 1.7 (Giovanelli et al., 1978), less than 2 mol% of the DOS_{SPE} was protein-derived. This low value is consistent with previous data on amino acid carbon yield (Davis and Benner, 2007) suggesting that labile DOS in form of sulfur containing amino acids is efficiently remineralized or transformed, even in the surface ocean.

For the molecular characterization of DOS, we used ultrahigh resolution mass spectrometry (FT-ICR-MS) and identified 803 unique molecular formulas containing predominantly one sulfur atom, 81 of which were exclusively identified in surface water ≤ 105 m (total number of S-formulas in the dataset: 81,037). None of the formulas we detected occurred uniquely at depth or matched the composition of a peptide. However, it is likely that other sulfur containing compounds were also present and not covered by our analytical window. The diversity of sulfur containing compounds identified by FT-ICR-MS and the average molecular S/C ratio in the EA decreased significantly from 0.06 ± 0.001 in surface water to 0.05 ± 0.001 in deeper water (≥ 200 m; $p < 0.001$; Fig. M1.2), whereas comparable trends in the SO were not observed. Similar to previous molecular studies on DOC (Flerus et al., 2012; Lechtenfeld et al., 2014), the most persistent S-formulas at depth showed higher unsaturation (lower molecular hydrogen/carbon ratio, Fig. M1.2) and slightly larger molecular size (427 ± 5.6 Da in surface water and 441 ± 10.9 Da ≥ 200 m).

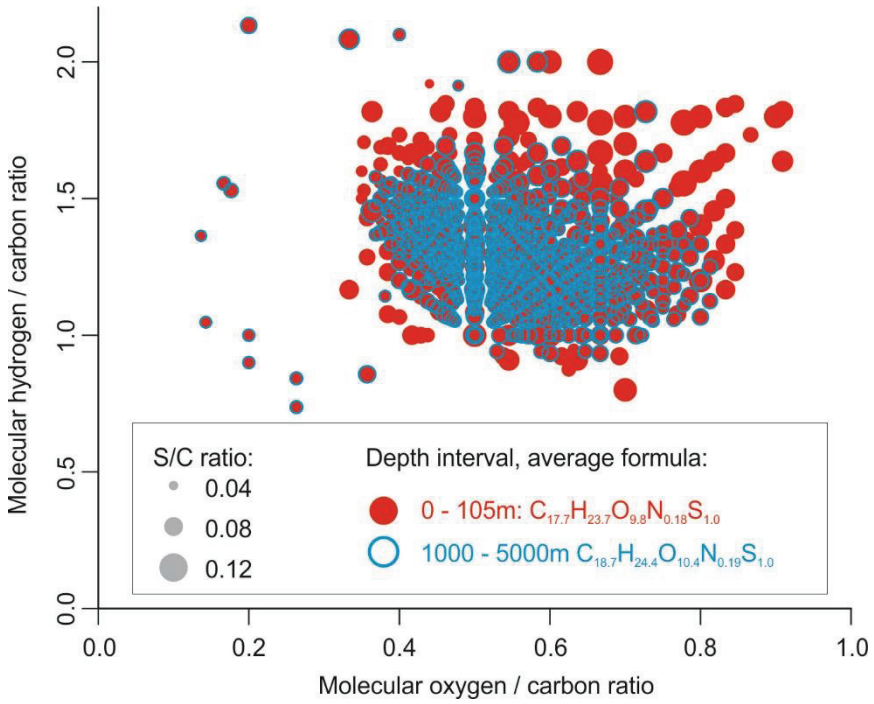

Figure M1.2. Molecular changes of sulfur containing compounds in the Eastern Atlantic Ocean. Every dot represents a specific sulfur-containing molecular formula. Each formula is represented by its molecular H/C and O/C ratio (van Krevelen plot). The size of the data points represents the molecular S/C ratio. Higher S/C ratios indicate a higher amount of sulfur in the formula. Colors represent two depth intervals: 0-105 m (red dots) and >1000 m (blue circles). In the surface, the number of different formulas (chemical diversity) was higher. Most unique sulfur compounds in the surface showed a higher content of hydrogen (saturation) and oxygen (oxidation). The average molecular formula for each depth interval is displayed.

The SPE method applied (Dittmar et al., 2008) yields lower extraction efficiencies for highly polar organic compounds (e.g. 22 % for marine DON) as compared to DOC (42 %) (Flerus et al., 2012; Lechtenfeld et al., 2014). Changes of the DOC and DON extraction efficiencies with depth, however, were insignificant (p_{DOC} = 0.85, p_{DON} = 0.45). Therefore, we can assume that the extraction yield for polar OS compounds is also lower than for DOC and independent of water depth. Using the average measured molar DOC_{SPE}/DOS_{SPE} ratio (Table M1.1) and the DOC concentrations in original seawater, we can reconstruct a conservative minimum for the original DOS concentration in seawater ($[DOS]_{MIN}$, Table M1.1, Eq. M1.1):

$$[DOS]_{MIN} = [DOC] \,/\, (DOC_{SPE}/DOS_{SPE}) \qquad \text{(M1.1)}$$

where [DOC] is the molar DOC concentration in original seawater and DOC_{SPE}/DOS_{SPE} is the measured molar elemental ratio in the extracts. The calculated $[DOS]_{MIN}$ concentrations were 0.34 ± 0.08 μmol L^{-1} and 0.19 ± 0.04 μmol L^{-1} in EA and SO surface waters, respectively (Table M1.1). This concentration range was consistent with previous data from the Sargasso Sea (0.04 – 0.4 μmol DOS L^{-1})

(Cutter et al., 2004). For comparison, the mean concentrations of dissolved DMS and DMSP in the surface of the EA during our cruise were 0.0036 μmol L^{-1} and 0.0032 μmol L^{-1}, respectively (Zindler et al., 2014), representing ~2 % of $[DOS]_{MIN}$ in the EA. The global average concentration for dissolved DMS and DMSP were previously estimated at 0.001 – 0.007 μmol L^{-1} (Lana et al., 2011) and 0.003 μmol L^{-1} (Kiene and Slezak, 2006), respectively, contributing only ~2.3 % of the total $[DOS]_{MIN}$.

Based on the global oceanic DOC inventory of 662 Pg C (Hansell et al., 2009) and depth-integrated molar DOC_{SPE}/DOS_{SPE} ratios, the minimum global oceanic DOS inventory (DOS_{MIN}) is 6.7 Pg S (= 6,700 Tg), ~600 Tg of which are present in the upper 200 m of the water column (Table M1.1, Fig. M1.3). If we assume that the molar C/S ratio of ~95 in phytoplankton is the lowest possible ratio for DOM, the maximum size of the global DOS inventory is 18.6 Pg S. Hence, DOS represents the major reservoir of organic S in the ocean, larger than OS in biomass, particles or volatile compounds combined (Fig. M1.3). More importantly, these numbers raise new questions on the marine sulfur budgets: Only 13 - 37 Tg S a^{-1} of the total DOS pool (red frame in Fig. M1.3) are released to the atmosphere as DMS (Yoch, 2002) and DOS degradation products such as carbonyl sulfide (COS; 0.4 Tg S a^{-1}) and carbon disulfide (CS_2; 0.3 Tg S a^{-1}, Fig. M1.3) (Yoch, 2002). In total, these fluxes represent less than 3 % of the annual sulfur assimilation of 1.36 Pg S a^{-1} by primary production, suggesting that rapid biogeochemical cycles of labile sulfur compounds (red cycle in Fig. M1.3) are superimposed on the large background of non-labile DOS (red frame in Fig. M1.3), which we consider to be derived from the microbial carbon pump (Jiao et al., 2010). Seasonal variation of C/S ratios by changes in production and microbial or photo-degradation has an important impact on the DOS_{MIN} estimates in the surface (Cutter et al., 2004). However, the value for our global DOS_{MIN} estimate is dominated by the relatively invariant C/S ratios of 266 ± 41 in the large water body below the photic zone (> 200 m) and therefore only marginally affected by seasonal effects. Many previous studies focused on the labile (and partly volatile) proportion of the DOS cycle (Fig. M1.3). This study enables important insights into the biogeochemistry of the vast pool of non-labile DOS. So far, the organic sulfur budgets cannot be closed, particularly because the connection between the rapid cycling of labile DOS and the non-labile proportion of the organic sulfur cycle remain unquantified.

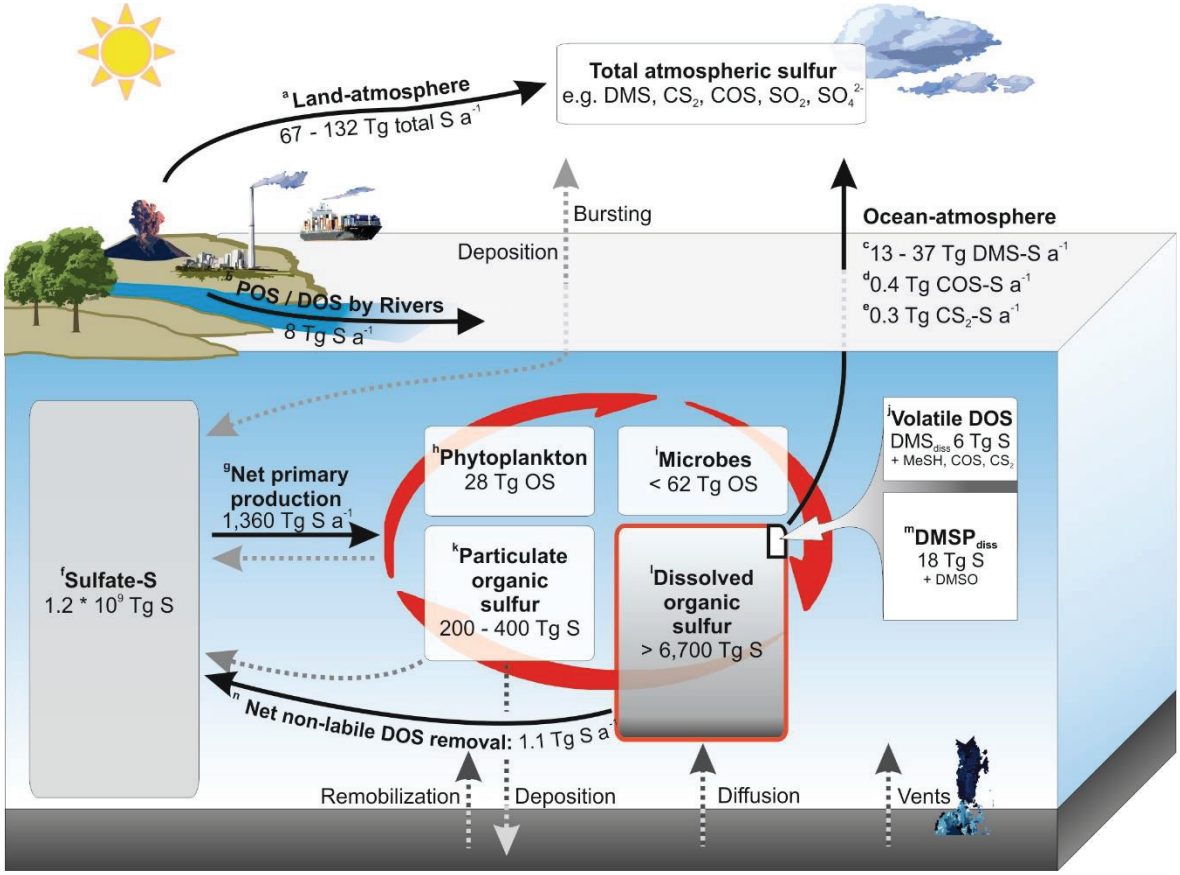

Figure M1.3[1]. Simplified marine organic sulfur cycle. Schematic overview of organic sulfur reservoirs and fluxes. All numbers refer to organic sulfur, except for the oceanic sulfate inventory and the land-atmosphere flux (total S). Known and calculated organic sulfur fluxes are shown as solid lines and unknown fluxes as dotted lines. The red circle indicates the rapid and important cycling of labile DOS compounds such as DMSP (depicted in the small white box). For corresponding data and references see Table M1.S3.

[1] It should be noted that in our published, original Fig. M1.3, the removal was incorrectly assigned as "refractory" and the sulfate reservoir was given to be $1.2*10^{12}$ Tg S instead of the correct $1.2*10^{9}$ Tg S (as mentioned in Manuscript 2). Here, the corrected version of Fig. M1.3 is presented.

Table M1.1. Average values and root mean square deviations of dissolved organic carbon and sulfur concentrations in the EA and SO and calculated global DOS_{MIN} inventory.

		Depth intervals				
		0-105 m	200 m	201-1000 m	>1000 m	Total*
East Atlantic Ocean	n†	106 (108)	21	5	11 (8)	143 (142)
	DOC (μmol L^{-1})	71 ± 12	54 ± 4	49 ± 5	46 ± 2	47 ± 3
	DOC_{SPE} (μmol L^{-1})	29 ± 5	23 ± 3	20 ± 1	20 ± 1	21 ± 1
	DOS_{SPE} (μmol L^{-1})	0.14 ± 0.02	0.10 ± 0.02	0.09 ± 0.03	0.07 ± 0.01	0.08 ± 0.01
	DOC_{SPE} / DOS_{SPE}	213 ± 25	235 ± 30	241 ± 47	276 ± 38	268 ± 39
	$[DOS]_{MIN}$ (μmol L^{-1})	0.34 ± 0.08	0.23 ± 0.04	0.21 ± 0.05	0.16 ± 0.03	0.18 ± 0.03
Southern Ocean	n†	22 (21)	3 (2)	3	3	31 (29)
	DOC (μmol L^{-1})	50 ± 11	48	48 ± 6	49 ± 6	49 ± 7
	DOC_{SPE} (μmol L^{-1})	21 ± 2	21 ± 1	21 ± 0.3	18 ± 4	19 ± 3
	DOS_{SPE} (μmol L^{-1})	0.08 ± 0.01	0.07 ± 0.003	0.07 ± 0.005	0.07 ± 0.001	0.07 ± 0.01
	DOC_{SPE} / DOS_{SPE}	262 ± 28	288 ± 17	294 ± 14	246 ± 29	255 ± 26
	$[DOS]_{MIN}$ (μmol L^{-1})	0.19 ± 0.04	0.16	0.16 ± 0.02	0.20 ± 0.01	0.19 ± 0.01
Total average	n†	128 (129)	24 (23)	8	14 (11)	174 (171)
	DOC (μmol L^{-1})	68 ± 14	53 ± 4	49 ± 5	47 ± 4	48 ± 5
	DOC_{SPE} (μmol L^{-1})	28 ± 5	23 ± 3	21 ± 1	20 ± 2	20 ± 2
	DOS_{SPE} (μmol L^{-1})	0.13 ± 0.03	0.10 ± 0.02	0.08 ± 0.02	0.07 ± 0.01	0.08 ± 0.01
	DOC_{SPE} / DOS_{SPE}	221 ± 31	241± 34	261 ± 46	270 ± 38	266 ± 39
	$[DOS]_{MIN}$ (μmol L^{-1})	0.31 ± 0.09	0.23 ± 0.04	0.19 ± 0.05	0.17 ± 0.03	0.18 ± 0.03
Global	DOC (Pg)[13]	47		138	477	662
	DOS_{MIN} (Pg)	0.6		1.4	4.7	6.7

* Depth-integrated values.

† Number of samples for the DOS_{SPE} analysis. Numbers in brackets are the numbers of samples for DOC analysis.

Acknowledgments: This work was supported by the DFG-Research Centre / Cluster of Excellence "The Ocean in the Earth System" and a PhD grant by the Deutsche Forschungsgemeinschaft (DFG) in the framework of the priority programme "Antarctic Research with comparative investigations in Arctic ice areas" (Grant KO 2164/8-1+2). We are grateful to RV *Polarstern* captain, crew and chief scientists Gerhard Kattner (ANTXXV-1) and Olaf Böbel (ANTXXV-2); I. Stimac is acknowledged for technical support with ICP-MS analysis and K.-U. Ludwichowski for support with methionine analysis; we thank C. Marandino for DMS and DMSP data; S. Frickenhaus is acknowledged for support with statistical analysis and B. Kanavati, M. Harir and J. Uhl for support with FT-ICR-MS analyses. G. Kattner and R. Alheit are acknowledged for helpful discussions and proof reading.

The data presented in this paper are available at the PANGEA data library (doi: 10.1594/PANGAEA.858568).

IV.2 Manuscript 2

Response to Comment on "Dissolved organic sulfur in the ocean: Biogeochemistry of a petagram inventory"

Boris P. Koch,[1,2,3] Kerstin B. Ksionzek,[1,2] Oliver J. Lechtenfeld,[1,7] S. Leigh McCallister,[4] Philippe Schmitt-Kopplin,[5,6] Jana K. Geuer,[1] Walter Geibert[1]

[1] Alfred Wegener Institute, Helmholtz Center for Polar and Marine Research, Am Handelshafen 12, 27570 Bremerhaven, Germany.

[2] MARUM Center for Marine Environmental Sciences, Leobener Straße, D-28359 Bremen, Germany.

[3] University of Applied Sciences, An der Karlstadt 8, 27568 Bremerhaven, Germany.

[4] Virginia Commonwealth University, Department of Biology, Center for Environmental Studies, 1000 West Cary Street, Richmond, VA 23284, USA.

[5] Helmholtz Zentrum München (HMGU), German Research Centre for Environmental Health, Analytical BioGeoChemistry (BGC), Ingolstädter Landstraße 1, D-85764 Neuherberg, Germany.

[6] Technische Universität München, Chair of Analytical Food Chemistry, Alte Akademie 10, 85354 Freising, Germany.

[7] UFZ-Helmholtz Centre for Environmental Research, Department of Analytical Chemistry, Permoserstraße 15, D-04318 Leipzig, Germany.

*Correspondence to: Boris.Koch@awi.de

Abstract: Dittmar et al. proposed that mixing alone can explain our observed decrease in marine dissolved organic sulfur with age. However, their simple model lacks an explanation for the origin of sulfur-depleted organic matter in the deep ocean and cannot adequately reproduce our observed stoichiometric changes. Using radiocarbon age also implicitly models the preferential cycling of sulfur that they are disputing.

Dittmar and co-workers (2017) claimed that the distribution of marine dissolved organic sulfur (DOS) reported in Ksionzek et al. (2016a) could be explained by simple water mass mixing alone. The authors calculated separate mixing models for the solid-phase extractable (SPE) fraction of dissolved organic carbon (DOC), nitrogen (DON), and DOS. They based their calculation on radiocarbon age and two endmembers – deep and surface ocean water - that differed in concentration, elemental composition and radiocarbon age of the dissolved organic matter (DOM).

We appreciate the interest in our publication; however, we disagree with their conclusions for three fundamental reasons: (i) Their mixing hypothesis considers deep-sea DOM as an independent end-member without reasoning for its origin or formation processes. (ii) Mixing without removal cannot adequately explain the stoichiometric changes that we observed. (iii) The authors mistakenly assumed that we exclusively addressed the removal of refractory DOS. Each of these aspects is addressed in detail below and rules out that mixing alone can explain the distribution of DOS and the depletion of nonlabile DOS.

We are well aware of the fact that the ocean consists of different water masses influenced by seasonal changes of the mixed-layer, deep-mixing, and circulation. Dittmar et al. outlined the accepted view that production in the ocean surface is the source for deep-sea DOM. Many previous stoichiometric studies [e.g., (Hopkinson and Vallino, 2005)] showed depletion of DON and dissolved organic phosphorus relative to DOC from surface to deep water, consistent with the DOS depletion and respective stoichiometric changes that we observed. Nonetheless, in their mixing model, Dittmar et al. treated surface and deep DOM as independent end-members (conservative mixing). Because the ultimate source of deep-ocean DOM is primary production, removal processes are fundamental to explain differences in concentration and stoichiometry (i.e., DOS_{SPE}/DOC_{SPE} ratio), as well as the differing methionine-S yield between surface and deep DOM that we observed. Calculating the DOS_{SPE} removal exclusively for the meso- and epipelagic showed little effect on the rate coefficient (Fig. M2.1).

Our results are in agreement with many previous studies reporting microbial alteration of marine DOM composition (Flerus et al., 2012; Hopkinson and Vallino, 2005; Jiao et al., 2010; Lechtenfeld et al., 2014; Ogawa et al., 2001; Stedmon and Markager, 2005). Dittmar and co-workers cited a recent study (Hansell and Carlson, 2013) that showed localized removal of refractory DOC in the deep Pacific. Hansell and Carlson conclude that the removal mechanisms are unknown and hypothesize that (i) the release of exoenzymes by microbial assemblages could lead to uptake of recalcitrant compounds,

(ii) solubilization of sinking particles could support cometabolism, or (iii) sinking particles or gel formation remove refractory DOC. Each of these processes would also contribute to our calculated DOS net removal.

By using radiocarbon age as a measure for mixing, Dittmar et al. introduce an inherent inconsistence: On the one hand, they correctly emphasize that bulk radiocarbon age is affected by preferential removal of labile DOM constituents above the pycnocline; on the other hand, they used radiocarbon age to infer conservative mixing over the entire water column.

Although it is unclear how Dittmar et al. "fine-tuned" [caption, figure 2 of (Dittmar et al., 2017)] endmember values to match their exponents to our approach, they reproduced our gradients by their mixing models. However, the authors neglected to compare relative differences between their mixing models [see figure 2 of (Dittmar et al., 2017)] and the resulting changes in elemental stoichiometry; if it was truly conservative mixing alone, each element would be equally affected. A simple way to illustrate this is to compare relative changes of their endmember concentrations for deep and surface water. The concentrations of DOS_{SPE} (0.08 μmol L^{-1}) and DON_{SPE} (0.7 μmol L^{-1}) in the deep are 50 % lower than surface concentrations (0.16 and 1.4 μmol L^{-1}, respectively) whereas DOC_{SPE} is only reduced by 39 %.

Mass spectrometry data from this and previous studies (Flerus et al., 2012; Lechtenfeld et al., 2014) provide independent measures that mixing alone might model but cannot explain complex compositional DOM dynamics. In a mixing-only scenario with two endmembers, one would expect a correlation of the peak magnitude for each observed mass with the mixing ratio (and age). Instead, we observed that only 65 % of the total peak magnitude in the mass spectra correlated with radiocarbon age, whereas 35 % was not correlated.

Although the SPE applied does not recover some of the most polar labile compounds, it does include molecules that are cycling on different time scales in the ocean, which led us to define the term "nonlabile" DOS_{SPE} (Ksionzek et al., 2016a). In the productive surface layer, this is reflected in higher methionine content, younger DOM_{SPE} radiocarbon age and unique sulfur-containing formulas. Thus, our DOS_{SPE} removal rate encompasses degradable compounds and processes that are faster than those relevant for refractory DOM alone. It should be noted that in figure 3 of (Ksionzek et al., 2016a), the removal was assigned incorrectly as "refractory" and the sulfate reservoir should be $1.2*10^9$ Tg S. Most important, the rate demonstrates that 99.9 % of the sulfur assimilated is subject to rapid cycling whereas the nonlabile DOS_{SPE} removal discussed by Dittmar et al. only represents a very minor flux (Fig. M2.1).

Dittmar et al. also claimed that persistent sulfonates dominate the DOS pool and mix conservatively in the ocean, based on a previous study using a non-quantitative method, in which steric hindrance was excluded a priori (Pohlabeln and Dittmar, 2015). Previous studies indeed identified relatively unreactive alkylsulfonates in marine DOM (Lechtenfeld et al., 2013), which are potentially derived from anthropogenic surfactants (Morales-Cid et al., 2009). However, other studies, using

independent methods, quantified additional reduced sulfur groups such as thioethers (identified as methionine in our dataset) and thiols (Al-Farawati and Van Den Berg, 2001), consistent with the fact that the amino acids methionine and cysteine are primary biogenic precursors of DOS.

Dittmar et al. overlooked that we explicitly mentioned that carbon in sulfur containing compounds most likely cycles on different time scales than bulk DOC. We are well aware that changes in radiocarbon age are likely to be faster than the time elapsed due to the removal of the labile and young DOM fraction (Lechtenfeld et al., 2014). Such a partitioning effect would have an effect on the absolute number for the net DOS removal (Fig. M2.1) but cannot support their mixing theory. On the contrary, the insight that DOS cycles faster than DOC supports the presence of a removal process.

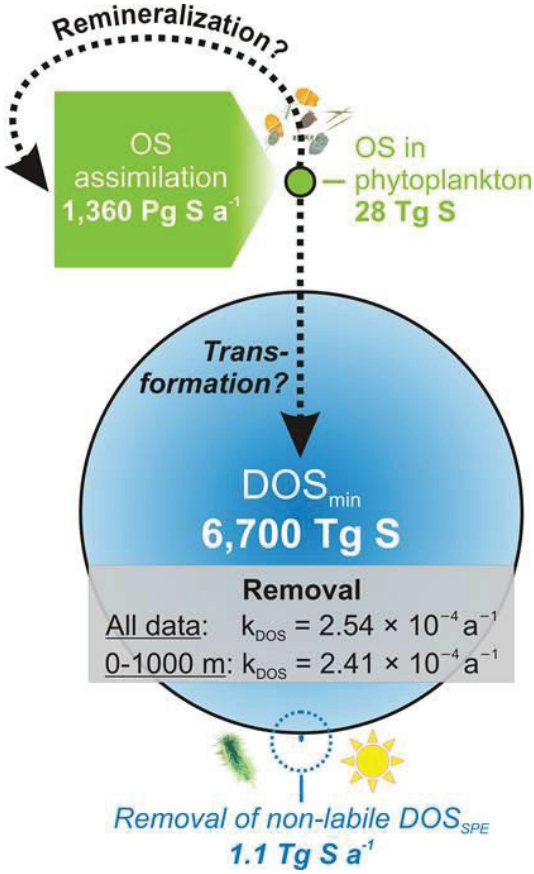

Figure M2.1. Scale representation of selected marine organic sulfur (OS) reservoirs and fluxes. Circle sizes represent the global sulfur inventory in phytoplankton and the minimum inventory of marine DOS. Squares represent annual fluxes. Removal of nonlabile DOS (within the dotted circle), represents less than one per mill of the annual sulfur assimilation by primary production (1360 Tg S year^{-1}). Calculating the removal rate for DOS above the pycnocline (<1000m), where existence of active removal is indisputable, only marginally reduces the coefficient compared to the calculation for the entire water column calculated in (Ksionzek et al., 2016a) (grey box). The major future scientific challenge is the unaddressed mineralization of organic sulfur derived from primary production and its conversion into nonlabile DOS (black dotted arrows).

Acknowledgments: This work was supported by the DFG-Research Centre / Cluster of Excellence "The Ocean in the Earth System" and a PhD grant by the Deutsche Forschungsgemeinschaft (DFG) in the framework of the priority programme "Antarctic Research with comparative investigations in Arctic ice areas" (Grant KO 2164/8-1+2).

IV.3 Manuscript 3

Stoichiometry, polarity, and organometallics in solid-phase extracted dissolved organic matter of the Elbe-Weser estuary

Kerstin B. Ksionzek[1,2,*], Jing Zhang[3], Kai-Uwe Ludwichowski[1], Dorothee Wilhelms-Dick[1], Scarlett Trimborn[1], Thomas Jendrossek[1], Gerhard Kattner[1], Boris P. Koch[1,2,4,*]

[1] Alfred Wegener Institute Helmholtz Center for Polar and Marine Research, Am Handelshafen 12, 27570 Bremerhaven, Germany.

[2] MARUM – Center for Marine Environmental Sciences, Leobener Straße, D- 28359 Bremen, Germany.

[3] State Key Laboratory of Estuarine and Coastal Research (SKLEC), East China Normal University (ECNU), 3663 Zhongshan Road North, Shanghai 200062, China

[4] University of Applied Sciences, An der Karlstadt 8, 27568 Bremerhaven, Germany.

*Corresponding authors

E-mails: Kerstin.Ksionzek@awi.de (KBK), Boris.Koch@awi.de (BPK)

Abstract

Dissolved organic matter (DOM) is ubiquitous in natural waters and plays a central role in the biogeochemistry in riverine, estuarine and marine environments. This study quantifies and characterizes solid-phase extractable DOM and trace element complexation at different salinities in the Weser and Elbe River, northern Germany, and the North Sea. Dissolved organic carbon (DOC), total dissolved nitrogen (TDN), Co and Cu concentrations were analyzed in original water samples. Solid-phase extracted (SPE) water samples were analyzed for DOC (DOC_{SPE}), dissolved organic nitrogen (DON_{SPE}), sulfur (DOS_{SPE}) and trace metal (^{51}V, ^{52}Cr, ^{59}Co, ^{60}Ni, ^{63}Cu, ^{75}As) concentrations. Additionally, different pre-treatment conditions (acidification vs. non-acidification prior to SPE) were tested. In agreement with previous studies, acidification led to generally higher recoveries for DOM and trace metals. Overall, higher DOM and trace metal concentrations and subsequently higher complexation of trace metals with carbon and sulfur-containing organic complexes were found in riverine compared to marine samples. With increasing salinity, the concentrations of DOM decreased due to estuarine mixing. However, the slightly lower relative decrease of both, DOC_{SPE} and DON_{SPE} (~77 %) compared to DOS_{SPE} (~86 %) suggests slightly faster removal processes for DOS_{SPE}. A similar distribution of trace metal and carbon and sulfur containing DOM concentrations with salinity indicates complexation of trace metals with organic ligands. This is further supported by an increase in Co and Cu concentration after oxidation of organic complexes by UV treatment. Additionally, the complexation of metals with organic ligands (analyzed by comparing metal/DOC_{SPE} and metal/DOS_{SPE} ratios) decreased in the order Cu > As > Ni > Cr > Co and thus followed the Irving-Williams order. Differences in riverine and marine trace metal containing DOM_{SPE} are summarized by their average molar ratios of $(C_{107}N_4P_{0.013}S_1)_{1000}V_{0.05}Cr_{0.33}Co_{0.19}Ni_{0.39}Cu_{3.41}As_{0.47}$ in the riverine endmember and $(C_{163}N_7P_{0.055}S_1)_{1000}V_{0.05}Cr_{0.47}Co_{0.16}Ni_{0.07}Cu_{4.05}As_{0.58}$ in the marine endmember.

Introduction

Dissolved organic matter (DOM) is actively cycling in natural waters and participates in most biogeochemical processes. Assessment of the DOM stoichiometry supports to unravel its origin and fate and to understand its role in different aquatic environments. The biogeochemistry of marine dissolved organic carbon, nitrogen and phosphorus (DOC/N/P) was extensively studied in the past, e.g. (Hansell and Carlson, 2002; 2015). In contrast, the knowledge on quantity, distribution, and the biogeochemical role of dissolved organic sulfur (DOS) in aquatic environments is limited, though not less important. We have previously estimated the global marine DOS inventory to range between 6.7 and 18.6 Pg S (Ksionzek et al., 2016a). In particular, rivers are known to be important sources of reduced carbon, nitrogen and phosphorus to coastal environments (Raymond and Spencer, 2015). Riverine DOM can be influenced by different transformation and removal processes along its way into

estuarine and marine water: salt-induced flocculation (Abdulla et al., 2010; Asmala et al., 2012), adsorption to particulate matter (Gogou and Repeta, 2010; Kaiser and Guggenberger, 2000), photo-oxidative remineralization (Miller and Moran, 1997), and uptake by heterotrophs (Elifantz et al., 2007; Sepers, 1977). Thus, typical concentrations of DOC and DON decrease over a salinity gradient from riverine to marine water (Abril et al., 2002; Cai et al., 2012). DOC/DON ratios usually also decrease from land to sea along the salinity gradient in estuaries (Ylöstalo et al., 2016) indicating differences in the stoichiometry of the organic matter precursors. In our previous study, we used existing literature and roughly estimated that the riverine transport of organic sulfur in particulate (POS) and dissolved form combined is about 0.25 Tmol S a^{-1} (8 Tg S a^{-1}) (Ksionzek et al., 2016a). In estuarine and marine environments, the concentration of sulfate (up to 29 mmol S L^{-1}) exceeds the concentration of DOS by up to five orders of magnitude. As the analysis of DOS has been analytically hampered, the composition and biogeochemistry of DOS remains widely unknown. Several studies focused primarily on volatile organic sulfur compounds, such as dimethylsulfide (DMS) and carbonyl sulfide (COS), because they are actively involved in climate processes (Bentley and Chasteen, 2004; Charlson et al., 1987; Lomans et al., 2002). However, those climate relevant organic sulfur compounds contribute less than 3 % to the total marine DOS pool (Ksionzek et al., 2016a).

Other organic sulfur compounds, such as sulfides and thiols, play an important role as ligands for organic metal complexes (Smith et al., 2002). Thiols build strong complexes with copper and account for a major part of the copper complexing ligand pool in surface seawater (Laglera and van den Berg, 2003; Vraspir and Butler, 2009). Silver and mercury are also known to bind strongly with organic sulfur species (Bell and Kramer, 1999; Ravichandran, 2004). Organic metal-complexing ligands can thus affect the mobility, toxicity, and bioavailability of several trace metals. Some metals or metalloids in aquatic ecosystems, such as As, Co, Cu, Cr, Ni, and V are essential micronutrients to support biological processes (Driscoll et al., 1994; Kolber et al., 1994; Twining and Baines, 2013; Twining et al., 2004), e.g Cu, Co, and Ni are essential for growth and control of marine phytoplankton populations (Sunda, 2012). This has also an indirect effect on bioproductivity, species composition and, in the long term, food web dynamics. However, in high concentrations, these metals can also cause toxic effects (Driscoll et al., 1994; Paytan et al., 2009). Reduced toxicity was found for some trace metals (e.g. Cu, Pb, Cd) in case of higher DOM complexation rates (De Schamphelaere et al., 2004; Schwartz et al., 2004). Moreover, trace metals can not only trigger the active production of organic ligands but also contribute to their persistence in surface waters: trace-metal complexation has a protective effect against oxidation of DOM-thiol groups (Hsu-Kim, 2007), whereas the production of copper-binding thiols is enhanced with increasing copper-levels (Croot et al., 2000; Dupont and Ahner, 2005; Dupont et al., 2004; Moffett and Brand, 1996). Besides quantity, the quality of DOM plays also an equally important role for trace metal complexation (Baken et al., 2011). Baken et al. found that increasing aromaticity lead to a higher trace metal affinity of DOM, indicating that aromatic humic substances can

act as major metal chelators (Baken et al., 2011). Matar et al. analyzed the influence of organic matter polarity on trace metal speciation and bioavailability and revealed that the hydrophobic DOM fraction has a lower binding capacity for Cu than the hydrophilic fraction, suggesting lowered Cu bioavailability in presence of hydrophilic DOM (Matar et al., 2013). Although DOM interactions with metals and the distribution and cycling of organic metal complexes are a growing field of interest, the influence of DOM and specifically of DOS compounds on transport, kinetics, bioavailability and toxicity of trace metals remains largely unknown.

Here we present results on the composition and distribution of DOM at different salinities sampled from the rivers Weser and Elbe in northern Germany to the marine waters of the North Sea. Our aim is to improve our knowledge on distribution and composition of organically bound trace metals. The major research questions/hypotheses are:

i. What is the concentration of solid-phase extractable DOS (DOS_{SPE}) in the rivers Elbe and Weser and how does it change with salinity? How does the stoichiometry (molar elemental ratios) of solid-phase extractable DOM (DOM_{SPE}) change with salinity within the Elbe-Weser-Estuary?
ii. Since some sulfur species, such as thiols, are known as trace-metal ligands, we hypothesize that the amount of organically-bound trace metals correlates with the relative contribution of DOS and DOM. Consequently, changes in DOM concentration with salinity should also be reflected in trace metal concentrations.
iii. How does DOM polarity change along the estuary and is this change connected to dissolved/complexed trace element concentrations?
iv. What is the influence of salinity and different sample pre-treatment conditions (pH 2 versus pH 8 extraction) on DOM and associated trace element composition?

Materials and Methods

Sample collection and processing

Six surface water samples were collected in June and July 2014 from Rivers Weser and Elbe, northern Germany (salinity ~0), and in the Southern North Sea (salinity ~33, Fig. M3.1, Table M3.1). The marine water sample (M1) and samples from the Elbe Estuary (E2, E3) were collected with a rosette sampler connected to a conductivity, temperature, and depth sensor (CTD) (expedition HE426 of *R/V Heincke*). In total, 36 CTD stations were performed to analyze background parameters, such as temperature and salinity. Other riverine samples from River Elbe (E1) and River Weser (W1, W2) were collected manually in glass bottles. Temperature, conductivity, and pH were measured in situ with a sensor (Cond 340i, WTW). No specific permissions were required for sampling and the field studies did not involve endangered or protected species. The sample processing workflow is presented in Fig. M3.2. All samples were filtered through pre-combusted GF/F filters (Whatman, 450 °C, 5 h, 0.7 µm

nominal pore size) with a maximum pressure < 200 mbar. Aliquots for DOC and nutrient analyses were stored at -20 °C in pre-cleaned high-density polyethylene (HDPE) bottles. Filtered water was either acidified to pH 2 (hydrochloric acid, suprapur, Merck) or processed without acidification (pH ~8). SPE was applied for DOM enrichment and desalting (Dittmar et al., 2008) and for each sample 500 mL of filtered water (pH 8 and pH 2) was extracted (PPL, 200 mg, Mega Bond Elut, Varian) in quadruplicates and each eluted with ~1 mL methanol (LiChrosolv, Merck; exact volume was determined by weighing) into pre-combusted glass vials. After extraction, DOM_{SPE} was stored at -20 °C until further analysis.

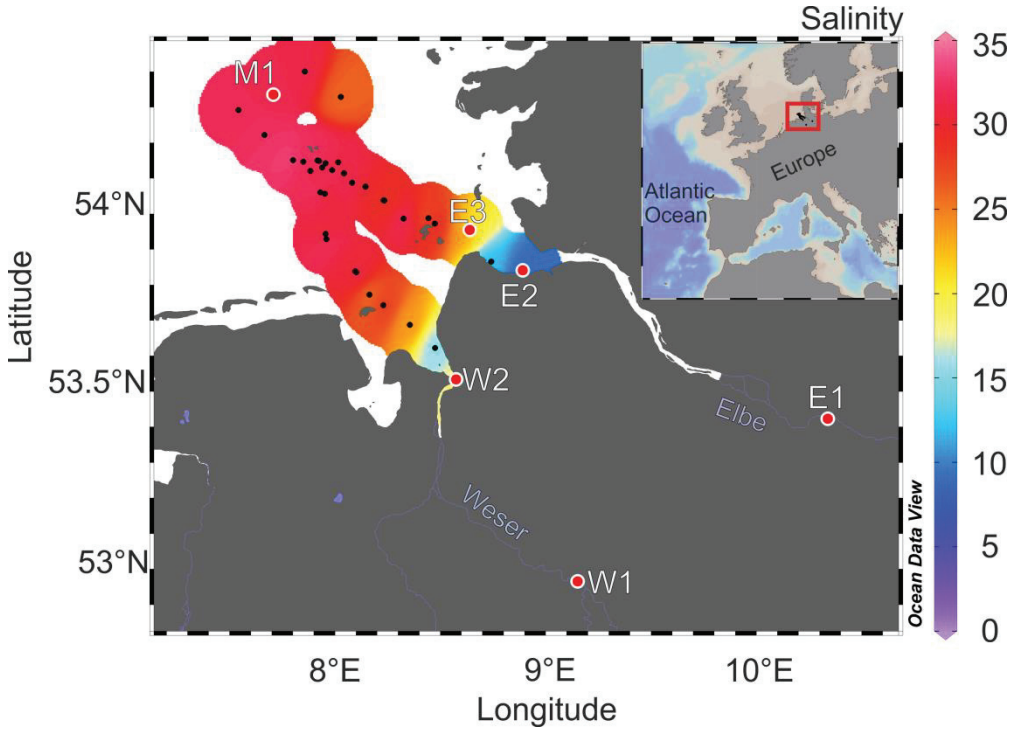

Fig M3.1. Map of sampling area. Sampling locations are marked as red dots, colors represent the surface salinity. Black dots represent stations, at which temperature and salinity were measured (Koch and Rohardt, 2016).

Table M3.1. Sampling locations and hydrographic conditions

Sample	Location	Date	Salinity	Temperature (°C)	Category
W1	52.965°N, 9.152°E	12.06.2014	0	21.1	Riverine endmembers
E1	53.423°N, 10.339°E	17.07.2014	0.27	22.6	
E2	53.841°N, 8.89167°E	14.06.2014	9.4	18.4	Estuarine samples
E3	53.95483°N, 8.6395°E	14.06.2014	17.4	17.9	
W2	53.534°N, 8.575°E	07.07.2014	18.1	19.5	
M1	54.3355°N, 7.7075°E	15.06.2014	32.9	12.8	Marine endmember

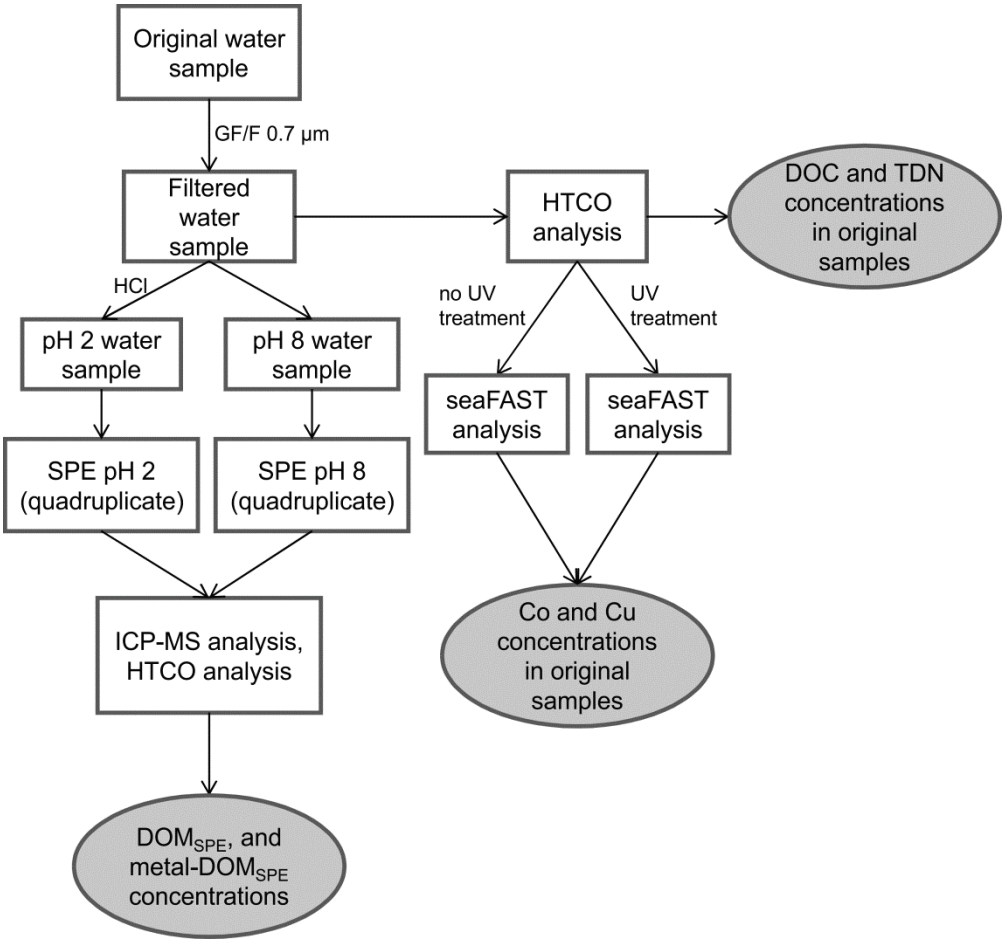

Fig M3.2. Sample processing workflow. The sample processing steps are represented as white boxes. Measured parameters are specified in grey boxes. DOC and total dissolved nitrogen (TDN) in original water samples were analyzed by high temperature catalytic oxidation (HTCO). The seaFAST analysis was used to determine Co and Cu concentrations in the original filtered water samples. Aliquots of original filtered water samples were solid-phase extracted in quadruplicates for each acidified and non-acidified sample. DOC and DON in solid-phase extracts (DOC_{SPE}, DON_{SPE}) were analyzed by HTCO. All other elements were analyzed by inductively coupled plasma mass spectrometry (ICP-MS).

DOC, TDN and DON analysis

Concentrations of DOC and total dissolved nitrogen (TDN) in filtered water were determined by high temperature catalytic oxidation (HTCO) and subsequent nondispersive infrared spectroscopy and chemiluminescence detection (TOC-VCPN analyzer, Shimadzu). For the determination of solid-phase extractable DOC (DOC_{SPE}, pH 2 and pH 8) and DON (DON_{SPE}, pH 2), 50 µL (250 µL for DON_{SPE}, pH 8) of each methanol extract was evaporated under N_2 and subsequently redissolved in 6.5 mL ultrapure water. All samples were acidified in the auto sampler (0.1 M HCl suprapur, Merck) and purged with O_2 for > 5 min to remove inorganic carbon. Performance of the instrument was recorded by the analysis of potassium hydrogen phthalate standard solutions and the deep-sea reference samples (DSR, Hansell research lab). Final DOC and TDN concentrations are average values of triplicate measurements. If the standard variation or the coefficient of variation of DOC values exceeded 0.1 µM or 1 %, respectively, up to two additional analyses were performed and outliers were eliminated. For DON, outliers of triplicate measurements were eliminated manually. The accuracy was ± 5 % for DOC and ± 7 % for DON.

ICP-MS analysis

For quantification of DOS_{SPE}, DOP_{SPE} and trace elements (^{51}V, ^{52}Cr, ^{59}Co, ^{60}Ni, ^{63}Cu, ^{75}As), an inductively coupled plasma mass spectrometer (ICP-MS, Element 2, Thermo Fisher Scientific) was equipped with a desolvation nebulizer (Apex Q, Elemental Scientific), a platinum guard electrode, and nickel sampler and skimmer cones. Prior to ICP-MS analysis, 50 µL of the extract was evaporated with N_2 gas and redissolved in 2 mL nitric acid (1 M, bidestilled, Merck). 50 µL of ^{103}Rh (50 ppb in the spike solution) were added as internal standard. The samples were sonicated for 10-15 min to ensure that all DOM was redissolved. The instrument was tuned daily for optimized plasma conditions and accurate mass calibration with a multi-element tuning solution (~0.1 ppb in MilliQ). Signals of ^{32}S and ^{75}As were recorded in a resolution of 4000 m/Δm, whereas all other elements were recorded in a resolution of 2000m/Δm, for which the instrument was modified to achieve a flat top peak shape (higher precision). Nitric acid (1 M, double destilled, Merck) was used for analysis blank. If the blank values for SPE were higher than the limit of detection (LOD), the extract concentrations were corrected for the respective blanks. Calibration standards for trace elements were prepared in concentrations of 0.001, 0.01, 0.05, 0.1, 0.5, 1, 5, 10, 50, 100, and 250 µg L^{-1} from a stock solution (100 mg L^{-1}, multi-element-standard, nonmetals, Spetec). Limits of detection (according to the German industry standard; DIN 32645) are given in S1 Table.

Trace element analysis of filtered seawater samples

We analyzed ^{59}Co and ^{63}Cu in original (filtered) water samples. All labware used for analysis was pre-cleaned according to Dick et al. (2008). Samples for dissolved trace metal analysis were acidified to pH

1.75 using bidistilled HNO_3. As organic ligands form complexes with Co and Cu which are relatively blind to the chelating resin and therefore pass through it without being extracted, one half of each sample was UV digested to analyze the total amount of Co and Cu (Biller and Bruland, 2012). For UV digestion, samples were filled into pre-cleaned PFA bottles and UV-oxidized for 1.5 h using a 450 W photochemical UV power supply from ACE GLASS (photochemical lamp number 7825; Power Supply number 7830). Two procedural blanks were processed the same way. Prior to analysis, each sample was spiked with Indium as internal standard (final concentration 1 ppb). The multi-element analyses of water samples were performed using a seaFAST system (Elemental Scientific Inc.) as described in Hathorne et al. (2012) coupled to ICP-MS (Element 2, Thermo Fisher Scientific). The ICP-MS was optimized every day to achieve oxide forming rates below 0.3 %. The ICP-MS was modified to achieve a flat top peak shape (higher precision) with a resolution of R = 2000. Quantification limits are 0.35 ng L^{-1} for ^{59}Co and 7.35 ng L^{-1} for ^{63}Cu. To assess the accuracy and precision of the method, the NASS-6 reference standard was analyzed in a 1:2 dilution at the beginning, in between and at the end of a batch run (n=5). For Cu, we found 208 ng L^{-1} with a relative standard deviation of 1.5 % (certified 248 ± 25 ng L^{-1}). The Student *t*-Test was used to compare our values to the certified ones (n = 5, 99 % significance level) and showed no significant difference. Within the GeoRem database Takano et al. reported Cu concentrations of 224 ng L^{-1}, which is in agreement with our findings (Jochum et al., 2005; Takano et al., 2013). Co is not certified for the NASS-6 standard. For this, only an indicative value is given in the certificate (15 ng L^{-1}). We found 11.2 ng L^{-1} with a precision of 0.6 %.

RP-HPLC analysis

Reversed phase high performance liquid chromatography (RP-HPLC) was performed on a LaChrom Elite™ HPLC-system (Hitachi) equipped with a pump (L-2130), autosampler (L-2200), column oven (L-2300), diode array detector (DAD, L-2450, 210 nm) and fluorescence detector (L-2485; excitation: 260 nm, emission: 430 nm) according to Koch et al. (2008). Of each methanol extract, 100 µL extract were diluted with 400 µL ultrapure water. Original water samples were analyzed without any pre-treatment. For each analysis, 30 µL of the methanol extract and 95 µL of original samples were injected respectively. The separation based on polarity (and molecular size) was performed using a reversed-phase column (4µm Hydro-RP 80 Å, 250 x 4.60 mm; Phenomenex, Synergi) and a solvent gradient (0 to 70 min) from 100 % ultrapure water (adjusted with low-concentrated NaOH (Merck, suprapur) to pH 7) to 100 % methanol (Merck, LiChrosolv, Table M3.2). Analysis blanks were performed with 100 µL methanol and 400 µL ultrapure water for the analysis of the extracts and ultrapure water only for the analysis of the original samples respectively. Peak areas of the samples were corrected for the respective blanks. Based on RP-HPLC analyses, we differentiated two major DOM_{SPE} fractions: the polar water-soluble fraction with a retention time < 24 min and the non-polar methanol soluble fraction with a retention time > 24 min. We calculated polar/non-polar ratios

($DOC_{pol}/DOC_{non-pol}$) to elucidate changes in DOM polarity with changing salinity. Since nitrate and nitrite can absorb in the DAD_{210nm} range, only fluorescence data were used for the evaluation of the DOM polarity characteristics in the original samples.

Table M3.2. Gradient for the chromatographic run. Water (adjusted to pH 7) and methanol were used as eluents.

Time [min]	Water [%]	Methanol [%]	Flow rate [mL min^{-1}]
0	100	0	0.2
6	100	0	0.2
20	0	100	0.4
35	0	100	0.4
45	100	0	0.3
55	100	0	0.2
65	100	0	0.2

Data evaluation and statistical analysis

Outliers in quadruplicate measurements of DOM_{SPE} concentrations were defined by Grubbs Test with a significance level of $\alpha = 0.5$. Statistical analysis was performed with the software *R*: Analysis of variances between the riverine (E1, W1) and marine (M1) endmember samples) was performed with Mann-Whitney-U-Test (function "wilcoxon.test" in the software *R*). Correlation of changing DOM, DOM_{SPE} and metal-DOM_{SPE} concentrations, respectively, with changing salinity was analyzed using correlation analysis (function "cor.test" in *R*). The variables were not manipulated prior to statistical analysis.

Results

Changes in DOM concentration and stoichiometry

The original DOC and TDN concentrations in the water samples decreased with increasing salinity from a maximum of 407 μmol L^{-1} and 190 μmol L^{-1}, respectively, in riverine water (W1) to 293 μmol L^{-1} DOC and 101 μmol L^{-1} TDN in estuarine water (E3), and 97 μmol L^{-1} DOC and 14 μmol L^{-1} TDN in the marine sample (M1; Fig. M3.3, Table M3.3).

For DOM_{SPE}, significantly higher concentrations were found for all elements in samples extracted at pH 2 compared to those extracted at pH 8 ($p < 0.001$). Therefore, this section focusses on the results of pH 2 extracts. Data on pH 8 extracts can be found in Tables M3.3 and M3.4.

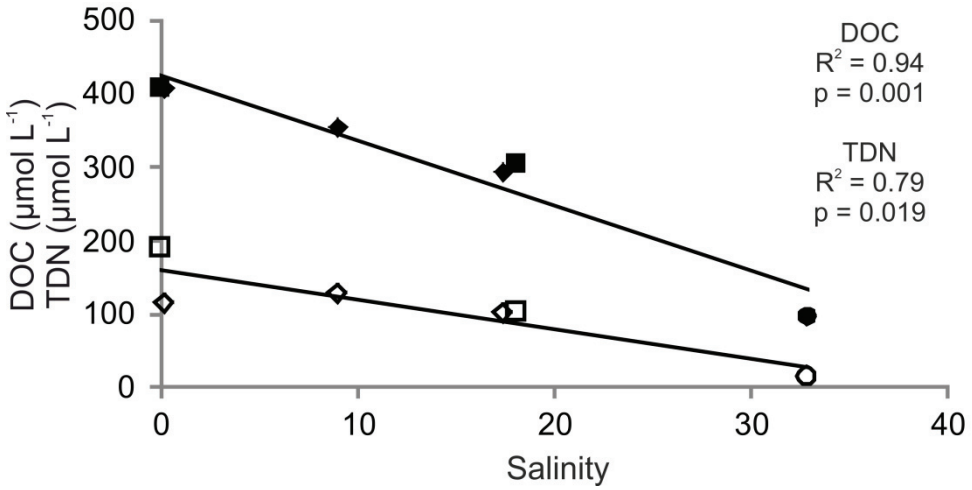

Fig M3.8. Changes of DOC (filled symbols) and TDN (unfilled symbols) concentrations of original water samples with salinity. Symbols represent sampling locations: River Weser (W1, W2; squares), River Elbe (E1 - E3; diamonds) and the marine station (M1; circles).

DOC_{SPE} concentrations of pH 2 extracted samples decreased significantly from 144 ± 4 µmol L^{-1} in the riverine endmember (W1) to 31 ± 1 µmol L^{-1} in the marine endmember sample (M1) ($p < 0.01$, Table M3.3). Using the DOC concentrations in the original samples and the DOC_{SPE} concentration, we calculated the DOC extraction efficiencies. The average DOC extraction efficiencies at pH 2 were 36 ± 2 %. No significant correlation of the extraction efficiency with salinity was found ($p > 0.05$).

DON_{SPE} concentrations of pH 2 extracted samples decreased significantly with increasing salinity from 6.3 ± 0.1 µmol L^{-1} in riverine water (E1) to 1.4 ± 0.0 µmol L^{-1} in seawater (M1) ($p = 0.01$). Differences of the average molar DOC_{SPE}/DON_{SPE} ratios of 24 ± 1 and 23 ± 1 were insignificant between pH 2 extracted riverine (E1, W1) and marine (M1) endmember (for pH 8 extracted samples however, they decreased significantly from 25 ± 1 to 22 ± 1 in riverine (E1, W1) and marine (M1) samples ($p = 0.01$)).

Similar to DOC_{SPE} and DON_{SPE}, concentrations of DOS_{SPE} and DOP_{SPE} were higher in pH 2 than in pH 8 extracted samples ($p < 0.001$, Table M3.3). DOS_{SPE} concentrations of pH 2 samples decreased significantly from 1.44 ± 0.02 µmol L^{-1} in riverine (E1) to 0.19 ± 0.02 µmol L^{-1} in marine water ($p = 0.01$). To address the influence of mixing of low and high salinity waters, we normalized DOS_{SPE} and DOP_{SPE} concentrations to DOC_{SPE} concentrations and thus calculated molar DOC_{SPE}/DOS_{SPE} ratios and DOC_{SPE}/DOP_{SPE} ratios, respectively. Average DOC_{SPE}/DOS_{SPE} ratios of pH 2 extracted riverine waters (E1, W1) were 103 ± 5 and increased to 162 ± 17 in the marine sample ($p = 0.01$). No differences in molar DOC_{SPE}/DOS_{SPE} ratios were found between pH 2 and pH 8 extracted samples.

Compared to DOS_{SPE}, DOP_{SPE} concentrations of pH 2 samples were two orders of magnitude lower and decreased significantly from 20.7 ± 0.7 nmol L^{-1} to 10.5 ± 2.1 nmol L^{-1} in riverine (E1) and marine water, respectively ($p < 0.001$). Molar DOC_{SPE}/DOP_{SPE} ratios of pH 2 extracted samples decreased significantly from riverine to marine water ($p < 0.01$).

Thus, average molar C:N:P:S ratios of pH 2 extracted samples were $C_{106}:N_4:P_{0.013}S_1$ for the riverine endmember (W1) and $C_{164}:N_7:P_{0.053}S_1$ for the marine endmember.

Changes in DOM polarity

Using reversed-phase chromatography, we found a good relationship of both fluorescence (260/430 nm) and absorption (210 nm) data (total peak areas) with measured DOC and DOC_{SPE} concentrations ($R^2 = 0.3$ and $p < 0.01$ for DOC concentrations of 0 - 40 µmol L^{-1} versus UV peak areas and $R^2 = 0.6$ and $p < 0.001$ for DOC concentrations > 100 µmol L^{-1} versus UV peak areas, M3.S1 Fig), confirming that UV absorption in the extracts serves as a suitable predictor of DOC concentration (Lechtenfeld et al., 2011). Lechtenfeld et al. (2011) showed that this correlation can also be found in individual chromatographic fractions. In this section, we will use integrated peak areas of fluorescence / adsorption as a proxy for DOC_{SPE} concentration.

Fluorescence data for the original samples confirmed decreasing DOC concentrations (peak areas) with increasing salinity (not shown). For the solid-phase extracted DOM, we found a significant linear correlation of decreasing polar peak areas with increasing salinity ($R^2 = 0.9$; $p < 0.01$), whereas no significant trend was found for non-polar peak areas. Hence, $DOC_{pol}/DOC_{non\text{-}pol}$ ratios significantly decreased with increasing salinity ($R^2 = 0.7$, $p = 0.035$).

In addition, absorption (Fig. M3.4) and fluorescence data (not shown) confirmed significantly higher DOC concentrations in pH 2 compared to pH 8 extracted samples ($p < 0.001$).

Absorption data showed significantly higher DOC_{SPE} concentrations (peak areas) at low salinity compared to high salinity samples ($p < 0.01$, Fig. M3.4). However, the DOC_{SPE} concentration (peak areas) in the estuarine samples E3 and W3 (salinity of 17.4 and 18.1, respectively) were similar to sample E2 at salinity 9.4 and thus deviated from the linear regression line ($R^2 = 0.96$, $p < 0.001$). For all extracts, the ratio of DOC derived from polar compounds compared to the total DOC concentration (DOC_{pol}/DOC_{tot}) was significantly higher in pH 2 compared to pH 8 samples ($p < 0.001$). In pH 2 extracted samples, DOC_{pol}/DOC_{tot} of 0.25 ± 0.02 in riverine samples (W1, E1) was significantly higher compared to 0.06 ± 0.02 % in marine samples ($p < 0.01$). Consequently, we observed a significant decrease of $DOC_{pol}/DOC_{non\text{-}pol}$ in pH 2 samples from 0.36 ± 0.03 in riverine water (W1) to 0.07 ± 0.02 in marine water ($p = 0.01$, Fig. M3.5A), whereas no significant changes in pH 8 samples occurred. However, if we focus on Elbe samples only, we observed a relative increase of $DOC_{pol}/DOC_{non\text{-}pol}$ ratios in estuarine water (Fig. M3.5A).

Table M3.3. Average DOM_{SPE} concentrations and molar DOC_{SPE}/DON_{SPE}, DOC_{SPE}/DOP_{SPE}, DOC_{SPE}/DOS_{SPE} ratios at the stations with different salinities. The values are averages of quadruplicate measurements (except of DOC and TDN). Stations are ordered by increasing salinity.

Sample	W1		E1		E2		E3		W2		M1	
Salinity	0		0.3		9		17.4		18.1		32.9	
DOC (µmol L^{-1})	407		407		354		293		304		97	
TDN (µmol L^{-1})	190		114		130		101		102		14	
pH	2	8	2	8	2	8	2	8	2	8	2	8
DOC_{SPE} (µmol L^{-1})	144 ± 4	37 ± 1	143 ± 6	31 ± 1	138 ± 2	33 ± 1	109 ± 4	28 ± 1	116 ± 2	30 ± 1	31 ± 1	10 ± 1
DON_{SPE}(µmol L^{-1})	5.9 ± 0.2	1.4 ± 0.1	6.3 ± 0.1	1.3 ± 0.0	9.4 ± 0.1	1.4 ± 0.1	5.7 ± 0.4	1.2 ± 0.1	5.3 ± 0.3	1.4 ± 0.2	1.4 ± 0.0	0.5 ± 0.1
DOC_{SPE}/DON_{SPE}	25 ± 1	26 ± 2	23 ± 1	24 ± 0	15 ± 0	24 ± 1	19 ± 1	25 ± 2	22 ± 1	23 ± 2	23 ± 1	20 ± 3
DOS_{SPE} (µmol L^{-1})	1.35 ± 0.10	0.35 ± 0.03	1.44 ± 0.02	0.30 ± 0.01	1.39 ± 0.10	0.34 ± 0.01	1.80 ± 0.59-	0.43 ± 0.12	0.89 ± 0.02	0.28 ±0.01	0.19 ± 0.02	0.14 ± 0.03
DOC_{SPE}/DOS_{SPE}	107 ± 5	110 ± 11	100 ± 3	105 ± 1	100 ± 6	98 ± 2	70 ± 26	71 ± 17	131 ± 4	109 ± 2	162 ± 17	80 ± 15
DOP_{SPE} (nmol/L)	17.1 ± 1.7	5.3 ± 0.5	20.7 ± 0.7	12.4 ± 0.3	14.8 ± 0.9	6.5 ± 0.6	17.3 ±1.8	6.9 ± 0.3	18.0± 0.2	6.4 ± 0.2	10.5 ± 2.1	5.2 ± 1.6
DOC_{SPE}/DOP_{SPE} *10^3	8.5 ± 0.8	7.2 ± 0.4	7.0 ± 0.4	2.4 ± 0.1	9.4 ± 0.6	5.3 ± 0.5	6.4 ± 0.6	4.2 ± 0.1	6.5 ± 0.2	4.9 ± 0.1	3.1 ± 0.5	2.2 ± 0.5

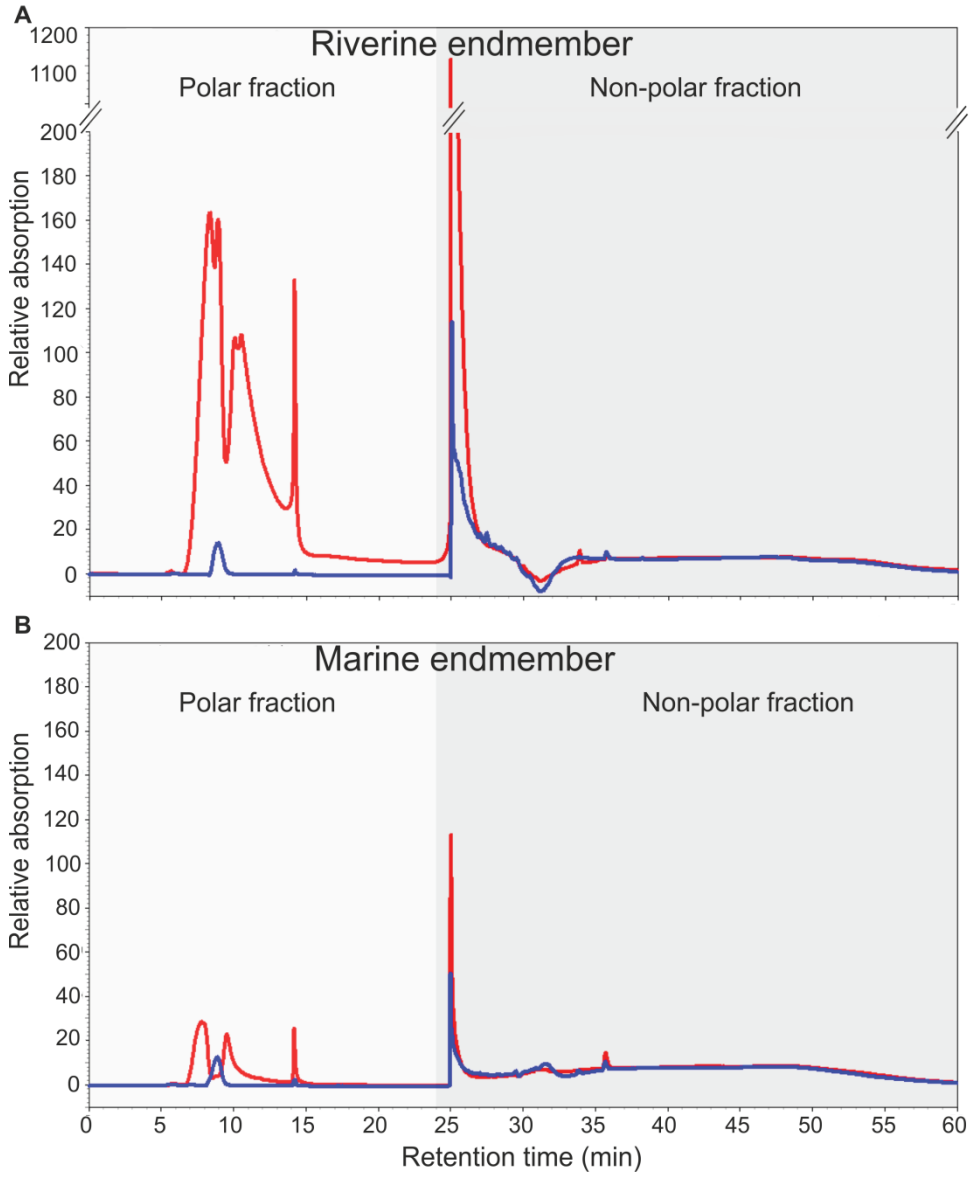

Fig. M3.4. UV absorption chromatograms of riverine and marine methanol extracts at 210 nm. (A) Chromatograms of riverine pH 2 (red) and pH 8 (blue) extracted samples. (B) Chromatograms of marine pH 2 (red) and pH 8 (blue) extracted samples.

Fluorescence data showed that DOC_{SPE} concentrations (peak areas) of both pH 2 and pH 8 extracted samples decreased with increasing salinity ($p < 0.001$). Overall, DOC_{pol}/DOC_{tot} of 0.68 ± 0.07 in pH 2 samples was significantly higher compared to 0.03 ± 0.01 in pH 8 samples ($p < 0.001$). DOC_{pol}/DOC_{tot} in both pH 2 and pH 8 extracted samples decreased significantly with increasing salinity ($p < 0.001$). This results in a significant increase in $DOC_{pol}/DOC_{non\text{-}pol}$ of 1.7 ± 0.2 to 2.1 ± 0.3 in pH 2 extracted riverine and marine samples, respectively, and from 0.01 ± 0.002 to 0.04 ± 0.01 in pH 8 extracted riverine and marine samples, respectively (Fig. M3.5B). Comparing the concentration of non-polar DOC ($DOC_{non\text{-}pol}$) between pH 2 and pH 8 samples, it is noteworthy that in pH 8 samples, $DOC_{non\text{-}pol}$ was only about half of the value in pH 2 samples. By contrast, the contribution of the $DOC_{non\text{-}pol}$ pool to the absorbance of pH 2 or pH 8 extracted samples was similar.

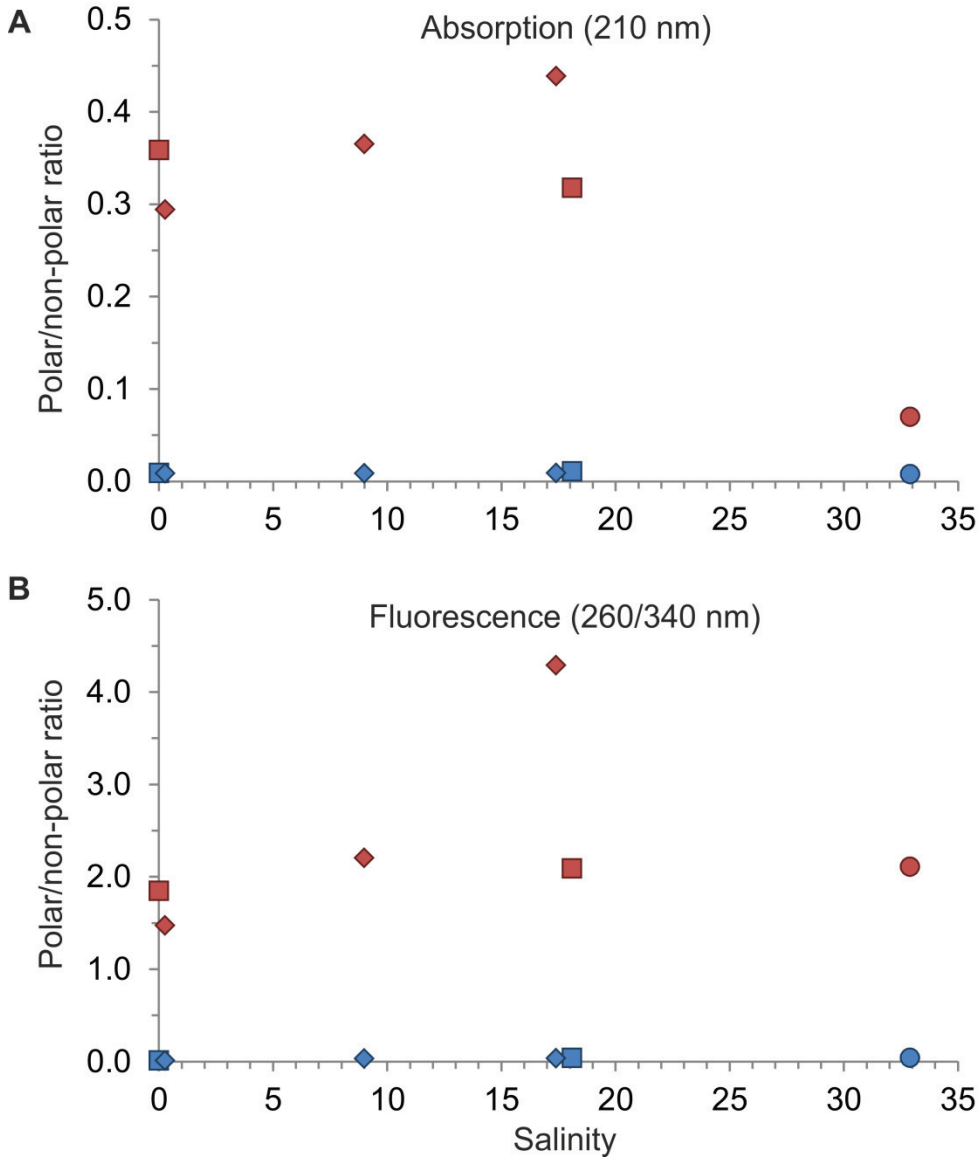

Fig M3.5. Changes in polar/non-polar peak area ratios of DOM_{SPE} samples with salinity changes. (A) Average polar/non-polar peak area ratios analyzed by UV spectroscopy (DAD_{210nm}) versus salinity and (B) average polar/non-polar peak area ratios analyzed by fluorescence spectroscopy (260/340 nm) versus salinity. The pH 2 extracted samples are indicated by red symbols, pH 8 extracted samples by blue symbols. Symbols represent sampling locations: River Weser (W1, W2; squares), River Elbe (E1 - E3; diamonds) and the marine station (M1; circles).

Trace metals

Concentrations of solid-phase extractable trace metals (metal-DOM_{SPE}) were generally higher in pH 2 compared to pH 8 extracts, with the exception of Ni-DOM_{SPE}. In pH 2 extracted samples, Co-DOM_{SPE}, Ni-DOM_{SPE}, Cu-DOM_{SPE}, and Cr-DOM_{SPE} concentrations decreased with increasing salinity, similar to DOC_{SPE} and DOS_{SPE} (Table M3.4). Although riverine Cu-DOM_{SPE} was significantly higher than in the marine sample ($p < 0.05$), we found a concentration maximum at E2 followed by a decrease with increasing salinity. V-DOM_{SPE} concentrations also increased in estuarine waters, followed by a

decrease in the high salinity marine water, but were highly distributed over all samples. Also, Cr-DOM_{SPE} concentrations were highly distributed. Nevertheless, we could also observe a significant decrease with increasing salinity over all Cr-DOM_{SPE} samples ($p < 0.01$). No significant differences between riverine and marine endmember concentrations were found for As-DOM_{SPE} and V-DOM_{SPE}. Process blanks were below the detection limit for Co-DOM_{SPE}, Ni-DOM_{SPE}, and Cu-DOM_{SPE}. Blanks for As-DOM_{SPE}, Cr-DOM_{SPE}, and V-DOM_{SPE} were measurable and about factor 2.0 – 5.8 lower for riverine and estuarine samples and by factor 1.2 - 2.4 lower for marine samples compared to the corresponding metal-DOM_{SPE} concentrations in the samples. To facilitate the subsequent comparison of the relative metal and sulfur content in DOM, we used C/metal ratios (similar to C/S ratios).

Similar to DON_{SPE}, DOP_{SPE} and DOS_{SPE}, the concentrations of metal-DOM_{SPE} were normalized to DOC_{SPE} (Table M3.4). The decrease in Co-DOM_{SPE} and Ni-DOM_{SPE} concentrations with increasing salinity was a more sensitive function of salinity than that of DOC_{SPE} decrease, resulting in a significant linear increase of the molar DOC_{SPE}/Co-DOM_{SPE} ($p < 0.01$) and DOC_{SPE}/Ni-DOM_{SPE} ratios ($p = 0.01$ Fig. M3.6). In contrast, DOC_{SPE}/As-DOM_{SPE} ratios decreased significantly with increasing salinity ($p < 0.01$). No significant differences between riverine and marine samples were found for DOC_{SPE}/Cr-DOM_{SPE}, DOC_{SPE}/Cu-DOM_{SPE} and V-DOM_{SPE}.

In pH 8 extracted samples, most concentrations of As-DOM_{SPE} and V-DOM_{SPE} were below the detection limit (LOD; cf. Table M3.4). Additionally, a high variance in quadruplicate measurements was found for the low concentrations of all trace metals in the marine samples, therefore those results were excluded from further discussion. Data of metal-DOM_{SPE} concentrations and DOC_{SPE}/metal-DOM_{SPE} ratios of pH 8 extracts can be found in Table M3.4.

To verify if DOS_{SPE} correlates with trace metals, we plotted DOC_{SPE}/metal-DOM_{SPE} ratios versus DOC_{SPE}/DOS_{SPE} ratios of pH 2 extracted samples (Fig. M3.7). We observed a significant negative linear correlation of DOC_{SPE}/As-DOM_{SPE} ($R^2 = 0.28$, $p = 0.01$) with DOC_{SPE}/DOS_{SPE} and a positive linear correlation for DOC_{SPE}/Co-DOM_{SPE} ($R^2 = 0.17$, $p = 0.05$). DOC_{SPE}/Cr-DOM_{SPE}, DOC_{SPE}/V-DOM_{SPE}, DOC_{SPE}/Ni-DOM_{SPE}, and DOC_{SPE}/Cu-DOM_{SPE} showed no correlation with DOC_{SPE}/DOS_{SPE} (Fig. M3.7). For pH 8 extracted samples, no significant correlation was found.

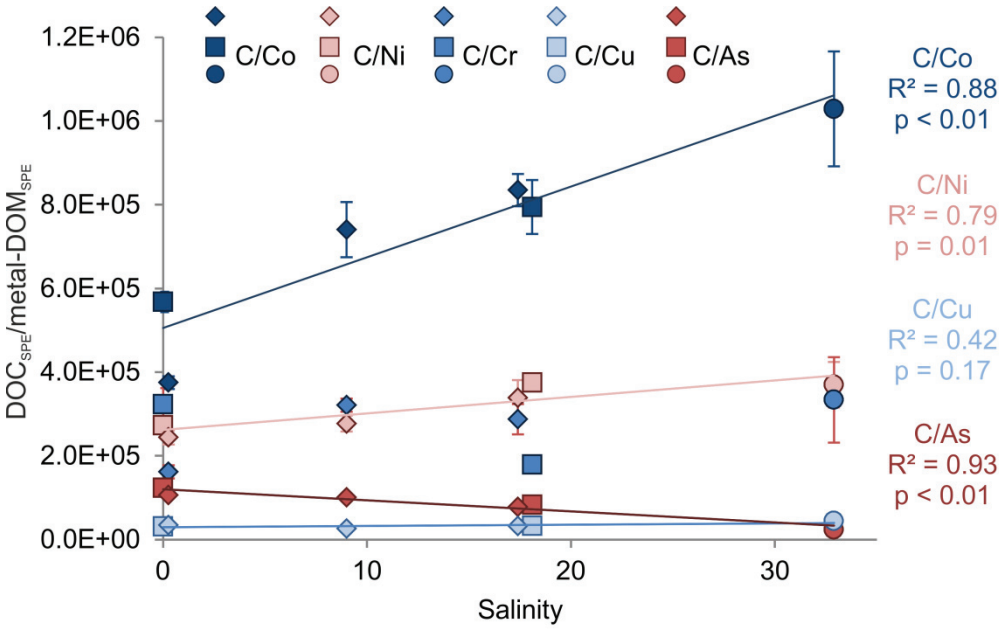

Fig. M3.6. Changes in trace-metal stoichiometry with salinity. Linear correlation of average molar DOC_{SPE}/metal-DOM_{SPE} ratios of pH 2 extracted samples (except of DOC_{SPE}/Cr-DOM_{SPE}, DOC_{SPE}/Cu-DOM_{SPE}, and DOC_{SPE}/V-DOM_{SPE}) versus salinity. Symbols represent sampling locations: River Weser (W1, W2; squares), River Elbe (E1 - E3; diamonds) and the marine station (M1; circles).

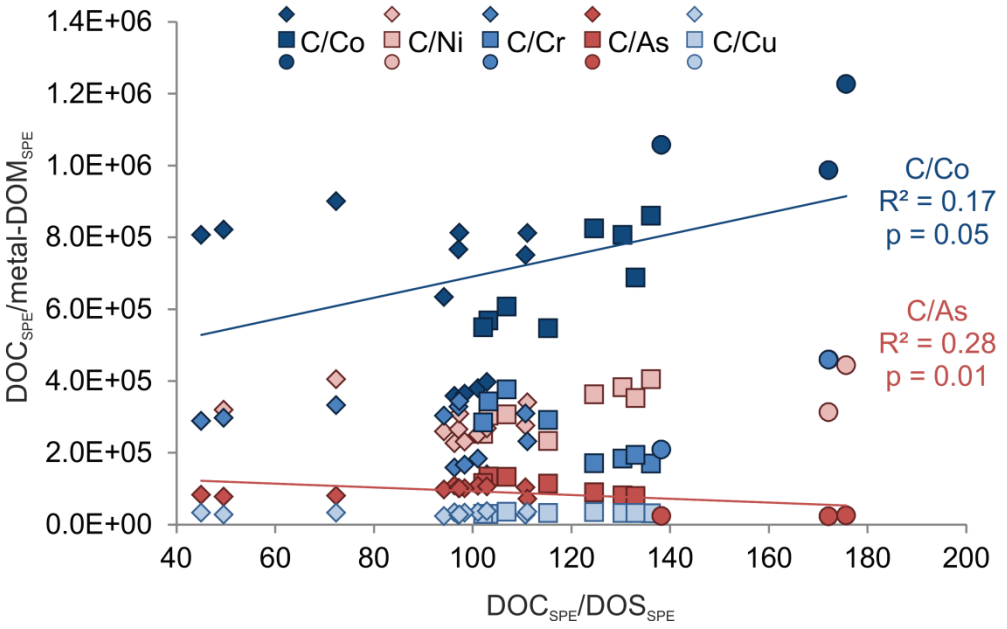

Fig. M3.7. Correlation of trace metal and DOS stoichiometry. Correlation of DOC_{SPE}/metal-DOM_{SPE} versus average DOC_{SPE}/DOS_{SPE} of pH 2 extracted samples. Linear correlation of DOC_{SPE}/Co-DO_{SPE} and DOC_{SPE}/As-DOM_{SPE} is shown. Symbols represent sampling locations: River Weser (W1, W2; squares), River Elbe (E1 - E3; diamonds) and the marine station (M1; circles).

Table M3.4. Average metal-DOM$_{SPE}$ concentrations and molar DOC$_{SPE}$/metal-DOM$_{SPE}$ ratios (/10^5) at the stations. The values are average values of quadruplicate measurements. All concentrations are given in nmol L^{-1}.

Sample	W1		E1		E2		E3		W2		M1	
pH	2	8	2	8	2	8	2	8	2	8	2	8
V-DOM$_{SPE}$	0.12 ± 0.04	0.04 ± 0.03	0.11 ± 0.00	≤ LOD	0.27 ± 0.03	-	0.09 ± 0.00	-	0.25 ± 0.01	0.02 ± 0.01	0.06 ± 0.04	≤ LOD
DOC$_{SPE}$/ V-DOM$_{SPE}$	11.5 ± 0.3	-	13.0 ± 0.5	-	5.2 ± 0.1	-	11.8 ± 0.4	-	4.8 ± 0.1	1.7 ±0.1	5.4 ±0 .2	-
Cr-DOM$_{SPE}$	0.45 ± 0.04	0.01 ± 0.00	0.90 ± 0.11	0.01 ± 0.00	0.43 ± 0.02	0.08 ± 0.06	0.39 ± 0.04	-	0.65 ± 0.04	0.02 ± 0.00	0.09 ± 0.05	0.05 ± 0.00
DOC$_{SPE}$/ Cr-DOM$_{SPE}$	3.2 ± 0.4	38.4 ± 5.2	1.6 ± 0.2	31.9 ± 9.6	3.2 ± 0.2	8.8 ± 8.0	2.9 ± 0.4	-	1.8 ± 0.1	16.7 ± 0.8	3.3 ± 1.0	2.3 ± 0.1
Co-DOM$_{SPE}$	0.25 ± 0.01	0.07 ± 0.01	0.38 ± 0.00	0.09 ± 0.00	0.19 ± 0.02	0.06 ± 0.00	0.13 ± 0.00	0.05 ± 0.00	0.15 ± 0.01	0.06 ± 0.01	0.03± 0.00	0.02 ± 0.01
DOC$_{SPE}$/ Co-DOM$_{SPE}$	5.7 ± 0.2	5.7 ± 0.6	3.8 ± 0.2	3.7 ± 0.1	7.4 ± 0.7	5.8 ± 0.4	8.4 ± 0.4	5.7 ± 0.5	7.9 ± 0.7	5.5 ± 0.4	10.3 ± 1.4	6.2 ± 1.5
Ni-DOM$_{SPE}$	0.53 ± 0.05	0.23 ± 0.06	0.59 ± 0.02	0.39 ± 0.01	0.5 ± 0.03	0.44 ± 0.03	0.33 ± 0.04	0.4 ± 0.01	0.31 ± 0.01	0.32 ± 0.01	0.09 ± 0.01	0.09 ± 0.01
DOC$_{SPE}$/ Ni-DOM$_{SPE}$	2.7 ± 0.3	1.8 ± 0.5	2.4 ± 0.2	0.8 ± 0.03	2.8 ± 0.2	0.8 ± 0.1	3.4 ± 0.4	0.7 ± 0.04	3.8 ± 0.2	1.0 ± 0.03	3.7 ± 0.6	1.1 ± 0.3
Cu-DOM$_{SPE}$	4.60 ± 0.39	2.30 ± 0.12	4.13 ± 0.10	1.76 ± 0.11	5.35 ± 0.39	4.46 ± 0.53	3.41 ± 0.41	4.30 ± 0.32	3.58 ± 0.18	3.89 ± 0.41	0.77 ± 0.18	1.40 ± 0.77
DOC$_{SPE}$/ Cu-DOM$_{SPE}$	0.3 ± 0.02	0.2 ± 0.01	0.4 ± 0.02	0.2 ± 0.01	0.3 ± 0.02	0.08 ± 0.01	0.3 ± 0.03	0.07 ± 0.01	0.3 ± 0.01	0.08 ± 0.01	0.4 ± 0.09	0.1 ± 0.05
As-DOM$_{SPE}$	0.63 ± 0.06	≤ LOD	0.82 ± 0.06	-	0.83 ± 0.04	-	0.87 ± 0.06	-	0.85 ± 0.08	0.15 ± 0.02	0.77 ± 0.06	0.11 ± 0.01
DOC$_{SPE}$/As -DOM$_{SPE}$	1.2 ± 0.1	-	1.1 ± 0.03	-	1.0 ± 0.02	-	0.8 ± 0.04	-	0.8 ± 0.05	0.5 ± 0.005	0.2 ± 0.01	0.2 ± 0.02

LOD: limit of detection

To assess the extraction efficiencies for metal-DOM, we determined the trace metal concentrations of Co and Cu in original seawater and compared them with Cu-DOM$_{SPE}$ and Co-DOM$_{SPE}$ (Table M3.5). Co and Cu concentrations in original water samples also decreased with increasing salinity (Fig. M3.8, Table M3.5). A significant linear correlation with salinity was found for UV-treated Co (Co$_{UV}$) concentrations only (Fig. M3.8). The application of UV digestion led to 300-500 % higher trace element concentrations compared to the untreated samples. Co extraction efficiencies were generally lower for pH 8 extracted samples compared to pH 2 extracted samples. Average extraction efficiencies of pH 2 extracted Co-DOM$_{SPE}$ were 8-45 % without UV digestion of original samples and 3-12 % with UV digestion, respectively. Co extraction efficiencies of riverine samples were significantly higher compared

to marine samples ($p < 0.001$). However, no correlations with salinity were observed. For pH 8 extracted samples, average Co-DOM_{SPE} extraction efficiencies were 5-19 % and 2-4 % for samples without and with UV digestion, respectively. No differences between riverine and marine samples were found. Average extraction efficiencies of pH 2 extracted Cu-DOM_{SPE} were 10-13 % without UV digestion of original samples and 9-11 % with UV digestion. For pH 8 extracted samples, Cu-DOM_{SPE} extraction efficiencies were 5-20 % and 6-17 % for samples without and with UV digestion, respectively. In contrast to Co-DOM_{SPE}, the extraction efficiencies of pH 8 extracted Cu correlated linearly with salinity ($R^2 = 0.98$, $p < 0.001$). Interestingly, Cu extraction efficiencies of pH 2 extracted samples showed no differences with increasing salinity, whereas Cu extraction efficiencies of pH 8 extracted samples increased with increasing salinity (Table M3.5).

Table M3.5. Dissolved Co and Cu concentrations in original water samples and corresponding average solid phase extraction efficiencies (extr. eff.).

		without UV digestion				with UV digestion			
Sample	Salinity (psu)	Co conc. (nmol L^{-1})	Co extr. eff. pH2/ pH8 (%)	Cu conc. (nmol L^{-1})	Cu extr. eff. pH2/ pH8 (%)	Co_{UV} conc. (nmol L^{-1})	Co_{UV} extr. eff. pH2/ pH8 (%)	Cu_{UV} conc. (nmol L^{-1})	Cu_{UV} extr. eff. pH2/ pH8 (%)
W1	0	1.20	21/6	35	13/7	4.143	6/11	41	11/6
E1	0.3	1.26	30/7	32	13/5	4.701	8/11	39	11/5
E2	9	0.35	54/17	51	11/9	1.526	12/9	57	9/8
E3	17.4	0.27	49/19	31	11/14	1.399	9/9	36	9/12
W2	18.1	0.35	42/16	36	10/11	1.308	11/10	35	10/11
M1	32.9	0.40	8/5	7	11/20	1.037	3/9	8	9/17

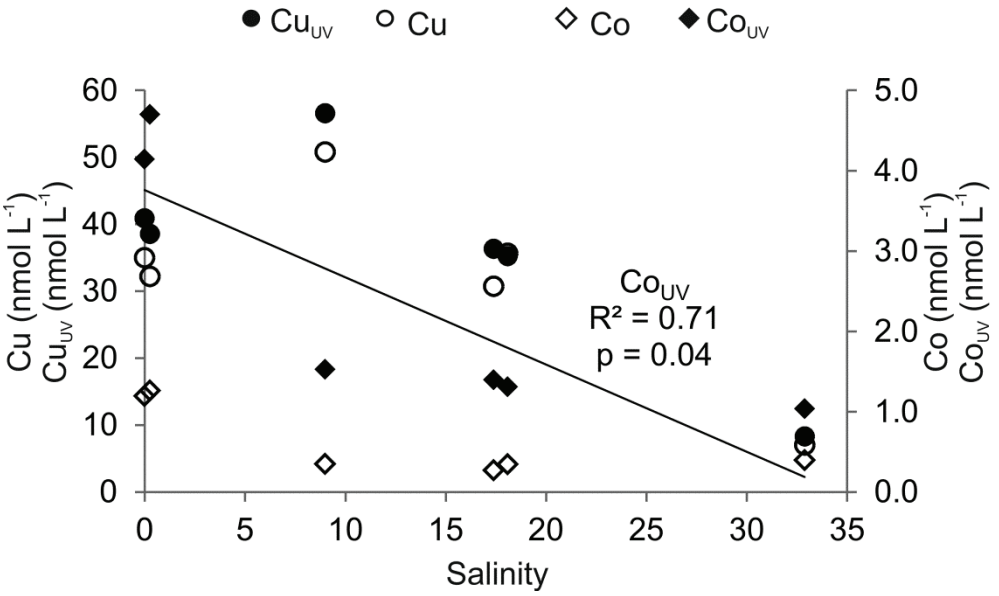

Fig. M3.8. Cu (circles) and Co (diamonds) concentrations with changing salinity. Symbols and correlation line represent pre-treatment conditions of original samples: with UV digestion (filled symbols, solid line) and without UV digestion (unfilled symbols).

Discussion

Stoichiometry and polarity characteristics of dissolved organic matter

The high DOM concentrations in the riverine endmember samples of Weser and Elbe River emphasized the importance of rivers as a DOM source to the coastal oceans as previously shown for many other regions from riverine to marine waters (Benner and Opsahl, 2001; Gonçalves-Araujo et al., 2015; Guo et al., 2007; Huguet et al., 2009). DOC concentrations in the estuarine and marine samples (E2, E3, M1; Table M3.3) were typical for the German Bight (76 – 209 μmol L^{-1} (Spitzy, 2005)). DOC_{SPE}, DON_{SPE}, and DOS_{SPE} concentrations as well as DOC_{SPE}/DON_{SPE} and DOC_{SPE}/DOS_{SPE} ratios are in accordance with values published for the North Sea (Pohlabeln and Dittmar, 2015) and Atlantic surface waters (Ksionzek et al., 2016a; Ksionzek et al., 2016b). Unlike the typical decrease of DOC/DON ratios from land to sea in estuaries (e.g. (Ylöstalo et al., 2016)), our pH 2 extracted samples showed almost constant molar DOC_{SPE}/DON_{SPE} ratios, probably due to an inefficient extraction of nitrogen compared to carbon (Flerus et al., 2012; Lechtenfeld et al., 2014). Ratios of pH 8 extracted samples were similar, but reflected the typical decrease of molar DOC_{SPE}/DON_{SPE} ratios with increasing salinity. Molar DOC_{SPE}/DOS_{SPE} ratios were higher and molar DOS_{SPE}/DON_{SPE} ratios lower in the riverine compared to the marine endmembers. Our average DOC_{SPE}/DOS_{SPE} ratios were 100 ± 3 and 107 ± 5 in the riverine endmember samples. Previous studies on DOS in freshwater and other aquatic systems are very scarce. Houle et al. found DOS concentrations of ~5.8 μmol L^{-1} (~185 μg L^{-1}) and DOC/DOS ratios of ~122 in several southwestern Québec lakes (Houle et al., 1995), values that are higher than those in our riverine samples. However, these lakes are influenced by terrestrial DOM

with high DOC and DOS concentrations from forest soils. Nevertheless, spatial differences can also cause differences in DOS concentrations. Some information on sulfur exists also for soil and particulate organic matter (POM), e.g. (Homann et al., 1990; Matrai and Eppley, 1989). Based on a molar C/S ratio of 119 for POC (Matrai and Eppley, 1989), the global flux of DOS and POS from rivers to the ocean accounts for 8 Tg S a^{-1} (Ksionzek et al., 2016a), a value that would be ~15 % higher if we use the C/S ratio from this study. Our numbers for the molar DOC_{SPE}/DOP_{SPE} ratios were very high compared to other studies (Hopkinson and Vallino, 2005), presumably due to inefficient DOP extraction for the cartridges used. However, this is speculative due to the limited available data.

The chromatographic data reflected also lower DOC_{SPE} concentrations at higher salinity. Since fluorescence represents only a small fraction of DOM_{SPE}, we focus on the absorbance data. In contrast to samples from the Weser River, $DOC_{pol}/DOC_{non\text{-}pol}$ ratios of riverine and estuarine samples of the Elbe River were significantly higher at higher salinity. Possible reasons might be differences in DOM sources or different residence times. Over all samples, however, no significant changes in $DOC_{pol}/DOC_{non\text{-}pol}$ ratios occurred within the group of pH 2 extracted riverine and estuarine samples (W1, W2, E1 - E3). Only for the marine endmember, a significant lower $DOC_{pol}/DOC_{non\text{-}pol}$ ratio was found. Riverine DOM is dominated by terrestrial sources, characterized by high polarity due to a high number of carboxyl groups, elevated C/N ratios and higher contribution of aromatic components (e.g. lignin and its degradation products) (Benner et al., 1992; Dittmar and Kattner, 2003) (resulting in higher $DOC_{pol}/DOC_{non\text{-}pol}$ ratios compared to marine samples, as found also in this study). DOM in marine samples, in contrast, originates mainly from phytoplankton and its degradation products and only 0.7 – 2.4 % appears to be from terrestrial sources (Opsahl and Benner, 1997). In estuaries, mixing of both, riverine and marine DOM occurs and results in changes of the DOM pool composition: with increasing salinity, molecular weight, carbohydrate and heteroelement content of DOM increases (Abdulla et al., 2010; Sleighter and Hatcher, 2008), while DOM aromaticity decreases (Abdulla et al., 2013). The highly significant correlation of decreasing DOM_{SPE} concentration with increasing salinity reflects mixing of riverine and marine DOM. However, due to the limited number of samples, precise statements about deviations from conservative mixing, as previously reported (e.g. (Gonçalves-Araujo et al., 2015)), would be speculative. To assess if all DOM_{SPE} compounds decreased in a similar range with increasing salinity, we compared the relative changes of DOC_{SPE}, DOS_{SPE} and DON_{SPE} endmember concentrations in riverine and marine samples. We found a similar reduction in DOC_{SPE} and DON_{SPE} concentrations of ~77 ± 1 % and a reduction in DOS_{SPE} concentration of 86 ± 1 %. These changes indicate that DOS_{SPE} decreased faster than DOC_{SPE} and DON_{SPE}. This is in accordance with previous studies in the oceanic water column, showing preferential depletion of sulfur (and phosphorous) relative to carbon (Hopkinson and Vallino, 2005; Ksionzek et al., 2016a). Similar to sulfur, nitrogen is also removed preferentially to carbon (Ksionzek et al., 2016a). It might be possible,

that in our study, the fast decrease in DON_{SPE} is masked by other DON_{SPE} sources along the estuary (such as agricultural and industrial sources, benthic flux, or microbial activity).

Although the mixing of DOM-rich riverine freshwater with marine water in estuaries is the major factor controlling DOM distribution and composition (Alling et al., 2010; Gonçalves-Araujo et al., 2015; Guo et al., 2007; Stedmon and Markager, 2003), relative changes in DOM stoichiometry indicate processes beyond estuarine mixing. Different sources and sinks control the amount, composition and reactivity of DOM in aquatic environments: biological release, phyto and zooplankton mediated processes (Castillo et al., 2010), decomposition of riverine DOM by marine bacteria (Rochelle-Newall et al., 2004), photo-bleaching and photo-degradation (Gonsior et al., 2014; Gonsior et al., 2013; Helms et al., 2013; Opsahl and Benner, 1998) as well as flocculation processes and sorption to sediments (Asmala et al., 2014; Benner and Opsahl, 2001; Guo et al., 2007). All of these processes might occur simultaneously, and it remains a major challenge to quantify the influence of each process on DOM composition.

Trace metal complexation and DOM composition

Co-DOM_{SPE}, Ni-DOM_{SPE}, and Cu-DOM_{SPE} concentrations decreased with salinity, a result of mixing of trace metal-rich riverine water with trace metal-poor marine water. Higher trace-metal concentrations in the riverine extracts suggest a terrestrial/benthic source for dissolved trace metals (Santschi et al., 1997; Wen et al., 1999) and/or differences in trace-metal/organic matter composition. Although statements about conservative or non-conservative mixing would be speculative due to the limited number of samples, we assume that other factors additionally to mixing must occur. Normalization of trace metals to carbon allows us to analyze differences between the decreases in DOC_{SPE} and metal-DOM_{SPE} concentrations. Unlike As-DOM_{SPE} and Cu-DOM_{SPE}, Co-DOM_{SPE} and Ni-DOM_{SPE} decreased disproportionately compared to DOC_{SPE}, similar to DOS_{SPE}. The rapid decrease of trace metal concentrations in the estuarine mixing zone is consistent with previous studies (Guo et al., 2000; Sholkovitz, 1978) and reasons might be (i) changes in trace metal and/or DOM sources, (ii) changes in DOM quality (polarity) and (iii) consumption. Some trace metals (e.g. V, Cr, and Cu) however, increased in estuarine waters and decreased at high salinity in the marine water.

The distributions of Co-DOM_{SPE}, Ni-DOM_{SPE}, Cu-DOM_{SPE}, and Cr-DOM_{SPE} concentrations with increasing salinity followed that of DOC_{SPE} and DOS_{SPE} concentrations, which implies that they are complexed with organic matter (e.g. via carboxylic, hydroxamate, or thiol groups), whereas V-DOM_{SPE}, and As-DOM_{SPE} distributions lead to assume a lower affinity for organic matter. From a study in the Northeast Pacific Ocean, it was estimated that > 99 % of total dissolved Cu in surface water is associated with strong organic complexes (Coale and Bruland, 1988). Complexation of Co und Cu is further indicated by relatively high extraction efficiencies for both trace metals. We assume that trace metals, which are not organically complexed would most likely not be captured by our extraction

method. The PPL sorbent has previously been shown to achieve high recovery rates for organic Cu (Waska et al., 2015).

The importance of organometallic complexes in DOM is supported by UV digestion prior to seaFAST analysis yielding 100-120 % higher Cu concentrations and up to 300-500 % higher Co concentrations in the original sample. In previous studies, Co concentrations increased also but only by 50-160 % (Biller and Bruland, 2012; Milne et al., 2010). These differences could be explained by spatial differences in the availability and composition of organic ligands. Since UV treatment/oxidation is used to destroy even very strong metal-organic complexes, the increase in Co and Cu concentrations after UV digestion indicates that a major part of Cu and Co in aquatic samples is organically complexed.

To explore the role of organic sulfur in organometallic complexes, we compared the values of metal-DOM_{SPE}/DOC_{SPE} and metal-DOM_{SPE}/DOS_{SPE} ratios in the pH 2 extracted riverine (W1) and marine (M1) endmember samples and found an increase in the following order: Cu > As > Ni > Cr > Co and As ≥ Cu > Ni > Cr > Co, respectively. This order is consistent with the Irving-Williams order, which has been used to compare the affinity of (colloidal) trace-metals to organic ligands (Guo et al., 2000; Mantoura et al., 1978). It is true for both, the affinity of trace metals to DOC_{SPE} and to DOS_{SPE}. According to our results, Cu has a higher affinity to (S-containing) organic ligands than Co and Cr irrespective of the salinity. Comparing the metal-DOM_{SPE} concentrations in riverine and marine endmember samples (Table M3.4), we can calculate the relative changes of metal-DOM_{SPE} concentrations as it has been done similarly for DOC_{SPE} and DOS_{SPE}. We found a relative decrease of metal-DOM_{SPE} with increasing salinity in the order Co (90 %) > Cr (87 %) > Ni (84 %) > Cu (82 %). Those differences in relative changes of the trace metal concentrations with increasing salinity are similar to DOS_{SPE} and DOC_{SPE} concentrations and cannot be explained by mixing alone. In fact, different transformation and removal processes (as mentioned in the introduction) can influence DOM concentration. The order in relative changes of metal-DOM_{SPE} concentrations with increasing salinity reflects again the Irving-Williams order, indicating that a higher relative decrease in metal-DOM_{SPE} concentration consequently reflects lower affinity to organic ligands. The stronger the affinity of trace metals to organic ligands, the more resistant are the metal-organic complexes against degradation processes.

Trace metal complexation to organic sulfur groups is further supported by the positive correlation of the ratio of DOC_{SPE}/Co-DOM_{SPE} with DOC_{SPE}/DOS_{SPE} (Fig. M3.7). Thus, we found indication for a correlation of Co and sulfur. Comparatively little is known about organic complexation of cobalt in aquatic environments. Studies in the Mediterranean Sea and the Scheldt Estuary suggest partial, but strong complexation of Co to organic ligands (Ellwood and van den Berg, 2001; Vega and van den Berg, 1997; Zhang et al., 1990). In organisms, Co and sulfur are coupled via the biosynthesis pathway of methionine: the enzyme methionine synthase is responsible for the regeneration and remethylation

of methionine from homocysteinie. In some microorganisms (e.g in *E. coli*), this enzyme requires the Co-containing cobalamin (vitamin B12) as a cofactor (Zydowsky et al., 1986).

Following the Irving-Williams order, we assume the affinity of Ni to organic carbon and sulfur groups to be between that of Cu and Co. It is known that about 10 – 60 % of Ni in coastal and marine waters is bound by organic ligands (Donat et al., 1994; Saito et al., 2004; Vraspir and Butler, 2009). However, it is unclear whether S-containing organic ligands play a role in nickel complexation and we did not find a significant correlation of DOC_{SPE}/Ni-DOM_{SPE} with DOC_{SPE}/DOS_{SPE} ratios in our samples.

Although our results suggest a higher affinity of Cu to sulfur than of Co (Irving-Williams order) we could not find a linear correlation of Cu-DOM_{SPE} with DOS_{SPE}. It is known that dissolved Cu in different aquatic environments is organically complexed by thiols (e.g. (Laglera and van den Berg, 2003)). Laglera and van den Berg analyzed copper-thiol complexes in estuarine waters of the Scheldt River, the Netherlands, and found a decrease in copper-thiol complex stability with increasing salinity (Laglera and van den Berg, 2003). However, thiol concentrations in marine waters are usually very low (< 10 nmol L^{-1}) (Al-Farawati and Van Den Berg, 2001; Dupont et al., 2006; Tang et al., 2000). Comparing these concentrations with the calculated minimum DOS concentration of 0.34 µmol L^{-1} in original seawater of the upper East Atlantic Ocean (Ksionzek et al., 2016a), it turns out that thiols contribute to only < 3 % of the DOS pool.

We can summarize the differences in riverine and marine trace metal containing DOM_{SPE} by their average molar ratios to be $(C_{107}N_4P_{0.013}S_1)_{1000}V_{0.05}Cr_{0.33}Co_{0.19}Ni_{0.39}Cu_{3.41}As_{0.47}$ in the riverine endmember (W1) and $(C_{163}N_7P_{0.055}S_1)_{1000}V_{0.05}Cr_{0.47}Co_{0.16}Ni_{0.07}Cu_{4.05}As_{0.58}$ in the marine endmember. Compared to the extended Redfield ratio by Ho et al. of $(C_{95}N_{12}P_{0.8}S_1)_{1000}Cu_{0.29}Co_{0.15}$ for marine phytoplankton (Ho et al., 2003), we found a considerably higher DOC_{SPE}/DOS_{SPE} ratio in the marine endmember sample, presumably as a result of a more advanced state of degradation. Additionally, we found lower DOC_{SPE}/Cu-DOM_{SPE} and DOC_{SPE}/Co-DOM_{SPE} ratios in our samples compared to marine phytoplankton.

Influence of salinity and sample pre-treatment on extraction and trace element complexes

The DOC extraction efficiencies of 36 ± 2 % for pH 2 extracted samples were lower than expected. However, compared to the extraction efficiency for marine DOC of 42 ± 7 % (n = 187) found in another study (Lechtenfeld et al., 2014), our values are still in the range of uncertainty. Possible reasons for the lower DOC extraction efficiencies might be (i) unknown influence of the source material (ii) too high original DOC measurements or (iii) a problem with the adsorber material. Nevertheless, the results of the quadruplicates of each treatment in our extractions were very consistent, reproducible and invariant, ensuring comparability of our samples.

It has been previously shown that changes in salinity and DOM quality (e.g. at different sample locations in estuaries) can affect DOM recovery via SPE (Chen et al., 2016; Kruger et al., 2011). However, we found no significant effect of salinity on the amount of recovered DOC. Similar DOC extraction efficiencies throughout different salinities suggest little or no fractionation effects as a result of changes in DOM quality. These findings are further supported by an additional experiment, in which low salinity samples from the Weser River were spiked with different concentrations of NaCl and extracted using PPL cartridges (M3.S1 File). The results also showed that the DOC extraction efficiency was not affected by salinity. However, structural changes (indicated by changes in polarity) were observed with changes in salinity, similar to our samples. Thus, we conclude that the polarity of some organic compounds can be reduced by the presence of salt. Structural changes with changes in ionic strength of the medium were also observed for humic acids (Tsutsuki and Kuwatsuka, 1984).

Acidification of samples prior to SPE yielded significantly higher DOM_{SPE} and metal-DOM_{SPE} concentrations in the methanol extracts compared with samples extracted at neutral pH and thus gave a more comprehensive picture to discuss changes in DOM stoichiometry and polarity characteristics with changing salinity. It has been shown that acidification leads to higher extraction efficiencies for natural organic matter due to the protonation of functional groups such as organic acids and phenols (Dittmar et al., 2008). Overall, our method is only suitable to extract specific fractions of the natural metal-organic complex pool: the strong acidic fraction in pH 2 extracted samples and the neutral/weak acidic fraction in pH 8 extracted samples, respectively (as defined by Waska et al., 2015). Cu-DOM_{SPE} extraction efficiencies were similar to those previously reported for acidified and non-acidified PPL extracts (Waska et al., 2015). Mills et al. reported decreasing extraction efficiencies of Cu-organic complexes with decreasing pH and mentioned that acidification to pH $\leq$ 4 did not allow the existence of stabile Cu-DOM_{SPE} complexes (Mills et al., 1982). However, another study indicates that also acid-stable Cu-containing compounds can occur in natural aquatic environments (Reddy et al., 1995). This contradiction reflects that the stability of Cu-organic complexes also depends on the acid-base characteristics of the Cu-binding functional groups and their competitive binding with H^+ and possibly other major ions such as Ca^{2+} and Mg^{2+}. In summary, acidification leads to two competing effects on the recovery of DOM_{SPE} and metal-DOM_{SPE}: (i) an increase in the carbon extraction efficiency due to the protonation of organic matter and (ii) a decrease in the complex extraction efficiency due to reduced stability of protonated/acidified organic complexes. For the riverine samples E1 and W1, acidification led to a relative increase by factor 3-4 in both DOC_{SPE} and DOS_{SPE} concentrations, respectively, compared to the non-acidified samples. For trace metals, the net effect of both processes is reflected in differences in average molar DOC_{SPE}/metal-DOM_{SPE} ratios of pH 2 and pH 8 extracted samples, respectively, which were about a factor of 1.5 - 2 for Cu and Ni while no net effect was observed for Co. For estuarine and marine samples however, the decrease in trace metals changed by factor 1.3 – 1.7 for Co and 3 – 4 for Ni and Cu, whereas the increase in DOC_{SPE} and DOS_{SPE}

concentrations remained similar to those found in riverine samples. Thus, we can conclude that acidification prior to SPE plays an important role, since it improves the recovery of both DOM_{SPE} and metal-DOM_{SPE}. As a result, we found higher extraction efficiencies for pH 2 extracted metal-DOM_{SPE} compared to pH 8 as similarly found for DOM_{SPE}. However, acidification likely leads to changes in the quality of organic ligands. In contrast to DOC and Co, we found a significant correlation of the Cu extraction efficiency with salinity. This can have several reasons: (i) differences in the quality of riverine and marine organic ligands (e.g. a higher binding strength of marine Co-complexing ligands) as indicated by differences in polarity or (ii) ionic strength of the medium. The first assumption is supported by a higher polarity of terrestrial DOM which goes along with lower DOC_{SPE}/metal-DOM_{SPE} ratios. The second assumption might be explained by an increasing amount of inorganic ions with increasing ionic strength of the medium that could compete with the trace metal ions.

Conclusion

In this study we presented the concentration and distribution of DOC_{SPE}, DON_{SPE}, DOS_{SPE}, and dissolved metal-DOM_{SPE} with changing salinity in two rivers draining to the North Sea. With regard to the research question/hypothesis stated in the introduction, we can conclude:

i. DOM_{SPE} concentrations decreased from riverine to marine waters. The differences in the relative changes in DOC_{SPE} and DOS_{SPE} concentration suggest a preferential removal of DOS_{SPE} over DOC_{SPE} (and DON_{SPE}).

ii. The concentration of some solid-phase extractable trace metals (^{52}Cr, ^{59}Co, ^{60}Ni, ^{63}Cu) was correlated with the DOC_{SPE} and DOS_{SPE} concentrations as a result of the presence of organic complexes. The positive correlations of the DOC_{SPE}/Co-DOM_{SPE} and DOC_{SPE}/Ni-DOM_{SPE} ratios with the DOC_{SPE}/DOS_{SPE} ratio and relatively high extraction efficiencies for Co and Cu suggest complexation of trace metals with organic carbon- and sulfur-containing ligands. Increasing Co and Cu concentrations after UV digestion further supported the presence of strong organic sulfur-trace metal complexes. The affinity of trace metals to (sulfur-containing) organic ligands followed the Irving-Williams order.

iii. DOM polarity reflected typical changes along the estuary from highly polar terrestrial DOM in riverine waters to non-polar DOM compounds in the marine water. This is reflected in a decreasing $DOC_{pol}/DOC_{non\text{-}pol}$ ratio with increasing salinity.

iv. Acidification prior SPE plays an important role and leads to a higher recovery of both DOM_{SPE} and metal-DOM_{SPE} compared to neutral SPE. Higher DOC yield by acidification is more important for the metal yield than the negative effect of acidification on complexation. On a qualitative scale, however, acidification can of course make a big difference for the recovery of different organic ligands.

Acknowledgements

We are grateful to captain and crew of RV *Heincke* (HE426); I. Stimac is acknowledged for technical support with ICP-MS analysis and Stephan Frickenhaus for his advice regarding statistical questions; we thank W. Geibert for helpful discussions.

Supporting Information

M3.S1 Fig. UV peak area at 210 nm versus DOC_{SPE} concentrations of all samples. A significant linear correlation was found for both fractions: the low concentrated fraction (all pH 8 extracted samples and the pH 2 extracted marine sample) with DOC_{SPE} concentrations from 0 – 40 μmol L^{-1} (unfilled symbols) and the high concentrated fractions (pH 2 extracted riverine and estuarine samples) with DOC_{SPE} concentrations > 100 μmol L^{-1} (filled symbols).

M3.S1 Table. Limits of detection for all elements analyzed by ICP-MS, given that solid-phase extraction was performed with an enrichment factor of 430. These values were calculated according to DIN 32645.

M3.S1 File. This file includes methodical information about the salt-spiking experiment of riverine samples.

IV.4 Manuscript 4

Quantification and biogeochemistry of dissolved organic sulfur in the southeastern Weddell Sea

Kerstin B. Ksionzek[1,2*], Walter Geibert[1], Kai-Uwe Ludwichowski[1], Ingrid Stimac[1], Svenja Ryan[1], Boris P. Koch[1,2,3]

[1] Alfred Wegener Institute Helmholtz Center for Polar and Marine Research, Bremerhaven, Germany.

[2] MARUM – Center for Marine Environmental Sciences, Bremen, Germany.

[3] University of Applied Sciences, Bremerhaven, Germany

*Corresponding author

E-mail: Kerstin.Ksionzek@awi.de

Abstract

The southern Weddell Sea is of major importance for the global ocean circulation, as this region is a key area for the formation of Weddell Sea Deep and Bottom Water (WSDW, WSBW). It is one of the least accessible regions of the world, so that only few studies addressed organic biogeochemical processes. In this study, we present nutrient and dissolved organic matter (DOM) data from five sections of an oceanographically and biological "hotspot", the Filchner trench and outflow aiming in the biogeochemical characterization of this area. In the ice-covered region of the Filchner trough, nutrient consumption in the surface water was limited due to low phytoplankton abundance, resulting in no significant differences in nitrate and phosphate concentrations of surface and bottom water. For silicate, we assume additional (e.g. sedimentary) sources, yielding higher concentrations in the bottom water, compared to the surface water. North of the Filchner sill and in an area where a polynya was located, nutrient concentrations followed typical nutrient depth profiles and were depleted in surface water compared to bottom water. The characterization of DOM comprises a basin-scale distribution of solid-phase extractable dissolved organic sulfur (DOS) in the Weddell Sea. Molar DOS versus dissolved organic nitrogen (DON) ratios were comparable to phytoplankton stoichiometry, indicating the predominant DOS source. Following the Ice Shelf Water (ISW, one of the major water masses inside the Filchner trench, which has its origin at the Filchner Ronne Ice Shelf), we found high DOC concentrations in the south, close to the ice shelf, which were decreasing along northward transport. Inside the Filchner trough, where primary production was limited due to higher ice coverage, the ice shelfs and sea ice were also important DOM sources. At few stations, we found elevated DOC concentrations in the bottom water, presumably as a result of downwelling of DOM-rich ISW. Evaluation of molar dissolved organic carbon (DOC) versus DOS and DON ratios, respectively, and comparison of relative reduction in DOC and DOS concentrations demonstrated preferential removal of DOS compared to DOC. However, DOC transformation and mineralization was not reflected in a correlation of DOC and apparent oxygen utilization (AOU).

Introduction

The Weddell Sea and the region of the Filchner depression are of major importance for the global oceanic circulation, since it is one of the largest areas for bottom water formation (Orsi et al., 1999; Reid and Lynn, 1971). Cold and dense Ice Shelf Water (ISW) from the Filchner-Ronne Ice Shelf flows northward along the Filchner trough and has its outflow region at the Filchner sill, from where it can reach the deepest parts of the Weddell Sea, due to its high density. The sill has a depth of ~600 m and thus acts as a barrier: only the upper layer of ISW can leave the

trough, whereas ISW in the bottom layer is circulating inside the trough (Carmack and Foster, 1975). Deeper water masses from the north cannot enter this region. On its way down the continental slope, ISW mixes with Warm Deep Water (WDW) of the Weddell Gyre and thus, contributes to dense water formation (Foldvik et al., 2004). Consequently, north of the Filchner sill, the deepest areas are dominated by Weddell Sea Deep Water (WSDW) and Weddell Sea Bottom Water (WSBW). The shallow shelf area east of the Filchner trough is dominated by East Shelf Water (ESW), a mixture of glacial melt water from the eastern Weddell Sea ice shelves, Winter Water (WW) and Modified Warm Deep Water (MWDW), which enters the Filchner sill at its eastern part and flows southwards - in the opposite direction of the ISW (Nicholls et al., 2009). MWDW is formed by mixing of WDW with WW or ESW.

WSDW is a major component of Antarctic Bottom Water (AABW), which is found in the deep waters of all oceans of the southern hemisphere. Since nutrient concentrations in the Weddell Sea are among the highest in the global oceans (Hoppema et al., 2015), bottom water formation in the Weddell Sea is an important mechanism transporting nutrient (and oxygen) rich waters from the surface into the deep ocean (Foldvik et al., 2004). Thus, the region of the Filchner outflow is considered a "hot spot" both in terms of oceanography and biology (Knust and Schröder, 2014; Kohlbach et al., 2019; Nachtsheim et al., 2019).

A similar vertical transport mechanism was assumed for sea-ice derived dissolved organic matter (DOM) (Knust and Schröder, 2014). For the Ross Sea, however, it has been shown that most of the dissolved organic carbon (DOC) is consumed during export to the deep ocean and thus, only represents a small source to the deep ocean (Bercovici et al., 2017). For the Weddell Sea, it has been shown that DOM is older and highly degraded compared to the East Atlantic (Flerus et al., 2012; Lechtenfeld et al., 2011) indicating that most of the fresh sea-ice derived DOM is also remineralized and not transported to the deep ocean. Nevertheless, during several cruises in the past, we observed increased DOC concentrations at some stations in the bottom water of the Weddell Sea. The high DOC radiocarbon age in the Weddell Sea contradicts with the observed elevated DOC concentrations. In this study, we tried to verify whether these increased concentrations are indeed present and elucidate potential causes.

In addition, this study focusses on the chemical characterization of DOM. An important component of DOM besides dissolved organic carbon (DOC), nitrogen (DON) and phosphorus (DOP), is dissolved organic sulfur (DOS), which represents the largest reservoir of organic sulfur in the ocean (Ksionzek et al., 2016a). Sulfur is an essential element for marine primary production and the sulfur cycle is tightly coupled to the C and N cycle. Volatile DOS compounds are involved in climate processes (Charlson et al., 1987), whereas other DOS compounds (e.g. thiols) act as important ligands for organic metal complexes (Smith et al., 2002). Due to the limited

accessibility of the Weddell Sea, only few information is available on DOS (Ksionzek et al., 2016a; Lechtenfeld et al., 2011). Most DOM studies focused on the quantification of DOC and DON in sea ice and the underlying water column (Doval et al., 2002; Kähler et al., 1997; Norman et al., 2011; Ogawa et al., 1999; Scott et al., 2000; Thomas et al., 2001; Wiebinga and de Baar, 1998). A few other studies analyzed the composition, degradation and bioavailability of DOM (Lechtenfeld et al., 2014; Shen et al., 2017). However, the chemical structures of DOM in general and DOS in particular, which are important to assess DOM bioavailability, remains largely unknown (Ksionzek et al., 2016). Thus, knowledge on the availability, distribution, molecular composition and biogeochemistry of DOS is limited.

This study aims to characterise the "hot spot" around the Filchner outflow in more detail from the biogeochemical view. To improve our understanding of the role of organic matter in cryo-pelagic and bentho-pelagic processes, seawater from different depths and water masses was sampled for inorganic nutrient, DOC and DOS analyses. A high spatial sampling resolution, particularly in surface and bottom water of the southern Weddell Sea, was essential to improve our mechanistic understanding of DOM biogeochemistry. By quantification and characterization of inorganic nutrients and DOM stoichiometry, we aim at following questions/hypotheses:

(i) How is the concentration and availability of inorganic and organic nutrients in the Filchner outflow and adjacent water masses?

(ii) As a result of earlier indications, we hypothesize that the biomass signal of extractable DOM (DOS/DON ratio) is invariant from surface to depth whereas the DOC/DON and DOC/DOS ratios of extractable DOM decrease from surface to bottom water and indicate DOM degradation.

(iii) What is the source for elevated DOC concentrations in the bottom water?

(iv) Is fresh DOM transported to deeper water and can sea-ice derived organic matter be thus detected in bottom water of the Southern Weddell Sea?

(v) Apparent oxygen utilization (AOU) might control organic carbon and sulfur speciation in the water column below the sea-ice and at the sediment-water interface. Thus, we explore whether a correlation of DOM and AOU can be found and if the molar DOC/AOU ratio can be applied to calculate the contribution of DOC degradation to AOU.

Materials and methods

Sample collection and processing

Water samples were collected between January and February 2014 during the expedition ANT XXIX/9 on *R/V Polarstern* to the southeastern Weddell Sea. This study focuses on six sections in the southwestern Weddell Sea (Fig. M4.1c): four east-west transects (78°S, 77°S, 76°S, section east-west (SEW)) and two north-south transects (section east (SE), section middle east (SME)). The sections 76°S, 77°S and 78°S have their easternmost end at the shallow eastern Weddell Sea shelf, while their western ends are reaching into the Filchner depression. The Filchner sill is crossed by SEW. At 40 stations, samples for nutrient and DOM analysis were taken. Samples were collected using a rosette sampler equipped with conductivity-temperature-depth (CTD) sensors (Seabird SBE 911plus), a fluorometer (WET Labs ECO AFL/FL) and an oxygen sensor (Seabird SBE 43). Oceanographic data measured at a total of 130 stations during this cruise were taken from (Schröder and Wisotzki, 2014). Apparent oxygen utilization (AOU) was calculated from dissolved oxygen concentrations [O_2] and the equilibrium oxygen saturation concentration [$O_{2\ sat}$] from the oceanographic dataset (Schröder and Wisotzki, 2014) using Eq. M4.1.

$$AOU = [O_{2\ sat}] - [O_2] \qquad \text{(Eq. M4.1)}$$

Our water sampling focused on gradients at the sea surface and near the sediment-water interface. Therefore, we sampled at higher depth resolution in the upper 100 m of the water column (including the fluorescence maximum) and above the seafloor. All samples were filtered through pre-combusted GF/F filters (Whatman, 450 °C, 5 h, 0.7 μm nominal pore size). Aliquots for DOC and nutrient analyses were stored at -20 °C. Filtered samples were acidified to pH 2 (hydrochloric acid, suprapur, Merck). For solid-phase extraction (SPE) of DOM 500 mL of seawater was extracted (PPL, 200 mg, Mega Bond Elut, Varian) and eluted with 1 mL of methanol (LiChrosolv, Merck) into pre-combusted glass vials (Dittmar et al., 2008). The solid-phase extracted DOM (DOM_{SPE}) was stored at -20 °C until further analysis to avoid esterification (Flerus et al., 2011).

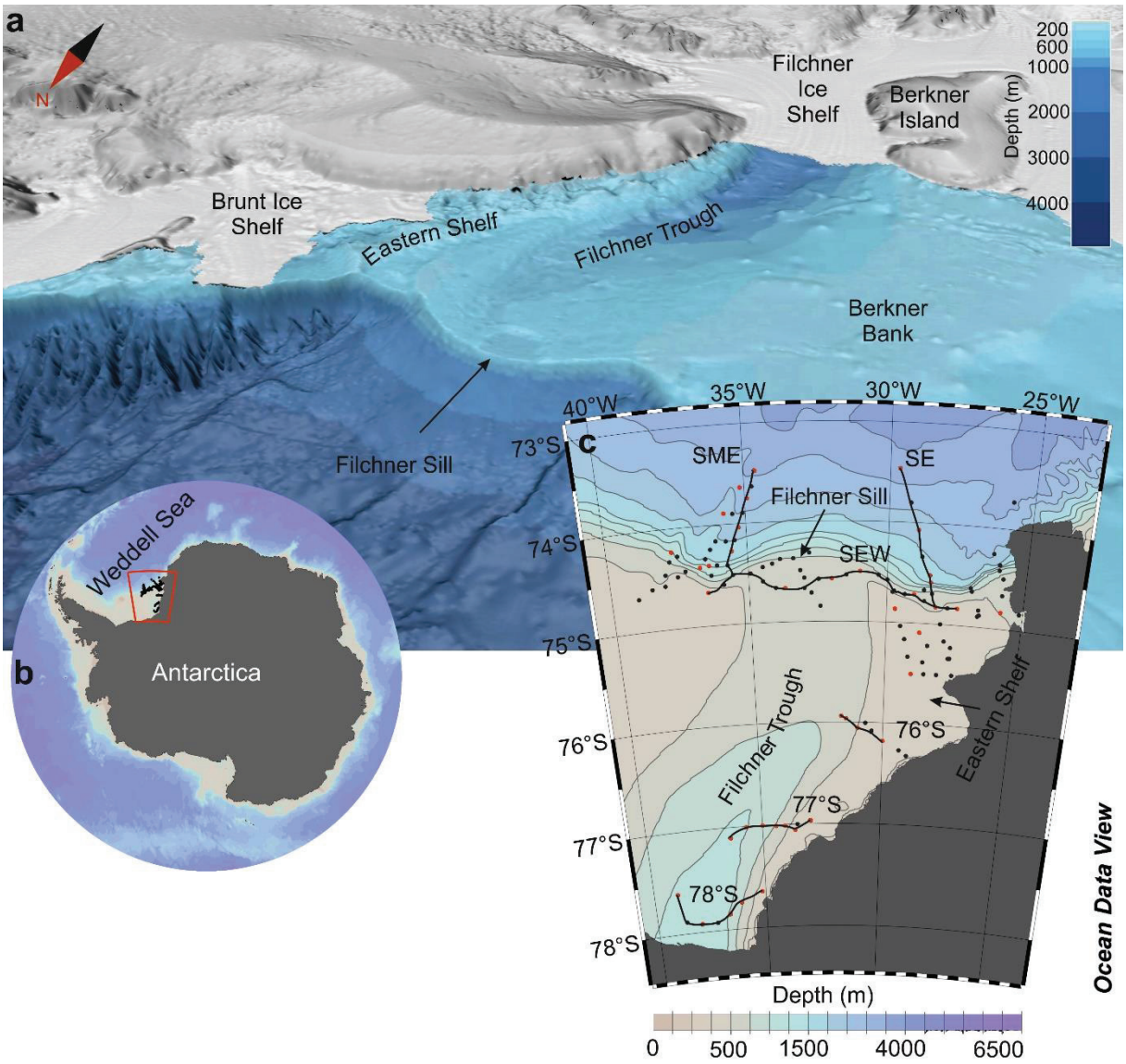

Figure M4.9. Sampling location in the southeastern Weddell Sea. a) 3D image of the seafloor topography of the southeastern Weddell Sea, showing the Filchner Trough and its outflow region. Data from the International Bathymetric Chart of the Southern Ocean (IBCSO) (Arndt et al., 2013). b) Map of Antarctica. The sampling region is indicated by the red box. Sampled stations are marked with black dots. c) Map of the sampled sections. The color scale and contours are of bathymetry. All CTD stations (salinity, temperature and oxygen data) are marked with grey dots. Stations where nutrient and DOM samples were taken are marked with red dots. The sections discussed in this study are indicated as black lines.

Nutrient and DOM analysis

Nutrient samples were analyzed for nitrate, nitrite, phosphate, silicate and ammonium concentrations using an autoanalyzer (Evolution III, Alliance instruments) with standard seawater methods (Kattner and Becker, 1991).

DOC concentrations in seawater and the solid-phase extractable DOC concentrations (DOC_{SPE}) were determined by high temperature catalytic oxidation and subsequent nondispersive infrared spectroscopy and chemiluminescence detection (TOC-V_{CPN} analyzer, Shimadzu). For external calibration, potassium hydrogen phthalate (KHP, Merck) was used. Aliquots of the methanol solid-phase extracts (50 µL) were evaporated under N_2 gas flow to complete dryness and subsequently redissolved in 6.5 mL ultrapure water for DOC analysis (DOC_{SPE}). All samples were acidified (0.1 M HCl suprapur, Merck) and purged with O_2 for >5 min. Performance of the instrument was recorded by analysis of in-lab KHP standard solutions and reference samples (deep sea reference, DSR, Hansell research lab). Final DOC concentrations are average values of triplicate measurements. If the standard variation or the coefficient of variation exceeded 0.05 µmol C L^{-1}, up to 2 additional analyses were performed and outliers were eliminated. The limit of quantification was 21 µmol C L^{-1}. The accuracy was ± 5 %.

Analysis of solid-phase extractable DON (DON_{SPE}) was performed for samples of the sections 78°S and SME in a second measurement by high temperature catalytic oxidation (TOC-V_{CPN} analyzer, Shimadzu) similar to the DOC_{SPE} measurement. For this, 240 µL aliquots of the methanol extracts were used. Final DON_{SPE} concentrations are average values of triplicate measurements. Outliers were eliminated manually. The limit of quantification was 11 µmol N L^{-1}. The accuracy was ± 5 %.

Quantification of solid-phase extractable dissolved organic sulfur (DOS_{SPE}) was performed on an inductively coupled plasma optical emission spectrometer (ICP-OES, iCAP 7400, Thermo, Bremen, Germany). Prior to ICP-OES analysis, 100 µL of the extract was evaporated with N_2 and redissolved in 1 mL nitric acid (1 M, double distilled, Merck). 1 mL of Yttrium (2 µg L^{-1} in the spike solution) was added as internal standard. The sulfur signal was detected at a wavelength of 182.034 nm. Nitric acid (1 M, double distilled, Merck) was used for analysis blank. Calibration standards were prepared in different concentrations from a stock solution (1000 mg L^{-1} Sulfur ICP-standard solution, Carl Roth). To assess the accuracy and precision of the method, the SLRS-5 reference standard (Boyko et al., 2012)was analyzed at the beginning, in between and at the end of each batch run. Although sulfur is not certified for SLRS-5, Yeghicheyan et al. (2013) reported S concentrations of 2347 – 2428 µg S L^{-1}, which is in agreement with our findings. Limit of detection (according to DIN 32645, n=7) was 0.957 µmol L^{-1} S. This corresponds to 0.002 µmol L^{-1} DOS_{SPE} in original seawater (average enrichment factor of 485).

Data evaluation and statistical analysis

Samples with DOC extraction efficiencies ≤ 30 % were excluded from evaluation and discussion of DOC concentrations. Outliers in DOC, DOC_{SPE}, and DOS_{SPE} concentration were

defined graphically with boxplots for each water mass: Values higher than the third quartile plus 1.5 times the interquartile range (IQR) or lower than the first quartile minus 1.5 times IQR were treated as outliers and were omitted in the following evaluation and discussion.

Statistical analysis was performed with the software *R*. Analysis of variances between two groups (surface water vs bottom water and/or Location north of the Filchner sill vs south of the Filchner sill) was performed with the Mann-Whitney-U Test. Analysis of variances between more than two groups (water masses) was performed using the Kruskal-Wallis Test. The relationship between several variables was investigated using Spearman's correlation.

Results

Water masses properties in the south-eastern Weddell Sea

Sampled Water masses

Eight different water masses were assigned based on salinity and potential temperature (T_{pot}) data (Schröder and Wisotzki, 2014) (Fig. M4.2): Antarctic Surface Water (AASW), WW, ISW, ESW, WDW, MWDW, WSDW and WSBW. These water masses were additionally categorized into "colder" water masses with T_{pot} = -1.7 ± 0.3 °C (AASW, WW, ISW, ESW) and "warmer" water masses with T_{pot} = -0.4 ± 0.7 °C (MWDW, WDW, WSDW, WSBW). WSBW was only observed from the oceanographic data set (Schröder and Wisotzki, 2014) and not sampled for nutrient and DOM analysis.

Although sampling took place in austral summer, the study area was characterized by high sea ice concentrations and low surface water temperatures (Fig. M4.3a). A polynya with warmer surface temperatures was located in the east between 75°S and 76°30´S (Fig. M4.3a). During our sampling period, the Weddell Sea was covered by AASW and ESW and below the surface, WW was found. ISW in the bottom water layer of the Filchner trough (sections 76°S, 77°S and 78°S) had its coldest temperatures in the south, close to the Filchner-Ronne Ice Shelf (Fig. M4.3b) and covered the whole Filchner trough at depths below ~200 m. Section SEW is crossing the sill from east to west. Here, MWDW was found below WW. Between 35°W and 32°W, the outflow of ISW was detected at a depth of ~400-600 m. The sections SE and SME were located north of the Filchner sill. They are directing from the shallow eastern and western end of the Filchner sill in the south into the deep Weddell basin in the north. SME is characterized by higher ice cover and lower surface temperatures than section SE (Fig. M4.3a). WDW covered a huge part of the Weddell Sea basin in depths of 500 - 2000 m. Below WDW, WSDW was found.

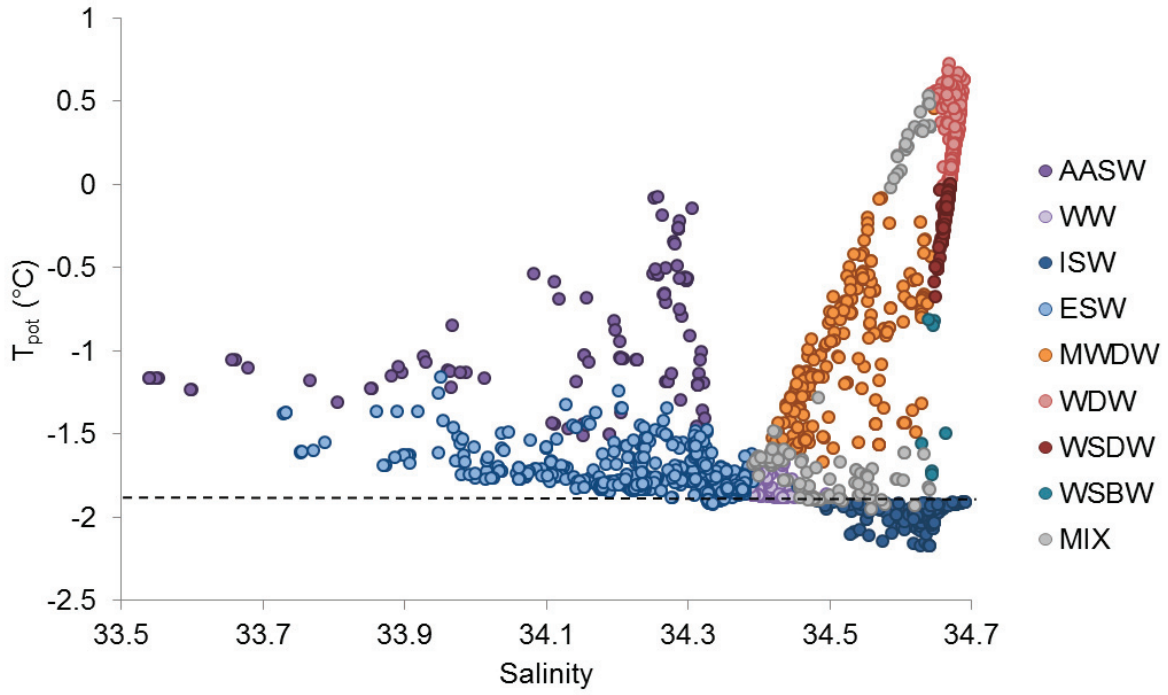

Figure M4.10. T-S-plot of CTD bottle data with color scale for water masses. The dashed line represents the freezing point temperature at one atmosphere pressure.

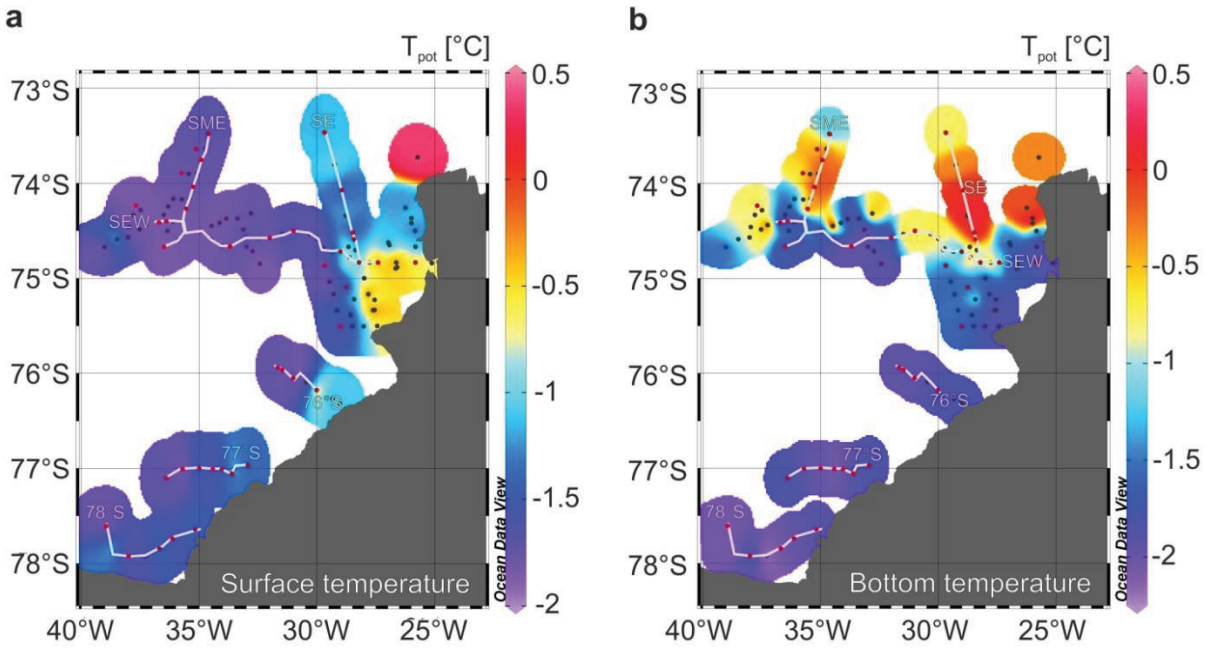

Figure M4.11. Temperature values along the cruise track. a) Surface and b) bottom depth temperature.

Apparent oxygen utilization

Mean AOU values were 66 ± 34 µmol L^{-1}. AOU values of samples from the deeper water column increased up to 141 µmol L^{-1} (Fig. M4.4). The lowest oxygen saturation was ~60 % and AOU values differed significantly between the water masses ($p < 0.001$, Fig. M4.4).

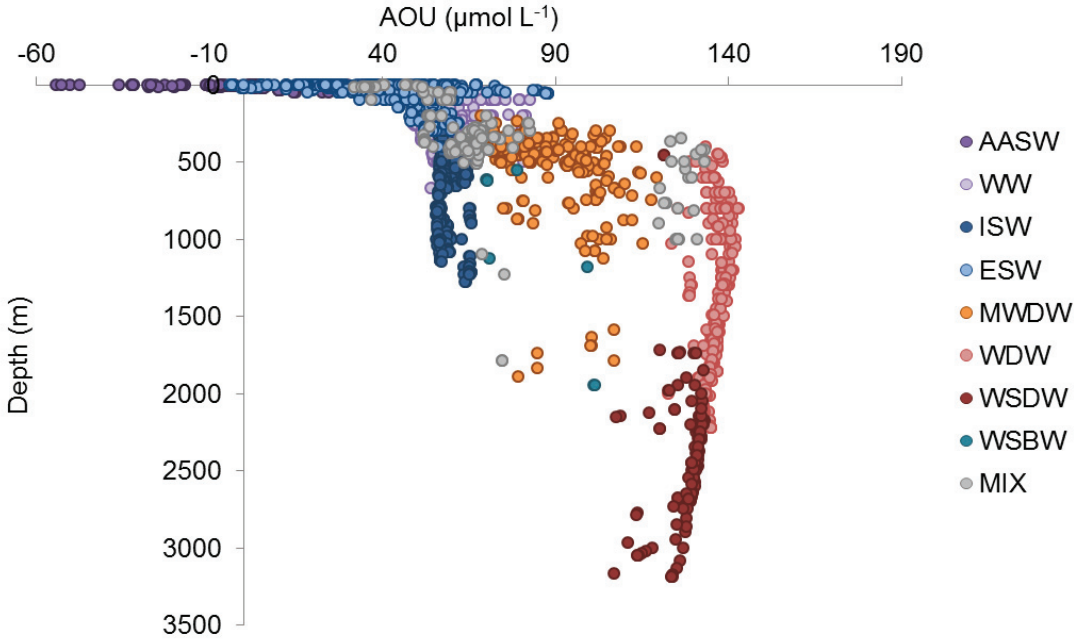

Figure M4.12. Apparent oxygen utilization (AOU) of the different water masses. Changes of AOU with depth are shown. Water masses are represented as colors.

Quantity and distribution of inorganic nutrients

Over all samples, average concentrations of phosphate, silicate and nitrate were significantly higher in bottom water (lowermost 100 m) compared to the surface water (uppermost 100 m, $p < 0.001$, Table M4.1). However, looking at sections 76°S, 77°S and 78°S inside the Filchner trough only, no significant differences between surface and bottom water were found for phosphate and nitrate but for silicate. In sections SEW, SE and SME, significant depth related differences were found for all nutrients. Nitrite and ammonium concentrations, in contrast to silicate, phosphate and nitrate, were significantly higher in surface water compared to bottom water ($p < 0.001$). Additionally, we found significantly higher silicate and nitrite concentrations north of the Filchner trench (SE, SEW and SME), where warmer water masses dominated the sampling area, compared to the region south of the Filchner sill ($p < 0.01$, Fig. M4.5a, Table M4.1). For nitrate, ammonium and phosphate, no significant differences were found between the section areas. Average NO_3/PO_4 ratios of 14.9 ± 1.5 did not differ significantly between surface and bottom water and the different water masses. Only between WW and WSDW, significant differences in NO_3/PO_4 ratio were found ($p < 0.01$).

Table M4.4. Average nutrient concentrations in surface and bottom water samples and the different water masses.

		NO_2^- (µmol L^{-1})	NH_4^+ (µmol L^{-1})	NO_3^- (µmol L^{-1})	$Si(OH)_4$ (µmol L^{-1})	PO_4^{3-} (µmol L^{-1})	NO_3^-/PO_4^{3-} ratio
Depth	Surface (n = 169)	0.09 ± 0.04	0.44 ± 0.21	23.81 ± 4.84	53.03 ± 10.40	1.62 ± 0.26	14.66 ± 1.53
	Bottom (n = 203)	0.07 ± 0.04	0.27 ± 0.17	25.71 ± 4.41	62.68 ± 14.64	1.72 ± 0.23	14.88 ± 1.29
Water masses	AASW (n = 17)	0.11 ± 0.05	0.52 ± 0.32	21.30 ± 5.53	52.29 ± 11.88	1.46 ± 0.34	14.54 ± 1.45
	WW (n = 36)	0.08 ± 0.03	0.26 ± 0.18	25.76 ± 4.45	55.83 ± 9.41	1.68 ± 0.22	15.25 ± 1.36
	ISW (n = 86)	0.06 ± 0.04	0.28 ± 0.18	25.79 ± 3.61	57.35 ± 7.07	1.74 ± 0.20	14.85 ± 1.22
	ESW (n = 98)	0.09 ± 0.04	0.43 ± 0.16	23.96 ± 4.70	52.58 ± 10.44	1.62 ± 0.24	14.71 ± 1.55
	MWDW (n = 25)	0.08 ± 0.04	0.27 ± 0.17	27.10 ± 4.57	64.82 ± 11.61	1.83 ± 0.24	14.75 ± 1.35
	WDW (n = 30)	0.07 ± 0.04	0.24 ± 0.16	25.22 ± 5.38	81.45 ± 19.92	1.71 ± 0.29	14.68 ± 1.43
	WSDW (n = 22)	0.08 ± 0.03	0.28 ± 0.11	24.52 ± 5.56	77.36 ± 20.60	1.68 ± 0.28	14.44 ± 1.15
	MIX (n = 27)	0.07 ± 0.03	0.30 ±0.26	26.54 ± 4.37	59.75 ± 11.56	1.79 ± 0.21	14.88 ± 1.50
Sections	SME (n = 56)	0.09 ± 0.04	0.34 ± 0.16	22.38 ± 5.45	56.71 ± 17.45	1.58 ± 0.24	14.02 ± 1.45
	SEW (n = 74)	0.09 ± 0.04	0.37 ± 0.23	24.60 ± 5.59	55.18 ± 13.13	1.66 ± 0.31	14.71 ± 1.37
	SE (n = 55)	0.08 ± 0.04	0.25 ± 0.15	25.28 ± 5.51	74.20 ± 23.71	1.69 ± 0.32	14.91 ± 1.41
	76°S (n = 29)	0.07 ± 0.04	0.25 ± 0.18	26.95 ± 2.38	59.08 ± 4.31	1.73 ± 0.13	15.54 ± 0.54
	77°S (n = 76)	0.07 ± 0.04	0.29 ± 0.16	26.62 ± 2.89	58.91 ± 4.20	1.70 ± 0.16	15.66 ± 0.45
	78°S (n = 55)	0.05 ± 0.03	0.44 ± 0.26	24.84 ± 3.44	56.04 ± 7.36	1.80 ± 0.21	13.87 ± 1.55
	Total (n = 341)	0.08 ± 0.04	0.33 ± 0.20	25.06 ± 4.70	59.72 ± 14.94	1.69 ± 0.25	14.79 ± 1.39

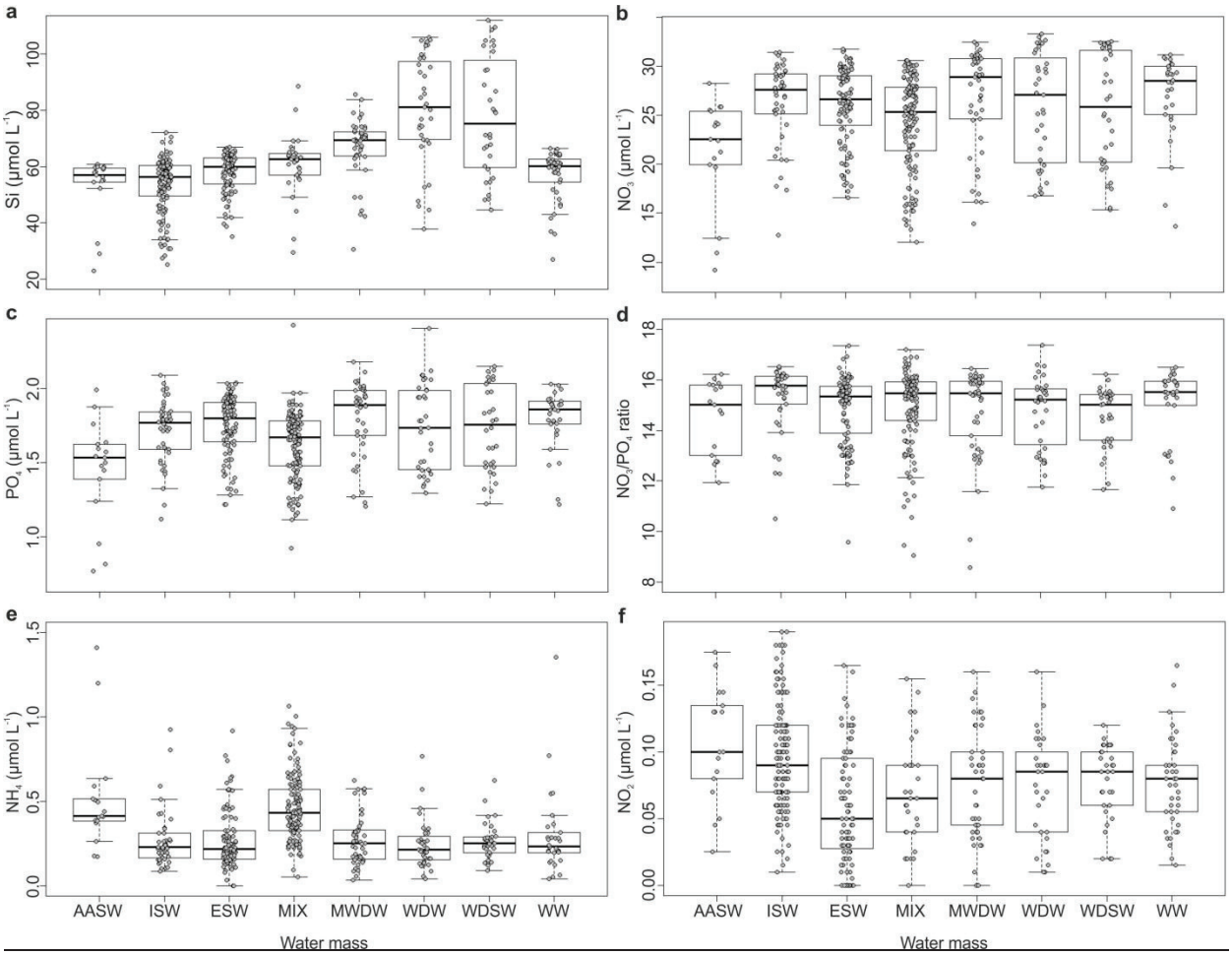

Figure M4.13. Variation in nutrient concentrations of the different water masses. Comparison of a) silicate, b) nitrate and c) phosphate concentrations, d) nitrate versus phosphate ratios, e) ammonium and f) nitrite concentrations.

Quantity and distribution of dissolved organic matter

Overall, DOC concentrations in original seawater samples varied from 38 - 69 µmol L^{-1} (47 ± 6 µmol L^{-1}, Table M4.2). DOC_{SPE} concentrations varied from 18 – 25 µmol L^{-1} (22 ± 1 µmol L^{-1}, Table M4.2). We found significant higher DOC concentrations in surface water (uppermost 100 m) compared to bottom water (lowermost 100 m, $p < 0.01$). DOC_{SPE} concentrations, however, did not differ significantly between surface and bottom water. However, we found significant higher DOC_{SPE} concentrations in colder water masses compared to warmer water masses ($p < 0.01$), whereas we found no differences for DOC concentrations. Significantly higher DOC concentrations were found north of the Filchner sill, compared to the area south of the sill ($p < 0.001$). For DOC_{SPE} in contrast, significantly higher concentrations were found south of the Filchner sill ($p < 0.001$). The average DOC extraction efficiency was 46 ± 7 %. We found no correlation of the extraction efficiency with the chemical composition (DOC_{SPE}/DOS_{SPE} ratio) of the samples.

DON_{SPE} was measured for the southernmost section 78°S and the section SME north of the Filchner sill. DON_{SPE} concentrations of 0.81 ± 0.05 μmol L^{-1} for section SME (warmer water masses) were significantly lower than average DON_{SPE} concentrations of 0.89 ± 0.08 μmol L^{-1} at section 78°S (colder water masses, $p < 0.001$, Table M4.2). No significant differences were found between surface and bottom water. Molar DOC_{SPE}/DON_{SPE} ratios of 25 ± 4 did not differ significantly between the two sections or between surface and bottom water.

Concentrations of DOS_{SPE} ranged from 0.05 to 0.30 μmol L^{-1} (0.08 ± 0.04 μmol L^{-1}) and were significantly higher in surface waters compared to bottom waters ($p = 0.001$, Table M4.2). Additionally, we found significant differences between colder and warmer water masses ($p < 0.001$), whereas no differences in DOS_{SPE} concentrations were found between the sampling locations north and south of the Filchner sill. Molar DOC_{SPE}/DOS_{SPE} ratios ranged from 89 – 438 (292 ± 70) and were significantly lower in surface waters compared to bottom waters ($p = 0.01$). Also, DOC_{SPE}/DOS_{SPE} ratios differed throughout the water masses, with significantly higher DOC_{SPE}/DOS_{SPE} ratios in warmer water masses compared to colder water masses ($p < 0.5$). However, no significant differences were found comparing the area north and south of the Filchner sill. Molar DOS_{SPE}/DON_{SPE} ratios of 0.12 ± 0.05 in section 78°S and 0.10 ± 0.03 in section SME differed significantly between the two sections ($p < 0.01$). Additionally, DOS_{SPE}/DON_{SPE} ratios were significantly higher in surface waters compared to bottom waters ($p < 0.05$).

The distribution of DOC, DOC_{SPE}, and DOS_{SPE} across the sections is shown in Figs. M4.6 and M4.7.

Table M4.5: Mean concentrations, molar elemental ratios and respective standard deviations of DOM in the different water masses. DON_{SPE} was analyzed for the two sections 78°S and SME, resulting in low sample numbers for each water mass. Thus, average values of DON_{SPE} concentration and molar DOC_{SPE}/DON_{SPE} and DOS_{SPE}/DON_{SPE} ratios are only given for the two sections and the comparison of surface and bottom water.

		DOC (µmol L^{-1})	DOC_{SPE} (µmol L^{-1})	DON_{SPE} (µmol L^{-1})	DOC_{SPE}/DON_{SPE} ratio	DOS_{SPE} (µmol L^{-1})	DOC_{SPE}/DOS_{SPE} ratio	DOS_{SPE}/DON_{SPE} ratio
Depth	Surface	48 ± 6	22 ± 1	0.86 ± 0.08	25 ± 2	0.09 ± 0.04	277 ± 76	0.12 ± 0.04
	Bottom	46 ±6	22 ± 1	0.84 ± 0.07	26 ± 2	0.08 ± 0.04	303 ± 66	0.10 ± 0.02
Water masses	AASW	48 ± 2	22 ± 1	-	-	0.09 ± 0.03	285 ± 65	-
	WW	45 ± 4	22 ± 1	-	-	0.11 ± 0.07	266 ± 90	-
	ISW	46 ± 5	22 ± 2	-	-	0.07 ± 0.01	302 ± 55	-
	ESW	48 ± 6	21 ± 2	-	-	0.09 ± 0.04	267 ± 79	-
	MWDW	44 ± 5	21 ± 2	-	-	0.07 ± 0.01	306 ± 42	-
	WDW	48 ± 6	21 ± 2	-	-	0.07 ± 0.02	295 ± 57	-
	WSDW	49 ± 8	21 ± 1	-	-	0.06 ± 0.01	331 ± 42	-
Sections	SME	51 ± 8	20 ± 1	0.81 ± 0.05	25.4 ± 1.9	0.07 ± 0.02	313 ± 66	0.10 ± 0.03
	SEW	47 ± 5	22 ± 2	-	-	0.09 ± 0.04	281 ± 73	-
	SE	48 ± 6	22 ± 2	-	-	0.07 ± 0.01	297 ± 47	-
	76°S	43 ± 4	22 ± 1	-	-	0.07 ± 0.01	303 ± 35	-
	77°S	45 ± 5	22 ± 1	-	-	0.08 ± 0.04	296 ± 81	-
	78°S	49 ± 7	22 ± 1	0.89 ± 0.08	25.4 ± 2.4	0.10 ± 0.04	260 ± 68	0.12 ±0.05
	Total	47 ± 6	21 ± 1	0.85 ± 0.08	25.4 ± 2.1	0.08 ± 0.04	292 ± 70	0.11 ± 0.03

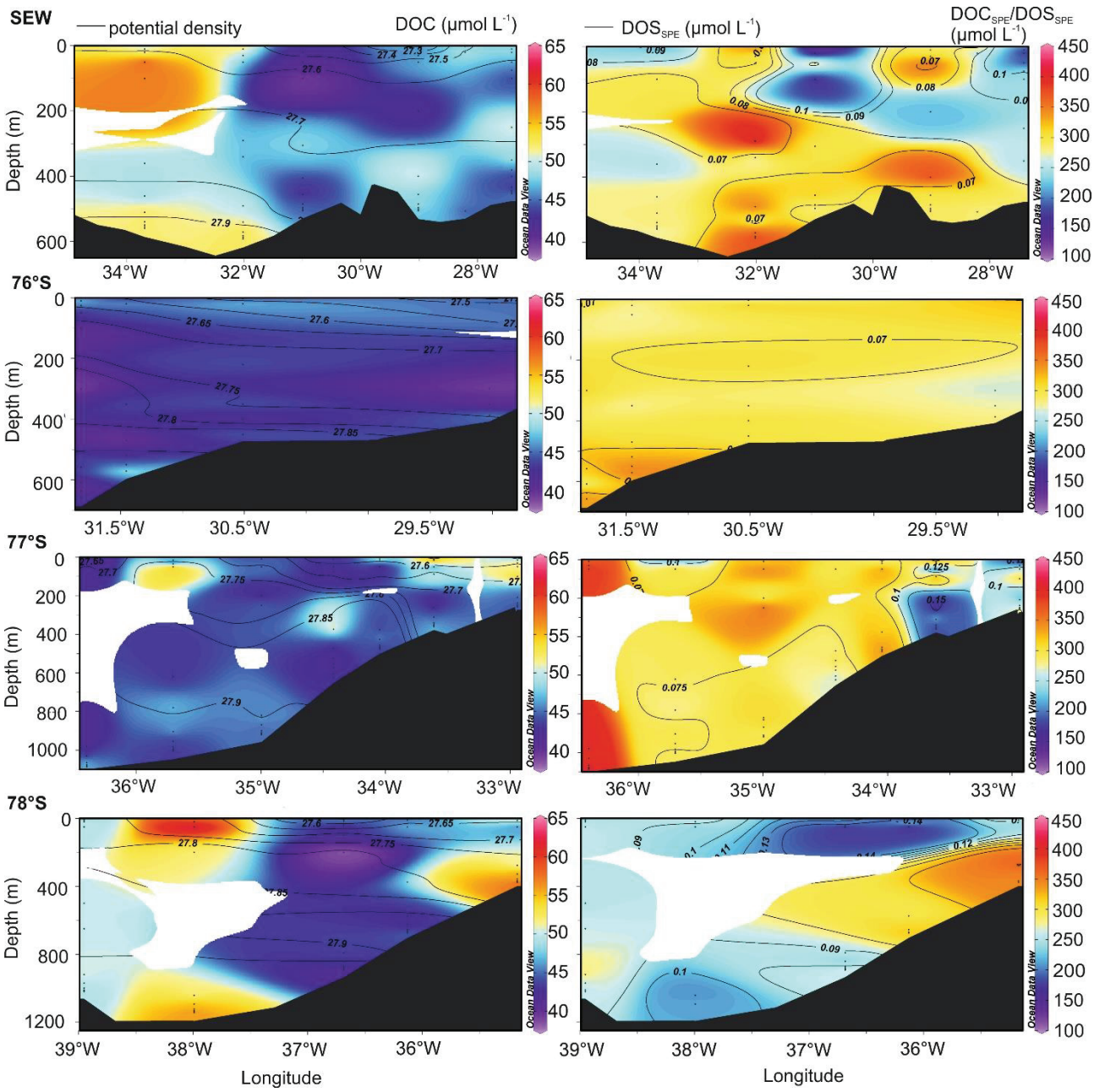

Figure M4.6. Changes in DOC, and DOS_{SPE} concentrations of sections SEW (first row), 76°S (second row), 77°S (third row) and 78°S (fourth row) along the Filchner trench from north to south. Left column: DOC concentrations in colors and potential density as contour lines. Right column: Molar DOC_{SPE}/DOS_{SPE} ratios in colors and DOS_{SPE} concentrations as contour lines.

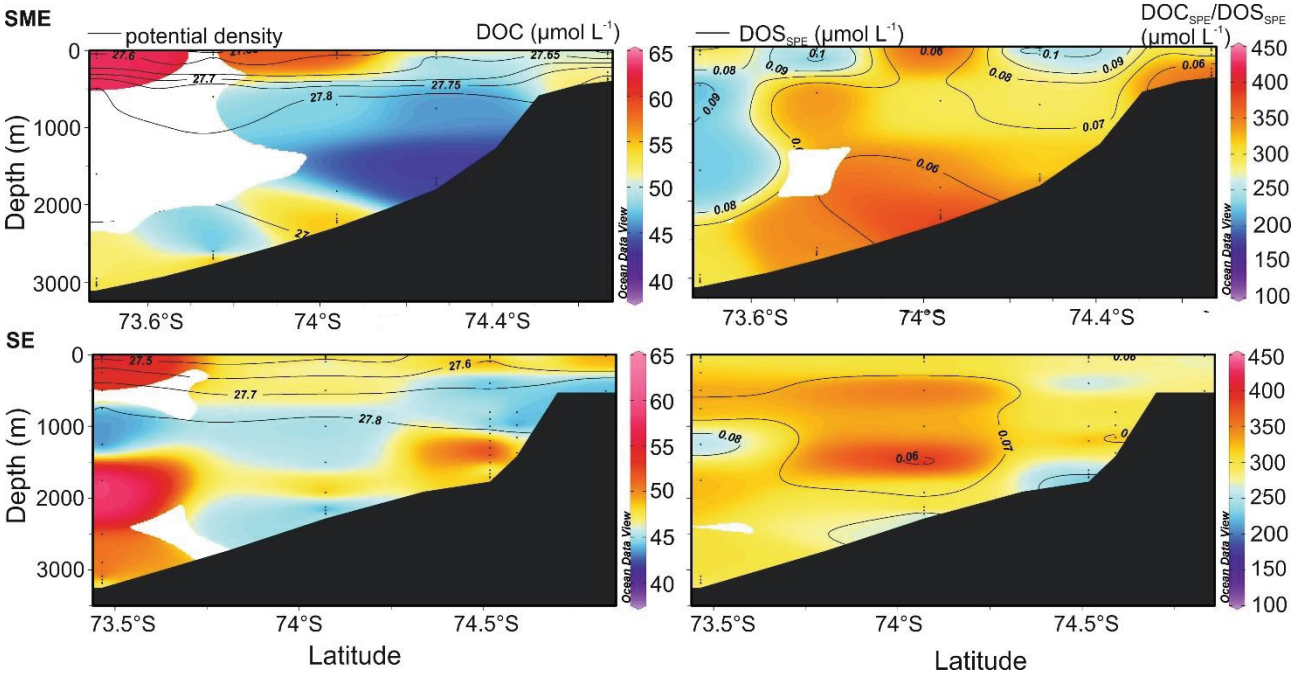

Figure M4.7. Changes in DOC and DOS_{SPE} concentrations of the sections SME (first row) and SE (second row). Left column: DOC concentrations in colors and potential density as contour lines. Right column: Molar DOC_{SPE}/DOS_{SPE} ratios in colors and DOS_{SPE} concentrations as contour lines.

To test if AOU controls organic carbon and sulfur speciation in the water column, concentrations of DOC, DOC_{SPE}, DON_{SPE}, and DOS_{SPE} were plotted against AOU and the significance and grade of a Spearman correlation was tested (Fig. M4.8).

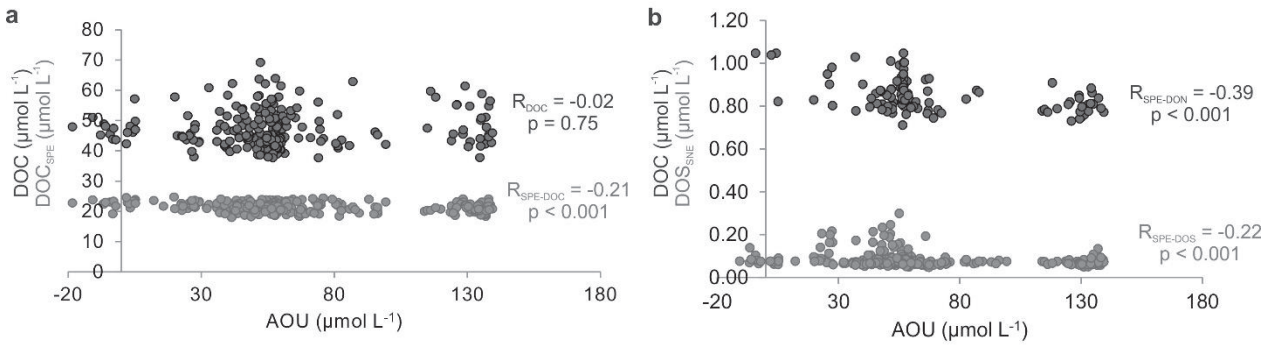

Figure M4.14. Correlation of DOM and AOU in the Weddell Sea. Spearman correlation of a) DOC and DOC_{SPE} and b) DON_{SPE} and DOS_{SPE} with AOU.

For our samples, we found a significant moderate negative correlation of DON_{SPE} with AOU ($p < 0.001$, Spearman's $R_{DON_AOU} = 0.39$Fig. 8b). No or only weak correlations of DOC, DOC_{SPE}, and DOS_{SPE} with AOU were found (Fig. M4.8a + b).

Discussion

Inorganic nutrient availability

Nutrient concentrations (Table M4.1) were in the lower range of values previously found in other regions of the Weddell Sea during austral summer ($[NO_3^-]$ ~15 – 35 µmol L^{-1}, $[PO_4^{3-}]$ ~1 – 2.5 µmol L^{-1}, $[Si(OH)_4]$ ~0 – 125 µmol L^{-1}, $[NO_2^-]$ ~0 – 0.2 µmol L^{-1}, and [NH4] ~1.8 µmol L^{-1}, Clarke et al. (2008); Hoppema et al. (2015)). Compared to other oceanic regions, the values are high due to the fact that nutrient consumption is limited by the availability of iron and thus, low phytoplankton abundance occurs (high-nutrient, low-chlorophyll region) (Martin et al., 1990). Since our cruise was performed during austral summer, when nutrient concentrations are depleted due to net consumption by algae, we could expect even higher nutrient concentrations during winter time (Clarke et al., 2008). The dissolved inorganic nitrogen (DIN) pool is mainly nitrate, with ammonium and nitrite together representing only ~1.7 % of the total DIN pool. Nitrate and phosphate concentrations showed a strong linear correlation (Spearman's $R = 0.85$, $p < 0.001$), representing a stoichiometry close to the Redfield ratio (mean NO3/PO4 ratio ~15).

Overall, concentrations of the major nutrients silicate, nitrate and phosphate were depleted in surface water compared to deeper water (by ~15 % for silicate and ~7 % for phosphate and nitrate, Table M4.1) and thus, followed common nutrient depth profiles (Hoppema et al., 2015; Nelson and Gordon, 1982). Inside the Filchner trough, however, phosphate and nitrate concentrations were not depleted in surface water compared to bottom water. The Filchner trough was largely ice-covered, resulting in low phytoplankton abundance (as estimated from the CTD fluorescence signal as proxy of the chlorophyll a concentration; data not shown) and thus, low nutrient consumption. Higher chlorophyll a concentrations and thus, lower nutrient concentrations were only found at the westernmost part of section 76°S, where a polynya was located. For silicate, in contrast, significant higher concentrations in bottom water compared to surface water were found not only north of the Filchner sill (as for nitrate and phosphate) but also inside the Filchner trough. Inside the Filchner trough, ISW and ESW are the predominant water masses. Thus, the ice shelves and sea ice, but also icebergs are most likely the major nutrient sources to the Filchner trough (Bertolin and Schloss, 2009; Duprat et al., 2016; Wadham et al., 2013). For silicate, we assume that sedimentary sources and weathering of rocks are responsible for the relatively higher concentration compared to nitrate and phosphate.

Nitrite and ammonium are products of microbial mineralisation of organic matter and usually do not follow the depth profiles of nitrate, silicate and phosphate. Accordingly, most stations inside and outside the Filchner trough showed maximum concentrations of nitrite (0.19 µmol L-1) and ammonium (1.41 µmol L-1) in the surface layer (AASW and ESW). Although nitrite usually is highest in the surface layer, we also found high nitrite concentrations in the bottom layer, e.g. in sections SEW

and SME. Our results confirm previous findings of significant non-zero nitrite concentrations throughout the water column of the Weddell Sea (Hoppema et al., 2015). It was hypothesized that – at these depths – nitrite was produced by decaying sinking phytoplankton blooms (Hoppema et al., 2015).

DOM in the Weddell Sea

Spatial differences and biogeochemical indications

DOC, DOC_{SPE}, DON_{SPE} and DOS_{SPE} concentrations were in accordance with values previously reported for the Atlantic sector of the Southern Ocean (Ksionzek et al., 2016a). In other regions of the Southern Ocean, e.g the Ross Sea, DOC concentrations in deeper water masses were ~40 μmol L^{-1} and thus, slightly lower than the values found in this study (Bercovici and Hansell, 2016; Bercovici et al., 2017). Spatial differences in DOM concentrations were located: Following the dominant water mass ISW from south to north through the Filchner trough (sections 78°S, 77°S and 76°S), we found a significant decrease in DOC, DOC_{SPE} and DOS_{SPE} concentrations and an increase in molar DOC_{SPE}/DOS_{SPE} ratios. North of the Filchner trough, in the outflow region, concentrations of DOC_{SPE} and DOS_{SPE} were even lower. For DOC however, concentrations north of the Filchner sill were as high as in the southernmost section 78°S. Also DON_{SPE} concentrations (which were analysed for two sections), were significantly higher in the south (section 78°S) compared to the north (SME). The Filchner trough is dominated by high salinity ISW which has its origin at the Filchner Ronne Ice Shelf and most likely contains high DOM concentrations derived from the ice shelf and sea ice (Thomas et al., 2001; Thomas and Papadimitriou, 2003; Zemmelink et al., 2008). ISW moves northward to the Filchner sill. On its way, DOM is transported northwards and likely degraded during that time, resulting in lower DOM concentrations in the northern part of the Filchner trough. In the area of the Filchner outflow, additional mixing with older water masses, low in DOM concentrations occurs, resulting in further decrease of DOM concentrations. To assess and compare the relative decrease of DOM_{SPE} compounds inside the Filchner trough, we compared DOC_{SPE} and DOS_{SPE} "endmember" concentrations at the sections 78°S and 76°S. Overall, the mean endmember concentrations differed significantly. We found a relative reduction in DOC_{SPE} concentration of ~3 % and DOS_{SPE} concentrations of ~30 %, indicating faster removal (higher lability) of DOS_{SPE} compared to DOC_{SPE}. Focusing at single water masses, e.g. ESW, these differences were even more pronounced with a DOC_{SPE} and DOS_{SPE} reduction of ~5 % and ~42 % respectively. This is in accordance with previous studies, showing preferential depletion of sulfur (as well as nitrogen and phosphorous) relative to carbon (Hopkinson et al., 2002; Ksionzek et al., 2016a; Ksionzek et al., 2018).

Over all samples, we found a significant moderate and strong positive correlation of DOS_{SPE} with DOC_{SPE} and DON_{SPE} respectively ($p < 0.001$, Spearmans's $R_{C/S} = 0.30$, $R_{S/N} = 0.51$). The molar DOC_{SPE}/DOS_{SPE} and DOC_{SPE}/DON_{SPE} ratios can be interpreted as degradation signals. Molar DOC_{SPE}/DOS_{SPE} ratios were higher than that of phytoplankton (average C/S ~95) and increased with

depth, reflecting the non-labile character of DOM and preferential DOS_{SPE} removal compared to DOC_{SPE} as discussed above. This finding is also consistent with the high radiocarbon age of DOM as previously found in the Southern Ocean (Flerus et al., 2012; Ksionzek et al., 2016a; Lechtenfeld et al., 2014). In contrast, molar DOC_{SPE}/DON_{SPE} ratios were rather invariant with depth, possibly due to an inefficient extraction of nitrogen compared to carbon (Flerus et al., 2012; Ksionzek et al., 2018; Lechtenfeld et al., 2014). This contradicts with increasing molar DOC_{SPE}/DON_{SPE} ratios and faster removal of DON_{SPE} (similar to DSO_{SPE}) compared to DOC_{SPE}, as previously found for the Atlantic sector of the Southern Ocean (Ksionzek et al., 2016a) and disagree our hypothesis as stated in the introduction. Higher DOC_{SPE}, DON_{SPE} and DOS_{SPE} concentrations and lower DOC_{SPE}/DOS_{SPE} ratios in the south compared to the area north of the Filchner sill, indicate the presence of "fresher" sea-ice or ice-shelf derived DOM. The molar DOS_{SPE}/DON_{SPE} ratio is used as biomass signal. Average molar DOS_{SPE}/DON_{SPE} ratios of 0.11 ± 0.03 were comparable to phytoplankton stoichiometry (S/N ~0.08) and values found in a previous study (Ho et al., 2003; Ksionzek et al., 2016a). This indicates a predominantly biogenic DOS imprint (Gonsior et al., 2011; Ksionzek et al., 2016a). In contrast, riverine DOM (predominantly terrestrial imprint) is characterized by higher S/N ratios of ~0.23 (Ksionzek et al., 2018). However, molar DOS_{SPE}/DON_{SPE} ratios of this study decreased with depth, which is in contrast to almost constant DOS_{SPE}/DON_{SPE} ratios throughout the water column as found in the East Atlantic and the Atlantic sector of the Southern Ocean (Ksionzek et al., 2016a).

DOM depths profiles - how to explain elevated DOC concentrations in bottom water?

Typical DOM depth profiles from the Southern Ocean and other studies around the world show elevated surface concentrations, which are decreasing with depth. However, in former expeditions to the Weddell Sea, elevated DOC concentrations were also found in bottom water. The Weddell Sea is one of the major areas for bottom water formation (Orsi et al., 1999; Reid and Lynn, 1971). Thus, we hypothesized that fresh DOM might be transported to deep water formation and sea-ice derived organic matter can be detected in bottom water of the Southern Weddell Sea. Until now, the data are fragmentary and do not allow for reliable conclusions. To investigate whether these increased concentrations are indeed present, we sampled in higher depth resolution in the upper 100 m of the water column and above the seafloor.

The depth profiles of some stations indeed revealed elevated DOC concentrations in the bottom water (e.g. Station 93 – 78°S, Stations 61+80 – 77°S, Stations 22+28 – 76°S, Station 181+189 – SEW). In general, possible reasons are: (i) downwelling of (freshly produced) surface DOM (DOC) and (ii) sedimentary efflux of DOM. In the following, evidence for each possibility will be discussed.

(i) Downwelling of (freshly produced) surface DOM

Elevated DOC concentrations were mostly found inside the Filchner trough. There, high saline DOM-rich ISW from the Filchner Ice Shelf is transported northward through the Filchner trough. Due to its high density, it covers the bottom layer of the trough and might thus contribute to elevated DOC concentrations in the bottom water. The Filchner sill at section SEW is the outflow region of ISW. Here, also elevated DOC bottom water concentrations were found. This indicates, that downwellig might indeed (at least partly) contribute to elevated DOC concentrations in bottom water.

(ii) Sedimentary DOM efflux

Additional analysis of pore water samples and the overlying water of sediment cores also sampled during our expedition, revealed high sediment pore water DOC concentrations up to 700 μmol L^{-1} (Geuer, 2015). However, elevated DOC concentrations in the overlying water of the sediment core were only sporadically observed. Nevertheless, the molecular composition of DOM in sediment pore water and the overlying water (analysed by Fourier-Transform-Ion–Cyclotron-Mass Spectrometry) was similar (Geuer, 2015), indeed suggesting sedimentary DOM efflux, as also found in other regions (Boto et al., 1989; Otto and Balzer, 1998). This indicates that sedimentary efflux of DOM cannot be excluded but is most likely not a major source for elevated bottom water DOC concentrations.

The relationship of AOU with DOM

Surface AOU concentrations were around zero, indicating ocean-atmosphere interactions of surface water. Negative values found in surface samples indicate supersaturation, e.g. due to primary production. Positive AOU values indicate undersaturation due to oxygen consumption, e.g. during DOM remineralization. AOU values were similar to those previously reported for the Southern Ocean (Iida et al., 2013; Yamashita et al., 2007).

The relationship of AOU and DOC has been intensively studied in the past. The grade of correlation ranges from no or weak correlation in the Southern California Bight and the Equatorial Atlantic Ocean (Hansell et al., 1993; Thomas et al., 1995) to good and even strong correlations in the Atlantic Ocean, the meso and bathypelagic North Atlantic and Mediterranean Sea and the North Pacific Subtropical Gyre (Abell et al., 2000; Carlson et al., 2010; Pan et al., 2014; Santinelli et al., 2010). Especially in surface water, no clear conclusions can be drawn when correlating changes in DOM (or nutrient) concentrations with changes in AOU. Here, AOU is not only dependent on microbial activity but also on atmospheric interactions. In deeper water masses however, not only correlations of DOC with AOU, but also of NO_3 with AOU (e.g. in the northeast Atlantic Ocean) has been found as indicator for biological utilization of oxygen during organic matter remineralization (Hansman et al., 2015). Previous studies used the DOC/AOU molar ratio, to calculate the contribution of DOC (or total organic carbon) degradation to AOU, which varies from < 20 % in equatorial regions to ~80 % in subtropical gyres (Pan et al., 2014).

We hypothesized that AOU also controls organic carbon and sulfur speciation in the water column below the sea-ice and at the sediment-water interface.

For our samples, we only found a moderate negative correlation of DON_{SPE} AOU. DOC, DOC_{SPE}, and DOS_{SPE} showed no or only weak correlations with AOU (Fig. M4.8a + b). However, the correlations observed, predominantly appear from mixing of the different water masses, controlling AOU distribution, which is also indicated by a significant correlation of salinity and AOU ($p < 0.001$, Spearman's $R = 0.75$). No correlation of DOM (and nutrients concentrations – see Supplements) was found when looking at the single water masses. Additionally, DOM in the Southern Ocean is mainly characterized by relatively high radiocarbon age (Ksionzek et al., 2016a; Lechtenfeld et al., 2014) and the DOM degradation index (which can be used to compare the degradation state/relative age of DOM (Flerus et al., 2012)) is quite high. It has been shown that the correlation of DOC and AOU is stronger for "younger" more labile samples of the upper 1000 m of the water column than for "older" non-labile samples of the bathypelagic realm e.g. in the Atlantic Ocean (Hansman et al., 2015). This is further supported by a strong correlation between the degradation index of DOM and AOU as found in the northeast Atlantic Ocean (Hansman et al., 2015). Thus, it seems reasonable to find no or only weak correlation of non-labile DOC and DOS with AOU.

Although we were not able to confirm our hypothesis for the Weddell Sea, it is still reasonable for other regions such as the Atlantic Ocean, where strong correlations of DOC and AOU were already found (Pan et al., 2014). Therefore, we compared AOU Data from the East Atlantic Ocean (World Ocean Atlas 2009: monthly data for November (Garcia et al., 2010)) with DOC, DOC_{SPE}, and DOS_{SPE} data from another expedition in the same region (Ksionzek et al., 2016a). We found moderate to strong significant negative correlations of DOC (Spearman's $R = 0.50$), DOC_{SPE} (Spearman's $R = 0.51$), DON_{SPE} (Spearman's $R = 0.39$) and DOS_{SPE} (Spearman's $R = 0.50$) with AOU ($p < 0.001$, Fig. M4.8). Here, only a weak but significant correlation of salinity and AOU was found ($p = 0.02$, Spearman's $R = -0.19$), indicating a less pronounced influence of water mass mixing on AOU distribution.

The observed correlations are higher than for the Weddell Sea samples, but mainly driven by the high surface DOM concentrations. In the upper water column, however, the oxygen consumption (increasing AOU) might at least partly be superimposed by oxygen input via ocean-atmosphere interactions. Thus, no conclusions on the contribution of DOM remineralization on oxygen consumption could be drawn. The non-labile character of DOM in water depth > 200 m results in relative constant background DOC, DOC_{SPE}, DON_{SPE} and DOS_{SPE} concentrations (Ksionzek et al., 2016a), while AOU further increased (Garcia et al., 2010). Thus, for samples from deeper water, no correlation of DOM with AOU was found at all.

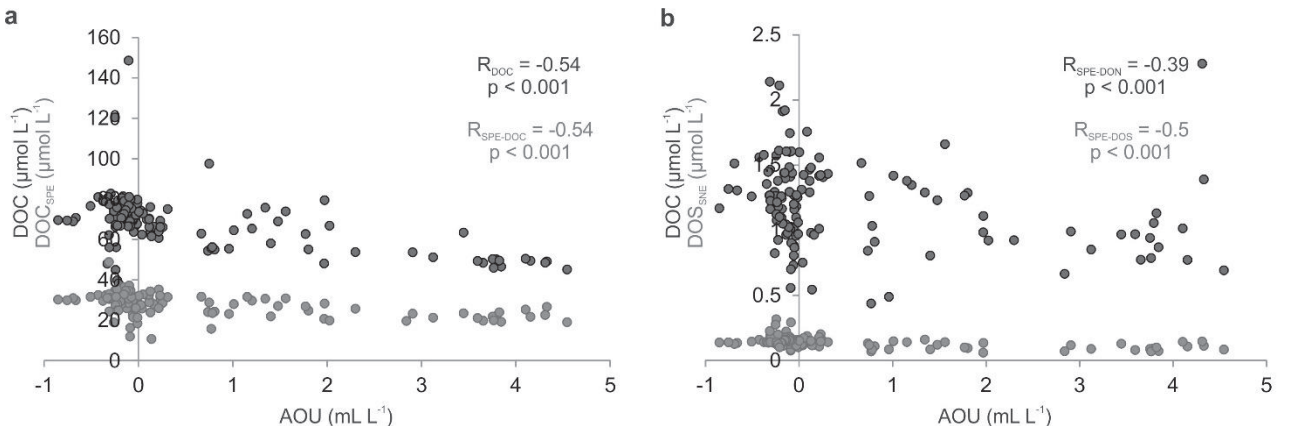

Figure M4.9. Correlation of DOM and AOU in the East Atlantic Ocean. Spearman correlation of a) DOC and DOC_{SPE} and b) DON_{SPE} and DOS_{SPE} with AOU.

Conclusion

In this study we presented concentrations and distribution of inorganic nutrients and DOM, including the first basin scale distribution of DOS_{SPE} in the Weddell Sea. With regard to the research questions/hypothesizes stated in the introduction, we can conclude:

(i) Inorganic nutrient and DOM concentrations were in accordance with values previously published for other regions of the Southern Ocean. North of the Filchner sill, nutrient concentrations followed typical nutrient depth profiles and were depleted in surface water compared to bottom water, whereas nutrient consumption in the surface water of the Filchner trough was limited due to the high ice cover and low phytoplankton abundance/ primary production. Limited primary production would also lead to lower DOM concentrations in the ice-covered sections of the Filchner trough. Nevertheless, we found significantly higher DOM concentrations in the southernmost section (78°S) close to the ice shelf compared to the northern section of the trough (76°S). This leads to suggest additional DOM sources from sea ice and the ice shelves. The assessment of the relative decrease of DOC_{SPE} and DOS_{SPE} during DOM transport inside the Filchner trough from south to north revealed significantly faster removal of DOS_{SPE} relative to DOC_{SPE}.

(ii) In this study, elevated DOC concentrations in the bottom water were found inside the Filchner trough and at the Filchner sill. We suggest downwelling of high salinity DOM-rich ISW and ESW as the major DOM source to the bottom water. There is also evidence for sedimentary DOM efflux, which, however, is most likely only a minor contributor to the elevated DOC concentration in the bottom water.

(iii) As hypothesized, molar DOC_{SPE}/DOS_{SPE} ratios decreased with depth, indicating DOM degradation. Molar DOC_{SPE}/DON_{SPE} ratios in contrast, were rather invariant with depth. Molar DOS_{SPE}/DON_{SPE} ratios - applied as a biomass signal - revealed comparability to phytoplankton

stoichiometry and thus, a predominant DOS source. In contrast to our hypothesis however, S/N ratios decreased with depth.

(iv) We found no correlation of DOM (or nutrients) with AOU in the southern Weddell Sea, which clearly results from DOM removal due to biological activity. In this study, AUO distribution was mainly driven by mixing of different water masses. Additionally, the non-labile character of DOM sampled in this study, revealed no significant contribution of DOM degradation to oxygen consumption.

Acknowledgements

This work was supported by the DFG-Research Centre / Cluster of Excellence "The Ocean in the Earth System". We thank on RV *Polarstern* captain, crew and chief scientist Rainer Knust, Claudia Burau is acknowledged for DON_{SPE} analysis. Michael Schröder, Wilma Huneke and Stefanie Semper are acknowledged for CTD data. We thank Mario Hoppema for helpful discussion on the nutrient data.

IV.5 Manuscript 5

The influence of dissolved organic matter on the marine production of carbonyl sulfide (OCS) and carbon disulfide (CS_2) in the Peruvian upwelling

S.T. Lennartz [1,a], M. von Hobe[2], D. Booge[1], H. Bittig[3], T. Fischer[1], R. Gonçalves-Araujo[4,5], K.B. Ksionzek[4,6], B.P. Koch[4,7,8], A. Bracher[4,8], R. Röttgers[9], B. Quack[1] , C.A. Marandino[1]

1 GEOMAR Helmholtz Centre for Ocean Research Kiel, Düsternbrooker Weg 20, 24105 Kiel, Germany

2 Forschungszentrum Jülich GmbH, Institute of Energy and Climate Research (IEK-7), Wilhelm-Johnen-Strasse, 52425 Jülich, Germany

3 Leibniz Institute for Baltic Sea Research Warnemünde, Seestraße 15, D-18119 Rostock

4 Alfred Wegener Institute Helmholtz Centre for Polar and Marine Research, Am Handelshafen 12, 27570 Bremerhaven, Germany

5 Aarhus University, Department of Bioscience, Frederiksborgvej 399, 4000 Roskilde, Denmark

6 MARUM Center for Marine Environmental Sciences, Leobener Straße, D-28359 Bremen, Germany.

7 University of Applied Sciences, An der Karlstadt, 27568 Bremerhaven

8 Institute of Environmental Physics, University of Bremen, 28334 Bremen, Germany

9 Helmholtz-Zentrum Geesthacht, 21502 Geesthacht, Germany

[a]now at: Insitute for Biology and Chemistry of the Marine Environment, University of Oldenburg, Oldenburg

Correspondence to: Sinikka T. Lennartz (sinikka.lennartz@uni-oldenburg.de)

Abstract. Oceanic emissions of the climate relevant trace gases carbonyl sulfide (OCS) and carbon disulfide (CS_2) are a major source to their atmospheric budget. Their current and future emission estimates are still uncertain due to incomplete process understanding and, therefore, inexact quantification across different biogeochemical regimes. Here we present the first concurrent measurements of both gases together with related fractions of the dissolved organic matter (DOM) pool, i.e. solid-phase extractable dissolved organic sulfur (DOS_{SPE}, n=24, 0.16±0.04 μmol L^{-1}), chromophoric (CDOM, n=76, 0.152±0.03) and fluorescent dissolved organic matter (FDOM, n=35) from the Peruvian upwelling region (Guayaquil, Ecuador to Antofagasta, Chile, October 2015). OCS was measured continuously with an equilibrator connected to an off-axis integrated cavity output spectrometer at the surface (29.8±19.8 pmol L^{-1}) and at four profiles ranging down to 136 m. CS_2 was measured at the surface (n=143, 17.8±9.0 pmol L^{-1}) and below, ranging down to 1000 m (24 profiles). These observations were used to estimate *in-situ* production rates and identify their drivers. We find different limiting factors of marine photoproduction: while OCS production is limited by the humic-like DOM fraction that can act as a photosensitizer, high CS_2 production coincides with high DOS_{SPE} concentration. Quantifying OCS photoproduction using a specific humic-like FDOM component as proxy, together with an updated parameterization for dark production, improves agreement with observations in a 1D biogeochemical model. Our results will help to better predict oceanic concentrations and emissions of both gases on regional and, potentially, global scales.

1 Introduction

Oceanic emissions play a dominant role in the atmospheric budget of the climate relevant trace gases carbonyl sulfide (OCS) and carbon disulfide (CS_2) (Chin and Davis, 1993; Kremser et al., 2016). OCS is the most abundant sulfur gas in the atmosphere, and CS_2 is its most important precursor. Both gases influence the climate directly (OCS) or indirectly (CS_2 by oxidation to OCS in the atmosphere), as OCS is a major supplier of stratospheric aerosols (Brühl et al., 2012; Crutzen, 1976), which exert a cooling effect on the atmosphere and can foster ozone depletion (Junge et al., 1961; Kremser et al., 2016). Furthermore, OCS has been suggested as a proxy to constrain global terrestrial gross primary production (Campbell et al., 2008; Montzka et al., 2007; Berry et al., 2013). The oceanic emissions of both gases have recently gained interest because they are suggested to account for a missing source of atmospheric OCS (Berry et al., 2013; Kuai et al., 2015; Glatthor et al., 2015; Launois et al., 2015). *In-situ* measurements of OCS in surface seawater are still limited, but those available suggest that oceanic emissions are too low to fill the proposed gap of 400-600 Gg S yr^{-1} in the atmospheric budget (Lennartz et al., 2017). Still, oceanic emission estimates are associated with high uncertainties (ca. 50 %) (Kremser et al., 2016; Whelan et al., 2018). Reducing these uncertainties for present and future emission estimates requires i) increasing the existing field data across various biogeochemical regimes and ii)

increasing process understanding and quantification in the whole water column to facilitate model approaches.

Most of the *in-situ* observations of OCS and CS_2 in seawater were reported from the Atlantic Ocean and adjacent seas, and mainly represent surface ocean measurements (see Whelan et al. (2018) for an overview). Here we report the first concurrent measurements in the surface ocean and the water column for both gases from the Peruvian upwelling. This region is one of the most biologically productive regions in the global ocean, due to the upwelling of nutrient rich water. The upwelling influences the pool of dissolved organic matter (DOM) exposed to sunlight by transporting DOM from the deep ocean to the surface. The DOM pool is relevant in this context, because it contains the precursors and photosensitizers for the photochemical production of OCS and CS_2 (Pos et al., 1998; Flöck et al., 1997; Uher and Andreae, 1997). Here we show measurements of chromophoric and fluorescent DOM as well as solid-phase extractable dissolved organic sulfur (DOS_{SPE}), in order to further specify drivers of production processes and improve parameterizations of production rates in biogeochemical models.

Chromophoric DOM (CDOM) is the fraction that absorbs light in the UV and visible range. CDOM contains photosensitizers that absorb light and facilitate photochemical reactions, and can undergo photodegradation itself (Coble, 2007). A part of the CDOM fraction fluoresces (FDOM), i.e. emits absorbed light at a shifted wavelength. Distinct groups of molecules have a specific fluorescence pattern, enabling the molecule classes such as humic substances or proteins (FDOM components) to be differentiated (Coble, 2007; Murphy et al., 2013). DOS_{SPE} is operationally defined as the dissolved organic sulfur retained by solid-phase extraction (Dittmar et al., 2008). The method favors the retention of polar molecules, which comprise approximately 40 % of the total dissolved organic carbon (DOC) in marine waters (Dittmar et al., 2008). Due to the operational definition, no direct comparison to the CDOM and FDOM pools is possible (Wünsch et al., 2018).

OCS is produced in the surface ocean by interaction of UV radiation with CDOM (Uher and Andreae, 1997), making coastal and shelf regions a hot spot for OCS production (Cutter and Radford-Knoery, 1993). A reaction pathway through an acylradical intermediate in addition to a thiyl (organic RS·) or sulfhydryl (inorganic SH·, from bisulfide) radical pathway has been proposed by Pos et al. (1998) based on incubation experiments. Indeed, the amount of OCS produced has been shown to depend on CDOM, more specifically the absorption coefficient at 350 nm (a_{350}), and a variety of organic sulfur-containing precursors, such as methionine or gluthathione (Zepp and Andreae, 1994; Flöck et al., 1997). a_{350} has been used as a proxy to calculate photochemical production of OCS previously (Preiswerk and Najjar, 2000). In addition, von Hobe et al. (2003) suggested a relationship between the photoproduction rate constant and a_{350}, making the overall photoproduction rate quadratic with respect to a_{350}. This dependency is based on the assumption that a_{350} can serve as a proxy for both photosensitizers and organic sulfur precursors on large spatial scales. Accordingly, a global

parameterization for photochemical production was developed based on a_{350}, by integrating data from the Atlantic, Pacific and Indian ocean (Lennartz et al., 2017). To improve this parameterization on a regional scale, we tested whether the precursors can be further specified by an easily measurable fraction of the DOM pool (FDOM components, DOS_{SPE}), without performing costly and potentially incomplete analysis on the molecular level. In addition, OCS is produced in a light-independent reaction termed dark production (Flöck and Andreae, 1996; Von Hobe et al., 2001). Two hypotheses exist to date: an abiotic reaction involving thiyl radicals formed by O_2 or metal complexes (Pos et al., 1998; Flöck et al., 1997; Flöck and Andreae, 1996), and a coupling to microbial processes during organic matter remineralization (Radford-Knoery and Cutter, 1994). Dark production is parameterized based on temperature and a_{350} derived from field data in the Atlantic Ocean and the Mediterranean Sea (Von Hobe et al., 2001). It is yet unclear whether this parameterization is valid on a global scale. Furthermore, OCS is degraded by hydrolysis yielding CO_2 and hydrogen sulfide (H_2S) or bisulfide (SH^-), in the following summarized as sulfide. The hydrolysis degradation rate increases strongly with temperature, and has been well quantified by a comprehensive laboratory study over a wide temperature range (Elliott et al., 1989) and by seawater incubation studies (Radford-Knoery and Cutter, 1994). Oceanic OCS concentrations have been modelled using surface box models on regional (von Hobe et al., 2003) and global scales (Lennartz et al., 2017), in the water column (von Hobe et al., 2003) as well as with a global 3D circulation model (Preiswerk and Najjar, 2000; Launois et al., 2015) based on the same or similar parameterizations as described above. Here we test whether subsurface concentrations can be numerically simulated by coupling the box model to a physical 1D water column host model.

Production and loss processes for CS_2 are less well constrained. Photochemical incubation studies indicate that the photoproduction of CS_2 has a similar wavelength-dependence (spectrally resolved apparent quantum yield, AQY), but only a quarter of the magnitude compared to OCS (Xie et al., 1998). It is currently unclear whether *in-situ* photoproduction rates of both gases co-vary on larger spatial scales. A covariation is expected only when identical drivers limit the production for both gases. Evidence for biological production comes from incubation studies (Xie et al., 1999), indicating varying CS_2 production for different phytoplankton species. Outgassing to the atmosphere appears to be the most important sink for CS_2 in the mixed layer (Kettle, 2000). Although CS_2 is hydrolyzed and oxidized by H_2O_2, the corresponding lifetimes are too long to rival emission to the atmosphere at the surface (Elliott, 1990). In addition to the known sinks, namely air-sea exchange, hydrolysis and oxidation, Kettle (2000) proposed a sink with a lifetime on the order of weeks, to match observed concentrations with a surface box model. No underlying mechanism for such a sink is currently known, hampering further model approaches.

The goal of this study is to quantify production rates for both gases in the Peruvian upwelling and to further specify their drivers. Surface concentrations and emissions to the atmosphere from the cruise

presented here are discussed in Lennartz et al. (2017). Here, we focus on processes in the water column. We use the comprehensive dataset together with simple biogeochemical models to increase the understanding and quantification of the cycling of both gases in the water column and to improve model capability to predict OCS and CS_2 seawater concentrations.

2 Material and Methods

2.1 Study area

The cruise ASTRA-OMZ on RV SONNE started in Guayaquil, Ecuador, on 05.10.2015 and reached Antofagasta on 22.10.2015 (Fig. M5.1). It covered several regimes from the open ocean to the coastal shelf between 5°N and 17°S. The hydrographic conditions encountered during this cruise have been described elsewhere (Stramma et al., 2016). The area off Peru belongs to one of the four major global eastern boundary upwelling systems (Chavez et al., 2008). A large oxygen minimum zone expands into the Pacific Ocean at depths between 100 and 900 m, resulting from weak ventilation and strong respiration (Karstensen et al., 2008). The cruise covered areas of open ocean with warm sea surface temperatures (SST) between 22-27°C (stations 1-6), and regions with colder SSTs below 20°C closer to the coast (stations 7-18). Upwelling occurred at the southernmost transects indicated by the lowest SSTs (15-18°C) encountered during that cruise (stations 15-18).

2.2 Measurement of trace gases

Carbonyl sulfide concentrations were determined with an off-axis integrated cavity output spectrometer (OA-ICOS, Los Gatos Inc., USA) coupled to a Weiss-type equilibrator (Lennartz et al., 2017). The Weiss-type equilibrator was supplied with 2-4 L min^{-1} of seawater from the hydrographic shaft of the ship 5 m below the surface. The sample gas stream from the headspace of the equilibrator was filtered (Pall Acro Filter, 0.2 μm) and dried (Nafion® dryer, Gasmet Perma Pure) before entering the cavity of the OCS analyzer. The outlet of the OCS analyzer was connected to the Weiss-equilibrator, as this recirculation method kept the concentration gradient between the water and gas phases small, enabling rapid equilibration.OCS calibrations using standards from permeation tubes (Fine Metrology, Italy) were performed before and after the cruise, showing good agreement. Details on the OA-ICOS spectrometer can be found in Schrade (2011). The precision of this set-up is 15 ppt, and the limit of detection is 180 ppt (corresponding to 4 pmol L^{-1} at 20°C). Additionally, independent samples for comparison measured with GC-MS (de Gouw et al., 2009; Schauffler et al., 1998) reflected <2 % difference between the NOAA scale and the perm tube standards. A corrected calibration led to a minor change in absolute concentrations of OCS compared to (Lennartz et al., 2017), which was on average +2 pmol L^{-1}. Marine boundary layer air was measured every hour for 10 min by pumping air from the ship's deck (ca. 35 m above sea level) through a metal tube (Decabon) with a chemically inert pump (KNF Neuberger). Resulting emissions are reported in (Lennartz et al., 2017).

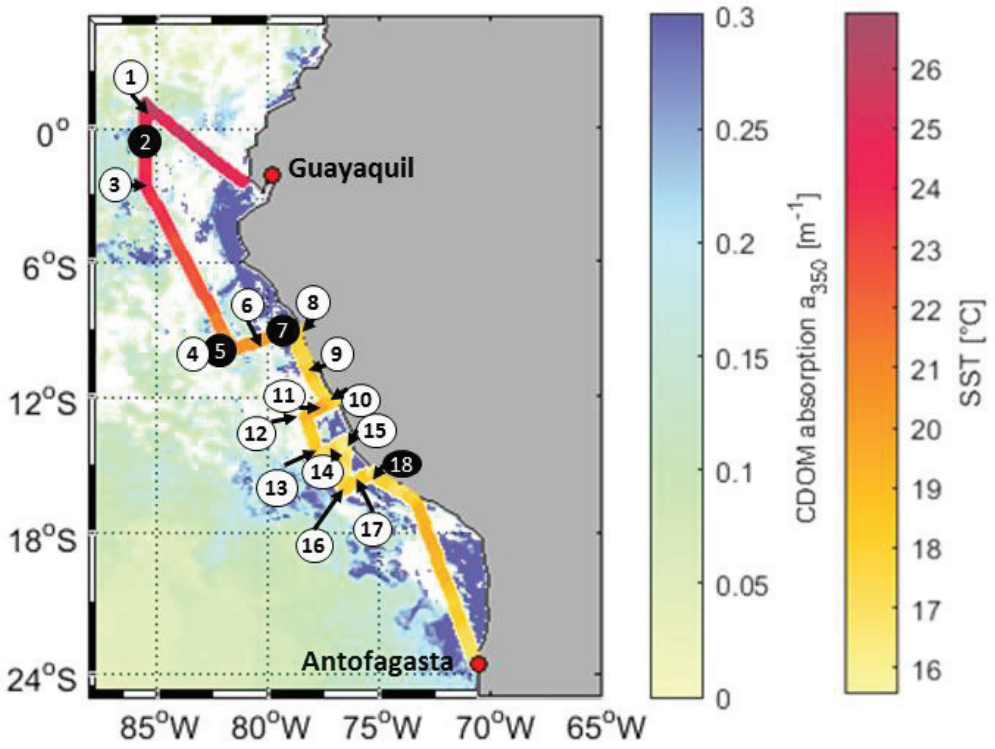

Figure M5.1: Cruise track of ASTRA-OMZ with stations 1-18 (in black circles: stations where OCS profiles were taken). The cruise track shows sea surface temperature (SST) measured onboard. For visualization only, the background is Aqua MODIS satellite data for the absorption of CDOM and detritus corrected from 443 nm to 350 nm with the mean slope of our in-situ measurements (0.0179, 300-450 nm, Aqua MODIS composite for October 2015). Note: As a monthly composite does not necessarily reflect the exact conditions during the cruise, in-situ measurements are illustrated in Fig. M5.2e. White areas: not satellite data available.

OCS depth profiles were obtained using a newly developed submersible pumping system. A rotary pump (Lowara, Xylem) connected to a 1" PTFE hose supplied the Weiss-equilibrator with 2-4 L seawater min^{-1}. The pump inlet was held at a constant depth for 10-15 min to ensure full equilibration at 4-6 depths during each profile.

CS_2 was measured with a purge and trap system attached to a gas chromatograph and mass spectrometer (GC/MS; Agilent 7890A/Agilent 5975C; inert XL MSD with triple axis detector) running in single-ion mode (Lennartz et al., 2017). 50 mL samples were taken in 1 to 3 hour intervals from the same underway system as for continuous OCS measurements. After purging for 15 min with helium (70 mL min^{-1}), the gas stream was dried with a Nafion® membrane drier (Gasmet Perma Pure) and trapped with liquid nitrogen for preconcentration. Hot water was used to heat the trap and inject CS_2 into the GC/MS. The retention time for CS_2 ($\frac{m}{z}$ =76, 78) was 4.9 min. The analyzed data were calibrated daily using gravimetrically prepared liquid CS_2 standards in ethylene glycol. During purging, 500 µL gaseous deuterated DMS (d3-DMS) and isoprene (d5-isoprene) were added to each sample as an internal standard to account for possible sensitivity drift between calibrations. The limit of detection

was 1 pmol L^{-1}. Discrete samples from depth profiles were obtained from the rosette sampler connected to a CTD. Note that OCS and CS_2 profiles were not obtained at the same time, but up to seven hours apart. The stations were defined by geographical location and not by a Lagrangian experiment following the same water mass, which explains temperature changes between OCS and CS_2 profiles for example at station 2 (see Fig. M5.2c, M5.S-Table 2).

2.3 Chromophoric dissolved organic matter (CDOM)

The spectral absorption coefficient of CDOM (a_{350}) was determined for samples collected from the CTD's Niskin bottles or from the underway system, here in a 3-hour interval. The sampled water was filtered through a sample-washed, 0.2 µm membrane (GWSP, Millipore) after pre-filtration through a combusted glass-fiber filter (GFF, Whatman). The optical density of the CDOM in the filtrate was analyzed using a spectrophotometric setup with a liquid waveguide capillary cell (LWCC, WPI; path length: 2.5 m) (Miller et al., 2002). Spectra were recorded for wavelengths between 270 to 700 nm at 2 nm spectral resolution for the sample filtrate and purified water as the reference, with sample and reference at room temperature. The absorption coefficient is determined from the obtained optical density using the Lambert-Beer law and corrected for salinity effect (see (Lefering et al., 2017) for details).

2.4 Fluorescent dissolved organic matter (FDOM)

Fluorescent dissolved organic matter (FDOM) was recorded in Excitation-Emission-Matrices (EEMs) with a UV-vis-spectrofluorometer (Hitachi F2700) from filtered seawater samples (0.2 µm, <200 mbar below atmospheric pressure) directly onboard. Excitation wavelengths ranged from 220 nm to 550 nm with a resolution of 10 nm. Emission wavelengths were recorded from 250 nm to 550 nm in 1 nm resolution at a photomultiplier voltage of 400 or 800 V, due to a change of method during the campaign (from 10 Oct 2015 onwards). For both voltages, calibration curves with quinine sulfate (5 to 30 ppb) in sulfuric acid were measured with R^2 of 0.9991 and 0.9971, respectively. EEMs were blank subtracted and Raman normalized (Murphy et al., 2013). The values are reported here in quinine sulfate QS units (QSU). A parallel factor analysis (PARAFAC) was performed using the drEEM Toolbox (Murphy et al., 2013; Stedmon and Bro, 2008) to separate the superimposed optical signals of different fluorophores ('components') in the EEMs. FDOM concentrations are reported here in quinine sulfate units (QSU, Murphy et al. (2013)), the conversion factor between QSUs and Raman units is 0.3540 and 0.4256, for each of the QS calibration (i.e. before and after the change in photomultiplier voltage), respectively. The components were compared to the database OpenFluor (Murphy et al., 2014) to identify similar components from previous studies in other environments.

2.5 Solid-phase extractable dissolved organic sulfur (DOS_{SPE})

DOS_{SPE} was sampled from the underway system or from submersible pump profiles directly into glass bottles and filtered through pre-combusted GF/F filters (Whatman, 450°C for >5h) at maximum 200 mbar below atmospheric pressure. 450 mL of each filtered samples were acidified to pH 2 (hydrochloric acid, suprapur, Merck), extracted according to Dittmar et al. (2008) (PPL, 1 g, Mega Bond Elut, Varian) and stored at -20°C until further analysis. For analysis, the PPL-cartridges were eluted with 5 mL of methanol (LiChrosolv, Merck). DOS_{SPE} was quantified with an inductively coupled plasma optical emission spectrometer (ICP-OES, iCAP 7400, Thermo Fisher Scientific). 100 µL of the extract was evaporated with N_2 and redissolved in 1 mL nitric acid (1 M, double distilled, Merck). 1 mL of Yttrium (2 µg L^{-1} in the spike solution) was added as internal standard. The sulfur signal was detected at a wavelength of 182.034 nm. Nitric acid (1 M, double distilled, Merck) was used for analysis blank. Calibration standards were prepared from a stock solution (1000 mg L^{-1} sulfur ICP-standard solution, Carl Roth). To assess the accuracy and precision of the method, the SLRS-5 reference standard was analyzed five times during the run. Although sulfur is not certified for SLRS-5, a previous study (Yeghicheyan et al., 2013) reported S concentrations of 2347 – 2428 µg S L^{-1}, which is in agreement with our findings. The limit of detection (according to German industry standard DIN 32645) was 1.36 µmol L^{-1} S corresponding to 0.015 µmol L^{-1} DOS_{SPE} in original seawater (average enrichment factor of 89.4).

2.6 Shortwave radiation in the water column

Underwater shortwave radiation was assessed through downwelling irradiance profiles obtained with the hyperspectral radiometer RAMSES ACC-VIS (TriOS GmbH, Germany). This instrument covers a wavelength range of 318 nm to 950 nm with an optical resolution of 3.3 nm and a spectral accuracy of 0.3 nm. Measurements were collected with sensor-specific automatically adjusted integration times (between 4 ms and 8 s). Radiometric profiles were collected down to the maximum where light could be recorded prior or after CDOM/FDOM sampling except at Station 7 where sampling took place at night only. Short wave radiation was approximated at this station with the shortwave radiation profile at station 6, which had similar properties in chlorophyll *a* distribution in the water column. Following the NASA protocols (Mueller et al., 2003), all downwelling irradiance profiles were corrected for incident sunlight (e.g. changing due to varying cloud cover) using simultaneously obtained downwelling irradiance at the respective wavelength, measured above the surface with another hyperspectral RAMSES irradiance sensor. Finally, these data were interpolated on discrete intervals of 1 m.

As surface waves strongly affect measurements in the upper few meters, deeper measurements that are more reliable can be further extrapolated to the sea surface. Each profile was checked and an appropriate depth interval was defined (ranging from 4-25 for Station 2 and 2-25 m for the other three

stations) to calculate the vertical attenuation coefficients for downwelling irradiance, [i.e. $K_d(\lambda,z)$] for the upper surface layer. With $K_d(\lambda,z)$ the subsurface irradiance $E_d^-(\lambda, 0\ m)$ were extrapolated from the profiles of $E_d(\lambda,z)$ within the respective depth interval. Finally, short wave radiation rad(z) and photosynthetic active radiation PAR(z) was calculated as the integral over $E_d^-(\lambda, z)$ for λ = 318 to 398 nm and for λ = 400 to 700 nm, respectively, for the depths above the lower limit of the respective depth interval and the originally measured $E_d^-(\lambda, z)$ for the depths below. Finally the euphotic depth Z_{eu} at each station was calculated from the *in-situ* PAR profiles as the 1 % light depth where PAR(z) 0.01 of PAR(z=0m).

2.7 Determination of gas diffusivity with microstructure profiles

Diapycnal diffusive gas fluxes, i.e. fluxes of dissolved gas compounds caused by turbulent mixing in direction perpendicular to the stratification, were calculated for the four stations 2, 5, 7 and 18. The diapycnal diffusive flux of a compound, φ_{dia} [pmol m^{-2} s^{-1}], is estimated as

$$\Phi_{dia} \approx \rho \cdot K_\rho \cdot \frac{\partial c}{\partial z} \qquad \text{(M5.1)}$$

where $\frac{\partial c}{\partial z}$ [pmol kg^{-1} m^{-1}] is the vertical gradient of gas concentration across a layer of ideally constant stratification and constant diffusivity, K_ρ [m^2 s^{-1}] is the diapycnal turbulent diffusivity, and ϱ [kg m^{-3}] is the water density. Fluxes can be estimated for depth ranges that are limited above and below by concentration measurements, and that do not vary systematically in stratification and turbulent mixing within. Particular focus is on fluxes to/from the mixed layer (ML), which however cause particular issues because of the sudden changes in stratification and mixing intensity at the mixed layer depth (MLD). That is why we approximate ML fluxes by fluxes through a transition zone at 5 to 15 m below the MLD, following Hummels et al. (2013), because stratification there is typically strong and relatively constant. MLD was defined here as the depth where the density has increased by an amount equivalent to a 0.5 K temperature decrease compared to the surface (Schlundt et al., 2014). The diapycnal turbulent diffusivity K_ρ was estimated from the average dissipation rate of turbulent kinetic energy, which in turn was estimated from profiles of velocity microstructure. Details on the methodology to estimate diapycnal fluxes of dissolved substances from microstructure measurements and concentration profiles can be found in Fischer et al. (2013) and Schlundt et al. (2014). The microstructure profiles were obtained with a tethered profiler (type MSS 90D of Sea & Sun Technology).

The depths where fluxes could be estimated were then used as upper and lower bounds of budget volumes. The difference of the diapycnal fluxes in and out of each volume determines convergence or divergence of the diapycnal flux. If other transport processes are negligible and if steady state is assumed, sources/sinks to compensate for the flux divergence/convergence can be determined.

Uncertainties of fluxes have been calculated by error propagation from measurement uncertainties of the gas concentrations and of the average K_ρ values. There are additional uncertainties not quantified, e.g. from the approximation of the average gas gradient, or from the neglect of other gas transport processes than diapycnal mixing. It should be noted that the diffusivity profile only represents current conditions during profiling, and can change on a daily basis due to varying stratification, surface winds etc.

2.8 Determination of OCS dark production rates

Dark production rates were determined from hourly averaged measured seawater concentrations shortly before sunrise (i.e. ca. 12-14 hours after concentration maximum of the previous day) or at depths below the euphotic zone. Concentration data from this study and a previous study from the Indian Ocean (Lennartz et al., 2017) were used to calculate dark production rates. The determination of dark production rates relies on the principle that in the absence of light, an equilibrium between dark production and loss by hydrolysis results in stable concentrations (Von Hobe et al., 2001). To ensure approximately steady state conditions, we averaged the concentrations one hour before sunrise and compared to the average of the previous hour. We only considered instances when the concentration before sunrise deviated less than 1 pmol L^{-1} from the previous hour for further calculation. These conditions were met at the beginning of the cruise (7 Oct to 12 Oct), when water temperatures ranged between 21-26°C and corresponding e-folding lifetimes of OCS due to hydrolysis 6 (7 Oct) -12 h (12 Oct). In steady state (early morning or below euphotic zone), dark production P_D [pmol L^{-1} s^{-1}] equals loss by hydrolysis L_H [pmol L^{-1} s^{-1}], the latter being the product of the steady-state concentration [OCS][pmol L^{-1}] and the rate constant k_h [s^{-1}] according to eq. M5.2:

$$P_D = L_H = [OCS] \cdot k_h \tag{M5.2}$$

The rate constant for hydrolysis, k_h [s^{-1}], was calculated according to Elliott et al. (1989), eq. M5.3 and 4:

$$k_h = e^{\left(24.3-\frac{10450}{T}\right)} + e^{\left(22.8-\frac{6040}{T}\right)} \cdot \frac{K_w}{a[H^+]} \tag{M5.3}$$

$$-log_{10}K_w = \frac{3046.7}{T} + 3.7685 + 0.0035486 \cdot \sqrt{S} \tag{M5.4}$$

with temperature T, salinity S, $a[H]^+$ the proton activity and K_w the ion product of seawater (Dickson and Riley, 1979).

The temperature dependency of the reaction rate P_D [pmol L^{-1} s^{-1}] can be described with an Arrhenius-relationship, resulting in the following equation (eq. M5.5) in its linearized form:

$$\ln\left(\frac{P_D}{a_{350}}\right) = \frac{a}{T} + b \quad \text{(M5.5)}$$

with a_{350} being the absorption coefficient of CDOM at 350 nm [m^{-1}], T the temperature [K] and a and b coefficients describing the temperature dependency of the reaction [-]. The production rate P_D is normalized to a_{350} (von Hobe et al., 2001). The parameters a and b in eq. M5.5 were derived from P_D (eq. M5.5) in the Arrhenius-plot to obtain a parameterization for dark production rate in relation to temperature and a_{350}.

Biases can potentially be introduced in two ways: 1) neglecting other sinks like air-sea exchange can lead to underestimations of the production rate. With wind speeds of 8 m s^{-1} and MLD on the order of 20-40m, life times due to air-sea exchange are in the order of days to weeks, and hence negligible. 2) Sampling less than two half lives after the maximum concentrations can lead to overestimations of the production rate. For the 11 and 12 October, samples considered for calculation of dark production rates were taken less than two half lives after the concentration maximum of the previous day. Since the concentration changed less than 1 pmol L^{-1} within two hours prior to this sampling, we consider the bias as within the range of the given uncertainty.

2.9 Surface box models to estimate photoproduction rate constants

The surface box model for OCS has already been used in Lennartz et al. (2017) to estimate OCS photoproduction rate constants. The model consists of parameterizations for the four processes hydrolysis (Elliott et al., 1989), dark production (Von Hobe et al., 2001), photoproduction (Lennartz et al., 2017) and air-sea exchange (Nightingale et al., 2000). *In-situ* measurements of meteorological, physical and biogeochemical parameters are used as model forcing. Photochemical production was calculated according to eq. M5.6:

$$\frac{dc_{photo}}{dt} = \int_{MLD}^{0} UV \cdot a_{350} \cdot p \quad \text{(M5.6)}$$

with $\frac{dc_{photo}}{dt}$ being the change in concentration due to photoproduction [pmol L^{-1} s^{-1}], UV the irradiance in the UV range [W m^{-2}], a_{350} the absorption coefficient of CDOM at 350 nm [m^{-1}] and the photoproduction rate constant p [pmol J^{-1}]. The model was set up in an inverse mode constrained by time series of OCS measurements $\left(\frac{dc}{dt}\right)$ to optimize the photoproduction rate constant p during each daylight period (13:00 to 23:00 h UTC) with a Levenberg-Marquardt-routine (MatLab version 2015a, Mathworks, Inc.). The scaling of the rate constant p can be seen as the contribution of the prescursors varying in concentration, as detailed in von Hobe et al. (2003).

An analogous model set-up was developed for CS_2, including only the processes of air-sea exchange and photoproduction. The estimated production rate hence compensates the sink of air-sea exchange. Processes without known parameterizations, such as possible biotic production and a potential

(chemical) sink are excluded at this stage (see discussion). More information on the model forcing parameters can be found in the supplementary material (S-Tab 1 and 2).

2.10 1D water column modules for OCS and CS_2

The Framework for Aqueous Biogeochemical Modelling (FABM) was used to couple the box model to a 1D water column model (Bruggeman and Bolding, 2014) and compare simulated concentrations to observations at stations 2, 5, 7 and 18. FABM provides the frame for a physical host model and a biogeochemical model, wherein the physical host is responsible for tracer transport and the biogeochemical model provides local source and sink terms. The physical host used here is the General Ocean Turbulence Model (GOTM), which is a 1D water column model simulating hydrodynamic and thermodynamic processes related to vertical mixing (Umlauf and Burchard, 2005). GOTM derives solutions for the transport equations of heat, salt and momentum.

In-situ measurements of radiation, temperature, salinity, CDOM and meteorological parameters were used as model forcing to represent conditions under which the concentration profiles were taken. Diurnal radiation cycles and constant meteorological conditions, salinity and water temperature were repeated for 5 days for OCS to obtain stable diurnal concentration cycles and 21 days for CS_2 due to its longer lifetime.

The same process parameterizations as for the box models were used as local source and sink terms in the 1D water column modules for OCS and CS_2 in FABM. Photochemical production was calculated in the wavelength-integrated approach (300-400 nm) described above in eq. M5.6, and in addition in a wavelength-resolved approach. For this purpose, we used *in-situ* measured, wavelength resolved downwelling irradiance profiles together with *in-situ* wavelength-resolved CDOM absorption coefficients to model the photoproduction of both gases in the water column based on previously published apparent quantum yields (AQY) by Weiss et al. (1995) for OCS and by Xie et al. (1998) for CS_2. We use the AQY by Weiss et al., since they were measured at the location closest to our study region (i.e. South Pacific). We assume they reflect the DOM composition in our study region best due to their similarity in a_{350}.. We note other observed AQYs (Zepp and Andreae, 1994; Cutter et al., 2004), which vary by up to two orders of magnitude. In addition, the photoproduction rate constant p of OCS in eq. M5.6 was calculated based on the relationship with FDOM component 2 developed in this study.

In addition, sensitivity tests were performed to further constrain production and consumption processes for CS_2. Here we assessed the sensitivity of the general shape of the profiles and did not focus on exact production rates, since both sink and source processes are too poorly constrained to derive reaction rates from single concentration profiles. Profiles were initialized with the lowest subsurface concentration of the respective measured profile: low enough to be able to assess whether in-situ photoproduction can explain concentration peaks below the mixed layer, but high enough to keep diapycnal fluxes out of the mixed layer in a reasonable range (in contrast to initializing with 0

pmol L^{-1}). The same meteorological conditions that occurred on the day of measurement were repeated for 21 days, i.e. ~2-3 times longer than the lifetime due to air-sea exchange. These sensitivity tests demonstrate 1) the sensitivity of surface CS_2 concentrations against diurnal mixed layer variations (simulations X98, X98d, X98s), and 2) the sensitivity of the subsurface CS_2 peak against the photoproduction rate constant and wavelength resolution (simulations X98x2, pfit, psfit). Testing the sensitivity against diurnal mixed layer variations is important because surface CS_2 concentrations depend on the amount of photochemical production occurring within the mixed layer. Air-sea exchange as the major sink for CS_2 within the mixed layer led to a relatively long lifetimes on the order of days to weeks during this cruise, so that the conditions during the days prior to the CS_2 profile measurements become important. Simulations with adjusted temperature and salinity profiles with a diurnally varying mixed layer between 10m-25m ('shallow' simulation X98s) and 25-50m ('deep' simulation X98d) were performed. For the second test, demonstrating the sensitivity of the subsurface peak, we chose station 5. This station provides the unique opportunity to assess a profile where the photic zone reaches below the ML, hence photoproduction might occur at depths where the sink of air-sea exchange is absent due to the bottom of the mixed layer acting as a barrier.We used two scenarios to assess the subsurface concentrations with one photoproduction rate constant *p* across the profile, which is consistent with surface concentrations: 1) a scenario during which the AQY by Xie et al. (1998) is scaled by a factor of 2 to match the surface concentration in a wavelength-resolved approach, and 2) a scenario where *p* is fitted with a wavelength-integrated approach (eq. M5.6) with (simulation psfit) and without (simulation pfit) allowing for an additional chemical first-order sink.

An overview of the model experiments is listed in Table M5.1, more information on the model forcing and set-up can be found in the supplementary material (M5.S-Table 2).

3 Results

3.1 CDOM, FDOM and DOS_{SPE}

DOM showed strong spatial variability in FDOM, but less in the DOS_{SPE} concentration and CDOM absorbance. CDOM, here shown as the absorption coefficient at 350 nm, was on average a_{350}=0.15 ±0.03 m^{-1} (coefficient of variation, c.o.v.: 0.2 m^{-1}). Highest absorption coefficients were found closest to the continent and in the upwelling-influenced region between 17-20°S (Fig. M5.2e), as expected in upwelling regions (Nelson and Siegel, 2013). This spatial pattern was consistent with the monthly composite of satellite data (Fig. M5.1).

Four different components of FDOM, representing groups of similarly fluorescing molecules, were isolated and validated with PARAFAC analysis. Components C1 (average±standard deviation 0.015±0.0119 QSU, c.o.v.: 0.79) and C4 (0.0091±0.0158 QSU, c.o.v.: 1.74) have their fluorescence peak in the UV part of the EEM (see supplements, M5.S-Fig. M5.1). They resemble the naturally occurring

amino acids tryptophane and tyrosine (Coble, 2007). Components C2 (0.0032±0.0027 QSU, c.o.v.: 0.84) and C3 (0.0032±0.0158 QSU, c.o.v.: 0.91) fluoresce in the visible range (VIS-FDOM) of the EEM. Their fluorescence pattern showed characteristics of humic-like substances, and were abundant especially in the southern part of the cruise, closer to the continent and upwelling region (C2 in Fig. M5.2f, M5.S-Fig. 1).

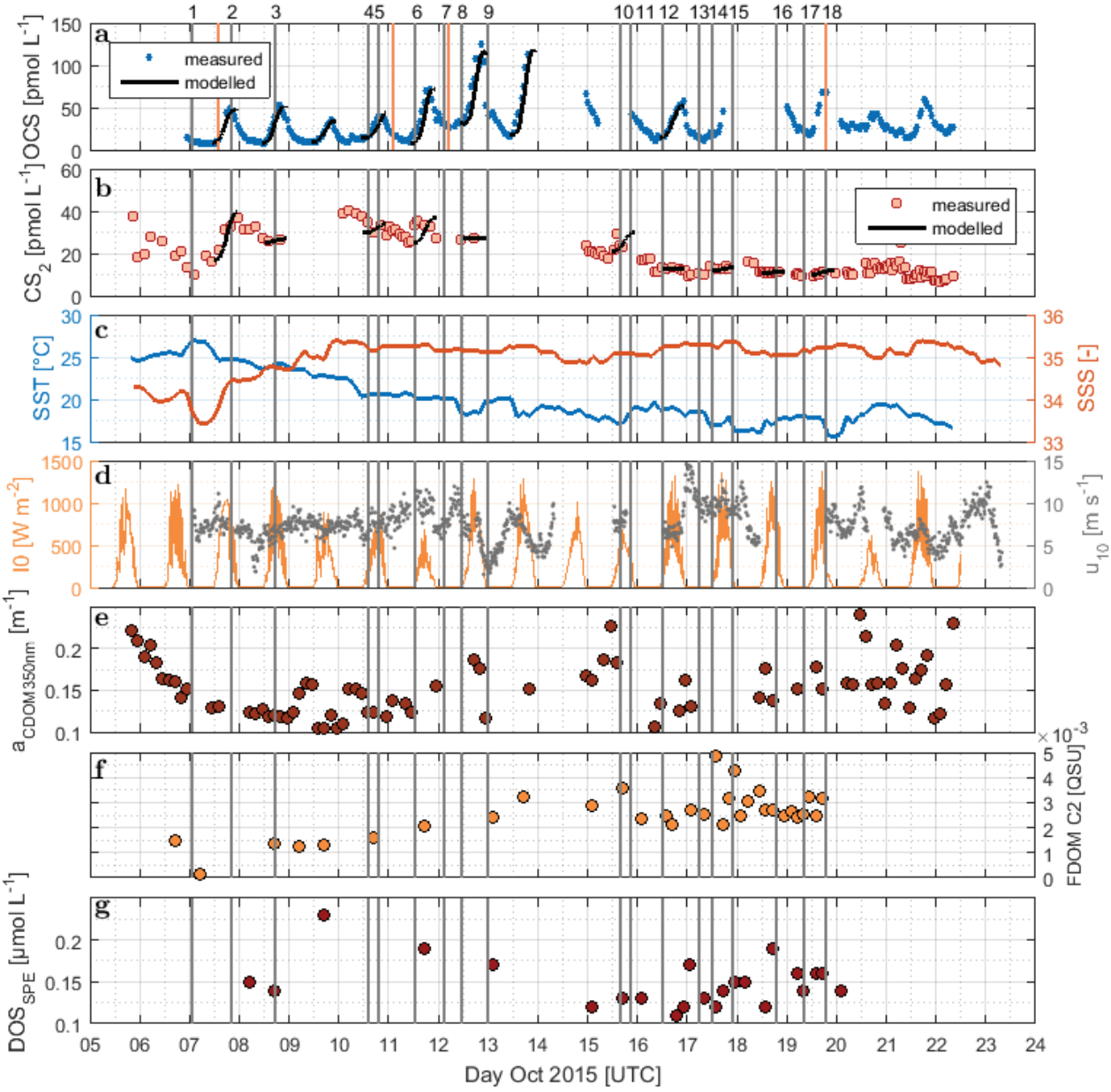

Figure M5.2: Time series of a) OCS, b) CS_2, c) SST and SSS, d) I0 and wind speed at 10m, e) absorption coefficient of CDOM at 350 nm, f) humic-like FDOM component 2, and g) DOS_{SPE} sampled from the underway system along the cruise track of ASTRA-OMZ from 5 to 23 October 2018. Vertical lines indicate stations of ASTRA-OMZ for comparison with location (see Fig. M5.1).

Table M5.1: Model experiments with 1D GOTM/FABM Modules for OCS and CS_2. AQY=apparent quantum yield.

Carbonyl Sulfide (OCS)				
	Photoproduction	**Dark prod.**	**Station**	**Description**
W95	AQY Weiss et al. (1995)	this study	2,5,7,18	wavelength resolved photoproduction, mixed layer constant
L17	Lennartz et al. (2017)	von Hobe et al. (2001)	2,5,7,18	wavelength integrated photoproduction, mixed layer constant
L19	This study (p based on FDOM C2)	this study	2,5,7,18	Wavelength integrated photoproduction, mixed layer constant

Carbon disulfide (CS_2)			
	Photoproduction	**Station**	**Description**
X98	AQY Xie et al. (1998)	5 2,7,18 in supplement	wavelength resolved photoproduction, mixed layer depth constant, no chemical sink
X98d	AQY Xie et al. (1998)	5	wavelength resolved photoproduction, deep diurnal mixed layer variation 25-50m, no chemical sink
X98s	AQY Xie et al. (1998)	5	wavelength resolved photoproduction, shallow diurnal mixed layer variation 10-25m, no chemical sink
X98x2	AQY Xie et al (1998) x2	5	wavelength resolved photoproduction, mixed layer depth constant, no chemical sink
pfit	fitted, inverse	5	wavelength-integrated (300-400 nm), test for simulation length of subsurface peak, optimized photoproduction rate constant p (eq. M5.6), no chemical sink
psfit	fitted, inverse	5	wavelength-integrated (300-400 nm), optimized photoproduction rate constant p (eq. M5.6) and first-order chemical sink.

Surface DOS_{SPE} only showed minor variations along the cruise track with concentrations of 0.16±0.05 μmol L^{-1} (c.o.v.: 0.31). Highest surface DOS_{SPE} concentrations were found in the 16°S transect connected to an active upwelling cell and in the open ocean part of the cruise (Fig. M5.2g).

DOS_{SPE} concentrations in the water column (not shown) decreased with depth, as also found in the eastern Atlantic Ocean and the Sargasso Sea (Ksionzek et al., 2016a). Concentrations decreased from 0.76 (5 m depth) to 0.33 μmol L^{-1} in 100 m at station 7, from 0.62 (25 m) to 0.49 μmol L^{-1} (125 m) at station 7 and from 0.49 (20m) to 0.28 μmol L^{-1} (115m) at station 18. At station 2, concentrations of 0.89-0.91 μmol L^{-1} were measured at a depth of 50-100m; no surface data is available.

3.2 Carbonyl Sulfide (OCS)

3.2.1 Horizontal and vertical distribution

OCS surface water concentrations ranged from 6.4 to 144.1 pmol L^{-1} (average 30.5 pmol L^{-1}) with strong diurnal cycles as described in Lennartz et al. (2017). Surface concentrations increased towards shelf and coast, and were highest along a shelf transect from 8° to 12° S and connected to a fresh upwelling patch around 16°S (Fig. M5.2a). Surface concentrations as well as emissions to the atmosphere are described in detail in Lennartz et al. (2017). The concentrations in the water column decreased with depth at stations 2, 7 and 18 to ca. 10 pmol L^{-1} below the euphotic zone with varying gradients. Profiles at stations 7 and 18 ranged down to the oxygen minimum zone, but the concentration profiles did not show any corresponding discontinuity. The shape of the concentration profile for station 5 differed from the other stations: here the profile had a convex shape down to 75 m, and it was the only station where a subsurface concentration peak was recorded at a depth of 136 m (Fig. M5.3).

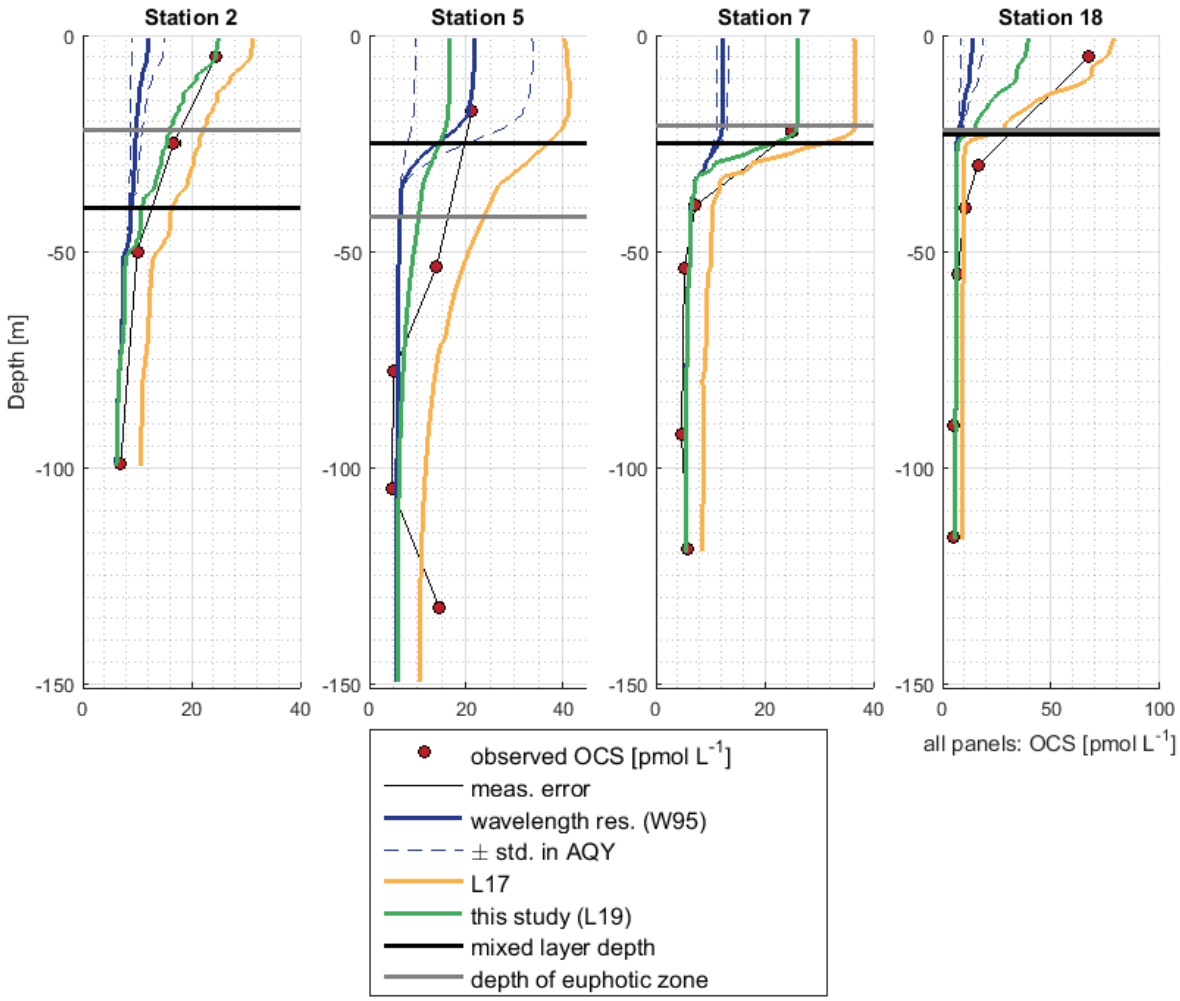

Figure M5.3: Profile measurements of OCS concentrations and 1D model results for the OCS model experiments described in Table M5.1.

3.2.2 Dark production

The dark production rates at the surface varied between 0.86 and 1.81 pmol L^{-1} h^{-1} along the northern part of the cruise track, and between 0.16 and 0.81 pmol L^{-1} h^{-1} in the four depth profiles below 50 m. The Arrhenius-type temperature dependency showed significantly increasing dark production rates with increasing temperature (Pearson's test, $p=5.66 \times 10^{-10}$). Dark production P_D both at the surface and at depth along the cruise track (Fig. M5.4) is described by the following Arrhenius-equation:

$$P_D = a_{350} \cdot \exp\left(-\frac{15182}{T} + 53.1\right) \quad \text{(M5.7)}$$

The Arrhenius-fit could not be improved using FDOM, DOS_{SPE} or O_2 instead of a_{350} (not shown). At station 5, the dark production rates at 50 and 136 m were larger than predicted for the temperature and the a_{350} present (Fig. M5.4).

The parameterization for dark production previously including only dark production rates from the North Atlantic, Mediterranean and North Sea (Von Hobe et al., 2001) was updated with the data from

the Peruvian upwelling and the Indian Ocean, and yields the following semi-empirical equation (eq. M5.8) (Fig. M5.4):

$$P_D = a_{350} \cdot \exp\left(-\frac{16692}{T} + 58.5\right) \quad \text{(M5.8)}$$

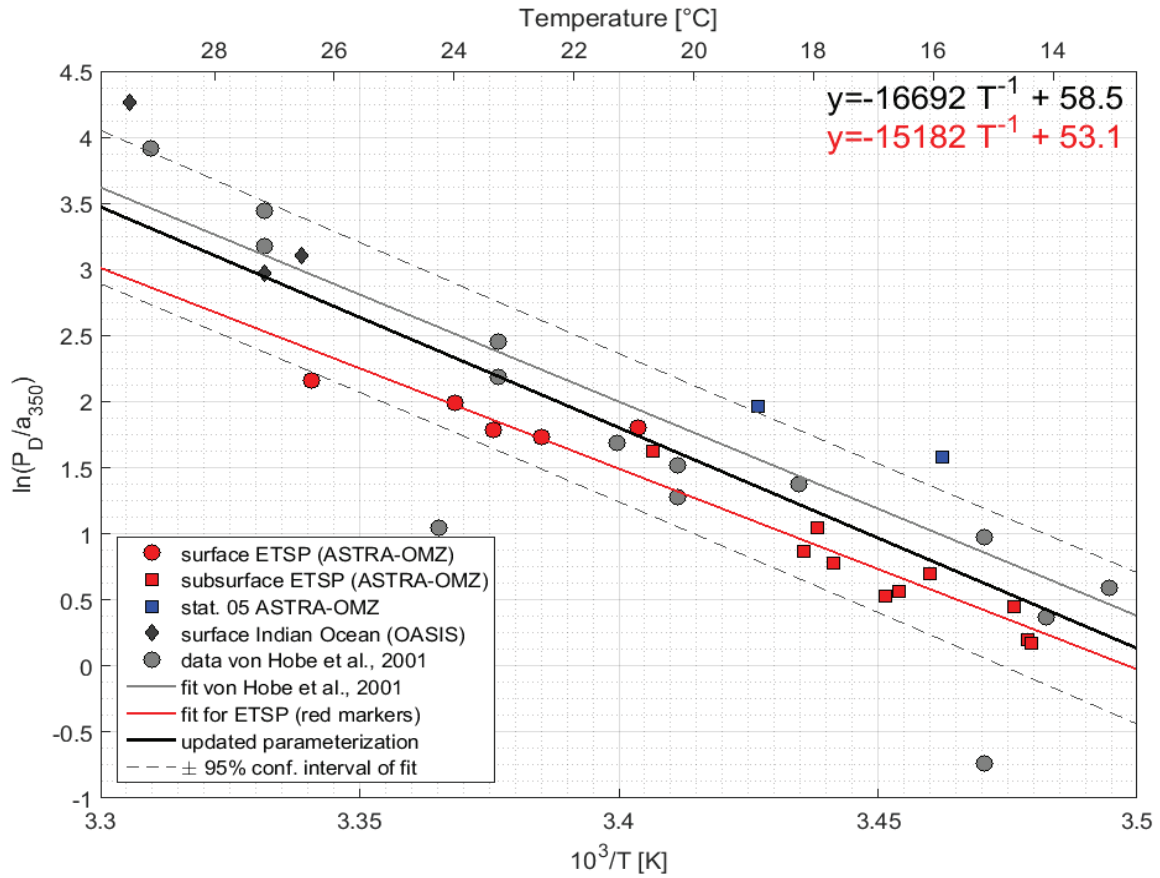

Figure M5.4: Arrhenius-plot of dark production rates from ASTRA-OMZ (this study, red and blue markers), data from the Indian Ocean (OASIS cruise, Lennartz et al. (2017)) and previously published rates (von Hobe et al., 2001, grey markers, note that P_D was converted from original units of pmol m^{-3} s^{-1} to pmol L^{-1} h^{-1}, for reconversion subtract 1.28). The red linear fit and equation shows the parameterization for ASTRA-OMZ only, whereas the black fit and equation is an updated parameterization including dark production rates from this and previous studies (see Von Hobe et al. (2001)).

3.2.3 Diapycnal fluxes

The diapycnal fluxes of OCS within the water column were derived from measured concentration and diffusivity profiles. OCS that was produced at the surface was mixed downwards in all four profiles. Diapycnal fluxes out of the mixed layer were always two or three orders of magnitude smaller than emissions to the atmosphere at stations 2, 5 and 7 with diapycnal fluxes of 8.2 x 10^{-4}, 2.4 x 10^{-4} and 3.8 x 10^{-3} pmol s^{-1} m^{-2}. An exception is station 18, where diapycnal fluxes (0.48 pmol s^{-1} m^{-2}) were almost half of the air-sea flux (-1.0 pmol s^{-1} m^{-2}).

3.2.4 Photoproduction

The photoproduction rate constants according to equation (M5.6) were previously derived from a surface box model and have already been discussed in Lennartz et al. (2017). For days with concurrent measurements of FDOM (7, 8, 9, 10, 13, 16 October 2015), the correlation between photoproduction rate constant and humic-like FDOM C2 was significant (Pearson's test, $p=0.014$, $R^2=0.81$, Fig. M5.5a). Measurements of FDOM (and a_{350}) during the period used for optimization of the photoproduction rate constant p (i.e. daylight period) were averaged for this correlation. The relationship was quantified by the following empirical equation (M5.9):

$$p = 85.8 \cdot [\text{FDOM C2}] + 828.76 \quad \text{(M5.9)}$$

with the photoproduction rate constant p [pmol J^{-1}] and the concentration of the FDOM component C2 [QSU]. The correlation with a_{350} only explains a variance of $R^2=0.01$ (n=7, i.e. 7, 8, 9, 10, 12, 13, 16 October 2015). R^2 increases to 0.3, when the respective days for FDOM C2 correlations are considered ($p>0.25$). C2 and a_{350} were not significantly correlated during these days ($p>0.2$, $R^2=0.36$), but showed a similar spatial trend all over the cruise track (Fig. M5.2). Although our experiment was not strictly Lagrangian, a_{350} only changed <0.05 m^{-1} within each respective fitting period. For FDOM C2, only 1-2 measurements per daylight period were available during the days when photoproduction rate constants were fitted, but variations of only 0.003 QSU per day were encountered during high frequency sampling towards the end of the cruise. This relationship thus carries some uncertainties, and will benefit from additional data from other regions.

OCS concentrations in the water column were simulated with the new module in the model environment of GOTM/FABM. While the AQY of Weiss et al. (1995) yielded surface concentrations of a factor 3-6 too small compared to observations, the L17 simulation overestimated concentrations in all cases up to twofold (Fig. M5.3). Deviations between simulation and measurements were reduced by using the updated dark production rate of this study and the linear correlation between FDOM C2 and p shown in Fig. M5.5a (eq. M5.9, see section 3.2.2). At station 18, surface concentrations were simulated lower than observed. The shapes of the concentration profiles were well reflected in the simulations except at station 5, where the subsurface concentration peaks at 55 m and 136 m were not adequately reproduced. Despite the different magnitude of the wavelength-resolved (W95) and wavelength-integrated (L17, L19) approaches, the shape of the photoproduction profile in the water column did not show major differences.

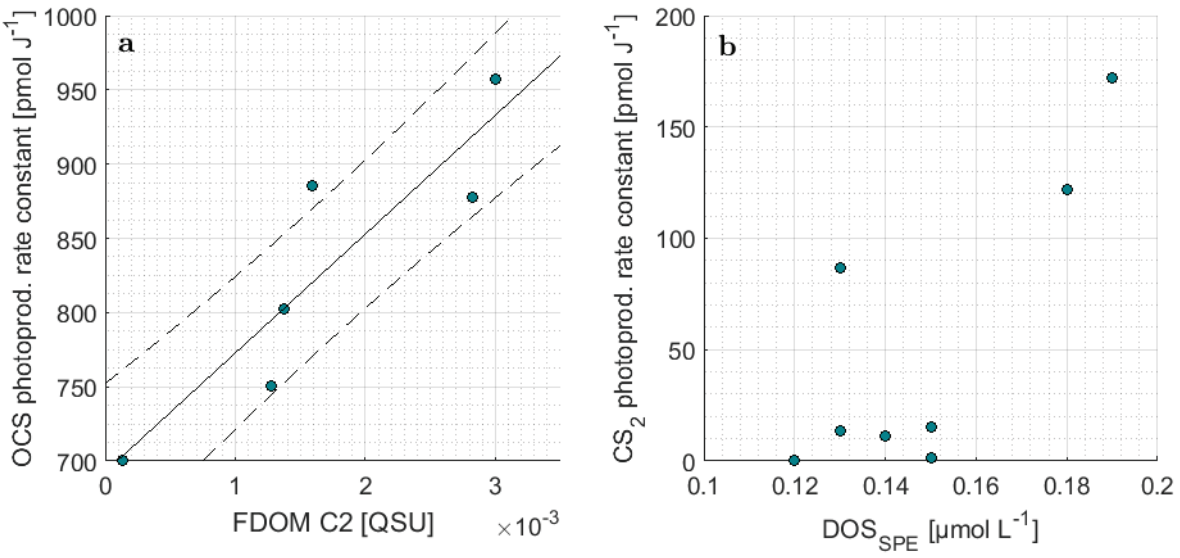

Figure M5.5: Correlations of the photoproduction rate constant from inverse surface box modelling for a) OCS and FDOM component C2 and b) CS_2 and DOS_{SPE}.

3.3 Carbon Disulfide (CS_2)

3.3.1 Horizontal and vertical distribution

The surface concentration of CS_2 during ASTRA-OMZ was in the lower picomolar range with an average of 17.8 ±8.9 pmol L^{-1} and displayed diurnal cycles only on some (e.g. 7 Oct 2015), but not at the majority of days (Fig. M5.3). The spatial pattern of sea surface concentrations was opposite to that of OCS, with highest concentrations distant from the shelf and lowest closer to the shore. Highest surface concentrations of CS_2 coincided with warm temperatures (Fig. M5.2b and 2c). Surface temperatures T [°C] and concentrations of CS_2 [pmol L^{-1}] were binned for daily averages, and yielded the following relationship (p=0.0026, R^2=0.61) of (eq. M5.10):

$$[CS_2] = 2.3\,T - 27.2 \qquad \text{(M5.10)}$$

The concentration profiles of CS_2 did not show a steep decrease with depth like OCS, but were more homogeneous (Fig. M5.6) apart from subsurface peaks below the mixed layer that occurred for example at stations 2, 5 and 18. The concentration in CS_2 profiles down to about 200m was distinctly higher in profiles where upwelling did not occur (stations 1 to 13, ~20 pmol L^{-1}) compared to stations in the Southern part of the cruise track (stations 15 to 18, ~10 pmol L^{-1}). This difference in concentrations throughout the water column reflected the pattern observed at the surface, where high concentrations coincide with high temperatures.

3.3.2 Diapycnal fluxes

The diapycnal fluxes of CS_2 within the water column revealed highest production at the surface except for station 18. Within the water column, CS_2 was redistributed downwards. Small *in-situ* sinks (stations 2, 7, and 18) and *in-situ* sources at different water depths (stations 2 and 18) within the water column were required to maintain convergences/divergences under a steady state assumption. Fluxes out of the ML were 7.6 x 10^{-4}, 3.3 x 10^{-4}, 1.9 x10^{-3} and 0.98 pmol s^{-1} m^{-2} at stations 2, 5, 7 and 18 and thus 1-3 orders of magnitude smaller than fluxes to the atmosphere. At station 18, diapycnal fluxes out of the ML and emissions to the atmosphere were at a similar magnitude (0.98 and -1.0 pmol s^{-1} m^{-2} respectively).

3.3.3 Photoproduction of CS_2

Photoproduction rate constants for CS_2 were determined using an inverse set up of the surface box model analogous to OCS, but including only photoproduction and air-sea exchange as source and sink terms. The resulting photoproduction rate constants were between 5 to 70 times smaller than those of OCS. Opposite to OCS, the rate constants did not covary significantly with any FDOM component ($p>>0.05$). A weak trend was detected for DOS_{SPE} ($p=0.08$, Spearman's $r^2=0.44$, $n=8$, Fig. M5.5), all other tested parameters did not show any correlation (FDOM C1-C4, CDOM).

The shape of the CS_2 concentration profiles was modelled for four stations (S-Fig. 2, supplements) with the scenarios described in Table M5.1. Concentrations in the mixed layer of stations 2,5 and 7 using the wavelength resolved AQY from Xie et al. (1998) yielded concentrations 4-6 times lower than observed (simulation X98).

The influence of mixed layer depth variations was tested in simulations X98d and X98s. Surface concentrations differed from the reference simulation X98 by <2.5 pmol L^{-1} (Fig. M5.7). The shape of the concentration profile, however, was sensitive to mixed layer variations, as indicated by the sensitivity simulations X98d and X98s. In these artificially created test scenarios, concentrations accumulated below the bottom of the deepest mixed layer during the simulation period.

The subsurface concentration peak was investigated with 1) simulation X98x2 with the wavelength-dependent AQY by Xie et al. (1998) scaled by a factor of 2 so that it matches CS_2 concentrations in the mixed layer, and 2) simulation pfit and psfit where a photoproduction rate constant in an integrated wavelength-approach (eq. M5.6) was fitted to observed profiles (corresponding to an evenly distributed AQY across wavelengths from 300-400 nm). Simulation X98x2 does not reproduce the subsurface peak, whereas simulations 'pfit' and 'psfit' are two possible scenarios to reproduce the observed peak (Fig. M5.7). Photoproduction rates for these simulations are shown in M5.S-Fig. 3 (see supplementary material).

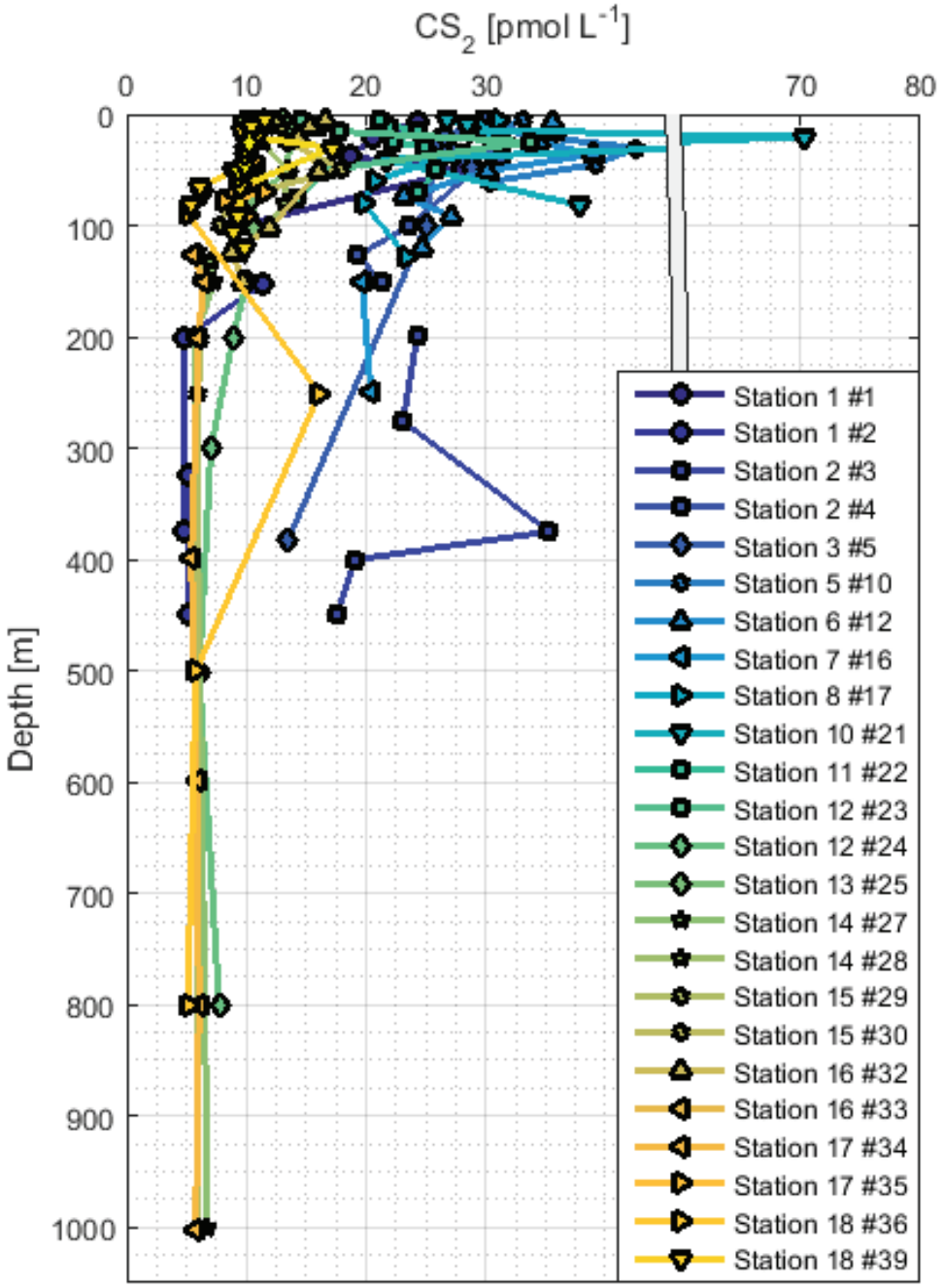

Figure M5.6. Concentration depth profiles for discrete measurements of CS_2 for open ocean regions (stations 1-5, blueish colors) and stations closer to the shelf (stations 6-13, green/yellow colors).

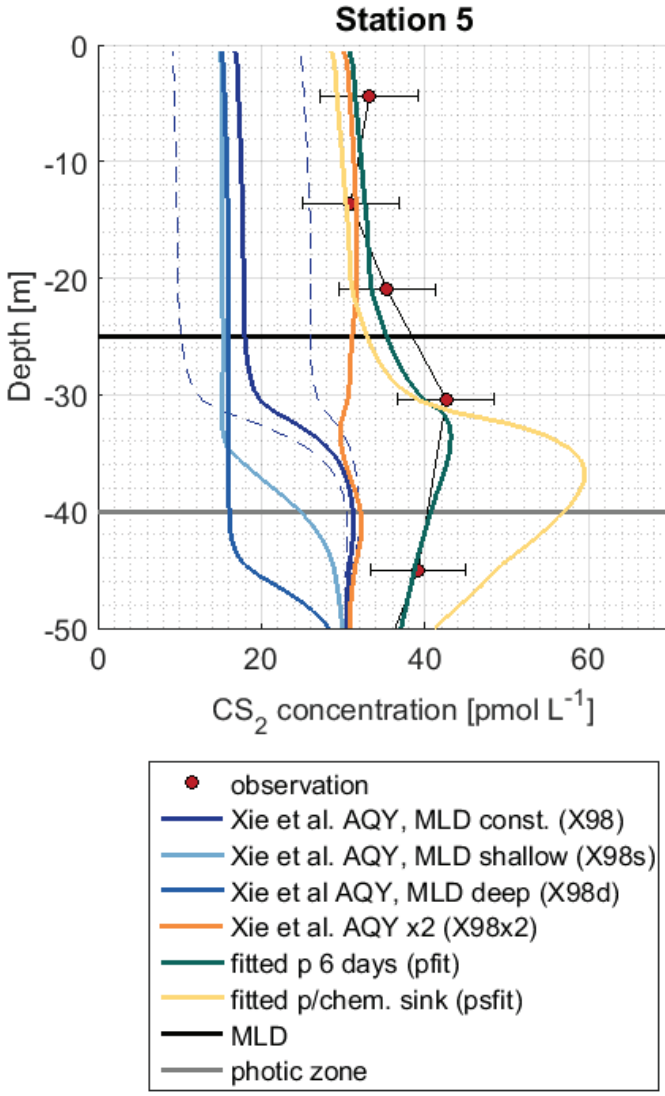

Figure M5.7. Observation and model sensitivity simulations at station 5. AQY=apparent quantum yield, MLD=mixed layer depth, chem. Simulation names in brackets refer to Table M5.1. Dashed lines indicate confidence interval of AQY as reported in Xie et al. (1998).

4 Discussion

4.1 Carbonyl Sulfide

The four profiles at stations 2, 5, 7 and 18 represent the first observations of OCS profiles in the upwelling area off Peru. They do not indicate any connection to a significant redox-sensitive process, as most profiles show a continuous decreasing shape as expected for photochemically produced compounds with a short lifetime in seawater. The independence from dissolved oxygen concentrations is in line with previous findings (Zepp and Andreae, 1994; Uher and Andreae, 1997). Station 5 was the only profile that differed in shape. This profile was measured in an eddy where downward mixing occurred (Stramma et al., 2016), which may explain the increased concentrations at 55 m. Profiles at station 7 and 18 reached down to the sediment, but did not show increased concentrations towards the

bottom. Increased sediment inputs, as e.g. reported from estuarine regions (Zhang et al., 1998), apparently do not play a large role in the studied region, and fluxes to the atmosphere are not affected.

The latter study also raises the question of near surface gradients, suggesting that our shallowest measurement depth of 5 m in both profile and underway sampling might underestimate the flux of OCS. On the other hand, strong near surface stratification acts as a barrier for air-sea exchange (Fischer et al., 2019), and could lead to a bias of the OCS flux if the sampling depth is below the barrier. Since it is difficult to perform underway sampling at shallower depths than a few meters, we cannot fully resolve this issue. However, given the low a_{350} compared to coastal and estuary regions as in Zhang et al. (1998), irradiation likely penetrates deeper into the water column in our study region than in the estuary in their study. Hence, photochemical production likely extended further down into the water column, which reduces the problem of underestimating the flux.

Dark production rates of up to 1.81 pmol L^{-1} h^{-1} in our study were at the upper end of the range of previously reported rates in the open ocean (Von Hobe et al., 2001; Ulshöfer et al., 1996; Flöck and Andreae, 1996; Von Hobe et al., 1999), but similar to those from the Mauritanian upwelling region (Von Hobe et al., 1999). Only incubation experiments in the Sargasso Sea showed higher production rates than reported here, ranging between 4-7 pmol L^{-1} h^{-1} (Cutter et al., 2004).Therein, the authors concluded that particulate organic matter heavily influences dark production. Although no sample-to-sample comparison to particulate organic carbon (POC) is possible for our OCS data, the general range of POC during our cruise was 12.1±6.1 μmol L^{-1} (145.2 μg L^{-1}), which is much higher than the POC (ca. 41 μg L^{-1}) reported from the Sargasso Sea (Cutter et al., 2004). We thus cannot confirm the influence of POC on dark production in the Peruvian upwelling, and do not find a direct biotic influence.

Our results together with previous studies show that tropical upwelling areas are globally important regions for OCS dark production, likely due to the combination of high a_{350} and moderate temperatures (15-18°C). The temperature dependency of the dark production (eq. M5.7 and 8) is very similar to the one found by Von Hobe et al. (2001) in the North Atlantic, North Sea and Mediterranean (Fig. M5.4). The similarity points towards a ubiquitous process across different biogeochemical regimes, as the dependence of the production rate on temperature and a_{350} is very similar for an oligotrophic region like the Sargasso Sea (Von Hobe et al., 2001) or the Indian Ocean during the OASIS cruise (Lennartz et al., 2017) and a nutrient rich and biologically very productive region such as the studied upwelling area. The fit in the Arrhenius-dependency could not be improved by other parameters than a_{350}, and showed no influence to dissolved O_2. The characteristics that make a molecule part of the CDOM pool, i.e. unsaturated bonds and non-bonding orbitals, also favor radical formation. OCS dark production is thus best described using abiotic parameters such as a_{350} and temperature, than biologically sensitive parameters such as dissolved O_2 or apparent oxygen utilisation as a proxy for remineralisation. This independence from biotic parameters supports the radical production pathway. The results are in line

with findings by Pos et al. (1998) showing that these molecules can form radicals in the absence of light e.g. mediated by metal complexes, and by Kamyshny et al. (2003) showing a positive correlation of dark production rate and temperature. However, the profile at station 5 provides some evidence that an additional process occurs in the subsurface. The concentration peak was visible in the up- and the downcast, but since we only observed it only once, we cannot conclusively rule out that the OCS peak at 136 m is an artefact. Still, similar subsurface peaks have been reported from stations in the North Atlantic by Cutter et al. (2004). They concluded that dark production is connected to remineralization.

Diapycnal fluxes at stations 2, 5, 7 and 18 indicate downward mixing from the surface to greater depths in all profiles. However, fluxes were several orders of magnitude smaller than emissions to the atmosphere, except for station 18. There, high diffusivities were observed using the microstructure probe, which most likely result from high internal wave activity as indicated by vertical water displacements of up to 30m during four CTD. . Diapycnal fluxes will change diurnally with the shape of the concentration profile and mixed layer variations, hence, the measurements here only represent a snapshot. Still, the difference in magnitudes between air-sea exchange and diapycnal fluxes seems to be valid at varying times of the days and regions in the studied area. Hence, neglecting diapycnal fluxes when calculating OCS concentrations in mixed layer box models leads only to minor overestimations of the concentrations.

An interesting finding is the significant correlation of the photoproduction rate constant p with FDOM C2 (humic-like FDOM), but not with $DOS_{SPE,}$ given a reported correlation of OCS and DOS in the Sargasso Sea where much higher DOS concentrations of ca. 0.4 μmol S L^{-1} were present (Cutter et al., 2004). It should be noted that the method to extract DOS_{SPE} in our study does not recover all DOS compounds, and we cannot exclude the possibility that this influences the missing correlation between p and DOS. In the studied area, OCS photoproduction is apparently not limited by the bulk organic sulfur, but rather by humic substances. The humic-like FDOM component C2 is an abundant fluorophore in marine (Catalá et al., 2015; Jørgensen et al., 2011), coastal (Cawley et al., 2012) and freshwater (Osburn et al., 2011) environments. This FDOM component seems to be especially abundant in the deep ocean (Catalá et al., 2015), which might be the reason for higher C2 surface concentrations in regions of upwelling, as evident in our study (Fig. M5.2) and reported by Jørgensen et al. (2011). The significant correlation of p with humic-like fluorophores in our study highlights the importance of upwelling and coastal regions for OCS photoproduction.

A significant correlation (i.e., a limitation) of OCS photoproduction with humic-like substances, but not with bulk DOS_{SPE} can be explained by two scenarios: Under the assumption that only organic sulfur is used to form OCS, the limiting factor is contained in the humic-like C2 fraction of the FDOM pool. The sulfur demand (75.8 pmol L^{-1}, the orange area in Fig. M5.7b) would need to be covered entirely by organic, sulfur-containing precursors. The limiting driver of this process is either organic molecules acting as photosensitizers or a sulfur-containing fraction of the DOM pool that correlates

with FDOM C2, but not bulk DOS_{SPE}. In that scenario, FDOM C2 can be used as a proxy for the OCS photoproduction rate constant. More data from other regions would help to quantify such a relationship. In a second possible scenario under the assumption that both organic and inorganic sulfur can act as a precursor, the sulfur demand could theoretically be covered by the sulfur generated by hydrolysis of OCS (i.e. 85.8 pmol L^{-1}, Fig. M5.7). In this case, FDOM C2 would only be limiting as long as enough organic or inorganic sulfur is present, for example when temperatures are high enough to recycle sulfur directly from OCS, or when other inorganic sulfur sources are present.

Incubation experiments have shown that inorganic sulfur is a precursor for OCS (Pos et al., 1998). It is not clear whether the mechanism proposed therein occurs under environmental conditions, because sulfide concentrations were higher than in most marine areas, but also yielded much higher OCS production rates in the magnitude of nM hr^{-1} compared to the magnitude of pM hr^{-1} under natural conditions. Furthermore, the conversion of sulfide to sulfate, rather than to OCS, is thermodynamically favored. Based on our data, we cannot resolve the question about the role of inorganic sulfur in OCS photoproduction, but our results are consistent with the reaction mechanism suggested by Pos et al. (1998). Incubation experiments at environmentally relevant sulfide concentrations, as well as *p*-DOS relationships across different temperature and DOM regimes will help to resolve this issue.

Our results show that FDOM C2 is a good candidate for a proxy for OCS photoproduction, but its sampling coverage is insufficient for global model approaches at the moment. On global scales, where p varies on a broader range than within the area covered by this study, a_{350} might still be an adequate, but not perfect predictor for this variation (Lennartz et al., 2017). On local scales, the parameterization for p based on a_{350} can be improved using FDOM C2.

In addition, we used parameterizations from previously reported 0D box models and from this study to assess their applicability to biogeochemical models coupled to a 1D physical host model. It should be noted, however, that the surface data shown here have been used, along with other data, to derive the parameterization for the photoproduction rate constant in Lennartz et al. (2017).

Photoproduction rates based on the wavelength-resolved simulation W95 underestimated observed concentrations in all cases. Other AQYs were not tested, but can be interpreted in a relatively straightforward way, since the AQYs of a given spectral shape is proportional to the OCS production and concentration (in steady state). Higher wavelength-resolved AQY as reported by Zepp and Andreae (1994) from the North Sea and the Golf of Mexico, as well as by Cutter et al. (2004) ranged from twofold to up to two magnitudes higher than the ones reported by Weiss et al. (1995). These differences in magnitude were attributed to the composition of the DOM pool. To reflect this influence of the DOM composition, Lennartz et al. (2017) parameterized the photoproduction rate constant (corresponding to an integrated AQY) to a_{350}, following the suggestion by von Hobe et al. (2003) that a_{350} can be used as a proxy for OCS precursors on larger spatial scales. Using this parameterization for photochemical production in the 1D water column model (simulation L19)

yielded simulated concentrations closer to, but higher than, observations (Fig. M5.3). Although the absolute concentrations for the AQY W95 did not match observations due to the reasons outlined above, the shape of the profile fits observations well. The simulations thus support the experimental findings in most of the previously published AQY work, i.e. the highest OCS yield at UV wavelengths for in-situ conditions.

The simulation using the updated dark production rate and scaling p with FDOM C2 (this study, L19) led to simulated concentrations closest to observations. Remaining deviations between simulated and observed profiles occur e.g. at station 5, possibly due to the reasons discussed above for dark production rates. At station 18, vertical water displacements of up to 30 m during four subsequent CTD casts were observed, most likely due to internal waves. This displacement could violate assumptions inherent to the 1D approach, i.e. influence of horizontal water transport. In general, our results show that simulating OCS concentrations in the water column is possible by applying surface box model parameterizations as local source and sink terms to a physical host model in the upwelling area off Peru with its specific DOM conditions. The approach is similar to the 1D model by von Hobe et al. (2003) for the Sargasso Sea, but the updated parameterizations yield a higher agreement in shape and actual concentrations of model simulation and observation.

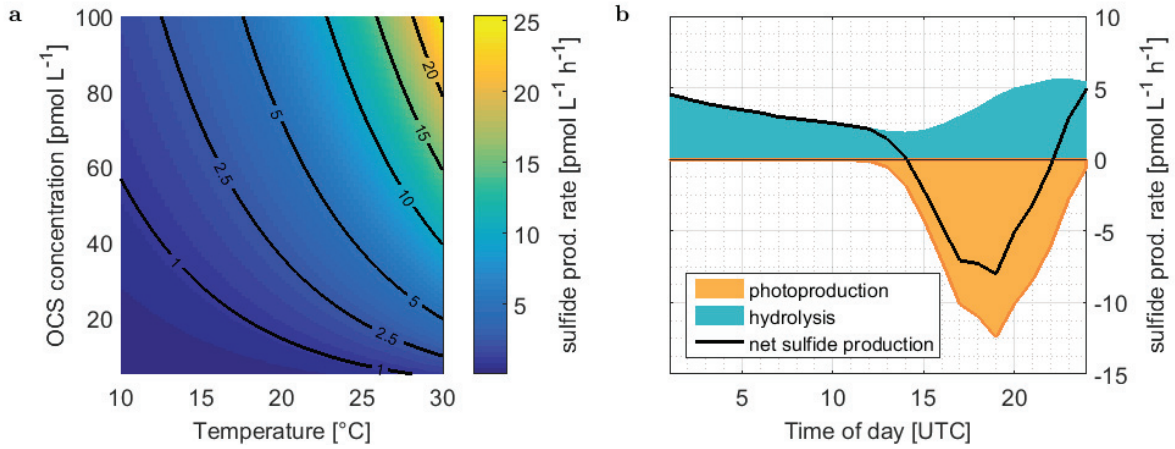

Figure M5.8: a) Rate of sulfide production due to OCS hydrolysis as a function of temperature and OCS concentration, calculated with eq. (*M5.*3)-(*M5.*4). b) Average consumption of S (organic or inorganic sulfide) by OCS photoproduction and production of sulfide during hydrolysis of ASTRA-OMZ (average 7 October – 14 October).

4.2 Carbon Disulfide

The CS_2 concentrations measured in this study were higher than those observed during an Atlantic transect (Kettle et al., 2001, average 10.9 pmol L-1, n=744), in the North Atlantic (13.4 pmol L^{-1}) and the Pacific (14.6 pmol L^{-1}) (Xie and Moore, 1999), but lower than those reported in a more recent

transect through the Atlantic (Lennartz et al., 2017). High concentrations of CS_2 coincided with elevated temperatures at the surface in our and in previous studies. The significant relationship between surface temperature and CS_2 concentrations corroborates previous findings. Xie et al. (1999) found a positive correlation between CS_2 concentration and SST for the Pacific and the North Atlantic with a linear relationship of $[CS_2] = 0.39t + 7.2$ (t=temperature in °C). Daily averages of our data close to the shelf (n=8, from 12 Oct onwards) between 15 and 20 °C fall within this relationship. However, daily averaged concentrations were higher than predicted according to this relationship further away from the coast at the beginning of our cruise at temperatures between 20 and 30°C (n=4). Overall, we confirm that CS_2 concentrations increase with increasing temperatures, but the exact relationship varies spatially. Reasons for this relationship could result from e.g. temperature-driven decay of precursor molecules, but remain speculative. The results are in line with findings by Gharehveran and Shah (2018), who found increased CS_2 formation with increasing temperatures in incubation experiments.

The surface box model to determine photoproduction rate constants of CS_2 is set-up as a very simple case, including only the processes of photoproduction and air-sea exchange. The rate constant p was only fitted for the increase in concentration during daylight, when photoproduction is expected to be much larger than potential other unknown, continuously acting sources or sinks. The photoproduction rate constant of CS_2 was highest when high DOS_{SPE} was present, indicating that the sulfur source might be limiting for this process. Organic sulfur is required to form CS_2 even if one S-atom originates from an inorganic S source (like possibly for OCS). A potential mechanism could include a precursor with an existing C-S double or single bond that reacts with either another organic sulfur radical or sulfide. This mechanism would rationalize the correlation with DOS being present for CS_2 and not for OCS. Laboratory studies showed that the organic sulfur compounds cystine, cysteine and (to a lesser extent) methionine are precursors for CS_2 photochemistry (Xie et al., 1998). Such organic sulfur-containing molecules are rare in the marine environment (Ksionzek et al., 2016a), which can explain the overall lower photoproduction rate constant of CS_2 compared to OCS. We found higher DOS_{SPE} concentrations in the upwelling area off Peru compared to other regions, but similar to DOS_{SPE} concentrations in the Mauretanian upwelling reported by Ksionzek et al. (2016a). There, elevated CS_2 concentrations were reported as well (Kettle et al., 2001). This spatial pattern suggests that upwelling regions might be hot spots for CS_2 photoproduction. It should be considered, however, that the extraction method used cannot recover all DOS compounds in seawater, so that the correlation between CS_2 and DOS_{SPE} may be influenced by the DOM composition.

Our simulation X98 at stations 2, 5, 7 and 18 underestimates mixed layer CS_2 concentrations, indicating spatial variations of the AQY, most likely due to changes in the DOM composition, as previously found for other gases (OCS: see above, carbon monoxide (Stubbins et al., 2011), DMS (Galí et al., 2016)). These results corroborate findings by Kettle (2000) and Kettle et al. (2001), who showed that the photoproduction of CS_2 was underestimated in some regions by the AQY from Xie et al.

(1998). The scaling factor was on the order of 1-10 in Kettle's studies, which is in line with our results (factor 2-4). In future model approaches, a photoproduction rate constant (expressing an integrated AQY) would need to be parameterized, and our results suggest that such parameterizations may rely on DOS or, on a global scale, DOC (since DOS covaries globally with DOC).

More detailed simulations were performed for station 5, because at this station, the photic zone extended below the mixed layer. The wavelength-dependence of the photochemical production is assessed with a 1D modelling approach, where the simulations 'X98x2' and 'pfit'/'psfit' reproduce surface concentrations, but differ in their wavelength-dependence of the photoproduction. In the simulation 'X98x2', the wavelength-dependent AQY was scaled to match surface concentrations, but failed to reproduce the observed subsurface peak at station 5, because photoproduction at wavelengths ~400 nm, that penetrate below the ML was too low. In this scenario, another production process is needed to reproduce the observed profile. Similar conclusions were drawn by Xie et al. (1998). They suggested biological production, as the peaks coincided with the peak of chlorophyll a. However, we did neither find any correlation with chlorophyll *a* nor with marker pigments representing various phytoplankton functional types (data source described in Booge et al. (2018)). A potential other dynamic process, e.g. downward mixing, that influences both gases cannot be ruled out, as concentrations for OCS were also higher than predicted around 50 m.

In our simulation 'pfit', a wavelength-integrated approach was adopted (eq. M5.6). Photoproduction is calculated with the integrated irradiation (300-400nm) and one rate constant, representing a wavelength-integrated AQY. In this simulation, photoproduction occurring at higher wavelengths, that are penetrating deeper into the water column, is higher compared to the wavelength-resolved simulation (see also M5.S-Fig. 3) and leads to the accumulation of CS_2 below the mixed layer.

The accumulation occured because the production is detached from the air-sea exchange sink. In this simulation, a period of 6 days was needed to accumulate enough CS_2 below the mixed layer to reproduce observed concentrations. This period highly depended on the actual production at wavelengths around 400 nm and can thus vary. With allowing for an additional sink process below the mixed layer (psfit) corresponding to an additional degree of freedom, observations can also be reproduced. Hence, it is possible to explain observed subsurface peaks by 1) photoproduction alone, if higher production is assumed at wavelength around 400 nm, the peak maximum depending on accumulation time and potential additional sink processes, or 2) via an additional production process only occurring shortly below the ML barrier, such as the biological production suggested by (Xie et al., 1999), or 3) by physical downward transport processes related to mixed layer dynamics (given the long CS_2 lifetime, such processes could be either slow but continuous mixing processes or strong one-time events such as storms). Slow sinks below the ML would conserve potential higher concentrations advected from surface waters due to the absence of air-sea exchange in the subsurface. The process leading to the observed profiles thus remains inconclusive. Our results highlight the importance of

Lagrangian experiments following the same water mass for compounds with a lifetime on the order of days. Information on the conditions prior to the profile measurements are needed to conclusively interpret the location and accumulation of subsurface peaks.

CS_2 was still detectable below 200 m, in concentrations around 5-10 pmol L^{-1} in shelf regions and around 20 pmol L^{-1} in open ocean regions (except station 1). This pattern reflects the spatial variation of surface concentrations, which were higher in the open ocean than at the shelf. The vertically relatively uniform concentration profiles suggest low degradation rates, and the travel distance of the water between the stations is too short to explain the concentration difference only by *in-situ* degradation. A Lagrangian approach would be helpful to resolve this issue. Some profiles display small local maxima in the region of the oxycline (not shown), but due to uncontrained subsurface source and sink processes, no conclusion can be drawn on whether a chemical or a physical process is responsible. The rather homogeneous concentrations below 200 m depth suggest slow *in-situ* degradation rates. As a result, physical processes resulting from currents, eddies or shelf processes might gain a higher importance for the distribution of CS_2 in the subsurface compared to the shorter lived gas, OCS. With sinks potentially acting on long timescales, CS_2 could possibly be transported from sources located further away, e.g. from contact to the sediment in shelf regions or subducted from the surface. Our results clearly show the limits of interpreting 1D concentration profiles for long lived compounds, with both subsurface sinks and source unconstrained. Incubation experiments using isotopically labelled CS_2 would be helpful to constrain source and sink processes independently.

5 Summary and conclusion

We show concurrent measurements of the gases OCS and CS_2 together with sulfur-containing and optically active fractions of the DOM pool in the upwelling area off Peru. The results indicate how the quality and composition of DOM influences the production processes of both gases, with implications for predicting their concentrations on regional and, potentially, global scales.

A parameterization for dark production of OCS is updated, resulting in a slight downward correction of the previously established parameterization. The photoproduction rate constant of OCS co-varies regionally with humic-like FDOM, and. more observations of OCS with humic-like DOM could help to improve parameterizations of OCS photoproduction. The absence of a correlation of the photoproduction rate constant with bulk DOS_{SPE} is not conclusively answered. Possible scenarios involve either a sulfur-containing precursor in a constant ratio FDOM C2, or surplus of sulfur via allocation from OCS hydrolysis. In both cases, FDOM C2 is a promising proxy on regional scales, and in case of scenario 1 also on global scales. In contrast to OCS, the availability of organic sulfur might be a limiting factor for the photochemical production of CS_2.

These different limitations of photochemical production of both gases have implications for the expected spatial pattern of their marine surface concentrations. Both, OCS dark and photochemical

production, correlate with optically active parts of the DOM pool, which are abundant at high latitudes, coastal and upwelling regions. Also, OCS is degraded by hydrolysis most efficiently in warm regions such as the tropics, resulting in longer lifetimes in high latitudes. Highest concentrations are thus expected in coastal regions of high latitudes, which is in line with observations. Increasing CS_2 photoproduction with increasing DOS_{SPE} concentrations suggests highest surface concentrations in tropical and subtropical regions, where highest DOC and DOS concentrations are expected. This spatial pattern is in line with the limited measurements available (Kettle et al., 2001). Regarding the tropical missing source of atmospheric OCS, the spatial pattern of oceanic emissions would then favour oxidation of emitted CS_2 to OCS as a potential candidate to fill the gap in the atmospheric budget. Our measurements likely represent CS_2 concentrations from the upper end of the range of tropical concentrations, since they were performed in a region with high DOS abundance. As an upper limit, a sulfur flux calculated with average values from this cruise (T=20.2°C, S=35, u10=7.3 m s^{-1}, CS_2=17.8 pmol L^{-1}) assumed for the whole tropical ocean (30°N-30°S, 1.95 x10^{14} m^2) results in an annual emissions of 268 Gg S as OCS. This flux, which represents an additional 140 Gg S to the global sulfur flux of CS_2 reported by Lennartz et al. (2017) is still too low to sustain a missing source of additional 400-600 Gg S yr^{-1} (800-1000 Gg S^{-1} yr^{-1} total oceanic OCS emissions).

Overall, we show that processes to model OCS distributions are well known and quantified and that the lifetime is sufficiently short to extend the parameterizations of the box model to a 1D water column model. OCS process understanding is better than for CS_2, for which sufficient process understanding to conclusively model subsurface concentrations is still lacking. Our results emphasize the importance of vertical dynamics for longer lived compounds such as CS_2 compared to the short lived OCS.

This study highlights the need for more *in-situ* measurements of OCS and CS_2 below the mixed layer in various biogeochemical regimes together with fractions of the DOM pool, to improve the suggested quantitative relationships across larger DOM variations. Subsurface processes, especially for CS_2, remain elusive and require concerted experimental and field studies.

Author contributions

S.T.L. and C.A.M. designed the study. Measurements and interpretation for essential parameters was performed by D.B. (CS_2), T.F. (microstructure profiles), R.G.-A. (PARAFAC), K.B.K. and B.P.K. (DOS_{SPE}), A.B. (radiation), R.R. (CDOM absorption). S.T.L. performed the simulations with support from H.B.. S.T.L., C.A.M. and M.v.H. synthesised the data. S.T.L. wrote the manuscript with contributions from all coauthors.

Acknowledgements

We acknowledge the help of the co-chief scientist, Damian Grundle and the crew and captain of the RV Sonne during ASTRA-OMZ to perform our measurements. We thank M. Lomas for providing

data on particulate organic carbon. This work was supported by the German Federal Ministry of Education and Research through the project ROMIC-THREAT (BMBF- FK01LG1217A and 01LG1217B), ROMIC- SPITFIRE (BMBF- FKZ: 01LG1205C) and SOPRAN, the DFG grants GR4731/2-1 and MA6297/3-1, as well as a PhD grant within the DFG-Research Centre/Cluster of Excellence "The Ocean in the Earth System". Additional funding for C.A.M. and S.T.L. came from the Helmholtz Young Investigator Group of C.A. M., TRASE-EC (VH-NG-819), from the Helmholtz Association through the President's Initiative and Networking Fund and the GEOMAR Helmholtz-Zentrum für Ozeanforschung Kiel. This work was co-funded by a PhD Miniproposal granted to S.T.L. from the Integrated School of Ocean Sciences (ISOS) of the Cluster of Excellence "The Future Ocean" at Kiel University, Germany, as well as GEOMAR Seedfunding. We thank NASA Goddard Space Flight Center, Ocean Ecology Laboratory, Ocean Biology Processing Group for providing access to satellite data of CDOM from Aqua MODIS. We thank C. Schlundt for her help in analyzing CS_2 samples and I. Stimac for her help in analyzing DOS_{SPE} samples.

V. Concluding Remarks

Aiming at the biogeochemical characterization of DOS_{SPE}, quantitative and compositional analysis was performed on DOM_{SPE} from different aquatic environments with a focus on the marine system. In the following, I will draw conclusions from the results of this thesis (Chapter IV), in the context of the aims and hypothesizes stated in Chapter III.

Abundance and distribution of DOS in aquatic systems

Since the concentration of inorganic sulfate exhibits the concentration of DOS by five orders of magnitudes, it has been assumed that sulfur hardly limits biological activity (Levine, 2016). Thus, the literature is lacking on DOS studies, covering not only advanced biogeochemical approaches but also basic quantification of marine DOS. Consequentially, one aim, which all studies presented in Chapter IV of this thesis have in common, was the quantification of DOS_{SPE} in each of the sampled regions. This represents the so far most comprehensive dataset of DOS in the ocean, including the first description of a DOS_{SPE} basin-scale distribution in the EA, the Atlantic sector of the SO, and the Weddell Sea. Hence, spatial differences but also differences throughout the water column were examined (Table 4). The highest concentrations of DOS_{SPE} (and DOC and DOC_{SPE}) were found in the riverine samples of the rivers Elbe and Weser. With increasing salinity from riverine waters through the estuary to marine waters, DOS_{SPE} concentrations decreased (along with DOC and DOC_{SPE} concentrations). Marine water samples were analyzed from various regions (Table 4): The lowest DOS_{SPE} concentrations detected in this study were found in polar waters and the deep ocean. Higher DOS_{SPE} concentrations were found in the upper water column of the EA, whereas the highest concentrations of marine DOS_{SPE} were found in the Peruvian upwelling (one of the most biologically productive regions in the global ocean).

In addition to the regional quantification of DOS_{SPE}, a first global marine DOS inventory of 6.7 – 18.6 Pg S was calculated, which highlights its significance: marine DOS represents the largest oceanic reservoir of organic sulfur. The minimum DOS inventory, however, does not cover compounds, which are not extractable by SPE, e.g. highly polar or volatile DOS compounds. Taurine for instance, an amino acid-like compound which is not extractable with the SPE method applied, was found in concentrations of up to ~16 nmol L^{-1} in the open ocean (Clifford et al., 2017), which is quite high compared to common oceanic concentrations of dissolved free amino acids. The missing data, however, do not affect the calculated global minimum inventory of marine DOS.

Until now, our understanding of the marine sulfur cycle is mostly based on labile sulfur-containing compounds of the DMSP cycle. Comparison of the global DMSP pool with the marine DOS

inventory, however, emphasizes that these compounds contribute to only < 2 % to the total marine organic sulfur inventory. Thus, there remain major gaps, especially in our understanding of the connection between the small, labile DOS pool and the large, non-labile DOS reservoir.

Table 4. Average DOC_{SPE} and DOS_{SPE} concentrations and DOC_{SPE}/DOS_{SPE} ratios at the different sampling locations analyzed in this thesis. For each sampling location, the number of analyzed samples (n) is given.

Sample location	n*	Average DOC_{SPE} concentration ($\mu mol\ L^{-1}$)	Average DOS_{SPE} concentration ($\mu mol\ L^{-1}$)	Average DOC_{SPE}/DOS_{SPE} ratio	Reference
Rivers Elbe and Weser	2 (2)	144	1.40	103	Manuscript 3
Elbe-Weser Estuary	3 (3)	121	1.36	100	
North Sea	1 (1)	31	0.19	162	
Peruvian Upwelling (surface)	- (64)	-	0.16	-	Manuscript 5
EA surface Ocean (0-105 m water depth)	106 (106)	29	0.14	213	Manuscript 1
EA deep Ocean (≥200 m depth)	37 (37)	22	0.09	248	
SO (Atlantic Sector)	31 (31)	21	0.08	266	
Weddell Sea	414 (373)	21	0.08	290	Manuscript 4

* Number of samples for DOC_{SPE} analyses. Number in parentheses represents the number of DOS_{SPE} samples.

Insights into the biogeochemistry of dissolved organic sulfur

Locally, riverine input or sedimentary efflux contributes to a certain extent to the marine DOS pool. The majority of marine DOM, however, derives from primary production. Also, for marine DOS, the analysis of DOS stoichiometry in marine surface waters revealed DOS_{SPE}/DON_{SPE} ratios comparable to phytoplankton stoichiometry and thus, confirmed a predominantly biogenic DOS source.

The results of this thesis reveal that water source and biogeochemical transition processes indeed control the elemental/molecular composition of DOS (as hypothesized in Chapter III). Average DOC_{SPE}/DOS_{SPE} ratios differed significantly between riverine/estuarine and marine samples. Fluvial DOM is characterized by lower DOC_{SPE}/DOS_{SPE} ratios than marine DOS. Differences in DOC_{SPE}/DOS_{SPE} ratios were also found between the different water masses of the Weddell Sea, indicating different origins and/or degradation stages.

About 800 different sulfur containing molecular formulas were identified in the EA. About 10 % of these formulas only occurred in the surface ocean (none of the detected formulas occurred uniquely at depth). Additionally, DOC_{SPE}/DOS_{SPE} ratios increased with increasing depth. These vertical changes in the chemical composition of DOS_{SPE} indicate DOS degradation and suggest that DOS is preferentially remineralized relative to DOC. Furthermore, the lifetime of non-labile DOC, DOC_{SPE}, and DOS_{SPE} was calculated based on the correlation of DOC, DOC_{SPE}, and DOS_{SPE} concentrations with DOC_{SPE} radiocarbon age. Comparison of the calculated lifetimes confirmed the suggestion of preferential remineralization of S relative to C. Although it is common use in DOM studies to define discrete organic matter fractions based on their lifetime (labile, semi-labile, or refractory DOM), it is important to consider that DOM degradation follows a continuum of reactivities (Flerus et al., 2012). The results of this study emphasize the different degradation kinetics of DOC and DOS, supporting the model of a continuous DOM degradation. For simplification, we only distinguished between labile and non-labile DOS.

The contribution of labile DOS to the total DOS pool has been estimated from the analysis of the sulfur containing amino acid methionine and its contribution to total DOS_{SPE}. It was found that < 2 mol % of DOS_{SPE} are protein-derived. Additionally, none of the ~800 detected molecular formulas matched the composition of a peptide. This reflects the non-labile character of the sampled DOS_{SPE} and suggests an efficient remineralization or transformation of labile DOS in the form of sulfur-containing amino acids, even in the surface ocean where DOM (and DOS) is produced by marine phytoplankton.

In a comment on the first manuscript of this thesis, it was stated that the distribution of DOM and thus the investigation of a decrease of DOS with age can be exclusively explained by water mass mixing (Dittmar et al., 2017). In Manuscript 2 of this thesis, we emphasized the importance of selective sulfur removal processes, beside and in addition to the obvious mixing of water masses with different DOM concentration and composition. The observed stoichiometric changes, the relative changes in endmember concentrations (surface ocean vs deep water) and changes in the chemical composition of surface and deep water samples emphasize the presence of an additional removal process (as also found for samples from the Weddell Sea). A faster removal of DOS_{SPE} relative to DOC_{SPE} was also confirmed for the transition from riverine to marine waters, where water mass mixing is known as the major factor controlling DOM distribution. Possible sinks and removal processes might be photo-bleaching and

photo-degradation, flocculation and sorption to sediments, and others. These processes might occur separately or simultaneously and the quantification of the influence of each process on DOM distribution and composition remains a major challenge.

Several factors can accelerate or restrain DOS degradation. Trace-metal complexation, for instance, has a protective effect against oxidation of DOM-thiol groups (Hsu-Kim, 2007). DOS and trace metal concentration and stoichiometry was analyzed for riverine, estuarine and marine samples and the influence of DOS on trace element complexation was discussed. Several findings indicated complexation of (sulfur containing) organic ligands with trace metals. A similar distribution of DOC_{SPE}, DOS_{SPE} and metal-DOM_{SPE} was found. Higher DOM and trace metal concentrations and subsequently higher complexation of trace metals with carbon and sulfur-containing organic complexes were found in riverine compared to marine samples. Additionally, we found an increase in Co and Cu concentrations after oxidation of organic complexes by UV treatment. By comparing the relation of trace metals to DOS_{SPE} (and DOC_{SPE}), we found, that the complexation affinity of metals to (sulfur containing) organic ligands followed the Irving-Williams order, irrespective of salinity.

I hypothesized that the contribution of biological activity to DOS removal is reflected in a correlation of AOU (as indicator for oxygen consumption due to biological activity) and DOS_{SPE} concentration) and tested this hypothesis for samples from the Weddell Sea. However, due to the non-labile character of the samples, no correlation of DOS_{SPE} (and DOC or DOC_{SPE}) with AOU was found. Although we could not confirm the hypothesis for the mostly non-labile Weddell Sea DOM, it might still be true for other regions where younger and more labile DOM occurs.

Another sink of DOS is its transformation to volatile sulfur compounds and its release to the atmosphere. Manuscript 5, to which I contributed DOS_{SPE} analyses, the possibility of a limiting effect of DOS_{SPE} availability on the production of the volatile sulfur compounds OCS and CS_2 was tested. A correlation between DOS_{SPE} concentration and the photoproduction rate constant of CS_2 was found, indeed indicating a limiting factor of DOS_{SPE} abundance on CS_2 production. For OCS production in contrast, this correlation was not found. However, since the SPE method applied does not recover all DOS compounds, the possibility that those compounds, which are not recovered, might influence OCS production cannot be excluded.

The results of this study clearly demonstrate that the marine DOS pool plays an important role in the global sulfur cycle, which is not only caused by its size. Especially the labile DOS compounds in the surface ocean are of major ecological and biogeochemical relevance and subject to very fast turnover rates. The characterization of these compounds and the assessment of the relative contribution of different DOS removal processes will help to further understand DOS biogeochemistry and to connect the small, labile DOS pool with the large, non-labile DOS pool.

KEY MESSAGES

DOS abundance, distribution and composition

- DOS is by far the largest reservoir of organic sulfur in the ocean.
- The distribution and elemental/molecular composition of DOS changes with water source (water mass) and biogeochemical transition processes.
- Labile DOS (e.g. methionine, DMSP, DMS) contributes to only ~2 % to the total DOS_{SPE}.

DOS biogeochemistry (sources, sinks, reactivity)

- DOS_{SPE} stoichiometry (S/N ratio) showed a predominantly biogenic imprint of DOS in the East Atlantic and Southern Ocean (Weddell Sea).
- DOS_{SPE} is removed preferentially to DOC_{SPE}.
  - Water mass mixing cannot solely account for DOS_{SPE} distribution. Additional removal processes must occur.
- DOS_{SPE} abundance is likely a limiting factor for marine CS_2 production, whereas no limiting influence was found for OCS production.
- We found indication for trace metal complexation to organic sulfur groups.
  - The affinity of trace metals to organic sulfur (and carbon) containing ligands follows the Irving-Williams order, irrespective of salinity.

VI. Perspectives

Marine DOS research is still at its infancy and within this study, some first fundamental aspects were addressed, such as the assessment of the global minimum marine DOS inventory. All findings of this study are based on the solid-phase extractable fraction of the bulk DOS pool. Our understanding of the biogeochemical processes driving the marine sulfur cycle is limited by the lack of information on the molecular structure and composition of DOS and its concentration in original seawater. Thus, it is necessary to expand the analytical window for the determination of DOS quantity and quality.

Analytical approaches

The major methodological challenge will be the analysis of the original DOS concentration and with this, the evaluation of the DOS extraction efficiency. Cutter et al. (2004) used a very promising technique. However, the applicability in the field/onboard of a research vessel remains to be tested.

The second challenge will be the chemical characterization of DOS. For this, several approaches can be applied:

Within this and other studies, FT-ICR-MS has been used to analyze the chemical composition of DOS. However, our knowledge is still fragmentary and the analysis of a bigger sample set from different aquatic environments is needed to better understand the differences in the chemical nature of aquatic DOS.

Another method, which has already been applied to analyze the chemical composition of DOS (e.g. in marine sediments and aquatic and soil humic substances), is X-ray absorption near edge structure (XANES) analysis (Vairavamurthy et al., 1993; Vairavamurthy et al., 1994; Xia et al., 1998). This method allows the qualitative identification of multiple organic sulfur oxidation states. Thus, comparison of the composition of several organic sulfur containing compound classes (such as thiols/sulfides, sulfate esters, sulfonates and sulfoxides) in samples from different environments is possible.

One-dimensional and multidimensional NMR spectroscopy is a powerful non-destructive tool for in-depth characterization of different functional groups and compounds classes. Whereas one dimensional ^{1}H and ^{13}C NMR spectroscopy provides near quantitative data (Hertkorn et al., 2013), multi-dimensional NMR spectroscopy provides information on the molecular structure and functionalities of DOM (Hertkorn et al., 2013; Hertkorn and Kettrup, 2005; Kaiser et al., 2003; Simpson, 2001). This method, however, also requires purification (desalting) and enrichment of DOM in the sample, similar to the mass spectrometric methods. Although ^{33}S NMR spectroscopy would be an advantage for DOS research, low sensitivity of the ^{33}S nucleus and the resulting very broad signals are major reasons for its limited use.

Isotopic analysis of $^{34}S/^{32}S$ ratios can be used to determine global DOS sources and pathways based on the isotopic DOS composition (Bottrell and Newton, 2006). For instance, based on the amount of ^{32}S or ^{34}S in DOS, it can be differentiated if this DOS results from biotic (^{34}S enrichment) or abiotic (^{32}S enrichment) production (Bottrell and Newton, 2006).

All these analytic tools can be applied to analyze bulk DOM (upon pretreatment, such as desalting and enrichment). Fractionation of bulk DOM based on different characteristics (e.g. polarity using HPLC) can be performed previously to gain deeper insights into the similarities and differences of several DOM fractions. For instance, HPLC-ICP-MS has been used for quantitative DOS analysis in DOM fractions of different polarity (Lechtenfeld et al., 2011). A further step could be to collect subsamples of these fractions after HPLC for subsequent analysis by NMR and/or FT-ICR-MS to link quantitative and qualitative information of the different fractions.

Biogeochemical questions

With these analytical tools, some fundamental gaps in our understanding of DOS biogeochemistry can be addressed.

Incubation and degradation experiments can be powerful tools for the investigation of DOS production and degradation rates/mechanisms. In combination with the analysis of the isotopic and molecular composition, sources, reaction pathways, and degradation rates of DOS under different environmental conditions (e.g. oxic vs. anoxic conditions) can be determined. Additional community studies will be important to assess biogeochemical interactions. A high resolution in time throughout the experiments is necessary to observe all changes in DOS concentration and composition on the way from DOS production to degradation and to fill the knowledge gaps in our understanding of the connection of the labile DOS pool with the non-labile DOS pool.

Changes in the molecular structure of marine and sedimentary DOS compounds can make these compounds unrecognizable to degradation by enzymes. However, the characteristics, that control whether a certain molecule will be mineralized or buried, are mainly unknown (Wasmund et al. 2017) and require in-depth chemical characterization of specific DOS compounds.

The analysis of sediment pore water samples will broaden the view on the role of heteroatomic organic matter in sedimentary processes (e.g. methanogenesis). Quantitative and qualitative information can be obtained by HPLC-ICP-MS analysis. Thus, differences between different regions and changes in the vertical distribution of DOS in sediment can be determined. A focus could be on the change of sulfur concentrations (and compositional changes) at different oxygen levels. Isotopic data were previously evaluated to constrain sulfur incorporation into sedimentary organic matter (Mossmann et al., 1991). Isotopic analysis will help us to further understand under which conditions biotic and abiotic pathways are preferred and to which extend they take place.

DOS-metal complexes in turn, can play an important role by affecting the toxicity and bioavailability of trace metals. A better understanding of the processes stabilizing or destabilizing these complexes (e.g. by thermal oxidation or photodegradation) will help to connect the global sulfur and trace-metal cycles.

Research on these and other questions will contribute to close some of the major gaps in our understanding of the marine sulfur cycle, which will be of interest to a broad scientific community.

VII. References

Abdulla, H.A.N., Minor, E.C., Dias, R.F. and Hatcher, P.G., 2010. Changes in the compound classes of dissolved organic matter along an estuarine transect: A study using FTIR and 13C NMR. *Geochim. Cosmochim. Acta*, **74**(13): 3815-3838.

Abdulla, H.A.N., Minor, E.C., Dias, R.F. and Hatcher, P.G., 2013. Transformations of the chemical compositions of high molecular weight DOM along a salinity transect: Using two dimensional correlation spectroscopy and principal component analysis approaches. *Geochim. Cosmochim. Acta*, **118**: 231-246.

Abell, J., Emerson, S. and Renaud, P., 2000. Distributions of TOP, TON and TOC in the North Pacific subtropical gyre: Implications for nutrient supply in the surface ocean and remineralization in the upper thermocline. *J. Mar. Res.*, **58**(2): 203-222.

Abril, G., Nogueira, M., Etcheber, H., Cabeçadas, G., Lemaire, E. and Brogueira, M.J., 2002. Behaviour of Organic Carbon in Nine Contrasting European Estuaries. *Estuar. Coast. Shelf Sci.*, **54**(2): 241-262.

Aiken, G.R., Hsu-Kim, H. and Ryan, J.N., 2011. Influence of Dissolved Organic Matter on the Environmental Fate of Metals, Nanoparticles, and Colloids. *Environ. Sci. Technol.* **45**(8): 3196-3201.

Al-Farawati, R. and Van Den Berg, C.M.G., 2001. Thiols in coastal waters of the western North Sea and English Channel. *Environ. Sci. Technol.*, **35**(10): 1902-1911.

Alling, V., Humborg, C., Mörth, C.-M., Rahm, L. and Pollehne, F., 2008. Tracing terrestrial organic matter by delta 34S und delta 13C signatures in a subarctic estuary. *Limnol. Oceanogr.*, **55**(6): 2549-2602.

Alling, V., Sanchez-Garcia, L., Porcelli, D., Pugach, S., Vonk, J.E., van Dongen, B., et al., 2010. Nonconservative behavior of dissolved organic carbon across the Laptev and East Siberian seas. *Glob. Biogeochem. Cycle*, **24**(4): GB4033.

Aluwihare, L.I., Repeta, D.J. and Chen, R.F., 1997. A major biopolymeric component to dissolved organic carbon in surface sea water. *Nature*, **387**(6629): 166-169.

Anderson, T.F. and Pratt, L.M., 1995. Isotopic Evidence for the Origin of Organic Sulfur and Elemental Sulfur in Marine Sediments, Geochemical Transformations of Sedimentary Sulfur. ACS Symposium Series. American Chemical Society, pp. 378-396.

Andreae, M.O., 1990. Ocean-atmosphere interactions in the global biogeochemical sulfur cycle. *Mar. Chem.*, **30**(1-3): 1-29.

Armstrong, R.A., Lee, C., Hedges, J.I., Honjo, S. and Wakeham, S.G., 2001. A new, mechanistic model for organic carbon fluxes in the ocean based on the quantitative association of POC with ballast minerals. *Deep Sea Res. Part II: Top. Stud. Oceanogr.*, **49**(1): 219-236.

Asmala, E., Bowers, D.G., Autio, R., Kaartokallio, H. and Thomas, D.N., 2014. Qualitative changes of riverine dissolved organic matter at low salinities due to flocculation. *J. Geophys. Res.: Biogeosciences*, **119**(10): 1919-1933.

Asmala, E., Stedmon, C.A. and Thomas, D.N., 2012. Linking CDOM spectral absorption to dissolved organic carbon concentrations and loadings in boreal estuaries. *Estuar. Coast. Shelf Sci.*, **111**: 107-117.

Baken, S., Degryse, F., Verheyen, L., Merckx, R. and Smolders, E., 2011. Metal Complexation Properties of Freshwater Dissolved Organic Matter Are Explained by Its Aromaticity and by Anthropogenic Ligands. *Environ. Sci. Technol.*, **45**(7): 2584-2590.

Bates, T.S., Kiene, R.P., Wolfe, G.V., Matrai, P.A., Chavez, F.P., Buck, K.R., et al., 1994. The cycling of sulfur in surface seawater of the northeast Pacific *J. Geophys. Res.-Oceans*, **99**(C4): 7835-7843.

Bell, R.A. and Kramer, J.R., 1999. Structural chemistry and geochemistry of silver-sulfur compounds: Critical review. *Environ. Toxicol. Chem.*, **18**(1): 9-22.

Benner, R. and Opsahl, S., 2001. Molecular indicators of the sources and transformations of dissolved organic matter in the Mississippi river plume. *Org. Geochem.*, **32**(4): 597-611.

Benner, R., Pakulski, J.D., McCarthy, M., Hedges, J.I. and Hatcher, P.G., 1992. Bulk Chemical Characteristics of Dissolved Organic Matter in the Ocean. *Science*, **225**: 1561-1564.

Bentley, R. and Chasteen, T.G., 2004. Environmental VOSCs - formation and degradation of dimethyl sulfide, methanethiol and related materials. *Chemosphere*, **55**(2): 291-317.

Bercovici, S.K. and Hansell, D.A., 2016. Dissolved organic carbon in the deep Southern Ocean: Local versus distant controls. *Glob. Biogeochem. Cycle*, **30**(2): 350-360.

Bercovici, S.K., Huber, B.A., DeJong, H.B., Dunbar, R.B. and Hansell, D.A., 2017. Dissolved organic carbon in the Ross Sea: Deep enrichment and export. *Limnol. Oceanogr.*, **62**(6): 2593-2603.

Berry, J., Wolf, A., Campbell, J.E., Baker, I., Blake, N., Blake, D., et al, 2013. A coupled model of the global cycles of carbonyl sulfide and CO2: A possible new window on the carbon cycle. *J. Geophys. Res.: Biogeosciences*, **118**(2): 842-852.

Bertilsson, S. and Jones Jr, J.B., 2003. Supply of Dissolved Organic Matter to Aquatic Ecosystems: Autochthonous Sources In: Findlay, S.E.G., Sinsabaugh, R.L. (Editors), Aquatic Ecosystems. Academic Press, Burlington, pp. 3-24.

Bertolin, M.L. and Schloss, I.R., 2009. Phytoplankton production after the collapse of the Larsen A Ice Shelf, Antarctica. *Pol. Biol.*, **32**(10): 1435-1446.

Biller, D.V. and Bruland, K.W., 2012. Analysis of Mn, Fe, Co, Ni, Cu, Zn, Cd, and Pb in seawater using the Nobias-chelate PA1 resin and magnetic sector inductively coupled plasma mass spectrometry (ICP-MS). *Mar. Chem.*, **130–131**: 12-20.

Booge, D., Schlundt, C., Bracher, A., Endres, S., Zäncker, B., and Marandino, C. A., 2018. Marine isoprene production and consumption in the mixed layer of the surface ocean – a field study over two oceanic regions. *Biogeosciences*, **15**, 649-667.

Boto, K.G., Alongi, D.M. and Nott, A.L.J., 1989. Dissolved organic carbon-bacteria interactions at sediment-water interface in a tropical mangrove system. *Mar. Ecol. Prog. Ser.*, **51**: 243-251.

Bottrell, S.H. and Newton, R.J., 2006. Reconstruction of changes in global sulfur cycling from marine sulfate isotopes. *Earth-Sci. Rev.*, **75**(1-4): 59-83.

Bowles, M.W., Mogollón, J.M., Kasten, S., Zabel, M. and Hinrichs, K.-U., 2014. Global rates of marine sulfate reduction and implications for sub–sea-floor metabolic activities. *Science*, **344**(6186): 889-891.

Brüchert, V. and Pratt, L.M., 1996. Contemporaneous early diagenetic formation of organic and inorganic sulfur in estuarine sediments from St. Andrew Bay, Florida, USA. *Geochim. Cosmochim. Acta*, **60**(13): 2325-2332.

Bruggeman, J. and Bolding, K., 2014. A general framework for aquatic biogeochemical models. *Environ. Model. Softw.*, **61**: 249-265.

Brühl, C., Lelieveld, J., Crutzen, P.J. and Tost, H., 2012. The role of carbonyl sulphide as a source of stratospheric sulphate aerosol and its impact on climate. *Atmos. Chem. Phys.*, **12**(3): 1239-1253.

Burdige, D.J., 2007. Preservation of Organic Matter in Marine Sediments: Controls, Mechanisms, and an Imbalance in Sediment Organic Carbon Budgets? *Chem. Rev.*, **107**(2): 467-485.

Cai, Y., Guo, L., Wang, X., Mojzis, A.K. and Redalje, D.G., 2012. The source and distribution of dissolved and particulate organic matter in the Bay of St. Louis, northern Gulf of Mexico. *Estuar. Coast. Shelf Sci.*, **96**: 96-104.

Campbell, J.E., Carmichael, G.R., Chai, T., Mena-Carrasco, M., Tang, Y., Blake, D.R., et al., 2008. Photosynthetic Control of Atmospheric Carbonyl Sulfide During the Growing Season. *Science*, **322**(5904): 1085-1088.

Carlson, C.A., Hansell, D.A., Nelson, N.B., Siegel, D.A., Smethie, W.M., Khatiwala, S., et al.., 2010. Dissolved organic carbon export and subsequent remineralization in the mesopelagic and bathypelagic realms of the North Atlantic basin. *Deep Sea Res. Part II: Top. Stud. Oceanogr.*, **57**(16): 1433-1445.

Carmack, E.C. and Foster, T.D., 1975. Circulation and distribution of oceanographic properties near the Filchner Ice Shelf. *Deep Sea Res. Oceanogr. Abstr.*, **22**(2): 77-90.

Castillo, C.R., Sarmento, H., Álvarez-Salgado, X.A., Gasol, J.M. and Marraséa, C., 2010. Production of chromophoric dissolved organic matter by marine phytoplankton. *Limnol. Oceanogr.*, **55**(1): 446-454.

Catalá, T.S., Reche, I., Fuentes-Lema, A., Romera-Castillo, C., Nieto-Cid, M., Ortega-Retuerta, E., et al., 2015. Turnover time of fluorescent dissolved organic matter in the dark global ocean. *Nature Commun.*, **6**: 5986.

Cawley, K.M., Butler, K.D., Aiken, G.R., Larsen, L.G., Huntington, T.G., McKnight, D.M., 2012. Identifying fluorescent pulp mill effluent in the Gulf of Maine and its watershed. *Mar. Pollution Bullet.*, **64**(8): 1678-1687.

Chari, N.V.H.K., Keerthi, S., Sarma, N.S., Pandi, S.R., Chiranjeevulu, G., Kiran, R., et al.., 2013. Fluorescence and absorption characteristics of dissolved organic matter excreted by phytoplankton species of western Bay of Bengal under axenic laboratory condition. *J. Experim. Mar. Biol. Ecol.*, **445**: 148-155.

Charlson, R.J., Lovelock, J.E., Andreae, M.O. and Warren, S.G., 1987. Oceanic phytoplankton, atmospheric sulphur, cloud albedo and climate. *Nature*, **326**(6114): 655-661.

Chavez, F.P., Bertrand, A., Guevara-Carrasco, R., Soler, P. and Csirke, J., 2008. The northern Humboldt Current System: Brief history, present status and a view towards the future. *Prog. Oceanogr.*, **79**(2-4): 95-105.

Chen, M., Kim, S., Park, J.-E., Kim, H.S. and Hur, J., 2016. Effects of dissolved organic matter (DOM) sources and nature of solid extraction sorbent on recoverable DOM composition: Implication into potential lability of different compound groups. *Anal. Bioanal. Chem.*, **408**(17): 4809-4819.

Chen, Y., Senesi, N. and Schnitzer, M., 1977. Information Provided on Humic Substances by E4/E6 Ratios. *Soil Sci. Soc. Am. J.*, **41**(2): 352-358.

Chin, M. and Davis, D.D., 1993. Global sources and sinks of OCS and CS2 and their distributions. *Glob. Biogeochem. Cycle*, **7**(2): 321-337.

Chuang, C.-Y., Santschi, P.H., Wen, L.-S., Guo, L., Xu, C., Zhang, S., et al., 2015. Binding of Th, Pa, Pb, Po and Be radionuclides to marine colloidal macromolecular organic matter. *Mar. Chem.,* **173**: 320-329.

Clarke, A., Meredith, M.P., Wallace, M.I., Brandon, M.A. and Thomas, D.N., 2008. Seasonal and interannual variability in temperature, chlorophyll and macronutrients in northern Marguerite Bay, Antarctica. *Deep Sea Res. Part II: Top. Stud. Oceanogr.*, **55**(18): 1988-2006.

Clifford, E.L., Hansell, D.A., Varela, M.M., Nieto-Cid, M., Herndl, G.J. and Sintes, E., 2017. Crustacean zooplankton release copious amounts of dissolved organic matter as taurine in the ocean. *Limnol. Oceanogr.*, **62**(6): 2745-2758.

Coale, K.H. and Bruland, K.W., 1988. Copper complexation in the Northeast Pacific. *Limnol. Oceanogr.*, **33**(5): 1084-1101.

Coble, P.G., 2007. Marine Optical Biogeochemistry: The Chemistry of Ocean Color. *Chem. Rev.*, **107**(2): 402-418.

Cole, J.J., 2013. The Carbon Cycle: With a Brief Introduction to Global Biogeochemistry. In: K.C. Weathers, D.L. Strayer and G.E. Likens (Editors), Fundamentals of Ecosystem Science. Academic Press, pp. 109-135.

Croot, P.L., Moffett, J.W. and Brand, L.E., 2000. Production of extracellular Cu complexing ligands by eucaryotic phytoplankton in response to Cu stress. *Limnol. Oceanogr.*, **45**(3): 619-627.

Crump, B.C., Kling, G.W., Bahr, M. and Hobbie, J.E., 2003. Bacterioplankton Community Shifts in an Arctic Lake Correlate with Seasonal Changes in Organic Matter Source. *Appl. Environ. Microbiol.*, **69**(4): 2253-2268.

Crutzen, P.J., 1976. The possible importance of CSO for the sulfate layer of the stratosphere. *Geophys. Res. Lett.*, **3**(2): 73-76.

Cutter, G. A., and Radford-Knoery, J., 1993. Carbonyl sulfide in two estuaries and shelf waters of the western north atlantic ocean, *Mar. Chem.*, **43**, 225-233.

Cutter, G.A., Cutter, L.S. and Filippino, K.C., 2004. Sources and cycling of carbonyl sulfide in the Sargasso Sea. *Limnol. Oceanogr.,* **49**(2): 555-565.

Davis, J. and Benner, R., 2007. Quantitative estimates of labile and semi-labile dissolved organic carbon in the western Arctic Ocean: A molecular approach. *Limnol. Oceanogr.,*, **52**(6): 2434-2444.

de Gouw, J.A., Warneke, C., Montzka, S.A., Holloway, J.S., Parrish, D.D., Fehsenfeld, F.C., et al.., 2009. Carbonyl sulfide as an inverse tracer for biogenic organic carbon in gas and aerosol phases. *Geophys. Res. Lett.*, **36**(5).

De Schamphelaere, K.A.C., Vasconcelos, F.M., Tack, F.M.G., Allen, H.E. and Janssen, C.R., 2004. Effect of dissolved organic matter source on acute copper toxicity to *Daphnia magna*. *Environ. Toxicol. Chem.*, **23**(5): 1248-1255.

Denis, M., Jeanneau, L., Pierson-Wickman, A.-C., Humbert, G., Petitjean, P., Jaffrézic, A., et al., 2017. A comparative study on the pore-size and filter type effect on the molecular composition of soil and stream dissolved organic matter. *Org. Geochem.*, **110**: 36-44.

Dick, D., Wegner, A., Gabrielli, P., Ruth, U., Barbante, C. and Kriews, M., 2008. Rare earth elements determined in Antarctic ice by inductively coupled plasma—Time of flight, quadrupole and sector field-mass spectrometry: An inter-comparison study. *Anal. Chim. Acta*, **621**(2): 140-147.

Dickson, A.G. and Riley, J.P., 1979. The estimation of acid dissociation constants in seawater media from potentionmetric titrations with strong base. I. The ionic product of water — K_w. *Mar. Chem.*, **7**(2): 89-99.

Dittmar, T., 2015. Chapter 7 - Reasons Behind the Long-Term Stability of Dissolved Organic Matter. In: Hansell, D.A., Carlson, C.A. (Editors), Biogeochemistry of Marine Dissolved Organic Matter (Second Edition). Academic Press, Boston, pp. 369-388.

Dittmar, T. and Kattner, G., 2003. Recalcitrant dissolved organic matter in the ocean: major contribution of small amphiphilics. *Mar. Chem.*, **82**(1): 115-123.

Dittmar, T., Koch, B.P., Hertkorn, N. and Kattner, G., 2008. A simple and efficient method for the solid-phase extraction of dissolved organic matter (SPE-DOM) from seawater. *Limnol. Oceanogr.: Methods*, **6**: 230-235.

Dittmar, T., Stubbins, A., Ito, T. and Jones, D.C., 2017. Comment on "Dissolved organic sulfur in the ocean: Biogeochemistry of a petagram inventory". *Science*, **356**(6340): 813-813.

Donat, J.R., Lao, K.A. and Bruland, K.W., 1994. Speciation of dissolved copper and nickel in South San Francisco Bay: a multi-method approach. *Anal. Chim. Acta*, **284**(3): 547-571.

Driscoll, C.T., Otton, J.K. and Ake, I., 1994. Trace Metals Speciation and Cycling. In: Moldan, B. and Cerny, J. (Editors), SCOPE 51: Biogeochemistry of Small Cachments. A Tool for Environmental Research. John Wiley & Sons.

Dupont, C.L. and Ahner, B.A., 2005. Effects of copper, cadmium, and zinc on the production and exudation of thiols by *Emiliania huxleyi*. *Limnol. Oceanogr.*, **50**(2): 508-515.

Dupont, C.L., Moffett, J.W., Bidigare, R.R. and Ahner, B.A., 2006. Distributions of dissolved and particulate biogenic thiols in the subartic Pacific Ocean. *Deep-Sea Res. Part I-Oceanogr. Res. Pap.*, **53**(12): 1961-1974.

Dupont, C.L., Nelson, R.K., Bashir, S., Moffett, J.W. and Ahner, B.A., 2004. Novel copper-binding and nitrogen-rich thiols produced and exuded by *Emiliania huxleyi*. *Limnol. Oceanogr.*, **49**(5): 1754-1762.

Duprat, L.P.A.M., Bigg, G.R. and Wilton, D.J., 2016. Enhanced Southern Ocean marine productivity due to fertilization by giant icebergs. *Nature Geosci.*, **9**: 219.

Durham, B.P., Sharma, S., Luo, H., Smith, C.B., Amin, S.A., Bender, S.J., et al.., 2015. Cryptic carbon and sulfur cycling between surface ocean plankton. *Proc. Natl. Acad. Sci.*, **112**(2): 453-457.

Eglinton, T.I. and Repeta, D.J., 2006. Organic matter in the contemporary ocean. In: Holland, H.D. and Turekian, K.K. (Editors), Treatise on Geochemistry. Elsevier Pergamon, Amsterdam, pp. 145–180.

Elifantz, H., Dittel, A.I., Cottrell, M.T. and Kirchman, D.L., 2007. Dissolved organic matter assimilation by heterotrophic bacterial groups in the western Arctic Ocean. *Aqu. Microbial. Ecol.*, **50**(1): 39-49.

Elliott, S., 1990. Effect of hydrogen peroxide on the alkaline hydrolysis of carbon disulfide. *Environ. Sci. Technol.*, **24**(2): 264-267.

Elliott, S., Lu, E. and Rowland, F.S., 1989. Rates and mechanisms for the hydrolysis of carbonyl sulfide in natural waters. *Environ. Sci. Technol.*, **23**(4): 458-461.

Ellwood, M.J. and van den Berg, C.M.G., 2001. Determination of organic complexation of cobalt in seawater by cathodic stripping voltammetry. *Mar. Chem.*, **75**(1): 33-47.

Fagerbakke, K.M., Heldal, M. and Norland, S., 1996. Content of carbon, nitrogen, oxygen, sulfur and phosphorus in native aquatic and cultured bacteria. *Aqu. Microbial Ecol.*, **10**(1): 15-27.

Falkowski, P., Scholes, R.J., Boyle, E., Canadell, J., Canfield, D., Elser, J., et al., 2000. The Global Carbon Cycle: A Test of Our Knowledge of Earth as a System. *Science*, **290**(5490): 291-296.

Falkowski, P.G., Barber, R.T. and Smetacek, V., 1998. Biogeochemical Controls and Feedbacks on Ocean Primary Production. *Science*, **281**(5374): 200-206.

Ferek, R.J. and Andreae, M.O., 1984. Photochemical production of carbonyl sulphide in marine surface waters. *Nature*, **307**(5947): 148-150.

Field, C.B., Behrenfeld, M.J., Randerson, J.T. and Falkowski, P., 1998. Primary Production of the Biosphere: Integrating Terrestrial and Oceanic Components. *Science*, **281**(5374): 237-240.

Fischer, T., Banyte, D., Brandt, P., Dengler, M., Krahmann, G., Tanhua, T., et al., 2013. Diapycnal oxygen supply to the tropical North Atlantic oxygen minimum zone. *Biogeosciences*, **10**(7): 5079-5093.

Fischer, T., Kock, A., Arévalo-Martínez, D. L., Dengler, M., Brandt, P., and Bange, H. W., 2019. Gas exchange estimates in the peruvian upwelling regime biased by multi-day near-surface stratification. *Biogeosciences*, **16**, 2307-2328.

Fitznar, H.P., Lobbes, J.M. and Kattner, G., 1999. Determination of enantiomeric amino acids with high-performance liquid chromatography and pre-column derivatisation with o-phthaldialdehyde and N-isobutyrylcysteine in seawater and fossil samples (mollusks). *J. Chromatogr. A*, **832**(1): 123-132.

Flerus, R., Lechtenfeld, O.J., Koch, B.P., McCallister, S.L., Schmitt-Kopplin, P., Benner, R., et al., 2012. A molecular perspective on the ageing of marine dissolved organic matter. *Biogeosciences*, **9**: 1935-1955.

Flöck, O.R. and Andreae, M.O., 1996. Photochemical and non-photochemical formation and destruction of carbonyl sulfide and methyl mercaptan in ocean waters. *Mar. Chem.*, **54**(1): 11-26.

Flöck, O.R., Andreae, M.O. and Dräger, M., 1997. Environmentally relevant precursors of carbonyl sulfide in aquatic systems. *Mar. Chem.*, **59**(1–2): 71-85.

Foldvik, A., Gammelsrød, T., Østerhus, S., Fahrbach, E., Rohardt, G., Schröder, M., et al., 2004. Ice shelf water overflow and bottom water formation in the southern Weddell Sea. *J. Geophys. Res.: Oceans*, **109**(C2): C02015.

Galí, M., Devred, E., Levasseur, M., Royer, S.-J. and Babin, M., 2015. A remote sensing algorithm for planktonic dimethylsulfoniopropionate (DMSP) and an analysis of global patterns. *Remote Sens. Environ.*, **171**: 171-184.

Galí, M., Kieber, D. J., Romera-Castillo, C., Kinsey, J. D., Devred, E., Pérez, G. L., et al., 2016. Cdom sources and photobleaching control quantum yields for oceanic dms photolysis. *Environ. Sci Technol.*, **50**, 13361-13370, 2016.

Garcia, H.E. et al., 2010. World Ocean Atlas 2009, Volume 3: Dissolved Oxygen, Apparent Oxygen Utilization, and Oxygen Saturation.

Geuer, J., 2015. Optimization of a method for the measurement of methionine and cysteine in seawater extracts, University of Applied Sciences Bremerhaven, Bremerhaven.

Gharehveran, M. M., and Shah, A. D., 2018. Indirect photochemical formation of carbonyl sulfide and carbon disulfide in natural waters: Role of organic sulfur precursors, water quality constituents, and temperature. *Environ. Sci Technol*, **52**, 9108-9117.

Giovanelli, J., 1987. Sulfur amino acids of plants: An overview, Methods in Enzymology. Academic Press, pp. 419-426.

Giovanelli, J., Mudd, S.H. and Datko, A.H., 1978. Homocysteine biosynthesis in green plants. Physiological importance of the transsulfuration pathway in *Chlorella sorokiniana* growing under steady state conditions with limiting sulfate. *J. Biol. Chem.*, **253**(16): 5665-5677.

Giovanelli, J., Mudd, S.H. and Datko, A.H., 1980. Sulfur Amino Acids in Plants. In: Stumpf, P.K. and Conn, E.E. (Editors), The Biochemistry of Plants. Academic Press, New York, pp. 453-505.

Glatthor, N., Höpfner, M., Baker, I.T., Berry, J., Campbell, J.E., Kawa, S.R., et al., 2015. Tropical sources and sinks of carbonyl sulfide observed from space. Geophys. Res. Lett.: 10,082–10,090.

Gogou, A. and Repeta, D.J., 2010. Particulate-dissolved transformations as a sink for semi-labile dissolved organic matter: Chemical characterization of high molecular weight dissolved and surface-active organic matter in seawater and in diatom cultures. *Mar. Chem.*, **121**(1): 215-223.

Gomez-Saez, G.V., Niggemann, J., Dittmar, T., Pohlabeln, A.M., Lang, S.Q., Noowong, A., et al.., 2016. Molecular evidence for abiotic sulfurization of dissolved organic matter in marine shallow hydrothermal systems. *Geochim. Cosmochim. Acta*, **190**: 35-52.

Gonçalves-Araujo, R. et al., 2015. From Fresh to Marine Waters: Characterization and Fate of Dissolved Organic Matter in the Lena River Delta Region, Siberia. *Front. Mar. Sci*, **2**(108).

Gonsior, M., Hertkorn, N., Conte, M.H., Cooper, W.J., Bastviken, D., Druffel, E., et al., 2014. Photochemical production of polyols arising from significant photo-transformation of dissolved organic matter in the oligotrophic surface ocean. *Mar. Chem.*, **163**: 10-18.

Gonsior, M., Peake, B.M., Cooper, W.T., Podgorski, D.C., D'Andrilli, J., Dittmar, T., et al., 2011. Characterization of dissolved organic matter across the Subtropical Convergence off the South Island, New Zealand. *Mar. Chem.*, **123**(1-4): 99-110.

Gonsior, M., Schmitt-Kopplin, P. and Bastviken, D., 2013. Depth-dependent molecular composition and photo-reactivity of dissolved organic matter in a boreal lake under winter and summer conditions. *Biogeosciences*, **10**(11): 6945-6956.

Guo, L. and Santschi, P.H., 1997. Composition and cycling of colloids in marine environments. *Rev. Geophys.*, **35**(1): 17-40.

Guo, L., Santschi, P.H. and Warnken, K.W., 2000. Trace metal composition of colloidal organic material in marine environments. *Mar. Chem.*, **70**(4): 257-275.

Guo, W., Stedmon, C.A., Han, Y., Wu, F., Yu, X. and Hu, M., 2007. The conservative and non-conservative behavior of chromophoric dissolved organic matter in Chinese estuarine waters. *Mar. Chem.*, **107**(3): 357-366.

Hansell, D.A., 2013. Recalcitrant Dissolved Organic Carbon Fractions. *Annu. Rev. Mar. Sci.*, **5**: 421-445.

Hansell, D.A. and Carlson, C.A., 2002. Biogeochemistry of marine dissolved organic matter. Academic Press, Amsterdam, 774 pp.

Hansell, D.A. and Carlson, C.A., 2013. Localized refractory dissolved organic carbon sinks in the deep ocean. *Glob. Biogeochem. Cycle*, **27**(3): 705-710.

Hansell, D.A. and Carlson, C.A., 2015. Biogeochemistry of marine dissolved organic matter. 2nd ed. Academic Press, Boston.

Hansell, D.A., Carlson, C.A., Repeta, D.J. and Schlitzer, R., 2009. Dissolved organic matter in the ocean - A controversy stimulates new insights. *Oceanogr*, **22**(4): 202-211.

Hansell, D.A., Williams, P.M. and Ward, B.B., 1993. Measurements of DOC and DON in the Southern California Bight using oxidation by high temperature combustion. *Deep Sea Res. Part I: Oceanogr. Res. Pap.*, **40**(2): 219-234.

Hansman, R.L., Dittmar, T. and Herndl, G.J., 2015. Conservation of dissolved organic matter molecular composition during mixing of the deep water masses of the northeast Atlantic Ocean. *Mar. Chem.*, **177**, Part 2: 288-297.

Hathorne, E.C., Haley, B., Stichel, T., Grasse, P., Zieringer, M. and Frank, M., 2012. Online preconcentration ICP-MS analysis of rare earth elements in seawater. *Geochem. Geophys. Geosyst.*, **13**(1): Q01020.

Hedges, J.I., Eglinton, G., Hatcher, P.G., Kirchman, D.L., Arnosti, C., Derenne, S., et al., 2000. The molecularly-uncharacterized component of nonliving organic matter in natural environments. *Org. Geochem.*, **31**(10): 945-958.

Hedges, J.I. and Mann, D.C., 1979. The characterization of plant tissues by their lignin oxidation products. *Geochim. Cosmochim. Acta*, **43**(11): 1803-1807.

Helms, J.R., Stubbins, A., Perdue, E.M., Green, N.W., Chen, H. and, Mopper, K., 2013. Photochemical bleaching of oceanic dissolved organic matter and its effect on absorption spectral slope and fluorescence. *Mar. Chem.*, **155**: 81-91.

Hertkorn, N., Benner, R., Frommberger, M., Schmitt-Kopplin, P., Witt, M., Kaiser, K., et al., 2006. Characterization of a major refractory component of marine dissolved organic matter. *Geochim. Cosmochim. Acta*, **70**(12): 2990-3010.

Hertkorn, N., Harir, M., Koch, B.P., Michalke, B. and Schmitt-Kopplin, P., 2013. High-field NMR spectroskopy and FTICR mass spectrometry: powerful discovery tools for the molecular level characterization of marine dissolved organic matter. *Biogeosciences*, **10**: 1583-1624.

Hertkorn, N. and Kettrup, A., 2005. Molecular Level Structural Analysis of Natural Organic Matter and of Humic Substances by Multinuclear and Higher Dimensional NMR Spectroscopy. Use of Humic Substances to Remediate Polluted Environments: From Theory to Practice. Springer Netherlands, Dordrecht, pp. 391-435.

Ho, T.Y., Quigg, A., Finkel, Z.V., Milligan, A.J., Wyman, K., Falkowski, P.G., et al., 2003. The elemental composition of some marine phytoplankton. *J. Phycol.*, **39**(6): 1145-1159.

Homann, P.S., Mitchell, M.J., Miegroet, H.V. and Cole, D.W., 1990. Organic sulfur in throughfall, stem flow, and soil solutions from temperate forests. *Can. J. For. Res.*, **20**(9): 1535-1539.

Hopkinson, C.S. and Vallino, J.J., 2005. Efficient export of carbon to the deep ocean through dissolved organic matter. *Nature*, **433**(7022): 142-145.

Hopkinson, C.S., Vallino, J.J. and Nolin, A., 2002. Decomposition of dissolved organic matter from the continental margin. *Deep-Sea Res. Part II-Top. Stud. Oceanogr.*, **49**(20): 4461-4478.

Hoppema, M., Bakker, K., van Heuven, S.M.A.C., van Ooijen, J.C. and de Baar, H.J.W., 2015. Distributions, trends and inter-annual variability of nutrients along a repeat section through the Weddell Sea (1996–2011). *Mar. Chem.*, **177**: 545-553.

Houle, D., Carignan, R., Lachance, M. and Dupont, J., 1995. Dissolved organic carbon and sulfur in southwestern Québec lakes: Relationships with catchment and lake properties. *Limnol. Oceanogr*, **40**(4): 710-717.

Hsu-Kim, H., 2007. Stability of Metal−Glutathione Complexes during Oxidation by Hydrogen Peroxide and Cu(II)-Catalysis. *Environ. Sci. Technol.*, **41**(7): 2338-2342.

Huguet, A., Vacher, L., Relexans, S., Saubusse, S., Froidefond, J.M. and Parlanti, E., 2009. Properties of fluorescent dissolved organic matter in the Gironde Estuary. *Org. Geochem.*, **40**(6): 706-719.

Hummels, R., Dengler, M. and Bourlès, B., 2013. Seasonal and regional variability of upper ocean diapycnal heat flux in the Atlantic cold tongue. *Prog. Oceanogr.*, **111**: 52-74.

Iida, T., Odate, T. and Fukuchi, M., 2013. Long-Term Trends of Nutrients and Apparent Oxygen Utilization South of the Polar Front in Southern Ocean Intermediate Water from 1965 to 2008. *PLOS ONE*, **8**(8): e71766.

Jasinska, A., Burska, D. and Bolalek, J., 2012. Sulfur in the marine environment. *Oceanol. Hydrobiol. Stud.*, **41**(2): 72-82.

Jiao, N., Herndl, G.J., Hansell, D.A., Benner, R., Kattner, G., Wilhelm, S.W., et al., 2010. Microbial production of recalcitrant dissolved organic matter: long-term carbon storage in the global ocean. *Nature*, **8**: 593-599.

Jochum, K.P., Nohl, U., Herwig, K., Lammel, E., Stoll, B. and Hofmann, A.W., 2005. GeoReM: A New Geochemical Database for Reference Materials and Isotopic Standards. *Geostand. Geoanal. Res.*, **29**(3): 333-338.

Jørgensen, B.B. and Kasten, S., 2006. Sulfur Cycling and Methane Oxidation. In: Schulz, H.D. and Zabel, M. (Editors), Marine Geochemistry. Springer Berlin Heidelberg, Berlin, Heidelberg, pp. 271-309.

Jørgensen, L., Stedmon, C.A., Kragh, T., Markager, S., Middelboe, M. and Søndergaard, M., 2011. Global trends in the fluorescence characteristics and distribution of marine dissolved organic matter. *Mar. Chem.*, **126**(1): 139-148.

Junge, C.E., Chagnon, C.W. and Manson, J.E., 1961. A World-wide Stratospheric Aerosol Layer. *Science*, **133**(3463): 1478-1479.

Kaiser, E., Simpson, A.J., Dria, K.J., Sulzberger, B. and Hatcher, P.G., 2003. Solid-State and Multidimensional Solution-State NMR of Solid Phase Extracted and Ultrafiltered Riverine Dissolved Organic Matter. *Environ. Sci. Technol.*, **37**(13): 2929-2935.

Kaiser, K. and Benner, R., 2009. Biochemical composition and size distribution of organic matter at the Pacific and Atlantic time-series stations. *Mar. Chem.*, **113**(1-2): 63-77.

Kaiser, K. and Guggenberger, G., 2000. The role of DOM sorption to mineral surfaces in the preservation of organic matter in soils. *Org. Geochem.*, **31**(7): 711-725.

Kamyshny, A., Goifman, A., Rizkov, D., and Lev, O., 2003. Formation of carbonyl sulfide by the reaction of carbon monoxide and inorganic polysulfides *Environ. Sci. Technol.*, **37**, 1865-1872.

Karstensen, J., Stramma, L. and Visbeck, M., 2008. Oxygen minimum zones in the eastern tropical Atlantic and Pacific oceans. *Prog. Oceanogr.*, **77**(4): 331-350.

Kattner, G. and Becker, H., 1991. Nutrients and organic nitrogenous compounds in the marginal ice zone of the Fram Strait. *J. Mar. Syst.*, **2**(3–4): 385-394.

Kettle, A. J., 2000. Extrapolations of the flux of dimethylsulfide, carbon monooxide, carbonyl sulfide and carbon disulfide from the oceans. PhD, Graduate Program in Chemistry, North York, Ontario.

Kettle, A.J. and Andreae, M.O., 2000. Flux of dimethylsulfide from the oceans: A comparison of updated data sets and flux models. *J. Geophys. Res.: Atmospheres*, **105**(D22): 26793-26808.

Kettle, A.J., Rhee, T.S., vonHobe, M., Poulton, A., Aiken, J. and Andreae, M.O.., 2001. Assessing the flux of different volatile sulfur gases from the ocean to the atmosphere. *J. Geophys. Res.: Atmospheres*, **106**(D11): 12193-12209.

Kiene, R.P. and Linn, L.J., 2000. The fate of dissolved dimethylsulfoniopropionate (DMSP) in seawater: Tracer studies using 35S-DMSP. *Geochim. Cosmochim. Acta*, **64**(16): 2797-2810.

Kiene, R.P., Linn, L.J., Gonzalez, J., Moran, M.A. and Bruton, J.A., 1999. Dimethylsulfoniopropionate and methanethiol are important precursors of methionine and protein-sulfur in marine bacterioplankton. *Appl. Environ. Microbiol.*, **65**(10): 4549-4558.

Kiene, R.P. and Slezak, D., 2006. Low dissolved DMSP concentrations in seawater revealed by small-volume gravity filtration and dialysis sampling. *Limnol. Oceanogr: Methods*, **4**(4): 80-95.

Knust, R. and Schröder, M., 2014. The Expedition PS82 of the Research Vessel POLARSTERN to the southern Weddell Sea in 2013/2014, Bremerhaven, Germany.

Koch, B.P. and Dittmar, T., 2006. From mass to structure: an aromaticity index for high-resolution mass data of natural organic matter. *Rapid Commun. Mass Spectrom.*, **20**(5): 926-932.

Koch, B.P., Ludwichowski, K.-U., Kattner, G., Dittmar, T., and Witt, M., 2008. Advanced characterization of marine dissolved organic matter by combining reversed-phase liquid chromatography and FT-ICR-MS. *Mar. Chem.*,**111**:233-41.

Koch, B.P. and Rohardt, G., 2016. Continuous thermosalinograph oceanography along HEINCKE cruise track HE426. Database: PANGAEA [Internet].

Koch, B.P., Witt, M., Engbrodt, R., Dittmar, T. and Kattner, G., 2005. Molecular formulae of marine and terrigenous dissolved organic matter detected by electrospray ionization Fourier transform ion cyclotron resonance mass spectrometry. *Geochim. Cosmochim. Acta*, **69**(13): 3299-3308.

Kohlbach, D., Lange, B.A., Graeve, M., Vortkamp, M. and Flores, H., 2019. Varying dependency of Antarctic euphausiids on ice algae- and phytoplankton-derived carbon sources during summer. *Mar. Biol.*, **166**(6): 79.

Kohnen, M.E.L., Schouten, S., Sinninghe Damsté, J.S., de Leeuw, J.W., Merrit, D., Hayes, J.M., 1992. The combined application of organic sulphur and isotope geochemistry to asses multiple sources of palaeobiochemicals with identical carbon skeletons. *Org. Geochem.*, **19**(4): 403-419.

Kolber, Z.S., Barber, R.T., Coale, K.H., Fitzwateri, S.E., Greene, R.M., Johnson, K.S., et al., 1994. Iron limitation of phytoplankton photosynthesis in the equatorial Pacific Ocean. *Nature*, **371**(6493): 145-149.

Kremser, S. Thomason, L.W., von Hobe, M., Hermann, M., Deshler, T., Timmreck, C. et al., 2016. Stratospheric aerosol—Observations, processes, and impact on climate. *Rev. Geophys.*, **54**: 278-335.

Kristensen, E., Ahmed, S.I. and Devol, A.H., 1995. Aerobic and anaerobic decomposition of organic matter in marine sediment: Which is fastest? *Limnol. Oceanogr*, **40**(8): 1430-1437.

Krogh, A., 1934. Conditions of Life in the Ocean. *Ecol. Monogr.*, **4**(4): 421-429.

Kruger, B.R., Dalzell, B.J. and Minor, E.C., 2011. Effect of organic matter source and salinity on dissolved organic matter isolation via ultrafiltration and solid phase extraction. *Aquat. Sci.*, **73**(3): 405-417.

Ksionzek, K.B., Lechtenfeld, O.J., McCallister, S.L., Schmitt-Kopplin, P., Geuer, J.K., Geibert, W., et al., 2016a. Dissolved organic sulfur in the ocean: Biogeochemistry of a petagram inventory. *Science*, **354**(6311): 456-459.

Ksionzek, K.B., Lechtenfeld, O.J., McCallister, S.L., Schmitt-Kopplin, P., Geuer, J.K., Geibert, W., et al., 2016b. Dissolved organic sulfur in solid-phase extracts of water samples obtained during POLARSTERN cruise ANT-XXV (PS73), Database: PANGAEA [Internet].

Ksionzek, K.B., Zhang, J., Ludwichowski, K.-U., Wilhelms-Dick, D., Trimborn, S., Jendrossek, T., et al., 2018. Stoichiometry, polarity, and organometallics in solid-phase extracted dissolved organic matter of the Elbe-Weser estuary. *PLOS ONE*, **13**(9): e0203260.

Kuai, L., Worden, J.R., Campbell, J.E., Kulawik, S.S., Li, K.-F., Lee, et al., 2015. Estimate of carbonyl sulfide tropical oceanic surface fluxes using Aura Tropospheric Emission Spectrometer observations. *J. Geophys. Res. Atmos.*, **120**(20): 11,012-11,023.

Kwint, R.L.J. and Kramer, K.J.M., 1996. Annual cycle of the production and fate of DMS and DMSP in a marine coastal system. *Mar. Ecol.-Prog. Ser.*, **134**: 217-224.

Laglera, L.M. and van den Berg, C.M.G., 2003. Copper complexation by thiol compounds in estuarine waters. *Mar. Chem.*, **82**(1–2): 71-89.

Lana, A., Bell, T.G., Simo, R., Vallina, S.M., Ballabrera-Poy, J., Kettle, A.J. et al., 2011. An updated climatology of surface dimethlysulfide concentrations and emission fluxes in the global ocean. *Glob. Biogeochem. Cycle*, **25**: 17.

Launois, T., Belviso, S., Bopp, L., Fichot, C.G. and Peylin, P., 2015. A new model for the global biogeochemical cycle of carbonyl sulfide - Part 1: Assessment of direct marine emissions with an oceanic general circulation and biogeochemistry model. *Atmos. Chem. Phys.*, **15**(5): 2295-2312.

Lechtenfeld, O.J., 2012. Biogeochemistry of marine dissolved organic matter: Molecular composition, reactivity and new methods, University of Bremen.

Lechtenfeld, O.J. et al., 2014. Molecular transformation and degradation of refractory dissolved organic matter in the Atlantic and Southern Ocean. *Geochim. Cosmochim. Acta*, **126**: 321-337.

Lechtenfeld, O.J., Kattner, G., Flerus, R., McCallister, S.L., Schmitt-Kopplin, P. and Koch, B.P., 2013. The influence of salinity on the molecular and optical properties of surface microlayers in a karstic estuary. *Mar. Chem.*, **150**: 25-38.

Lechtenfeld, O.J., Koch, B.P., Geibert, W., Ludwichowski, K.U. and Kattner, G., 2011. Inorganics in Organics: Quantification of Organic Phosphorus and Sulfur and Trace Element Speciation in Natural Organic Matter Using HPLC-ICPMS. *Anal. Chem.*, **83**(23): 8968-8974.

Lee, P.A., de Mora, S.J. and Levasseur, M., 1999. A review of dimethylsulfoxide in aquatic environments. *Atmosphere-Ocean*, **37**(4): 439-456.

Lefering, I., Röttgers, R., Utschig, C. and McKee, D., 2017. Uncertainty budgets for liquid waveguide CDOM absorption measurements. *Appl. Opt.*, **56**(22): 6357-6366.

Lennartz, S.T., Marandino, C.A., von Hobe, M., Cortes, P., Quack, B., Simo, R., et al., 2017. Direct oceanic emissions unlikely to account for the missing source of atmospheric carbonyl sulfide. *Atmos. Chem. Phys.*, **17**(1): 385-402.

Levine, N.M., 2016. Putting the spotlight on organic sulfur. *Science*, **354**(6311): 418-419.

Lindroth, P. and Mopper, K., 1979. High performance liquid chromatographic determination of subpicomole amounts of amino acids by precolumn fluorescence derivatization with o-phthaldialdehyde. *Anal. Chem.*, **51**(11): 1667-1674.

Lipp, J.S., Morono, Y., Inagaki, F. and Hinrichs, K.-U., 2008. Significant contribution of Archaea to extant biomass in marine subsurface sediments. *Nature*, **454**(7207): 991-994.

Liss, P.S. et al., 2014. Short-Lived Trace Gases in the Surface Ocean and the Atmosphere, Ocean-Atmosphere Interactions of Gases and Particles. Springer.

Lomans, B.P., van der Drift, C., Pol, A. and Op den Camp, H.J.M., 2002. Microbial cycling of volatile organic sulfur compounds. *CMLS*, **59**(4): 575-588.

Lorbacher, K., Dommenget, D., Niiler, P. P., and Köhl, A., 2006. Ocean mixed layer depth: A subsurface proxy of ocean-atmosphere variability. *J. Geophys. Res.: Oceans*, **111**, C07010 .

Mantoura, R.F.C., Dickson, A. and Riley, J.P., 1978. The complexation of metals with humic materials in natural waters. *Estuar. Coast. Mar. Sci.*, **6**(4): 387-408.

Martin, J.H., Gordon, R.M. and Fitzwater, S.E., 1990. Iron in Antarctic waters. *Nature*, **345**(6271): 156-158.

Matar, Z., Chebbo, G., Troupel, M., Boudhamane, L., Parlanti, E., Uher, E,. et al., 2013. Influence of Organic Matter from Urban Effluents on Trace Metal Speciation and Bioavailability in River Under Strong Urban Pressure. In: Xu, J., Wu, J. and He, Y. (Editors), Functions of Natural Organic Matter in Changing Environment. Springer Netherlands, Dordrecht, pp. 517-521.

Matrai, P.A. and Eppley, R.W., 1989. Particulate organic sulfur in the waters of the Southern California Bight. *Glob. Biogeochem. Cycle*, **3**(1): 89-103.

Miller, R.L., Belz, M., Castillo, C.D. and Trzaska, R., 2002. Determining CDOM absorption spectra in diverse coastal environments using a multiple pathlength, liquid core waveguide system. *Cont. Shelf Res.*, **22**(9): 1301-1310.

Miller, W.L. and Moran, M.A., 1997. Interaction of photochemical and microbial processes in the degradation of refractory dissolved organic matter from a coastal marine environment. *Limnol. Oceanogr*, **42**(6): 1317-1324.

Mills, G.L., Hanson, A.K., Quinn, J.G., Lammela, W.R. and Chasteen, N.D., 1982. Chemical studies of copper-organic complexes isolated from estuarine waters using C18 reverse-phase liquid chromatography. *Mar. Chem.*, **11**(4): 355-377.

Milne, A., Landing, W., Bizimis, M. and Morton, P., 2010. Determination of Mn, Fe, Co, Ni, Cu, Zn, Cd and Pb in seawater using high resolution magnetic sector inductively coupled mass spectrometry (HR-ICP-MS). *Anal. Chim. Acta*, **665**(2): 200-207.

Moffett, J.W. and Brand, L.E., 1996. Production of strong, extracellular Cu chelators by marine cyanobacteria in response to Cu stress. *Limnol. Oceanogr.*, **41**(3): 388-395.

Moffett, J.W., Zika, R.G. and Brand, L.E., 1990. Distribution and potential sources and sinks of copper chelators in the Sargasso Sea. *Deep Sea Res. Part A. Oceanogr. Res. Pap.*, **37**(1): 27-36.

Montzka, S.A., Calvert, P., Hall, B.D., Elkins, J.W., Conway, T.J., Tans, P.P., et al., 2007. On the global distribution, seasonality, and budget of atmospheric carbonyl sulfide (COS) and some similarities to CO2. *J. Geophys. Res.*, **112**(D9).

Mopper, K., Kieber, D.J. and Stubbins, A., 2015. Chapter 8 - Marine Photochemistry of Organic Matter: Processes and Impacts. In: Hansell, D.A., Carlson C.A. (Editors), Biogeochemistry of Marine Dissolved Organic Matter (Second Edition). Academic Press, Boston, pp. 389-450.

Mopper, K. and Lindroth, P., 1982. Diel and depth variations in dissolved free amino acids and ammonium in the Baltic Sea determined by shipboard HPLC analysis. *Limnol. Oceanogr*, **27**(2): 336-347.

Mopper, K., Zhou, X., Kieber, R.J., Kieber, D.J., Sikorski, R.J. and Jones, R.D., 1991. Photochemical degradation of dissolved organic carbon and its impact on the oceanic carbon cycle. *Nature*, **353**(6339): 60-62.

Morales-Cid, G., Gebefugi, I., Kanawati, B., Harir, M., Hertkorn, N., Rossello-Mora, R., et al., 2009. Automated microextraction sample preparation coupled on-line to FT-ICR-MS: application to desalting and concentration of river and marine dissolved organic matter. *Anal. Bioanal. Chem.*, **395**(3): 797-807.

Moran, M.A., Kujawinski, E.B., Stubbins, A., Fatland, R., Aluwihare, L.I., Buchan, A., et al., 2016. Deciphering ocean carbon in a changing world. *PNAS*, **113**(12): 3143-3151.

Moran, M.A., Reisch, C.R., Kiene, R.P. and Whitman, W.B., 2012. Genomic Insights into Bacterial DMSP Transformations. *Annu. Rev. Mar. Sci.*, Vol 4, 4: 523-542.

Moran, M.A. and Zepp, R.G., 1997. Role of photoreactions in the formation of biologically labile compounds from dissolved organic matter. *Limnol. Oceanogr*, **42**(6): 1307-1316.

Morel, F.M.M. and Price, N.M., 2003. The Biogeochemical Cycles of Trace Metals in the Oceans. *Science*, **300**(5621): 944-947.

Mossmann, J.-R., Aplin, A.C., Curtis, C.D. and Coleman, M.L., 1991. Geochemistry of inorganic and organic sulphur in organic-rich sediments from the Peru Margin. *Geochim. Cosmochim. Acta*, **55**(12): 3581-3595.

Mueller, J. L., Fargion, G. S., McClain, C. R., Pegau, S., Zanefeld, J., Mitchell, B. G., et al., 2003. Ocean optics protocols for satellite ocean color sensor validation, revision 4, volume iv: Inherent optical properties: Instruments, characterizations, field measurements and data analysis protocols.

Murphy, K.R., Stedmon, C.A., Graeber, D. and Bro, R., 2013. Fluorescence spectroscopy and multi-way techniques. PARAFAC. *Anal. Methods*, **5**(23): 6557-6566.

Murphy, K.R., Stedmon, C.A., Wenig, P. and Bro, R., 2014. OpenFluor– an online spectral library of auto-fluorescence by organic compounds in the environment. *Anal. Methods*, **6**(3): 658-661.

Nachtsheim, D.A., Ryan, S., Schröder, M., Jensen, L., Oosthuizen, W.C., Bester, M.N., et al., 2019. Foraging behaviour of Weddell seals (Leptonychotes weddellii) in connection to oceanographic conditions in the southern Weddell Sea. *Prog. Oceanogr.*, **173**: 165-179.

Nelson, D.M. and Gordon, L.I., 1982. Production and pelagic dissolution of biogenic silica in the Southern Ocean. *Geochim. Cosmochim. Acta*, **46**(4): 491-501.

Nelson, N.B. and Siegel, D.A., 2013. The Global Distribution and Dynamics of Chromophoric Dissolved Organic Matter. *Annu. Rev. Mar. Sci.*, **5**: 447-476.

Nicholls, K.W., Østerhus, S., Makinson, K., Gammelsrød, T. and Fahrbach, E., 2009. Ice-ocean processes over the continental shelf of the southern Weddell Sea, Antarctica: A review. *Rev. Geophys.*, **47**(3): n/a-n/a.

Nightingale, P.D. Malin, G., Law, C.S., Watson, A.J., Liss, P.S., Liddicoat, M.I., et al., 2000. In situ evaluation of air-sea gas exchange parameterizations using novel conservative and volatile tracers. *Glob. Biogeochem. Cycle*, **14**(1): 373-387.

Ogawa, H., Amagai, Y., Koike, I., Kaiser, K. and Benner, R., 2001. Production of Refractory Dissolved Organic Matter by Bacteria. *Science*, **292**(5518): 917-920.

Ogawa, H. and Tanoue, E., 2003. Dissolved organic matter in oceanic waters. *J Oceanogr.*, **39**(2): 129-147.

Opsahl, S. and Benner, R., 1997. Distribution and cycling of terrigenous dissolved organic matter in the ocean. *Nature*, **386**(6624): 480-482.

Opsahl, S. and Benner, R., 1998. Photochemical reactivity of dissolved lignin in river and ocean waters. *Limnol. Oceanogr*, **43**(6): 1297-1304.

Orsi, A.H., Johnson, G.C. and Bullister, J.L., 1999. Circulation, mixing, and production of Antarctic Bottom Water. *Prog. Oceanogr.*, **43**(1): 55-109.

Osburn, C.L., Wigdahl, C.R., Fritz, S.C. and Saros, J.E., 2011. Dissolved organic matter composition and photoreactivity in prairie lakes of the U.S. Great Plains. *Limnol. Oceanogr*, **56**(6): 2371-2390.

Otto, S. and Balzer, W., 1998. Release of dissolved organic carbon (DOC) from sediments of the N.W. European Continental Margin (Goban Spur) and its significance for benthic carbon cycling. *Prog. Oceanogr.*, **42**(1): 127-144.

Pan, X., Achterberg, E.P., Sanders, R., Poulton, A.J., Oliver, K.I.C. and Robinson, C., 2014. Dissolved organic carbon and apparent oxygen utilization in the Atlantic Ocean. *Deep Sea Res. Part I: Oceanogr. Res. Pap.*, **85**: 80-87.

Passier, H.F., Böttcher, M.E. and Lange, G.J.D., 1999. Sulphur Enrichment in Organic Matter of Eastern Mediterranean Sapropels: A Study of Sulphur Isotope Partitioning. *Aquat. Geochem.*, **5**(1): 99-118.

Payne, C.D. and Price, N.M., 1999. Effects of cadmium toxicity on growth and elemental composition of marine phytoplankton. *J. Phycol.*, **35**(2): 293-302.

Paytan, A. et al., 2009. Toxicity of atmospheric aerosols on marine phytoplankton. *PNAS*, **106**(12): 4601-4605.

Peuravuori, J. and Pihlaja, K., 1997. Molecular size distribution and spectroscopic properties of aquatic humic substances. *Anal. Chim. Acta*, **337**(2): 133-149.

Piccolo, A., Zaccheo, P. and Genevini, P.G., 1992. Chemical characterization of humic substances extracted from organic-waste-amended soils. *Biores. Technol.*, **40**(3): 275-282.

Pilson, M.E.Q., 2013. An Introduction to the Chemistry of the Sea. Cambridge University Press, New York.

Pohlabeln, A.M., 2017. Marine dissolved organic sulfur – Sources, fate, and structural characteristics, Carl von Ossietzky University Oldenburg, Oldenburg.

Pohlabeln, A.M. and Dittmar, T., 2015. Novel insights into the molecular structure of non-volatile marine dissolved organic sulfur. *Mar. Chem.*, **168**(0): 86-94.

Pohlabeln, A.M., Gomez-Saez, G.V., Noriega-Ortega, B.E. and Dittmar, T., 2017. Experimental Evidence for Abiotic Sulfurization of Marine Dissolved Organic Matter. *Front. Mar. Sci.*, **4**(364).

Pos, W.H., Riemer, D.D. and Zika, R.G., 1998. Carbonyl sulfide (OCS) and carbon monoxide (CO) in natural waters: evidence of a coupled production pathway. *Mar. Chem.*, **62**(1): 89-101.

Preiswerk, D., and Najjar, R. G., 2000. A global, open-ocean model of carbonyl sulfide and its air-sea flux, *Glob. Biogeochem. Cycle*, **14**, 585-598.

Quinn, P.K. and Bates, T.S., 2011. The case against climate regulation via oceanic phytoplankton sulphur emissions. *Nature*, **480**(7375): 51-56.

Radford-Knoery, J. and Cutter, G.A., 1994. Biogeochemistry of dissolved hydrogen sulfide species and carbonyl sulfide in the western North Atlantic Ocean. *Geochim. Cosmochim. Acta*, **58**(24): 5421-5431.

Ravichandran, M., 2004. Interactions between mercury and dissolved organic matter - A review. *Chemosphere*, **55**(3): 319-331.

Raymond, P.A. and Spencer, R.G.M., 2015. Chapter 11 - Riverine DOM. In: Hansell, D.A. and Carlson, C.A. (Editors), Biogeochemistry of Marine Dissolved Organic Matter (Second Edition). Academic Press, Boston, pp. 509-533.

Reddy, K.J., Wang, L. and Gloss, S.P., 1995. Solubility and mobility of copper, zinc and lead in acidic environments. *Plant Soil*, **171**(1): 53-58.

Redfield, A.C., Ketchum, B.H. and Richards, F.A., 1963. The influence of organisms on the composition of sea-water. In: Hill, M.N. (Editor), The Sea. Wiley Interscience, New York, pp. 26-79.

Reid, J.L. and Lynn, R.J., 1971. On the influence of the Norwegian-Greenland and Weddell seas upon the bottom waters of the Indian and Pacific oceans. *Deep Sea Res. Oceanogr. Abstr.*, **18**(11): 1063-1088.

Repeta, D.J., 2015. Chapter 2 - Chemical Characterization and Cycling of Dissolved Organic Matter. In: Hansell, D.A. and Carlson, C.A. (Editors), Biogeochemistry of Marine Dissolved Organic Matter (Second Edition). Academic Press, Boston, pp. 21-63.

Roberts, T., 2015. Sulphur Compounds. In: Moretto, L.M. and Kalcher, K. (Editors), Environmental Analysis by Electrochemical Sensors and Biosensors. Nanostructure Science and Technology. Springer New York, pp. 1047-1067.

Rochelle-Newall, E.J., Pizay, M.-D., Middelburg, J., J. , Boschker, H.T.S. and Gattuso, J.-P., 2004. Degradation of riverine dissolved organic matter by seawater bacteria. *Aquat. Microbial. Ecol.*, **37**(1): 9-22.

Saito, M.A., Moffett, J.W. and DiTullio, G.R., 2004. Cobalt and nickel in the Peru upwelling region: A major flux of labile cobalt utilized as a micronutrient. *Glob. Biogeochem. Cycle*, **18**(4): GB4030.

Santinelli, C., Nannicini, L. and Seritti, A., 2010. DOC dynamics in the meso and bathypelagic layers of the Mediterranean Sea. *Deep Sea Res. Part II: Top. Stud. Oceanogr.*, **57**(16): 1446-1459.

Santschi, P.H., Lenhart, J.J. and Honeyman, B.D., 1997. Heterogeneous processes affecting trace contaminant distribution in estuaries: The role of natural organic matter. *Mar. Chem.*, **58**(1): 99-125.

Sarmiento, J.L. and Gruber, N., 2006. Ocean Biogeochemical Dynamics. Princeton, NJ, Princeton University Press.

Schauffler, S.M., Atlas, E.L., Flocke, F., Lueb, R.A., Stroud, V. and Travnicek, W., 1998. Measurements of bromine containing organic compounds at the tropical tropopause. *Geophys. Res. Lett.*, **25**(3): 317-320.

Schlundt, M., Brandt, P., Dengler, M., Hummels, R., Fischer, T., Bumke, K., et al., 2014. Mixed layer heat and salinity budgets during the onset of the 2011 Atlantic cold tongue. *J. Geophys. Res.: Oceans*, **119**(11): 7882-7910.

Schmidt, F., Elvert, M., Koch, B.P., Witt, M. and Hinrichs, K.-U., 2009. Molecular characterization of dissolved orgenic matter in pore water of continental shelf sediments. *Geochim. Cosmochim. Acta*, **73**: 3337-3358.

Schmitt-Kopplin, P. et al., 2012. Dissolved organic matter in sea spray: a transfer study from marine surface water to aerosols. *Biogeosciences*, **9**(4): 1571-1582.

Schrade, S., 2001. Ground based measurements of carbon dioxide and other climatically relevant trace gases using off-axis integrated-cavity-output-spectroscopy (icos). Diploma Thesis, RWTH Aachen, Germany.

Schwartz, M.L., Curtis, P.J. and Playle, R.C., 2004. Influence of natural organic matter source on acute copper, lead, and cadmium toxicity to rainbow trout (Oncorhynchus mykiss). *Environ. Toxicol. Chem.*, **23**(12): 2889-2899.

Sepers, A.B.J., 1977. The utilization of dissolved organic compounds in aquatic environments. *Hydrobiologia*, **52**(1): 39-54.

Shaked, Y. and Lis, H., 2012. Disassembling Iron Availability to Phytoplankton. *Front. Microbiol.*, **3**(123).

Sholkovitz, E.R., 1978. The flocculation of dissolved Fe, Mn, Al, Cu, Ni, Co and Cd during estuarine mixing. *Earth Planet. Sci. Lett.*, **41**(1): 77-86.

Shooter, D., 1999. Sources and sinks of oceanic hydrogen sulfide – an overview. *Atmosph. Environ.*, **33**(21): 3467-3472.

Simpson, A., 2001. Multidimensional solution state NMR of humic substances: A practical guide and review. *Soil Sci.*, **166**(11): 795-809.

Sipler, R.E. and Bronk, D.A., 2015. Chapter 4 - Dynamics of Dissolved Organic Nitrogen. In: Hansell, D.A. and Carlson, C.A. (Editors), Biogeochemistry of Marine Dissolved Organic Matter (Second Edition). Academic Press, Boston, pp. 127-232.

Sleighter, R.L., Chin, Y.-P., Arnold, W.A., Hatcher, P.G., McCabe, A.J., McAdams, B.C., et al., 2014. Evidence of Incorporation of Abiotic S and N into Prairie Wetland Dissolved Organic Matter. *Environ. Sci. Technol. Lett.*, **1**(9): 345-350.

Sleighter, R.L. and Hatcher, P.G., 2008. Molecular characterization of dissolved organic matter (DOM) along a river to ocean transect of the lower Chesapeake Bay by ultrahigh resolution electospray ionization Fourier tranform ion cyclotron resonance mass spectrometry. *Mar. Chem.*, **110**: 140-152.

Smith, D.S., Bell, R.A. and Kramer, J.R., 2002. Metal speciation in natural waters with emphasis on reduced sulfur groups as strong metal binding sites. *Comp. Biochem. Physiol. C-Toxicol. Pharmacol.*, **133**(1-2): 65-74.

Spitzy, A., 2005. Water chemistry measurements of different Sites. Database: PANGAEA [Internet].

Stedmon, C.A. and Bro, R., 2008. Characterizing dissolved organic matter fluorescence with parallel factor analysis: a tutorial. *Limnol. Oceanogr: Methods*, **6**(11): 572-579.

Stedmon, C.A. and Markager, S., 2003. Behaviour of the optical properties of coloured dissolved organic matter under conservative mixing. *Estuar. Coast. Shelf Sci.*, **57**(5–6): 973-979.

Stedmon, C.A. and Markager, S., 2005. Tracing the production and degradation of autochthonous fractions of dissolved organic matter by fluorescence analysis. *Limnol. Oceanogr*, **50**(5): 1415-1426.

Stramma, L. et al., 2016. Observed El Niño conditions in the eastern tropical Pacific in October 2015. *Ocean Sci.*, **12**(4): 861-873.

Stubbins, A., Law, C., Uher, G., and Upstill-Goddard, R., 2011. Carbon monoxide apparent quantum yields and photoproduction in the tyne estuary. *Biogeosciences*, **8**, 703-713.

Summers, R.S., Cornel, P.K. and Roberts, P.V., 1987. Molecular size distribution and spectroscopic characterization of humic substances. *Sci. Tot.Environ.*, **62**: 27-37.

Sunda, W.G., 2012. Feedback Interactions between Trace Metal Nutrients and Phytoplankton in the Ocean. *Front. Microbiol.*, **3**: 204.

Takano, S., Tanimizu, M., Hirata, T. and Sohrin, Y., 2013. Determination of isotopic composition of dissolved copper in seawater by multi-collector inductively coupled plasma mass spectrometry after pre-concentration using an ethylenediaminetriacetic acid chelating resin. *Anal. Chim. Acta*, **784**: 33-41.

Tang, D., Hung, C.-C., Warnken, K.W. and Santschi, P.H., 2000. The distribution of biogenic thiols in surface waters of Galveston Bay. *Limnol. Oceanogr*, **45**(6): 1289-1297.

Tarnocai, C., Canadell, J.G., Schuur, E.A.G., Kuhry, P., Mazhitova, G. and Zimov, S., 2009. Soil organic carbon pools in the northern circumpolar permafrost region. *Glob. Biogeochem. Cycle*, **23**(2): n/a-n/a.

Thomas, C., Cauwet, G. and Minster, J.-F., 1995. Dissolved organic carbon in the equatorial Atlantic Ocean. *Mar. Chem.*, **49**(2–3): 155-169.

Thomas, D.N., Kattner, G., Engbrodt, R., Giannelli, V., Kennedy, H., Haas, C., et al., 2001. Dissolved organic matter in Antarctic sea ice. In: Jeffries, M.O. and Eicken, H. (Editors), Annals of Glaciology, Vol 33. Annals of Glaciology. Int Glaciological Soc, Cambridge, pp. 297-303.

Thomas, D.N. and Papadimitriou, S., 2003. Biogeochemistry of Sea Ice. In: Thomas, D.N. and Dieckmann; G.S. (Editors), Sea Ice, pp. 267-302.

Thomas, R., 2008. Practical Guide to ICP-MS: A Tutorial for Beginners, Second Edition. Practical Guide to Icp-Ms: A Tutorial for Beginners, Second Edition. Crc Press-Taylor & Francis Group, Boca Raton, 1-339 pp.

Thume, K., Gebser, B., Chen, L., Meyer, N., Kieber, D.J., Pohnert, G., 2018. The metabolite dimethylsulfoxonium propionate extends the marine organosulfur cycle. *Nature*, **563**(7731): 412-415.

Thurman, E.M., 1985. Organic geochemistry of natural waters. Kluwer Academic Publisher Group.

Toming, K., Tuvikene, L., Vilbaste, S., Agasild, H., Viik, M., Kisand, A., et al., 2013. Contributions of autochthonous and allochthonous sources to dissolved organic matter in a large, shallow, eutrophic lake with a highly calcareous catchment. *Limnol. Oceanogr*, **58**(4): 1259-1270.

Tripp, H.J., Kitner, J.B., Schwalbach, M.S., Dacey, J.W.H., Wilhelm, L.J., Giovannoni, S.J., 2008. SAR11 marine bacteria require exogenous reduced sulphur for growth. *Nature*, **452**(7188): 741-744.

Tsutsuki, K. and Kuwatsuka, S., 1984. Molecular size distribution of humic acids as affected by the ionic strength and the degree of humification. *Soil Sci. Plant Nut.*, **30**(2): 151-162.

Twining, B.S. and Baines, S.B., 2013. The Trace Metal Composition of Marine Phytoplankton. *Annu. Rev. Mar. Sci.*, **5**(1): 191-215.

Twining, B.S., Baines, S.B., Fisher, N.S. and Landry, M.R., 2004. Cellular iron contents of plankton during the Southern Ocean Iron Experiment (SOFeX). *Deep Sea Res. Part I: Oceanogr. Res. Pap.*, **51**(12): 1827-1850.

Uher, G. and Andreae, M., 1997. Photochemical production of carbonyl sulfide in North Sea water: A process study. *Limnol. Oceanogr*, **42**(3): 432-442.

Ulshöfer, V.S., Flock, O.R., Uher, G. and Andreae, M.O., 1996. Photochemical production and air-sea exchange of carbonyl sulfide in the eastern Mediterranean Sea. *Mar. Chem.*, **53**(1): 25-39.

Ulshöfer, V.S., Uher, G. and Andreae, M.O., 1995. Evidence for a winter sink of atmospheric carbonyl sulfide in the northeast Atlantic Ocean. *Geophys. Res. Lett.*, **22**(19): 2601-2604.

Umlauf, L. and Burchard, H., 2005. Second-order turbulence closure models for geophysical boundary layers. A review of recent work. *Cont. Shelf Res.*, **25**(7): 795-827.

Vairavamurthy, A., Manowitz, B., Luther, G.W. and Jeon, Y., 1993. Oxidation state of sulfur in thiosulfate and implications for anaerobic energy metabolism. *Geochim. Cosmochim. Acta*, **57**(7): 1619-1623.

Vairavamurthy, A., Zhou, W., Eglinton, T. and Manowitz, B., 1994. Sulfonates: A novel class of organic sulfur compounds in marine sediments. *Geochim. Cosmochim. Acta*, **58**(21): 4681-4687.

Vairavamurthy, M.A., Orr, W., L. and Manowitz, B., 1995a. Geochemical Transformations of Sedimentary Sulfur: An Introduction, Geochemical Transformations of Sedimentary Sulfur. ACS Symposium Series. American Chemical Society, pp. 1-14.

Vairavamurthy, M.A., Schoonen, M.A.A., Eglinton, T.I., Luther, G.W. and Manowitz, B., 1995b. Geochemical Transformations of Sedimentary Sulfur. ACS Symposium Series, 612. American Chemical Society, 484 pp.

Vega, M. and van den Berg, C.M.G., 1997. Determination of Cobalt in Seawater by Catalytic Adsorptive Cathodic Stripping Voltammetry. *Anal. Chem.*, **69**(5): 874-881.

Vila-Costa, M., Simó, R., Harada, H., Gasol, J.M., Slezak, D., Kiene, R.P., 2006. Dimethylsulfoniopropionate Uptake by Marine Phytoplankton. *Science*, **314**(5799): 652-654.

Vogt, M. and Liss, P.S., 2013. Dimethylsulfide and Climate, In: Le Quéré, C. and Saltzman, E.S., (Editors). Surface Ocean–Lower Atmosphere Processes. American Geophysical Union, pp. 197-232.

von Hobe, M., Cutter, G.A., Kettle, A.J. and Andreae, M.O., 2001. Dark production: A significant source of oceanic COS *J. Geophys. Res.*, **106**(C12): 31217.

von Hobe, M., Kettle, A.J. and Andreae, M.O., 1999. Carbonyl sulphide in and over seawater: Summer data from the northeast Atlantic Ocean. *Atmos. Environ.*, **33**(21): 3503-3514.

von Hobe, M., Najjar, R.G., Kettle, A.J. and Andreae, M.O., 2003. Photochemical and physical modeling of carbonyl sulfide in the ocean. *J. Geophys. Res.: Oceans*, **108**(C7).

Vraspir, J.M. and Butler, A., 2009. Chemistry of Marine Ligands and Siderophores. *Annu. Rev. Mar. Sci.*, **1**: 43-63.

Wadham, J.L., De'ath, R., Monteiro, F.M., Tranter, M., Ridgwell, A., Raiswell, R., et al., 2013. The potential role of the Antarctic Ice Sheet in global biogeochemical cycles. *Earth Environ. Sci. Trans. Royal Soc. Edinburgh*, **104**(1): 55-67.

Wakeham, S.G., Lee, C, Hedges, J.I., Hernes, P.J., Peterson, M.J., 1997. Molecular indicators of diagenetic status in marine organic matter. *Geochim. Cosmochim. Acta*, **61**(24): 5363-5369.

Waska, H., Koschinsky, A., Ruiz Chancho, M.J. and Dittmar, T., 2015. Investigating the potential of solid-phase extraction and Fourier-transform ion cyclotron resonance mass spectrometry (FT-ICR-MS) for the isolation and identification of dissolved metal–organic complexes from natural waters. *Mar. Chem.*, **173**: 78-92.

Wasmund, K., Mußmann, M. and Loy, A., 2017. The life sulfuric: microbial ecology of sulfur cycling in marine sediments. *Environ. Microbiol. Rep.*, **9**(4): 323-344.

Weishaar, J.L., Aiken, G.R., Bergamaschi, B.A., Fram, M.S., Fujii, R., Mopper. K., 2003. Evaluation of Specific Ultraviolet Absorbance as an Indicator of the Chemical Composition and Reactivity of Dissolved Organic Carbon. *Environ. Sci. Technol.*, **37**(20): 4702-4708.

Weiss, P.S., Andrews, S.S., Johnson, J.E. and Zafiriou, O.C., 1995. Photoproduction of carbonyl sulfide in South Pacific Ocean waters as a function of irradiation wavelength. *Geophys. Res. Lett.*, **22**(3): 215-218.

Wen, L.-S., Santschi, P., Gill, G. and Paternostro, C., 1999. Estuarine trace metal distributions in Galveston Bay: importance of colloidal forms in the speciation of the dissolved phase. *Mar. Chem.*, **63**(3–4): 185-212.

Werne, J.P., Hollander, D.J., Lyons, T.W. and Sinninghe Damsté, J.S., 2004. Organic sulfur biogeochemistry: Recent advances and future research directions. Sulfur Biogeochemistry - Past and Present. In: Amend, J.P., Edwards, K.J. and Lyons, T.W. (Editors). Geological Society of America, pp. 0.

Werne, J.P., Lyons, T.W., Hollander, D.J., Formolo, M.J., Sinninghe Damsté, J.S., 2003. Reduced sulfur in euxinic sediments of the Cariaco Basin: sulfur isotope constraints on organic sulfur formation. *Chem. Geol.*, **195**(1): 159-179.

Whelan, M.E., Lennartz, S.., Gimeno, T.E., Wehr, R., Wohlfahrt, G., Wang, Y., et al., 2018. Reviews and syntheses: Carbonyl sulfide as a multi-scale tracer for carbon and water cycles. *Biogeosciences*, **15**(12): 3625-3657.

Willey, J.D., Kieber, R.J., Eyman, M.S. and Avery, G.B., 2000. Rainwater dissolved organic carbon: Concentrations and global flux. *Glob. Biogeochem. Cycle*, **14**(1): 139-148.

Wu, J., Boyle, E., Sunda, W. and Wen, L.-S., 2001. Soluble and Colloidal Iron in the Oligotrophic North Atlantic and North Pacific. *Science*, **293**(5531): 847-849.

Wufuer, R. et al., 2014. Interaction of dissolved organic matter with Hg(II) along salinity gradient in Boston Lake. *Geochem. Internation.*, **52**(12): 1072-1077.

Wünsch, U.J., Stedmon, C.A., Tranvik, L.J. and Guillemette, F., 2018. Unraveling the size-dependent optical properties of dissolved organic matter. *Limnol. Oceanogr.*, **63**(2): 588-601.

Xia, K., Weesner, F., Bleam, W.F., Helmke, P.A., Bloom, P.R., Skyllberg, U.L., 1998. XANES Studies of Oxidation States of Sulfur in Aquatic and Soil Humic Substances. *Soil Sci. Soc. Am. J.,* **62**(5): 1240-1246.

Xie, H. and Moore, R.M., 1999. Carbon disulfide in the North Atlantic and Pacific oceans. *J. Geophys. Res.: Oceans*, **104**(C3): 5393-5402.

Xie, H., Moore, R.M. and Miller, W.L., 1998. Photochemical production of carbon disulphide in seawater. *J. Geophys. Res.: Oceans*, **103**(C3): 5635-5644.

Xie, H., Scarratt, M.G. and Moore, R.M., 1999. Carbon disulphide production in laboratory cultures of marine phytoplankton. *Atmosph. Environ.*, **33**(21): 3445-3453.

Yamashita, Y. and Tanoue, E., 2003. Chemical characterization of protein-like fluorophores in DOM in relation to aromatic amino acids. *Mar. Chem.*, **82**(3): 255-271.

Yamashita, Y., Tsukasaki, A., Nishida, T. and Tanoue, E., 2007. Vertical and horizontal distribution of fluorescent dissolved organic matter in the Southern Ocean. *Mar. Chem.*, **106**(3-4): 498-509.

Yeghicheyan, D., Bossy, C., Bouhnik Le Coz, M., Douchet, C., Granier, G., Heimburger, A., et al, 2013. A Compilation of Silicon, Rare Earth Element and Twenty-One other Trace Element Concentrations in the Natural River Water Reference Material SLRS-5 (NRC-CNRC). *Geostand. Geoanal. Res.*, **37**(4): 449-467.

Ylöstalo, P., Seppälä, J., Kaitala, S., Maunula, P. and Simis, S., 2016. Loadings of dissolved organic matter and nutrients from the Neva River into the Gulf of Finland – Biogeochemical composition and spatial distribution within the salinity gradient. *Mar. Chem.*, **186**: 58-71.

Yoch, D.C., 2002. Dimethylsulfoniopropionate: Its sources, role in the marine food web and biological degradation to dimethylsulfide. *Appl. Environ. Micobiol.*, **68**(12): 5804-5815.

Zemmelink, H.J., Houghton, L., Dacey, J.W.H., Stefels, J., Koch, B.P., Schröder, M., et al., 2008. Stratification and the distribution of phytoplankton, nutrients, inorganic carbon, and sulfur in the surface waters of Weddell Sea leads. *Deep Sea Res. Part II: Top. Stud. Oceanogr.*, **55**(8): 988-999.

Zepp, R.G. and Andreae, M.O., 1994. Factors affecting the photochemical production of carbonyl sulfide in seawater. *Geophys. Res. Lett.*, **21**(25): 2813-2816.

Zhang, H., Van Den Berg, C.M.G. and Wollast, R., 1990. The determination of interactions of cobalt (II) with organic compounds in seawater using cathodic stripping voltammetry. *Mar. Chem.*, **28**(4): 285-300.

Zhang, L., Walsh, R. S., and Cutter, G. A., 1998. Estuarine cycling of carbonyl sulfide: Production and sea-air flux. *Mar. Chem.*, **61**, 127-142.

Zindler, C., Marandino, C.A., Bange, H.W., Schutte, F. and Saltzman, E.S., 2014. Nutrient availability determines dimethyl sulfide and isoprene distribution in the eastern Atlantic Ocean. *Geophys. Res. Lett.*, **41**(9): 3181-3188.

Zydowsky, T.M., Courtney, L.F., Frasca, V., Kobayashi, K., Shimizu, H., Yuen, L.D., et a, 1986. Stereochemical analysis of the methyl transfer catalyzed by cobalamin-dependent methionine synthase from *Escherichia coli B. J. Am. Chem. Soc.*, **108**(11): 3152-3153.

VIII. Addendum

The addendum to this thesis contains reprints of the supplementary materials to the published and submitted manuscripts 1, 3 and 5 and the draft of the supplementary material to manuscript 4 (in preparation). The content of the reprints is unchanged and the (reference) style and labeling of figures and tables is adapted to the general format of this thesis. The references are included in the reference chapter of this thesis.

Supplementary Material to Manuscript 1

Dissolved organic sulfur in the ocean: Biogeochemistry of a petagram inventory

Kerstin B. Ksionzek, Oliver J. Lechtenfeld, S. Leigh McCallister, Philippe Schmitt-Kopplin, Jana K. Geuer, Walter Geibert, Boris P. Koch

Materials and Methods

Sample collection and processing

Water samples were collected in November and December 2008 (expedition ANTXXV/1 and 2 of *R/V Polarstern*) along a transect in the East Atlantic Ocean and the Atlantic sector of the Southern Ocean (i.e. south of 45° S) (Flerus et al., 2012; Lechtenfeld et al., 2014). Surface water samples (2 m water depth) were taken with a towed fish sampler. Other water samples were taken with the rosette sampler connected to a CTD. 6 L of each sample was filtered through pre-combusted GF/F filters (Whatman, 450 °C, 5 h, 0.7 μm nominal pore size) with a maximum pressure < 200 mbar. Aliquots for DOC and nutrient analyses were stored in pre-combusted glass ampules at -20 °C. Filtered samples were acidified to pH 2 (hydrochloric acid, suprapur, Merck). 5 L of seawater were extracted (PPL, 1 g, Mega Bond Elut, Varian) and eluted with 5 mL of methanol (LiChrosolv, Merck) into pre-combusted glass ampules (Dittmar et al., 2008). Extracts were stored at -20 °C until further analysis.

Analytical methods

DOC, nutrient, ^{14}C, and FT-ICR-MS analysis and data evaluation were performed as described previously (Flerus et al., 2012; Lechtenfeld et al., 2014). Analysis of DON_{SPE} was carried out simultaneously to DOC_{SPE} analysis by high temperature catalytic oxidation (TOC-V_{CPN} analyser, Shimadzu) (Dittmar et al., 2008).

To ensure that SPE completely removed sulfate from the samples, we analyzed sulfate in the extracts: An aliquote of the methanol extract (100 μL) was evaporated with N_2 and redissolved in 1 mL MilliQ water. We then added a solution of $BaCl_2$ in excess after which no precipitation of $BaSO_4$ was observed.

For organic sulfur quantification, an inductively coupled plasma sector field mass spectrometer (ICP-MS, Element 2, Thermo Fisher Scientific) was equipped with a desolvation nebulizer (Apex Q, Elemental Scientific), a platinum guard electrode, nickel sampler and skimmer cones. Prior to ICP-MS analysis, 50 μL methanol extract was evaporated with N_2 and redissolved in 5 mL nitric acid (1 M, double distilled, Merck). 50 μL of ^{103}Rh (50 ppb in the spike solution) were added as an internal standard. The samples were sonicated for 10-15 min to ensure that all DOM was redissolved. ICP-MS operating conditions are given in Table S2. The instrument was tuned daily for optimized plasma conditions and accurate mass calibration with a multi-element tuning solution (~0.1 ppb in HNO_3). Signals of ^{32}S and ^{103}Rh were recorded. Nitric acid (1 M, double destilled, Merck) was used for analysis blank. Calibration standards were prepared in different concentrations from a stock solution (100 μg mL^{-1}, multi-element-standard, nonmetals, Spetec) and external calibration was performed daily prior to the sample analyses. Limit of detection (according to DIN 32645, n=9) was 11 μmol L^{-1} S. This corresponds to 0.011 μmol L^{-1} DOS_{SPE} in original seawater (average enrichment factor of 1046).

Random controls of measured DOS_{SPE} values analyzed by standard addition yielded a relative accuracy of ~10 %.

Methionine quantification was performed using reversed-phase high performance liquid chromatography (RP-HPLC). 200 µL of each extract were pipetted into combusted glass ampules. Samples were dried with N_2 and redissolved in 1 mL MilliQ and 1 mL hydrochloric acid (30 %, ~9.6 mol L^{-1}). The gaseous phase of the ampules was flushed with N_2 before closure. Samples were heated in a drying oven at 110 °C for 20 hours. The ampules were opened and 0.8925 mL borate buffer for hydrolysis was added. The pH was adjusted to approximately 8.5 with NaOH (approx. 20 %, suprapur, Merck). The HPLC system (Agilent Technologies 1200 Series, 1260 Infinity Series) was equipped with a binary pump (G1312A), autosampler (ALS G1329A), column oven (TCC G1316A) and fluorescence detector (FLD G1321A). Column oven temperature was 32 °C and the total injection volume was 20 µL. The separation was performed using a reversed-phase column (Phenomenex Synergi 4 µm, Hydro-RP 80 Å, 150 x 2 mm, with precolumn Phenomenex KrudKatcher Ultra HPLC in-line filter (0.5 µm depth filter x 0.004" ID); constant flow at 0.45 mL min^{-1}) and a solvent gradient (0 to 76 min) from 97 % sodium acetate (NaAc, suprapur, Merck), adjusted to pH 6 with hydrochloric acid (suprapur, Merck) and 3 % acetonitrile (CH_3CN, Merck) to 3 % NaAc and 9 % CH_3CN. Fluorescence was measured at 230 nm excitation and 440 nm emission wavelengths and the average retention time for methionine was 39.91 ± 0.41 min.

Calculation of the long-term degradation rate for non-labile DOS_{SPE}

A subset of FT-ICR MS peaks from 24 samples from the EA was used to model the age of bulk DOC_{SPE} (Lechtenfeld et al., 2014). Peak magnitudes, which showed a significant correlation with measured ^{14}C values were subsumed and implemented in a calibration function. This function was applied to the total FT-ICR MS dataset, resulting in calculated ^{14}C values.

Measured DOS_{SPE} concentrations were plotted versus measured and calculated ^{14}C values (Fig. S1B). Eq. S1 describes the bulk DOS_{SPE} degradation:

$$[DOS]_{SPE} = 0.27\ e^{-0.000254*age}\ \mu mol\ L^{-1} \quad (S1)$$

where $[DOS]_{SPE}$ is the bulk DOS_{SPE} concentration at a certain age. We calculated $[DOS]_{SPE}$ both for the minimum and maximum age of the sample set (2241 a; $[DOS]_{SPE}$ = 0.14 µmol L^{-1} 5331 a; $[DOS]_{SPE}$ = 0.05 µmol S L^{-1}, respectively). This results in a degradation of non-labile DOS_{SPE} of $2.7*10^{-5}$ µmol S L^{-1} a^{-1}. Based on a global ocean volume of $1.3*10^{21}$ L, the global DOS_{SPE} removal is $3.5*10^{16}$ µmol S a^{-1} (1.12 Tg S a^{-1}).

Calculation of the lifetime of DOC_{SPE} and DOS_{SPE}

The lifetime τ is defined as the time over which the DOM concentration decreases to $1/e$ of its initial value. It relates to the degradation rate coefficient k in the following way:

$$\tau = 1/k \quad \text{(S2)}$$

The degradation rate coefficients for DOC_{SPE} and DOS_{SPE} are $k_{DOC} = 1.53*10^{-4}$ a^{-1} and $k_{DOS} = 2.54*10^{-4}$ a^{-1} respectively. This results in a lifetime of DOC_{SPE} and DOS_{SPE} of $\tau_{DOC} = 6536$ a and $\tau_{DOS} = 3937$ a.

Calculation of $[DOS]_{MIN}$

The calculation of DOS_{MIN} was performed according to Eq. S1. The $[DOS]_{MIN}$ concentrations were calculated for each depth interval, using the measured original DOC concentrations and the measured average DOC_{SPE}/DOS_{SPE} ratios (Table M1.1).

The global DOS_{MIN} inventory is based on depth-integrated DOC_{SPE}/DOS_{SPE} ratios and the global DOC inventory (Hansell et al., 2009).

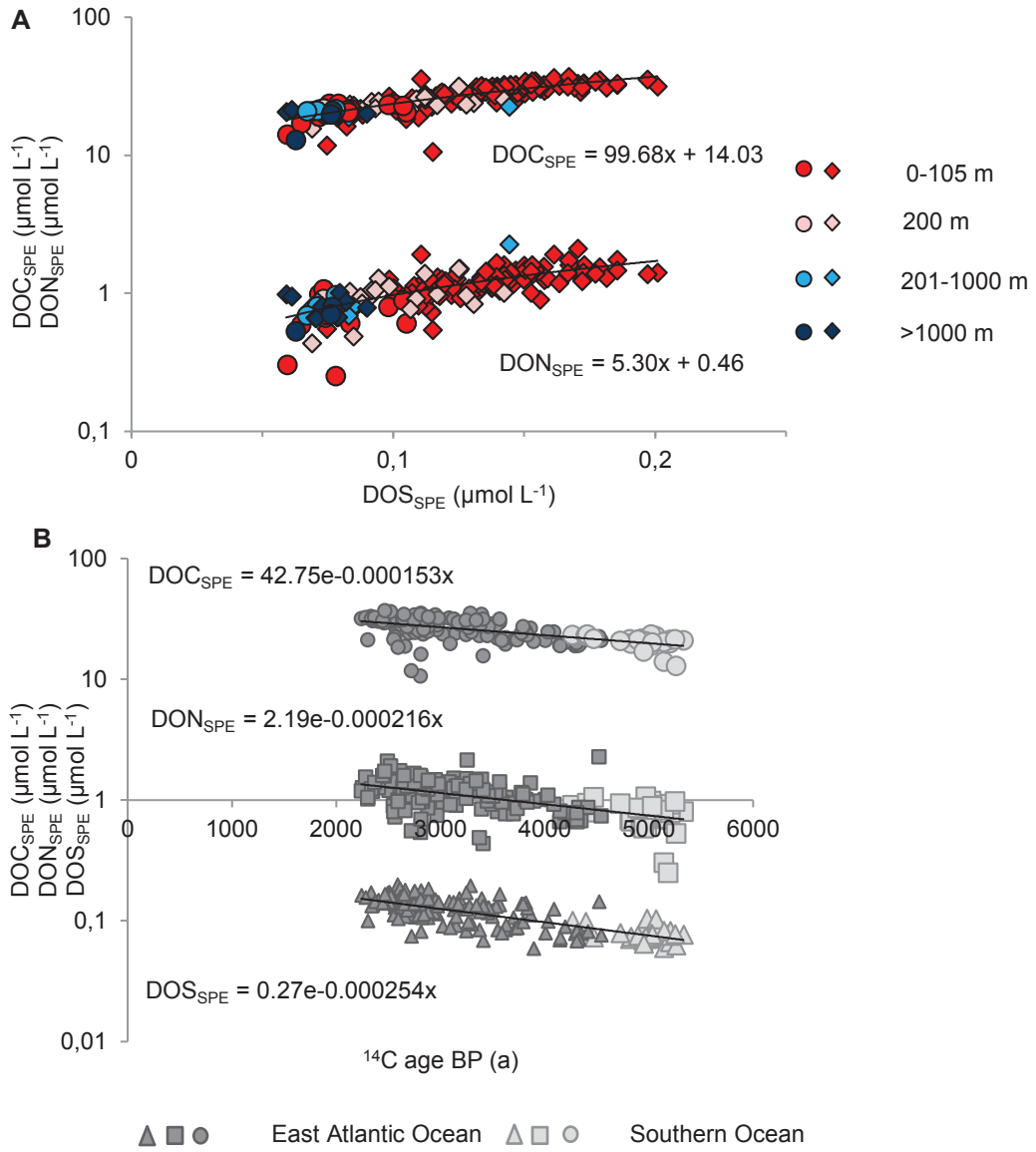

Fig. M1.S1. Correlation of DOS_{SPE} with DOC_{SPE}, DON_{SPE} and ^{14}C age. (A) DOS_{SPE} vs. DOC_{SPE} ($R = 0.86$, $p < 0.001$) and DOS_{SPE} vs. DON_{SPE} ($R = 0.75$, $p < 0.001$): Linear correlation of East Atlantic Ocean samples (diamonds) and Southern Ocean samples (circles) at different depth intervals (colors). (B) Bulk DOC_{SPE} (circles), DON_{SPE} (squares) and DOS_{SPE} (triangles) concentrations in the East Atlantic Ocean (dark grey) and Southern Ocean (light grey) vs. calculated ^{14}C age of the DOC_{SPE} samples. ^{14}C age is given in years before present (BP). Based on first order kinetics, the removal rates for DON_{SPE} and DOS_{SPE} were similar and significantly faster than for DOC_{SPE} ($p < 0.001$).

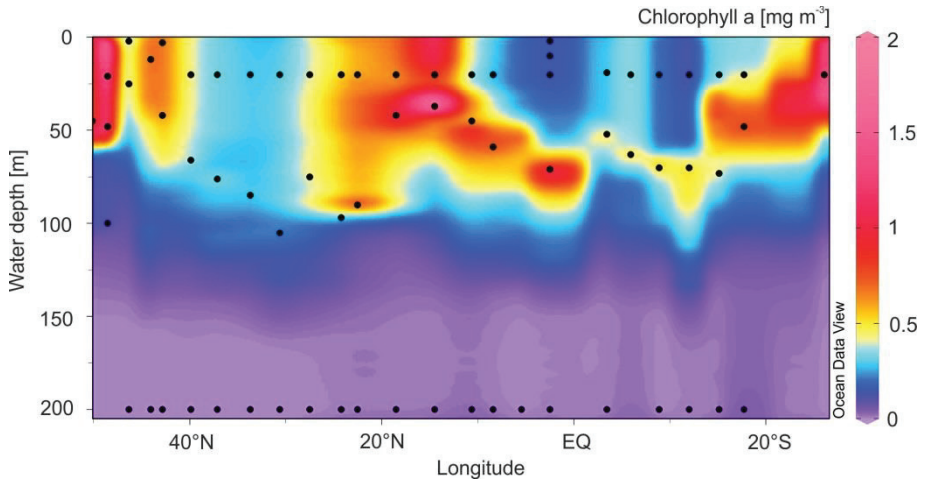

Fig. M1.S2. Chlorophyll a concentration in the upper 200m along the transect through the East Atlantic (note the nonlinearity of the color bar). The black dots represent the sampling locations of DOC_{SPE} and DOS_{SPE}. The chlorophyll a concentrations were calculated using fluorescence data from the CTD (Dr. Haardt) and HPLC data. No correlation was found between chlorophyll a and DOC_{SPE} or DOS_{SPE}.

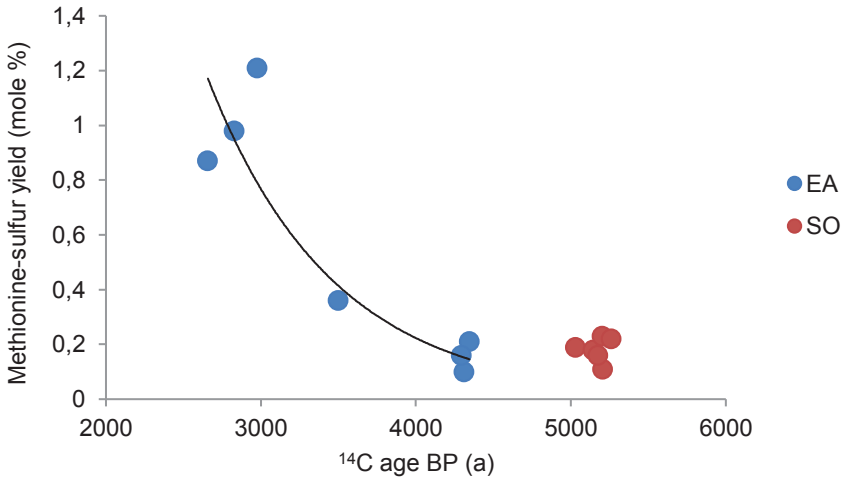

Fig. M1.S3. Methionine-sulfur yield. Decrease of the molar methionine-sulfur yield (mole % of methionine-S versus total DOS_{SPE}) with calculated ^{14}C age in the East Atlantic (EA, blue circles). For the Southern Ocean samples (SO, red circles) a decrease methionine-sulfur yield was not observed.

Table M1.S1. Definition of DOS fractions.

Term	Definition
DOS	Dissolved organic sulfur in original seawater.
DOS_{SPE}	Fraction of DOS isolated by solid-phase extraction.
Volatile DOS	Small organic sulfur compounds such as DMS, COS, CS_2 in the surface water, which contribute to ocean-atmosphere fluxes.
Non-volatile DOS	Dissolved organic sulfur compounds, which do not evaporate at normal temperatures and pressures (as opposed to volatile compounds).
Labile DOS	Dissolved organic sulfur compounds (e.g. DMSP and amino acids), which do not accumulate in the surface ocean due to their short lifetimes (hours to days).
Non-labile DOS	All other (solid-phase extractable) dissolved organic sulfur compounds with longer lifetimes (typically more than 1.5 years).
$[DOS]_{MIN}$	Estimated minimum concentration of dissolved organic sulfur in original seawater, calculated from the molar DOC concentration in original seawater and the molar bulk DOC_{SPE}/DOS_{SPE} ratio in the extracts (according to Eq.S1).

Table M1.S2. ICP-MS operating conditions.

ICP-MS operating conditions	
RF power	1236 W
Ar sample gas	1.15 L min^{-1}
Ar auxiliary gas	1.11 L min^{-1}
Ar cool gas	16 L min^{-1}
Data acquisition	
Scan type	EScan
Samples per peak	20
Sample time	20 ms
Integration window	60 %
Integration type	Average
Resolution	Medium (4000 m/Δm)
Regression type	Linear

Table M1.S3. Selected elements of the sulfur cycle in numbers.*

Parameter	Values	References
(a) Total land-atmosphere S flux (R)	67-132 Tg S a^{-1}	Roberts (2015)
(b) Global river-ocean flux of POS/DOS (A)	8 Tg S a^{-1}	Calculated: global DOC and POC input (0.2 Pg DOC a^{-1}, 0.15 Pg POC a^{-1}) (Eglinton and Repeta, 2006); molar C/S ratio of POC (~119) (Matrai and Eppley, 1989)
(c) Global ocean-atmosphere flux of DMS (R)	13 – 37 Tg S a^{-1}	Kettle and Andreae (2000)
(d) Global ocean-atmosphere flux of COS (A)	0.4 Tg S a^{-1}	Yoch (2002)
(e) Global ocean-atmosphere flux of CS_2 (A)	0.3 Tg S a^{-1}	Yoch (2002)
(f) Global oceanic sulfate pool	$1.2*10^9$ Tg S	Calculated oceanic sulfate concentration (Pilson, 2013): 29 mmol L^{-1}; global ocean volume: $1.3*10^{21}$ L)
(g) Sulfur assimilation by phytoplankton (A)	1,360 Tg S a^{-1}	Calculated (Field et al., 1998; Ho et al., 2003)
(h) Global organic sulfur in phytoplankton	28 Tg S	Calculated (Falkowski et al., 1998; Ho et al., 2003)
(i) Global organic sulfur in microbes	<62 Tg S	Calculated: global marine biomas (3 Pg C) (Cole, 2013) minus glob phytoplankton biomass (1 Pg C (Falkowski et al., 1998); molar C/ ratio of bacteria (Fagerbakke et a 1996): ~86
(j) Global DMS_{diss} in seawater	6 Tg S	Calculated (Zindler et al., 2014)
(k) Global particulate organic sulfur (R)	200 - 400 Tg S	Calculated (Eglinton and Repeta, 2006; Matrai and Eppley, 1989)
(l) Global DOS_{MIN} content	6,700 Tg S	This study
(m) Global $DMSP_{diss}$ in seawater (A)	18 Tg S	Calculated (Zindler et al., 2014)
(n) Net removal rate of refractory DOS (A)	$2.7*10^{-5}$ μmol L^{-1} a^{-1} (~1.1 Tg S a^{-1})	This study

* Values are given as average (A) or range (R)

Supplementary Material to Manuscript 3

Stoichiometry, polarity, and organometallics in solid-phase extracted dissolved organic matter of the Elbe-Weser estuary

Kerstin B. Ksionzek, Jing Zhang, Kai-Uwe Ludwichowski, Dorothee Wilhelms-Dick, Scarlett Trimborn, Thomas Jendrossek, Gerhard Kattner, Boris P. Koch

M3.S1 file. This file includes methodical information about the salt-spiking experiment of riverine samples.

To estimate the influence of salt on the extraction efficiency of DOM, low salinity Weser River samples (Fig. M3.SF1) were taken, and filtered using a stainless steel in-line filter holder (Sartorius type 16275), a peristaltic pump, a pre-filter (GF/F. 13400-142-K. Sartorius) and a membrane filter (cellulose acetate. 0.2 μm pore size. 11107-142-G. Sartorius). The first 500 mL of every filtration were rejected. Samples were stored in the dark at 4°C until further analysis. For the spiking-experiment, the samples were mixed with defined amounts of pre-combusted sodium chloride (NaCl, 500 °C. 5 h). The amount of added NaCl increased continuously in five steps (0, 8.75. 17.5, 26.25, 35 g/L). The final salinities of the sample R1/R2 are given in Table 1. 150 mL of each sample was acidified to pH 2, extracted (PPL, 200 mg. Mega Bond Elut, Agilent Technologies) and eluted with 1.5 mL of methanol (LiChrosolv. Merck) into pre-combusted glass vials. DOC and DOC_{SPE} concentrations were determined by high temperature catalytic oxidation. DOC in original water samples were measured directly. For analysis of DOC_{SPE}, 50 μL of the extract were evaporated under N_2 and subsequently redissolved in 7 mL ultrapure water.

Final DOC and DOC_{SPE} concentrations and according extraction efficiencies are given in Table M3.FS1.

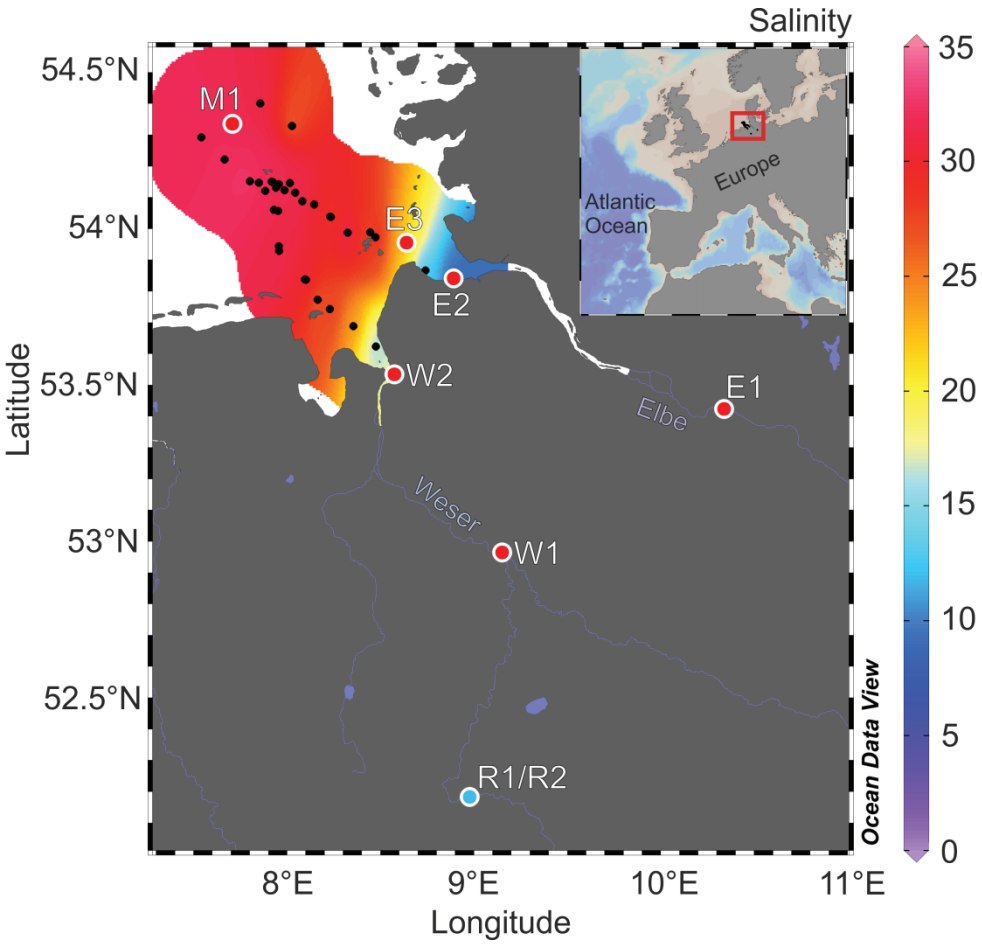

Fig M3.SF1. Sampling location of the Weser River samples R1 and R2 (blue dot). Color represents the surface salinity. Black dots represent stations, at which temperature and salinity were measured. Red dots represent stations, at which samples for DOM and trace element analysis were taken.

Table M3.SF1. DOC and DOC_{SPE} concentrations and according extraction efficiencies of the sodium chloride spiked Weser riverine samples R1 and R2.

Sample	DOC (µmol L^{-1})	DOC_{SPE} (µmol L^{-1})	Salinity	Extraction efficiency (%)
		138	0.9	56
		136	9.5	55
R1	247	137	18.1	55
		129	26.7	52
		128	35.3	51
		116	0.8	58
		112	9.4	56
R2	201	113	18.0	56
		115	26.6	57
		118	35.2	59

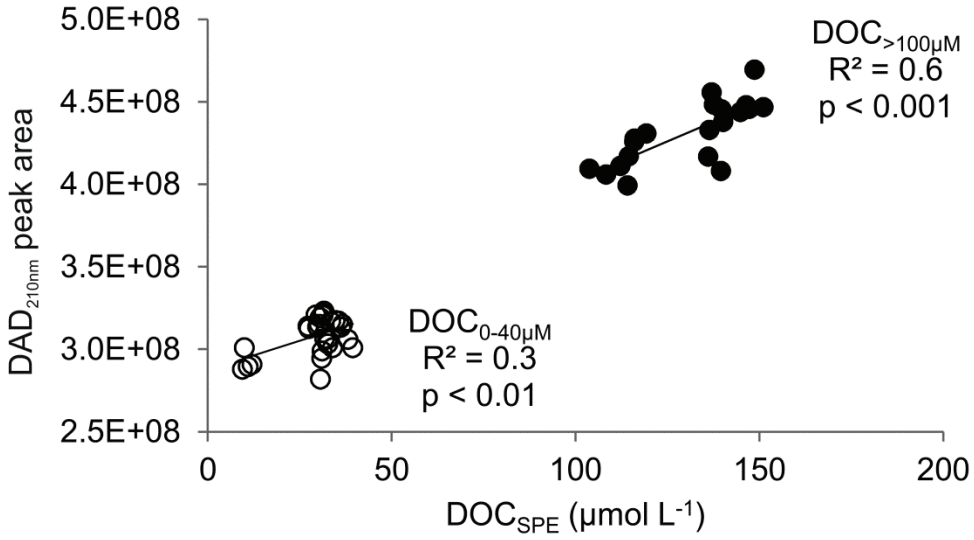

M3.S1 Fig. UV peak area at 210 nm versus DOC_{SPE} concentrations of all samples. A significant linear correlation was found for both fractions: the low concentrated fraction (all pH 8 extracted samples and the pH 2 extracted marine sample) with DOC_{SPE} concentrations from 0 – 40 µmol L^{-1} (unfilled symbols) and the high concentrated fractions (pH 2 extracted riverine and estuarine samples) with DOC_{SPE} concentrations > 100 µmol L^{-1} (filled symbols).

M3.S1 Table. Limits of detection for all elements analyzed by ICP-MS, given that solid-phase extraction was performed with an enrichment factor of 430. These values were calculated according to DIN 32645.

Isotope	Limit of detection
^{31}P	3.402 nmol L^{-1}
^{32}S	0.044 µmol L^{-1}
^{51}V	0.013 nmol L^{-1}
^{52}Cr	0.042 nmol L^{-1}
^{55}Mn	0.027 nmol L^{-1}
^{59}Co	$6.27*10^{-3}$ nmol L^{-1}
^{60}Ni	0.050 nmol L^{-1}
^{63}Cu	0.342 nmol L^{-1}
^{75}As	0.334 nmol L^{-1}

Supplementary Material to Manuscript 4

Quantification and biogeochemistry of dissolved organic sulfur in the southeastern Weddell Sea

Kerstin B. Ksionzek,Walter Geibert, Kai-Uwe Ludwichowski, Ingrid Stimac, Svenja Ryan, Boris P. Koch

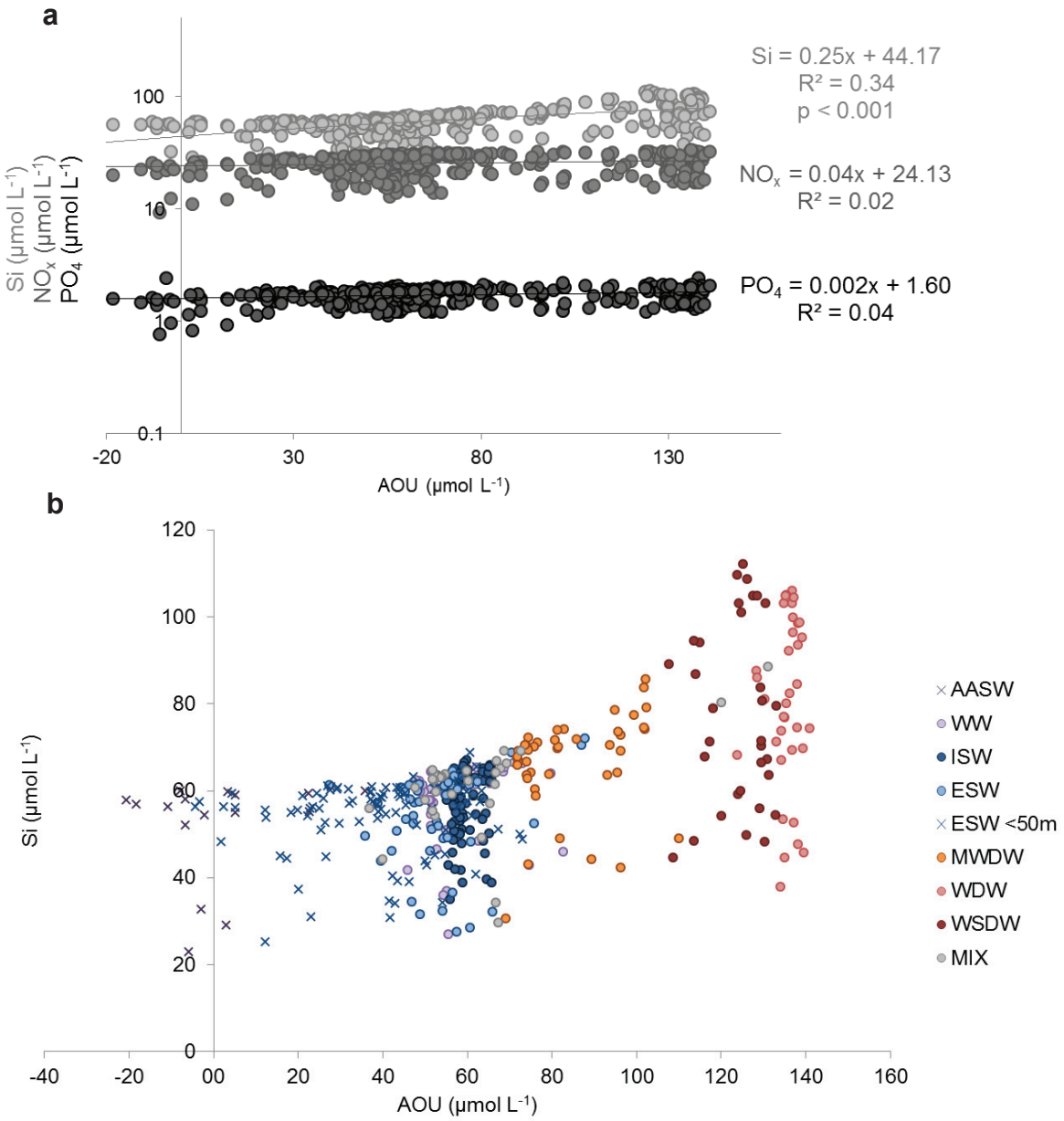

Figure M4.S1. Correlation of nutrients with AOU in the Weddell Sea. a) Correlation of silicate (light grey), NO_x (NO_3 + NO_2, grey) and phosphate (dark grey) concentrations with AOU. b) Correlation of silicate concentration with AOU in the Weddell Sea with color scale for water masses. A cross represents a sample from the sea surface (0-50 m).

Supplementary Material to Manuscript 5

The influence of dissolved organic matter on the marine production of carbonyl sulfide (OCS) and carbon disulfide (CS2) in the Peruvian upwelling

S.T. Lennartz, M. von Hobe, D. Booge, H. Bittig, T. Fischer, R. Gonçalves-Araujo, K.B. Ksionzek, B.P. Koch, A. Bracher, R. Röttgers, B. Quack , C.A. Marandino

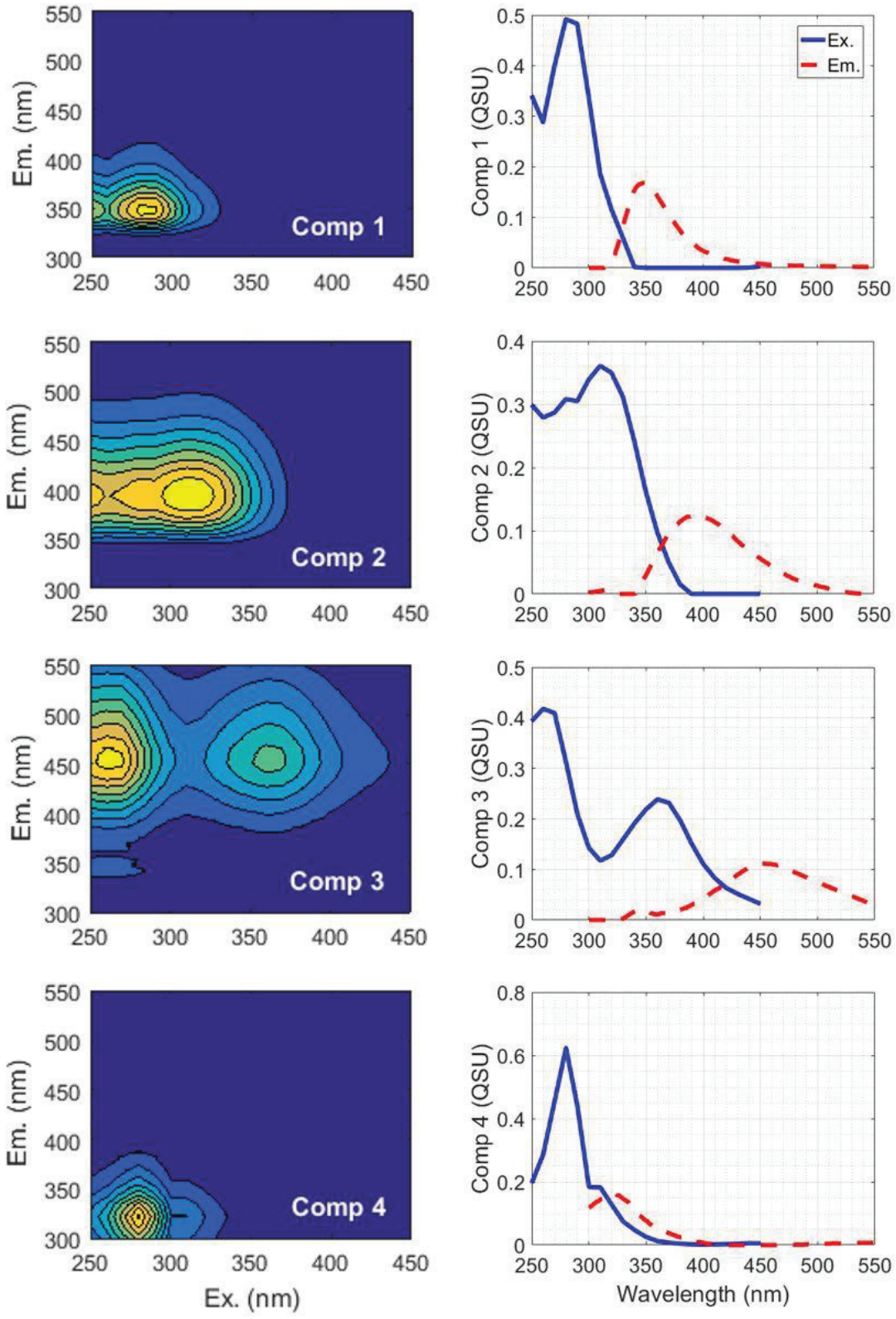

M5.S-Figure 1. Three-dimensional fluorescence landscapes (left) and the excitation and emission spectra (right) for a four component model derived from PARAFAC analysis for fluorescent dissolved organic matter (FDOM). C1 and C4 fluoresce in the UV range and represent protein-like fractions, whereas C2 and C3 fluoresce in the visible range and represent humic-like fractions of the DOM pool.

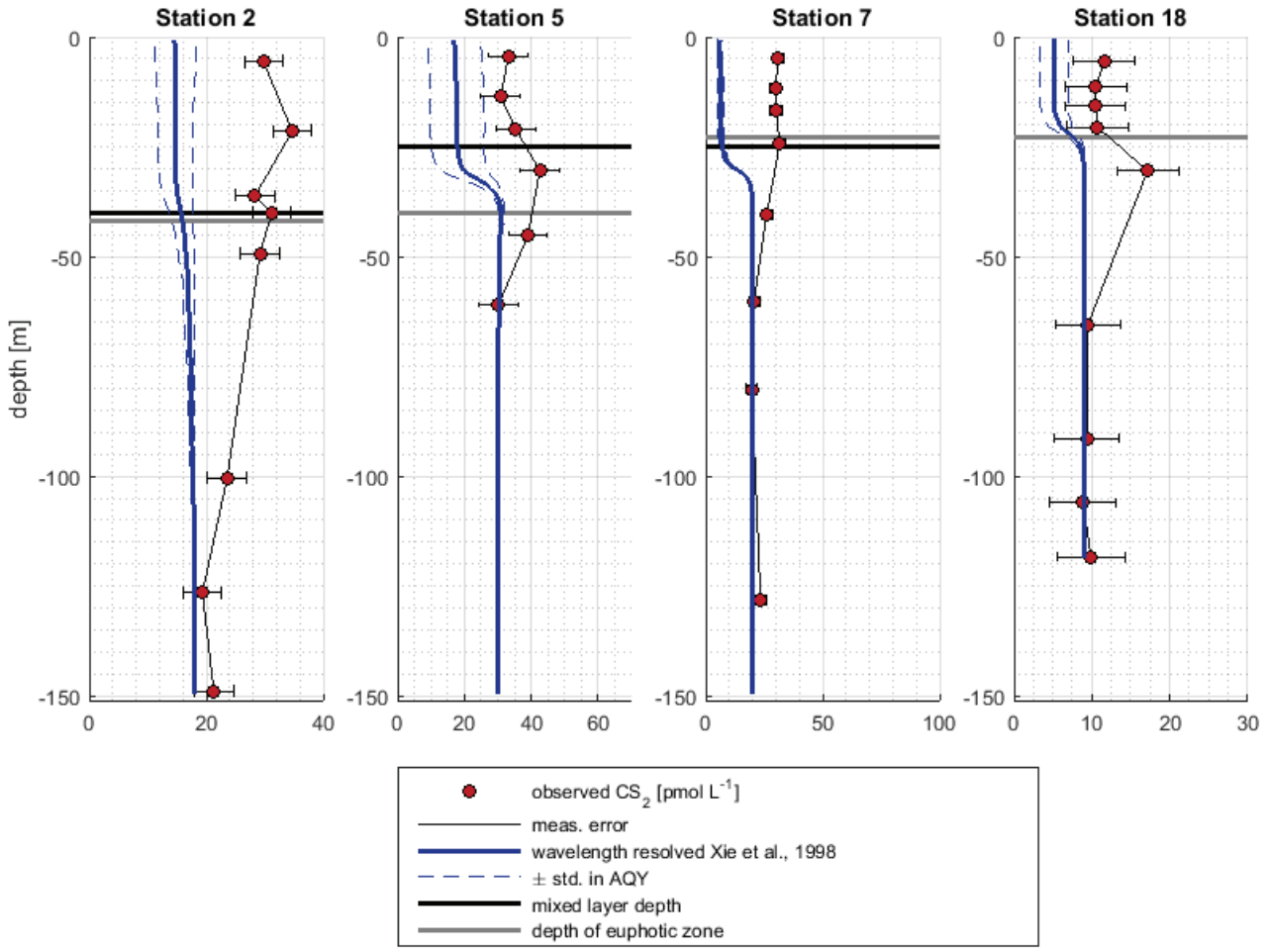

M5.S-Figure 2. Profile measurements of CS2 concentrations and 1D FABM/GOTM model results for the CS2 model experiments using the apparent quantum yield (AQY) reported by Xie et al. (1998). All concentrations in pmol L-1.

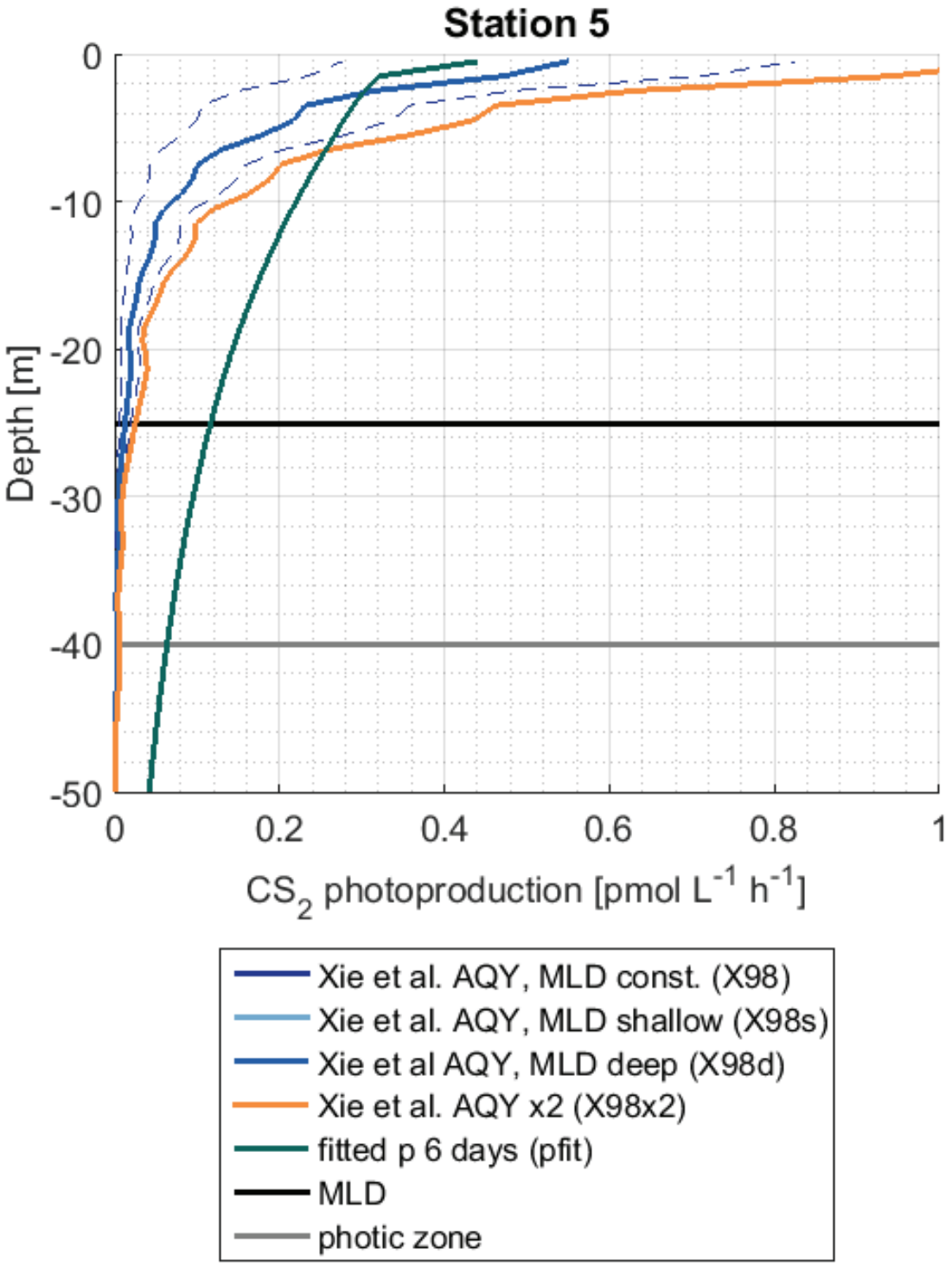

M5.S-Figure 3. Photoproduction for CS_2 in the water column in simulations for station 5.

M5.S-Table 1: Forcing parameter for the box model and the FABM/GOTM 1D water column model.

Parameter	Box model	FABM/GOTM module
CDOM a_{350}	in-situ measurements, 3-hourly measurements	in-situ measurements from CTD casts at stations, constant for the duration of the simulation
UV radiation	Global radiation from shipboard measurements (10 min. averages), corrected to UV radiation as described in von Hobe et al. (2003) and Lennartz et al. (2017)	4 % of global radiation from the host (GOTM), penetration depth and profile shape from in-situ measurements integrated over the wavelengths 300-400nm
Temperature	Continuous in-situ measurements, Seabird MicroCat SBE41	In-situ measurements from CTD, constant for the duration of the simulation
Salinity	Continuous in-situ measurements, Seabird MicroCat SBE41	In-situ measurements from CTD, constant for the duration of the simulation
pH	fixed value 8.1	fixed value 8.1
Air pressure	In-situ measurements	In-situ measurements, daily average, constant for the duration of the simulation
Atmospheric mixing ratio	OCS: sampled onboard, ca. 3-hourly resolution, for quality control: air canister samples analysed at RSMAS (Schauffler et al., 1998; de Gouw et al., 2009) CS_2: no measurements availabe, assumed mixing ratio of 0 ppt	OCS: sampled onboard, for quality control: air canister samples analysed at RSMAS (Schauffler et al., 1998; de Gouw et al., 2009), daily averages CS_2: no measurements availabe, assumed mixing ratio of 0 ppt
Wind speed	measured onboard, corrected to 10 m height, 10 minute averages	In-situ measurements, corrected to 10m height, daily average, constant for the duration of the simulation
Mixed layer depths	obtained from CTD profiles, using the Lorbacher (Lorbacher et al., 2006) criterion, 0-4 times per day	-

M5.S-Table 2: Model forcing for the simulations in GOTM/FABM.

	Station 2		Station 5		Station 7		Station 18	
	OCS	**CS_2**	**OCS**	**CS_2**	**OCS**	**CS_2**	**OCS**	**CS_2**
location	0.00° N 85.50°W	0.00° N 85.50°W	10.00°S 81.92°W	10.00°S 81.92°W	9.18° S 79.46° W	9.18° S 79.46° W	15.32 °S 75.27 °W	15.32 °S 75.27 °W
Date of 2015 UTC	7.10. 16h	7.10.2015 23h	11.10. 3h	10.10. 19h	12.10. 9h	12.10. 3h	19.10. 20h	19.10. 18h
length of simulation [days]	5	21	5	21, 6	5	21	5	21
depth of simulation [m]	100	150	150	150	120	150	120	120
SST [°C]	24.3	20.5	20.6	20.6	20.1	20.1	15.6	15.71
average T [°C]	21.1	19.3	17.5	17.6	17.9	17.3	14.7	14.6
average S [-]	34.9	34.9	35.1	35.1	35.1	35.1	35.0	35.0
average a_{350} [m^{-1}]	0.13	0.13	0.12	0.12	0.14	0.14	0.14	0.14
abs. coef. n	8.8	8.8	6.5	6.5	4.1	4.1	4.5	4.5
Wind speed [m s^{-1}]	8.1	8.1	8.6	8.6	6.7	6.7	8.8	8.8
rel. hum. [%]	100.0	100.0	77.8	77.8	80.9	80.9	88.0	88.0
air pressure [hPa]	1011.3	1011.3	1011.9	1011.9	1013.9	1013.9	1016.7	1016.7
cloud coverage [-]	0.1	0.1	0.1	0.1	0.1	0.1	0.1	0.1